BEHAVIOUR OF CONCRETE FILLED STEEL TUBULAR COLUMNS WITH DIFFERENT CROSS-SECTIONS

Ph.D. THESIS

by

HEAVEN SINGH

DEPARTMENT OF CIVIL ENGINEERING
INDIAN INSTITUTE OF TECHNOLOGY ROORKEE
ROORKEE – 247 667 (INDIA)
November, 2014

BEHAVIOUR OF CONCRETE FILLED STEEL TUBULAR COLUMNS WITH DIFFERENT CROSS-SECTIONS

A THESIS

Submitted in partial fulfilment of the requirements for the award of the degree of

DOCTOR OF PHILOSOPHY

in

CIVIL ENGINEERING

by

HEAVEN SINGH

DEPARTMENT OF CIVIL ENGINEERING
INDIAN INSTITUTE OF TECHNOLOGY ROORKEE
ROORKEE – 247 667 (INDIA)
November, 2014

INDIAN INSTITUTE OF TECHNOLOGY ROORKEE
ROORKEE

CANDIDATE'S DECLARATON

I hereby certify that the work which is being presented in the thesis entitled **"BEHAVIOUR OF CONCRETE FILLED STEEL TUBULAR COLUMNS WITH DIFFERENT CROSS-SECTIONS",** in partial fulfilment of the requirements for the award of the Degree of Doctor of Philosophy and submitted in the Department of Civil Engineering of the Indian Institute of Technology Roorkee is an authentic record of my own work carried out during the period from July, 2009 to November, 2014 under the supervision of **Dr. P. K. Gupta,** Professor, Department of Civil Engineering, Indian Institute of Technology Roorkee.

The matter presented in the thesis has not been submitted by me for the award of any other degree of this or any other Institute.

(HEAVEN SINGH)

This is to certify that the above statement made by the candidate is correct to the best of my knowledge.

(P. K. Gupta)
Supervisor

Date:

ACKNOWLEDEGEMENT

|| Awwal Allah Noor Upaya Kudrat Ke Sab Bande

Ek Noor Te Sab Jag Upjeya Kaun Bhale Kau Mande ||

At the outset, I would like to acknowledge my sincere gratitude and appreciation to my guide **Dr. Pramod Kumar Gupta**, Professor, Department of Civil Engineering, Indian Institute of Technology Roorkee, for his guidance and time throughout my research work. He was always available and eager to help and advise, whether my problem be professional or personal. His cooperation, support and motivation are the primary reason for my completion of this dissertation. This research would not have been possible without his inspiration.

I also sincerely thank **Dr. Ashok Kumar Ahuja**, Professor, Department of Civil Engineering, for his valuable suggestions and guidance.

I would like to take this opportunity to express my sincere gratitude to all faculty members of Department of Civil Engineering, Indian Institute of Technology Roorkee, especially members of my Student Research Committee, namely **Dr. Akhil Upadyay**, **Dr. Pradeep Bhargava** and **Dr. Yogendra Singh**.

I would like to sincerely thank all the laboratory technical staff of Department of Civil Engineering, IIT Roorkee. Special Thanks go to **Mr. Chetan Chand, Mr. Surendra Sharma, Mr. Anil Sharma** for their untiring efforts in helping and facilitating the research work of Ph.D. students like me.

I take this chance to give special thanks to my CFST colleagues, Ziyad Kubba, Mr. Virendra Kumar Verma and Mr. Susheel Katariya. Without our technical discussions regarding the research work, my knowledge of this subject would have been far limited than it presently is. Another sincere round of thanks is due to Ziyad Kubba, as he was my partner, guide and colleague in laboratory work. I would frankly say that I was deeply enriched by his grasp of technical fundamentals and wealth of experience, professional as well as personal.

I would express my dearest gratitude to my fellow research scholars, with some of whom I have come to share a special bond over the duration of my thesis. Praveen Kamath is the first and foremost on that list. The times I spent and the memories I shared with him will always etched in

my memory. He was always there as a friend whenever I needed him. Thank you for your undending support.

I would also like to thank my fellow Research scholars Virendra Kumar, Aasif Hussain Shah, Shakeel Waseem, Govardhan Bhat and Tushar Kanti Dey for their help, support and the good times we spent in Azad Bhawan.

My friends from M.Tech batches deserve a special mention, as they are very close to my heart. I thank Jitendra, Sahil, Pradeep Kumar, Pradeep Singh, Ravi, Ajay, Adil, Shrikanth, Ankit, Nikhil, Bhushan and Ravindra. And last but not the least, a special thanks to Hitesh Lakhani, for being a dear friend, and constant troubleshooter in ABAQUS. Thank you all for making my stay at IIT Roorkee a very enjoyable and pleasant one. My close friends Gaurav, Satveer, Aditya, Maninder, Gurikbal and Gagan also deserve a special mention. Many Thanks to all of you.

No words of mine can be sufficient to express my thanks and respect to my Parents. They have been a constant and untiring source of support and motivation to me all through this time. My sisters Navpreet, Mankiran and Kamalpreet Kaur have always been a guiding light in my life. I hope, they shall always continue to be my torchbearers and inbspire me towards new goals in this life.

Some people come into your life as strangers, but very quickly that become an eternal part of it, as if they were always there. This tribute is to thank my dearest brother-in-laws, Jaswinder Singh, Mandeep Singh and Parminder Singh, who were always there for me, as friends, guides and elders, to share their experiences and guide me through this journey.

At the end, I thank the Almighty, for giving me his blessing throughout my research work and providing me strength enough to finish this task.

ABSTRACT

In the modern world, there are severe constraints on building space. The skyrocketing prices of land and construction equipments have fuelled the movement of the construction industry towards high-rise buildings. There is also a need for more space for thoroughfare, which has led to the need for smaller cross-sectional sizes in columns. These new demands have researchers to innovate and develop new construction methods to satisfy these requirements.

Concrete Filled Steel Tubular Columns (CFT) have slowly begun to emerge as an alternative to the traditional construction practices. Over the last two decades, CFT columns have been used in many tall structures and bridges all over the world. These columns are constructed by filling the hollow volume of steel tubes with concrete. A composite section such as CFT provides the advantages of both its constituents. Concrete imparts Compressive strength and stiffness while steel tube improves the tensile strength and ductility. The composite action between steel tube and concrete affords many other benefits like improved seismic resistance and reduction in member sizes.

The present study investigates the behaviour of different types of Concrete Filled Steel Tubular Columns. Three different core configurations, namely concrete filled single steel tube (CFST), Concrete filled Double steel tube (CFDST) and Reinforced Concrete filled steel tube (RCC-CFST) of such columns were investigated. The Double Skin consisted of a hollow steel tube (of smaller diameter) inside an outer steel tube. The annulus between the two tubes was filled with concrete. The RCC-CFST specimens were designed by redistribution of total area of steel. This was achieved by replacing a steel tube of higher wall thickness with a steel tube of lower wall thickness. The difference in area of steel between the two cross-sections was supplied by traditional longitudinal reinforcement. This allowed the author to investigate the difference in behavior of tubular columns having same area of steel but different core configurations, i.e. CFST and RCC-CFST.

A total of 81 experimental specimens were tested in this work. Three different cross-sectional shapes which include circular, square and rectangular were used for every core configuration. Lengths, thicknesses and cross-sectional dimensions were also varied for individual specimens of each shape. Structural response of different cross-sectional shapes was studied and the results of all tested specimens were compared. The variations in load carrying capacity, mode of deformation and ductility with respect to core configuration, cross-sectional shape, thickness of steel tubes and length of the specimens were investigated and reported.

The strength of the specimens obtained from experimental investigations was compared with the nominal load capacity obtained by direct summation of plastic strengths of the constituent materials. Increase in strength (over the nominal capacity) was reported for all tested specimens. The peak enhancement in strength of circular specimens was observed in RCC-CFST specimens, whereas the CFST single skin specimens showed the maximum enhancement in square and rectangular columns.

The primary mode of deformation of the composite column was observed as the local buckling of steel tube accompanied by the crushing of concrete core. Breakage of bond was observed between steel and concrete at location of local buckling, leading to loss of confinement. Local buckling of circular specimens was initiated by yielding of steel tube followed by crushing of adjoining concrete core near the mid height in general and extended to the ends of the specimens

From the experimental studies on ductility, it was concluded that the circular specimens showed predominantly strain hardening behaviour, while the square and rectangular specimens showed strain softening characteristics. The maximum ductility in circular specimens was observed in CFST specimens. On the other hand, RCC-CFST columns showed higher ductility in square and rectangular columns.

The experimental investigations on effect of increase in length of specimens showed that strength and ductility decrease with increase in length of specimens. The decrease in ductility was more in samples with higher thickness of steel tube.

The experimental studies on the redistribution of area of steel using longitudnal reinforcing bars as compensation for steel tube showed encouraging results for circular specimens. It was noted that for the circular specimens, it was feasible to replace a tube of higher thickness with a tube of lower thickness (and rebars) while maintaining the strength and ductility. However, loss of ductile behaviour and strength was reported in RCC-CFST square and rectangular specimens.

Eight International Codes were used to evaluate the theoretical axial load capacities of tested specimens. The results showed that Canadian Code (S016) and Chinese Code (CECS) give the best estimate for strength of circular specimens. On the other hand, Chinese Codes GJB and CECS gave the closest approximations for square and rectangular columns respectively.

Numerical simulations were performed for all the tested specimens. Three-dimensional nonlinear finite element models were prepared for all the specimens in the commercial FE software ABAQUS 6.8. The details of the modeling procedure and simulation of contact behaviour between steel and concrete are explained in detail. The numerical models were validated with fifty-four single skin specimens (circular, square and rectangular) selected from the literature. The proposed numerical model was then successfully extended to simulation of Double Skin and Reinforced CFST columns of different cross-sectional shapes and lengths.

A new concept of study of confinement pressure was introduced for the circular CFST specimens. Using the results from numerical simulation, an attempt was made to calculate the lateral confining pressure for circular specimens using ABAQUS. The numerically obtained values pressure were then compared with value of lateral confining calculated using theoretical material model from literature. It was seen that the confining pressure for short columns from numerical simulations matched well with the corresponding values from theoretical model. However, the theoretical model was found to overestimate the confinement pressure for composite columns of higher lengths.

At the end, an attempt was also made to calculate the strains induced during the actual experimental process, using a new technique known as Digital Image Correlation (DIC). A typical circular specimen was tested and analyzed using this process. The experimental strains were compared with strain values for the same from ABAQUS at specific locations. It was noticed that the values from numerical simulations agreed acceptably with the experimental (DIC) values.

TABLE OF CONTENTS

CHAPTER THREE

EXPERIMENTAL PROGRAM

CHAPTER FOUR

NUMERICAL SIMULATIONS - THEORY AND MODELLING

CHAPTER FIVE

COLUMNSWITH CIRCULAR CROSS-SECTIONS

CHAPTER SIX

COLUMNSWITH SQUARE CROSS-SECTIONS

CHAPTER SEVEN

SPECIMENS.WITH RECTANGULAR CROSS-SECTIONS

CHAPTER EIGHT

CONCLUSIONS

LIST OF SYMBOLS

A_c	Cross-sectional area of concrete core
A_s	Cross-sectional area of steel tube
A_{se}	Effective cross-sectional area of square steel tube calculated based on D_e
A_{sc}	Equivalent area of composite section
A_{si}	Cross-sectional area of inner steel tube
A_{so}	Cross-sectional area of outer steel tube
AE_{eff}	Effective axial stiffness of composite section
A_r	Area of reinforcement bars
A_g	Gross area of composite section
B	Width of rectangular section (smaller dimension)
B_o	Width of rectangular section (smaller dimension) of outer tube
B_i	Width of rectangular section (smaller dimension) of inner tube
CI	Confinement index
D	Outer diameter of circular steel tube, width of square section tube, greater Dimension of rectangular tube
D_c	Diameter of concrete core in circular columns
D_o	Outer diameter of outer steel tube
D_i	Inner diameter of inner steel tube
D_e	Effective width of steel plate in box CFST
DI	Ductility index
E_c	Modulus of elasticity of unconfined concrete

E_{cc}	Modulus of elasticity of confined concrete
E_{cm}	Secant modulus of elasticity for structural concrete according to Euro Code
E_{ct}	Tangent modulus of elasticity of concrete
E_s	Modulus of elasticity of steel tube
E_{st}	Tangent modulus of elasticity of steel tube
EI_{eff}	Flexural stiffness of composite section
E_r	Modulus of elasticity of reinforcement bars
f	Coefficient of friction between CFST specimen and machine end platens
FA	Fine aggregate
f'_c	Uniaxial unconfined compressive strength of concrete cylinder
f_{cm}	Mean compressive strength of concrete core
f_{crs}	Critical buckling stress of steel column
f_{crc}	Critical buckling stress of concrete column
f'_{cu}	Uniaxial unconfined compressive stress of concrete cube
f'_{cc}	Uniaxial confined compressive strength of concrete
f_{ck}	Characteristics compressive strength of concrete
f_{ct}	Tensile strength of concrete
f_{cp}	Numerically obtained value of lateral confining pressure at displacement corresponding to peak load carrying capacity
f_l	Lateral (radial) stress in mortar core
f_h	Hoop stress developed in steel tube
f_y	Nominal yield stress of steel tube

f_{yi}	Yield stress of inner steel tube
f_{yo}	Yield stress of outer steel tube
f_{sl}	Longitudinal stress in the steel tube at failure
f_{scy}	Equivalent stress of composite section
f_{bl}	Local buckling strength
f_u	Uniaxial residual ultimate strength of confined concrete
f_{yt}	Yield stress of steel tube in tension
f_{yc}	Yield stress of steel tube in compression
f_{yr}	Yield stress of reinforcement bars
I_s	Moment of inertia of steel
I_c	Moment of inertia of concrete
I_g	Moment of inertia of composite section
I_r	Moment of inertia of reinforcement bars
k_1	Empirical confinement factor for calculating the confined concrete strength
k_2	Empirical confinement factor for calculating the strain corresponding to Confined concrete strength
k_3	Material degradation parameter for confined concrete
L	Length of the column
L_e	Effective buckling length of column
Mu	Coefficient of friction between steel tube and concrete core in a CFST specimen
P_{cr}	Critical buckling load of CFST
P_{crc}	Critical buckling load of concrete column

P_{crs}	Critical buckling load of steel column
P_{uc}	Ultimate axial load of concrete column
P_{us}	Ultimate axial load of steel column
P_{5y}	Axial load corresponding to five times the yield strain,
P_y	Axial yield load
P_s	Load carried by steel tube (steel contribution)
P_c	Load carried by concrete core (concrete contribution)
P_n	Nominal cross-sectional capacity of CFST column
P_e	Euler buckling load of CFST column
P_{es}	Euler buckling load of steel column
r_c	Radius of gyration of concrete core
r_s	Radius of gyration of steel tube
R1	Parameter for effective width ratio
R	Ratio relation
R_E	Modular ratio
R_σ	Stress ratio
R_ε	Strain ratio
t	Wall thickness of steel tube
t_o	Wall thickness of outer steel tube
t_i	Wall thickness of inner steel tube
ν_c	Poisson's ratio of concrete

ν'_e	Empirical parameter
ν_s	Poisson's ratio of steel
$\nu_{s\,max}$	Maximum Poisson's ratio of empty steel tube
ν_{CFST}	Poisson's ratio of Concrete Filled steel tube
ε	Axial strain
ε_c	Axial strain in unconfined concrete
ε_{cc}	Axial strain of confined concrete
ε'_c	Strain corresponding to maximum stress in unconfined concrete
ε'_{cc}	Strain corresponding to maximum stress in confined concrete
ε'_u	Strain corresponding to the point of ultimate strength of confined concrete, f_u.
ε_u	Strain corresponding to ultimate axial load
$\emptyset$	Strength reduction factor
$\emptyset_c$	Nominal resistance factor for concrete in Canadian Code
$\emptyset_s$	Nominal resistance factor for steel in Canadian Code
Δ	Displacement at any particular point
Δ_u	Displacement corresponding to ultimate axial load
Δ_y	Displacement corresponding to yield load
λ_{cs}	Cross-sectional slenderness
ε_p	Axial strain corresponding to the ultimate load
$\varepsilon_{85\%}$	Axial strain when the load falls to 85% of the ultimate load
γ_s	strength reduction factor for steel tube

γ_c	Strength reduction factor for concrete core
λ_c	slenderness parameter of concrete column
λ_c'	Relative slenderness parameter of concrete column
λ_s	Slenderness parameter of steel column
λ_s'	Relative slenderness parameter of steel column
λ_m	Maximum cross-sectional slenderness permitted to be used according to AISC code
λ_r	Maximum cross-sectional slenderness permitted to be classified as non-compact section according to AISC code
λ_p	Maximum cross-sectional slenderness permitted to be classified as a compact section according to AISC code
$\bar{\lambda}$	Relative slenderness parameter
$\bar{\lambda}_c$	Relative slenderness parameter of concrete column
$\bar{\lambda}_s$	Relative slenderness parameter of steel column
η_c	Confinement parameter for concrete core according to Euro Code 4
η_s	Confinement parameter for steel according to Euro Code 4
α	Imperfection factor
ξ	Confinement factor
χ	Reduction factor for ultimate capacity according to Euro Code 4

LIST OF FIGURES

LIST OF TABLES

CHAPTER ONE

INTRODUCTION

1.1. GENERAL

Advances in construction materials and technologies go hand in hand with infrastructure development. Many years ago, steel and RCC framed structures replaced masonry structures as multi-storeyed buildings became more common. New types of concrete, namely high performance and high strength concrete were developed to improve the strength and performance of reinforced concrete construction as compared to steel structures. Further research has resulted in the advent of two new types of steel-concrete composite sections, first being a concrete section with rolled steel sections embedded inside and the second a hollow steel tube filled with concrete.

1.2 COMPOSITE STRUCTURES

The use of steel tubular members has gained prominence in civil engineering constructions in the last few decades. However, local and global instability do not allow the steel tubular members to realize their full plastic cross-sectional capacity. One of the possible ways to improve the stability of the tubular members is to fill the hollow tube with materials like concrete. A composite section made of these two materials combines the benefits of both the materials. The concrete provides compressive strength and stiffness while steel gives tensile strength and ductility. Further, better performance against imposed loads due to wind and earthquakes make these sections attractive for use as composite columns in high-rise buildings. Such members generally need a smaller cross-sectional size than corresponding RC columns, thereby also satisfying the requirements of more flexibility in floor area.

Two types of composite columns are being commonly used in the framed structures (Shanmugam and Lakshmi, 2001); composite members in which the steel sections are enclosed in concrete (Figure 1.1 (a), referred to as Steel Reinforced Concrete (SRC)) and hollow steel tubes filled with concrete, better known as Concrete Filled Steel Tube (CFST; Figure 1.1 (b)).

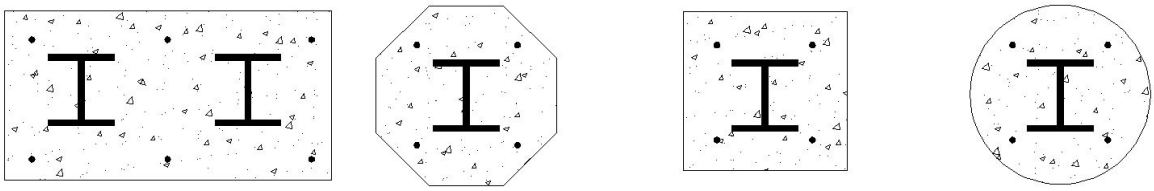

(a) Steel Reinforced Concrete (SRC) column cross-sections

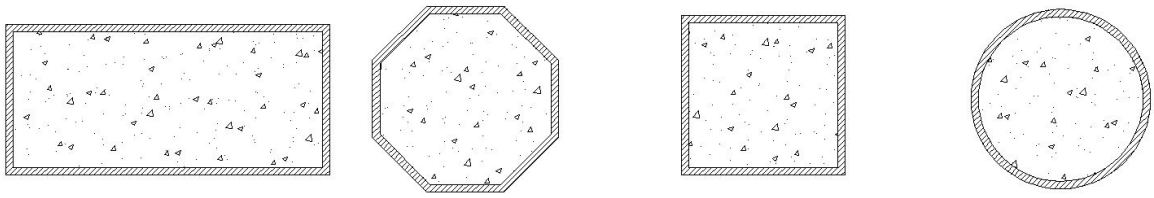

(b) Concrete Filled Steel Tubular (CFST) column cross-sections

Figure 1.1 Common cross-sections for composite columns

SRC columns consist of external concrete, longitudinal reinforcing bars, ties to restrain these bars and an embedded steel section. These composite columns are widely employed in construction of seismic resistant structures. The outer concrete section is susceptible to cracking under heavy flexural loads imposed by earthquake action. This may reduce overall section stiffness. However, steel core carries the additional lateral shear forces and improves the ductile response of the composite members. (Shams and Saadeghvaziri, 1997).

CFST columns are composed of concrete filled inside an empty steel tube. The interaction between steel tube and concrete core makes the CFST column system a cost effective and efficient member in structural applications. Hence, CFST columns are being successfully used around the world in bridge piers, bridge girders, high-rise buildings and arch bridges. Moreover, CFST columns also allow some unique “architectural expressions”, since they can be constructed easily (Baidya et al., 2012).

1.3 APPLICATIONS OF CFST

In general, peripheral columns in high-rise buildings experience higher stresses as compared to internal core columns and walls. Owing to their higher load resistance, CFST columns have been used as external columns in many tall buildings all around the world (Baidya et al., 2012). Some of these are summarized below:

Name of the Building	Location	No. of Storeys/ Building Height	Compressive strength of Concrete (MPa)	Special Features, if any	Reference
International Labor Organization	Geneva	NA	NA	NA	Shams and Saadeghvaziri, 1997
Casselden Place	Melbourne	43 storey	80	NA	Shams and Saadeghvaziri, 1997
Two Union Square	Seattle	57 storey	130	NA	Shams and Saadeghvaziri, 1997
Commerzbank	Frankfurt	63 storey/ 300 m high	NA	Triangular CFST columns	Uy, 1998-a
Shimizu high-rise building	Tokyo	550 m high	NA	Circular CFST columns	Uy, 1998-a
Queensbury House	London	6 storey	NA	Double Skin (tube in tube	Hicks et al., 2002

A few other applications of CFST are given below:

- External CFST columns have been provided on each longitudinal face of the building inside **Fleet Place House, London** (8-storey high) office block. The building has clear spans on the inside (Hicks et al., 2002).

- **Peckham Library, London** uses slender CFST columns to give a striking appearance (Hicks et al., 2002).

- **Maupre Valley Viaduct, Charolles**, France is a seven span viaduct with a total span of 324 meters and individual spans of upto 53.5 metres long. Inclined corrugated webs form a triangular section with the concrete deck, and connect to a 610mm steel tube at their lower edge. The tube is filled with concrete to improve stability of the tube and help distribute the support reactions (Fichier: Diapos ESDEP Anglais, Slides and Commentary).

- **Sainsbury's, Camden Town, London,** is a 43 m wide shopping mall spanned by curved steel towers at 7.2 metres centre to centre, which are further supported on T-shaped towers. The towers consist of tubular steel columns filled with concrete (Fichier: Diapos ESDEP Anglais, Slides and Commentary).

- **Banque Nationale de Paris, France,** has 12 A-shaped frames, 4 on each side, supporting girders over a span of 20 m. The A-frames consist of I-section filled with concrete (Fichier: Diapos ESDEP Anglais, Slides and Commentary)**.**

- **Bank of China, Hong Kong,** is a 369 m high building, with different plan form at different levels. The whole structure is supported by just 4 large corner columns of composite construction connected together by giant diagonals in the form of concrete filled steel box members (Fichier: Diapos ESDEP Anglais, Slides and Commentary).

- Hundreds of **Arch Bridges** of different spans and types in **China** use CFST columns (Chen and Wang, 2009).

Figure 1.2 shows the photographs of some of the structures discussed above.

International Labor Organization, Geneva

Two Union Square, Seattle

Commerzbank, Frankfurt

Casselden Place, Melbourne

Shimizu high-rise Building, Tokyo

Queensbury House, London

Maupre Valley Viaduct, Charolles, France

Sainsbury, Camden Tower, London

Bank of China, Hong Kong

Figure 1.2 Constructed Structures for CFST members from different countries

1.4 BENEFITS OF CFST COLUMNS

The composite action between steel tube and concrete core is the key to the enhanced properties of CFST columns as compared to equivalent reinforced concrete columns, steel columns and SRC columns (Gourley et al., 2008; Shams and Saadeghvaziri, 1997).

Structural benefits of CFST

Due to interaction between steel and concrete, CFST offers combined structural advantages of steel and concrete.

The presence of steel in the cross-section of CFST member gives many distinct advantages:

- Steel confines the concrete core which significantly increases the tensile strength and bending resistance due to higher section modulus of the section since the steel is now placed at the periphery (farthest from the centre). The confinement also enhances the compressive strength, corresponding strain and ductility of the concrete core.
- Steel tube helps to mitigate the large brittleness inherent in high strength concrete, when such concrete is used as infill for CFST.
- Since the elastic modulus of steel is approximately 8-10 times that of concrete, the presence of steel tube improves the stiffness of CFST member

Filling core of the CFST member with concrete also gives many benefits:

- Concrete core stops the inward buckling and delays the local buckling of steel tube. This allows the steel tube to withstand substantially larger deformation relative to that of hollow section.
- Concrete adds axial and flexural stiffness to the steel tube so that the axial and flexural strength are enhanced without increasing the outer dimensions of the columns.
- Since the steel tube acts as an outer cover, drying shrinkage and creep of concrete are considerably reduced as compared to ordinary reinforced concrete.

Economic benefits of CFST

- As compared to steel columns, the composite sections may require thinner steel sections without local buckling because the concrete core would force all buckling modes outward. (Uy, 1998-b).
- The need for transverse reinforcement in the form of ties or spirals is eliminated as compared with reinforced concrete columns.
- It is possible to erect the steel tube columns for many stories as the erection process is independent of concrete curing time. This allows for speedy construction process
- Since the steel tube acts as formwork for the infill concrete, considerable savings in construction materials can be obtained. Thus cost of formworks and the cost of labor charges for formworks shall be saved.
- Higher load carrying capacity due to the confinement effect results in smaller cross-sectional sizes, thus allowing more usable floor area, especially with circular CFST.

1.5 OBJECTIVE AND SCOPE OF THE PRESENT STUDY

The present research work primarily intends to study, explore and compare the behavior of CFST columns for different geometries, dimensions and core configurations. It has been observed that there is a distinct lack of studies on CFDST and RCC-CFST columns. Further, the effect of slenderness ratio on the response of CFST columns of different core configurations is an area completely untouched by researchers. The major objectives of this study are thus three-fold:

1. To generate a database of experimental results for CFST columns of various core configurations, such as Double skin CFST (CFDST) and Reinforced Concrete CFST (RCC-CFST). The effect of slenderness ratio, diameter (or width) – to - thickness ratio and cross-sectional shapes on such columns has also been studied.

2. To prepare a numerical model capable of representing the elastic and post-peak behavior of above mentioned CFST columns. For this purpose, a three dimensional nonlinear finite element model has been proposed using ABAQUS (ABAQUS 6.8, 2008) and validated with results from literature. The model has then been used to simulate and verify the response of experimentally tested specimens.

3. To study the variation of lateral confining pressure provided by steel to concrete across the height of the compression specimen. The existing models assume a constant confinement pressure for CFST columns irrespective of column length or core configuration. The numerical model proposed in point 2 has been used to obtain and study the changes in confining pressure along the sample length as well as with respect to slenderness ratio and core configurations.

1.6 METHODOLOGY OF THE STUDY

In the present research work, experimental and numerical studies have been performed for understanding the concrete filled steel tube columns. In these investigations, steel tubes of different geometries and cross-sections filled with normal strength concrete have been utilized. Three different cross-sectional shapes are investigated:

- Circular cross-section columns
- Square cross-section columns
- Rectangular cross-section columns

Three different core configurations are considered for each cross-sectional shape:

- Concrete filled steel tube (CFST)
- Concrete filled double steel tube (CFDST)
- Reinforced concrete filled steel tube (RCC-CFST)

Cross-sectional dimensions, thicknesses and length of tubes are also varied for every cross-sectional shape and core configuration.

1.7 ORGANIZATION OF THE THESIS

The thesis is presented in a planned sequence for easy understanding. The topics are presented in eight chapters:

Chapter One gives a brief idea about the composite members, their applications and advantages. A brief idea of the objective and methodology of the research work is also given.

Chapter Two covers detailed review of the available literature concerning concrete filled steel tubular (CFST) columns of various geometries and dimensions.

Chapter Three describes the details of experimental programs and material properties. Different testing procedures and data collection methods are also explained.

Chapter Four explains the Finite Element model used for modeling CFST columns with different cross-sections. The chapter also provides validation of the proposed model with wide range of experimental results chosen from available literature.

Chapter Five describes the results of experimental and numerical investigations on CFST specimens having circular cross-sections and three different core configurations (CFST, RCC-CFST and CFDST). The experimental results are further compared with recommendations for calculation of load carrying capacity using eight International codes. This chapter also presents a numerical study on the confinement pressure provided by steel tube to the concrete core. A new technique called Digital Image Correlation to estimate the strain distribution of the CFT during actual experimental test has also been discussed briefly.

Chapter Six covers the results of experimental and numerical investigations on CFST specimens having square cross-sections and three different core configurations (CFST, RCC-CFST and CFDST). The experimental results are further compared with recommendations for calculation of load carrying capacity using seven International codes.

Chapter Seven presents the results of experimental and numerical investigations on CFST specimens having rectangular cross-sections and three different core configurations (CFST, RCC-CFST and CFDST). The experimental results are further compared with

recommendations for calculation of load carrying capacity using seven International codes.

Chapter Eight shows a comparison of experimental and numerical results of all CFST columns illustrated in Chapters Five, Six and Seven. This chapter presents the major conclusions drawn from this thesis. Finally, the major contributions of these investigations and scope for future are also covered.

CHAPTER TWO

REVIEW OF LITERATURE

2.1 GENERAL

Space constraints and high cost of land have fuelled the movement towards high rise multi-storied construction in past few years. Most commercial structures nowadays demand higher floor area, which implies the need for smaller column size. This has resulted in intensive research efforts to improve the strength and performance of concrete as a construction material (Natarajan and Srividya, 2005); it is still being conducted in various parts of the world (Jaafar et al., 2002; Sofi et al., 2007; Alhozaimy et al., 2012-b; Laskar and Talukdar, 2008-a; Laskar and Talukdar, 2008-b; Laskar and Talukdar, 2008-c).Efforts are also being made to make the process of making concrete more eco-friendly(Wu et al., 2010; Raman et al., 2011; Ramesh et al., 2012) by replacing cement with supplementary cementitious materials (Natarajan, 2005; Ramesh et al., 2010; Ramesh et al., 2012; Alhozaimy et al., 2012-a), with recycled concrete being the frontrunner in this field (Yang et al., 2006; Yang et al., 2008)

Research on behavior of RC and steel structures is also going on continuously. While some of the researchers carried out studies on full scale structural systems (Balendra, 1983; Menon and Reddy, 1998; Menon, 2001; Thanoon et al., 2004-b; Rai and Prasad, 2005-a; Rai and Prasad, 2005-b; Rai et al., 2006; Gao et al., 2013), many others studied performance of isolated structural elements in detail (Thanoon et al., 2004-a; Revathi and Menon, 2005; Borsaikia et al., 2006; Natarajan and Shifana Fatima, 2007; Ganesh et al., 2010; Chakrabarti et al., 2012-a; Chakrabarti et al., 2012-b; Chakrabarti et al., 2013-a; Chakrabarti et al., 2013-b). Many investigations have also been performed for improving the seismic response of structures (Agrawal, 2003; Dasgupta et al., 2003; Agrawal and Chourasia, 2005).

The unique properties of CFST members have drawn the attention of many researchers during last few decades. As a result, their behavior has been investigated through experimental, numerical and analytical methods throughout the world. The first recorded use of CFST member as columns was in 1901. Steel tubes were filled with concrete to prevent corrosion of inner surface of tubes.

2.2 MECHANISM AND COMPOSITE ACTION

Gardner and Jacobson (1967) presented a detailed insight into the behaviour of short CFST columns. The authors explained the basic mechanism of failure of such columns. In the early stages of loading, Poisson's ratio of steel is greater than that of concrete. The steel tube thus expands radially outwards more than concrete; consequently, the steel tube does not restrain the concrete. Hence, the initial circumferential hoop stress developed in steel tube is compressive and the concrete is under lateral tension. As the load is increased, micro cracks start developing in concrete. The Poisson's ratio of the concrete core exceeds that of the steel. After this point, the steel tube restrains the concrete core and the hoop stress in steel tube become tensile. At this stage of loading, the concrete core and steel tube undergo triaxial state of stress and steel tube offers confinement to the concrete core. This reduces the yield stress of steel tube in the circumferential direction (hoop stress) and lowers the confining pressure on the concrete. Hence, there is a load transfer from steel tube to concrete core, because the steel tube cannot sustain the yield stress longitudinally in the presence of hoop tension (Gourley et al., 2008).

Gardner and Jacobson (1967) calculated the hoop stress developed in steel tube as:

$$f_h = \frac{D-2t}{2t} f_l \tag{2.1}$$

where f_h is tensile hoop stress generated in steel tube and D and t are outer diameter and thickness of steel tube, respectively.

Richart et al. (1928) found that longitudinal compressive strength of confined concrete increases in direct proportion to the lateral confining pressure. A formula was proposed for calculating the equivalent compressive strength of confined concrete:

$$f'_{cc} = f'_c + k_1 . f_l \tag{2.2}$$

where f'_{cc} is compressive strength of the confined concrete, and k_1 is an empirical confinement factor was determined experimentally to be about 4.1.

Gardner and Jacobson (1967) tested stub CFST columns in different loading conditions to study the effect of loading condition on the mechanism of failure. The specimens were tested in compression where (i) steel tube was loaded alone, (ii) concrete core was loaded alone and (iii)

both steel and concrete were loaded simultaneously. It was expected that for concrete core loaded specimens, steel tube does not carry any longitudinal stresses (as in case of spirally reinforced concrete columns). Thus, such loading condition of the composite column idealizes the use of the steel tube to provide confining pressure for the concrete core only. However, experimental results showed that longitudinal stress was also developed in steel tube. Such behaviour indicated that there was a bond between steel tube and concrete core. This bond induces a triaxial state of stress in steel tube which significantly reduces the yield stress. On the other hand, the load carrying capacity for the steel tube only loaded samples was quite close to that of hollow steel tube.

Furlong (1967) concluded on the basis of experimental study that steel tube and concrete core may carry the load separately till 90% of the load carrying capacity of the composite member. The author suggested that Poisson's ratio of plain concrete is lower than that of steel tube up to longitudinal strain of 0.001. Thus, it is expected that the lateral expansion of two materials may cause separation between the steel tube and concrete core. Micro cracking of concrete occurs at strain above 0.001. Poisson's ratio of the concrete core approaches that of steel and confinement may occur corresponding to strain 0.002.

Knowles and Park (1970) reported that the volume of concrete core decreases during initial loading stage. The decrease in volume was generally observed to occur until 95.4% of the peak load carrying capacity (on average) and a corresponding longitudinal strain of 0.002. Beyond this stage, the volume of the concrete core was found to increase, thereby resulting in confinement of concrete core from the steel tube.

Hatzigeorgiou (2008) proposed an empirical formula for calculating the hoop stress (f_h) as:

$$\frac{f_h}{f_y} = \exp\left[\ln\left(D/t\right) + \ln\left(f_y\right) - 11\right] \leq 1.0 \tag{2.3}$$

The author proposed separate formulae for calculating the yield stress of steel tube in tension (f_{yt}) and in compression (f_{yc}):

$$f_{yt} = 0.5\left(f_h + \sqrt{4{f_y}^2 - 3{f_h}^2}\right) \tag{2.4}$$

$$f_{yc} = 0.5\left(f_h - \sqrt{4{f_y}^2 - 3{f_h}^2}\right) \quad (2.5)$$

2.3 STIFFNESS

Furlong (1967) studied experimentally the axial and flexural stiffness of circular and square CFST columns and beam columns. Neglecting bond between steel tube and concrete core, the author suggested the following formulas:

$$AE_{eff} = A_c E_c + A_s E_s \quad (2.6)$$

$$E I_{eff} = E_c I_c + E_s I_s \quad (2.7)$$

Where AE_{eff} and EI_{eff} are effective axial and flexural stiffness of composite section, respectively, E_c and E_s are modulus of elasticity of concrete and steel, respectively. For predicting the critical buckling load of long columns, radius of gyration (r) of the composite section was proposed as:

$$r = \sqrt{\frac{E_c I_c + E_s I_s}{A_c E_c + A_s E_s}} \quad (2.8)$$

Based on the experimental results of Huang et al. (2002), the authors calculated the stiffness of composite section to identify the composite action. The slope of the initial part of the axial load-axial strain curve for experimental data with the strain between 0.05% and 0.1% calculated by linear regression was defined as the sliffness of composite section. The measured values were compared with calculated values using formula proposed by Furlong (1967). The results showed that the formula proposed by Furlong (1967) overestimates the stiffness particularly for square specimens.

2.4 LOAD CARRYING CAPACITY

Gardner and Jacobson (1967) performed experimental studies which showed that load carrying capacity of CFST columns was higher than the nominal load carrying capacity calculated by simply adding the strengths of steel tube and concrete core acting individually. The authors proposed an equation for predicting the load carrying capacity of short CFST specimens:

$$P_u = A_c f'_c + \frac{k_1}{2} A_s f_h + A_s f_{sl} \quad (2.9)$$

where, P_u is ultimate load carrying capacity, A_c, A_s are area of concrete core and steel tube, respectively, f'_c is compressive strength of unconfined concrete and f_{sl} is longitudinal stress in steel tube. The authors also reported that for short specimens, f_h and f_{sl} may be considered equal to yield stress of steel tube. The confinement parameter (k_1) was considered as 4 in this study.

For long CFST columns, the authors proposed the following for predicting the critical buckling load (P_{cr}) of such columns using tangent modulus of elasticity:

$$P_{cr} = \pi^2\left(\frac{E_{st}\, I_s + E_{ct}\, I_c}{L_e^2}\right) \tag{2.10}$$

where E_{st} and E_{ct} are tangent modulus of elasticity of steel and concrete, respectively, I_s and I_c are moment of inertia of steel and concrete, respectively and L_e is the effective buckling length of specimen. E_{st} was obtained from tension tests, while the concrete properties were found by using a stub column test.

Neogi et al. (1969) reported that the failure load of CFST specimens was greater than the sum of compressive strength of the steel tube and concrete core. The authors further suggested that shear failure in CFST may occur due to triaxial stress state of steel tube before the load transfer from steel tube to concrete core is complete. Thus in some cases, the load capacity may actually decrease.

A model based on tangent modulus theory was proposed by Knowles and Park (1970) for predicting the load carrying capacity of long CFST specimens. The ultimate load of CFST was calculated as the simple algebraic summation of the tangent modulus loads for the steel tube and the concrete core acting as independent columns. The design equation was compared against the experimental results presented by Knowles and Park (1969). It was observed that the results of the proposed equation were in good agreement with experimental results for the square specimens, but significantly lesser than their experimental counterparts for circular CFST columns. Hence, the authors concluded that as chance for triaxial stress state may happen for concrete core, the concrete strength may also increase correspondingly.

Johansson (2002) experimentally investigated the change in strength and ductility of short circular CFST columns subjected to axial compression. Two loading conditions, namely (i) entire section loaded and (ii) concrete core only loaded were investigated for CFST columns having same outer

diameter but increasing wall thickness. The efficiency of confinement was evaluated by two parameters; confinement index (CI) and ductility index (DI). Confinement index was defined as:

$$CI = \frac{A_s f_y}{A_c f_c'} \tag{2.11}$$

Ductility index was defined as the ratio between axial load corresponding to five times the yield strain ($P_{5\varepsilon_y}$) divided by the axial yield load (P_y):

$$DI = \frac{P_{5\varepsilon_y}}{P_y} \tag{2.12}$$

Based on DI values, the post-yield behaviour of CFST columns was classified into three groups; strain softening characteristics, elastic-perfectly-plastic characteristics, and strain hardening characteristics. The experimental results showed that specimens having confinement index lesser than one were generally accompanied by a strain softening behaviour due to shear plane failure. In case of specimens having confinement index more than one, a plastic or strain hardening behaviour was observed due to crushing failure of concrete. The experimental results also showed that the condition of loading (entire section loaded or concrete core only loaded) does not significantly change the shape of the load-displacement curves. However, since steel contributed in carrying the applied load from the very outset in entire section loaded columns, the author reported that the initial stiffness of the composite columns slightly increased when both steel and concrete were loaded. The author also reported that the CFST filled with high strength concrete need a thicker steel tube to achieve the same ductility as a CFST filled with normal strength concrete.

An experimental and analytical study was conducted by Huang et al. (2002) to study the response of stiffened and unstiffened circular and square CFST columns in axial compression. Steel tubes having D/t ratio from 40 to 150 were tested in this study. The higher ratios were chosen to study the difference in behaviour of thin and thick tubes filled with concrete. The results showed that the steel tube enhances the load carrying capacity and ductility of specimens. Elastic-perfectly-plastic post-peak behaviour was observed as for circular specimens having D/t equal to 40. Strain softening behaviour was noted for the remaining columns.

Giakoumelis and Lam (2004) investigated the effect of grade of concrete and wall thickness of steel tube on the load carrying capacity of short circular CFST columns. The specimens were filled

with three grades of concrete viz. 30, 60, and 100 MPa. The tested specimens were short columns with L/D = 2.61 and 2.62 to eliminate the effect of slenderness. Yield stress of steel was obtained by testing hollow steel tube samples in axial compression. The experimental results showed that columns filled with normal strength concrete reached the ultimate load with large shortening. On the other hand, columns filled with high strength concrete reached the peak load with small axial shortening (≈ 3 mm).

Gupta et al. (2007) conducted an experimental and computational study to investigate the behaviour of fly ash based concrete filled in circular steel tube columns under axial load. Fly ash was added as three different compositions of 15%, 20%, and 25% of cementitious material. The results showed that as D/t ratio increases, load carrying capacity of CFST columns decreases. Further, the load carrying capacity also reduced with increase in specimen length, as expected.

The compressive strength of confined concrete (f'_{cc}) was calculated in the analytical study conducted by Liang and Fragomeni (2009) as:

$$f'_{cc} = \gamma_c f'_c + 4.1 f_l \tag{2.13}$$

where f'_c is strength reduction factor that accounts for effects of the column size, the quality of concrete, and loading rate on the unconfined concrete compressive strength and is calculated as:

$$\gamma_c = 1.85 D_c^{-0.135} \qquad (0.85 \leq \gamma_c \leq 1.0) \tag{2.14}$$

where D_c is diameter of concrete core. Confining pressure (f_l) was calculated as:

$$f_l = 0.7\,(\nu_{CFST} - \nu_{s\,max})\frac{2t}{D-2t} f_y \qquad for \frac{D}{t} \leq 47 \tag{2.15 a}$$

$$f_l = 0.006241 - 0.0000357(D/t) \qquad for\ 47 \leq D/t \leq 150 \tag{2.15 b}$$

where ν_{CFST} is Poisson's ratio of composite CFST column and $\nu_{s\,max}$ is the maximum possible Poisson's ratio of empty steel tube and it was considered in this study as 0.5. The parameter ν_{CFST} was calculated using empirical formula:

$$\nu_{CFST} = 0.2312 + 0.3582\nu'_e - 0.1524\left(\frac{f'_c}{f_y}\right) + 4.843\,\nu'_e\left(\frac{f'_c}{f_y}\right) - 9.169\left(\frac{f'_c}{f_y}\right)^2 \tag{2.16}$$

where ν_e' is an empirical parameter calculated based on D/t ratio as:

$$\nu_e' = 0.881 \times 10^{-6} \left(\frac{D}{t}\right)^3 + 2.58 \times 10^{-4} \left(\frac{D}{t}\right)^2 + 1.953 \times 10^{-2} \left(\frac{D}{t}\right) + 0.4011 \quad (2.17)$$

An analytical model was also proposed in this study to calculate the axial strength of circular CFST columns. The proposed model was given as:

$$P_u = f'_{cc} A_c + \gamma_s f_y A_s \quad (2.18)$$

where γ_s is strength factor for the steel tube that accounts for the effect of horizontal tensile hoop stresses, strain hardening, geometric imperfection, and residual stresses, calculated as:

$$\gamma_s = 1.458 \left(\frac{D}{t}\right)^{-0.1} \qquad (0.9 \leq \gamma_s \leq 1.1) \quad (2.19)$$

Oliveira et al. (2009) experimentally investigated the load carrying capacity of CFST columns of different lengths filled with different grades of concrete. Steel tube of 114.3 mm outer diameter and 3.35 mm wall thickness were filled with four grades of concrete; C30 (f'_c= 30 MPa), C60 (f'_c= 60 MPa), C80 (f'_c= 80 MPa), and C100 (f'_c= 100 MPa). Four lengths of CFST columns with respect to to the outer diameter were tested in axial loading; L3D (L/D=3), L5D (L/D=5), L7D (L/D=7) and L10D (L/D=10). The experimental results showed that the mode of failure was a function of the L/D ratio and strength of concrete core. The columns having L3D failed predominantly in short column failure mode, i.e. by initial crushing of the concrete core and local buckling which was observed after reaching the yield stress of steel tube. The post-peak behaviour showed a significant increase in the cross-sectional dimensions without any major loss of load capacity for these specimens, even at large strains. The L5D CFST specimens failed by shear failure of the concrete core at an axial strain of about 0.004. Shear failure was also observed for columns having L7D filled with C80 and C100 concrete core. Significant loss of load capacity was observed after shear failure occurred. The specimens having L7D filled with C30 and C60 grades of concrete and L10D specimens filled with all grades of concrete showed Euler Buckling.

2.5 BOND STRENGTH

Furlong (1968) studied bond behaviour of CFST columns. Specimens were tested in pairs, i.e. one bonded normal CFST specimen (non-greased) was tested along with an Un-bonded specimen. The

un-bonded samples were prepared by using a coating of axle file grease between steel and concrete surfaces. The samples were tested under axial loading. The comparison of experimental results between un-bonded and bonded samples showed negligible difference between the two specimens. It was concluded that the contact pressure exerted by steel tube to concrete core is the only interaction between two materials and bond strength between steel tube and concrete core is negligible. Similar observations were reported for CFST specimens filled with normal strength concrete by Giakoumelis and Lam (2004). However, they observed that the bond between steel tube and concrete core affects the behavior of CFST specimens filled with high strength concrete.

Shakir-Khalil and Zeghiche (1989) carried out "Push-out bond-slip" tests to investigate the bond strength between steel tube and concrete core for rectangular CFST specimens. In the study, the CFST were loaded on concrete core only using a rigid steel plate until sliding occurred between steel and concrete. The load corresponding to the point of sliding was taken as failure load. The failure load was then divided by the surface area of contact between steel and concrete to determine the bond strength. The resulting bond strength varied in the range of 0.26-0.37 MPa. The authors reported that this bond strength was lower as compared to the bond strength between concrete and steel bars in reinforced concrete and as compared to bond strength between concrete and steel in circular CFST. Two reasons were proposed for this observation. First reason was that the effect of shrinkage of concrete in such columns would be opposed to its effect in the reinforced concrete. The second reason was that change in the shape of rectangular cross-section would have a less beneficial effect on the bond strength than in the case of circular cross-section.

2.6 CROSS-SECTIONAL SHAPE

Furlong (1967) observed that the effect of confinement by steel tube was more pronounced in circular cross-sections than in square cross-sections. This can be attributed to the fact that circular cross-sections develop uniform hoop stress all round the circumference to provide effective lateral confinement, while confinement in square sections is largely absent in the central part. However, thick square tubes with flat sides may relatively offer some confinement at the corners.

Shakir-Khalil and Zeghiche (1989) experimentally and numerically investigated the behaviour of axially and eccentrically loaded rectangular CFST columns. The tested specimens were full scale composite columns of about 3m length, representing a typical storey height in multi-storied structures. One column was loaded in axial loading condition; two columns each were loaded in

uniaxial bending about the major axis and minor axis; and two columns were loaded in biaxial bending. One short column having same configuration and filled with same concrete was also tested in order to determine the load carrying capacity of short CFST column. The load carrying capacity of hollow steel tube was also determined for each column by testing short hollow steel tubes. It was reported that the axially loaded short composite column failed by yielding of steel tube and crushing of concrete core. The long column behaved elastically whose response could be predicted by the Euler approach, where the initial effect of imperfection is neglected. All the full scale columns failed by Global buckling without any sign of local buckling. The experimental results were also compared with predicted results using British Standard (BS 5400, 2005). The codal results were in good agreement with experimental results.

Schneider (1998) experimentally and numerically investigated axially loaded circular, square, and rectangular CFST columns. The effect of cross-sectional shape and steel wall thickness on the ultimate load carrying capacity such composite columns was studied by testing fourteen specimens (three circular, five square and six rectangular cross-sections). The experimental load-displacement curves presented in this study showed that the circular tube shapes exhibited strain hardening behaviour in post yield stage of loading. Strain hardening behaviour was also observed for square and rectangular specimens having higher thicknesses. All the specimens showed local buckling after the yielding of composite columns only. Axial ductility at the point of observed local buckling was calculated as the ratio of axial displacement at that point to axial displacement corresponding to point of yield load. The ductility varied from 6 to 8 for all specimens with strain hardening behaviour. The corresponding value was 2 to 4 for samples with strain softening behaviour. A parameter named ductility index was proposed by the author as the ratio of axial displacement at ultimate axial load to yield load. It was observed that the ultimate load was reached at ductility index of about 2 for the specimens with strain softening and around 10 for specimens with strain hardening behaviour. The average ratio of axial to yield load was 1.07 for specimens with strain softening and 1.41 for specimens with strain hardening characteristics.

Uy (2000) experimentally tested thirty Box CFST columns under purely axial load as well as combined axial compression and flexural loads. The columns were fabricated using 3 mm nominal thickness steel plate. The experimental results showed a rapid decline in load carrying capacity after ultimate load in axially loaded specimens. The reduction in load was comparatively lower for columns subjected to combined loading. Moreover, the both steel and concrete loaded CFST

columns showed much more brittle post peak behaviour as compared to steel only loaded columns. The author reported that this reduction in ductility justifies the existing capacity reduction factor for Load and Resistance Factor Design (LRFD) philosophies adopted throughout the world. The author stated that the capacity reduction factor for steel columns have been typically calibrated for axial compression at 0.9, whereas those for reinforced concrete columns are much lower at 0.6. However, the author reported that the capacity reduction factor for composite columns with slender plates in this study was less than 0.9 and it might be used as a mixed capacity reduction factor for steel and reinforced concrete columns. Mode of failure was studied for column and beam column specimens. The experimental results showed that the failure in columns was primarily compression failure initiated by crushing of concrete followed by local buckling of steel plates

Based on the experimental results, the author proposed an analytical model for calculating the axial strength of box CFST columns using a concept of effective area of steel. This effective area of steel depends on a proposed effective width model calculated as:

$$\frac{D_e}{D} = 0.65\sqrt{\frac{f_{bl}}{f_y}} \tag{2.20}$$

where D_e is effective width of steel plate, D is actual width of steel plate and f_{bl} is local buckling strength calculated as:

$$f_{bl} = \frac{k\pi^2 E_s}{12(1-\nu_s^2)\left(\frac{D}{t}\right)^2} \tag{2.21}$$

in which, k is buckling coefficient is taken as 10.31 for CFST and 4 for hollow tube; ν is Poisson's ratio of steel. The capacity of axially loaded box CFST was proposed in this study as:

$$P_u = f_c A_c + f_y A_{se} \tag{2.22}$$

where A_{se} is effective area of four steel plates calculated using D_e.

Susantha et al. (2001) proposed a formula to calculate the maximum confining pressure in circular, box, and octagonal CFST columns. The change of the Poisson ratio of concrete (ν_c) and steel ($\nu_{s\,max}$) with loading stages of CFST column were investigated and correlated with the yield

strength of steel tube for calculating the hoop stress for circular CFST. The hoop stress was calculated as:

$$f_h = (\nu_{CFST} - \nu_{s\,max})\, f_y \tag{2.23}$$

where ν_{CFST} parameter was calculated as given in Equation 2.13 and $\nu_{s\,max}$ was taken as 0.5 as defined in Equation 2.13. The lateral confining pressure was calculated as:

$$f_l = \frac{2t}{D-2t} f_h \tag{2.24}$$

The compressive strength of confined concrete was calculated from the formula proposed by Richart et al. (1928) and using confining factor k_1 as 4.0:

$$f'_{cc} = f'_c + 4.0\, f_l \tag{2.25}$$

The authors proposed a formula for calculating the lateral confining pressure in box and octagonal CFST, based on results of selected specimens where the local buckling could be neglected. The proposed equations are:

$$f_l = -6.5R1\frac{(f'_c)^{1.46}}{f_y} + 0.12(f'_c)^{1.03} \quad \text{For box CFST columns} \tag{2.26}$$

$$f_l = -35R1\frac{(f'_c)^{1.35}}{f_y} + 0.22(f'_c)^{1.02} \quad \text{For octagonal CFST columns} \tag{2.27}$$

where parameter R1 represents the width of box or octagonal cross-sections and outer diameter of circular cross-sections to thickness ratio given as:

$$R1 = \frac{D}{2t}\frac{f_y}{E_s}\sqrt{3(1-\nu_s^2)} \quad \text{For circular CFST columns} \tag{2.28}$$

$$R1 = \frac{B}{t}\sqrt{\frac{12(1-\nu_s^2)}{4\pi^2}}\sqrt{\frac{f_y}{E_s}} \quad \text{For box and octagonal CFST columns} \tag{2.29}$$

The local buckling strength was calculated as:

$$\frac{f_{bl}}{f_y} = 0.8 + \frac{0.025}{R1^2} \leq 1.0 \quad \text{For circular CFST columns} \tag{2.30}$$

$$\frac{f_{bl}}{f_y} = \frac{1.2}{R1} - \frac{0.3}{R1^2} \leq 1.0 \qquad \text{For box and octagonal CFST columns} \qquad (2.31)$$

Rectangular and square CFST specimens were tested by Han (2002) to study the effect of cross-sectional shape and aspect ratio (ratio of the length of the longer side (D) to the length of the shorter side (B)) on the behaviour of these columns. The aspect ratios of the specimens were varied between 1 and 1.75. Two parameters viz. Confining index (CI) and ductility index (DI) were calculated as:

$$CI = \frac{A_s f_y}{A_c f_{ck}} \qquad (2.32)$$

$$DI = \frac{\varepsilon_{85\%}}{\varepsilon_u} \qquad (2.33)$$

where ε_u is axial strain corresponding to the peak load, and $\varepsilon_{85\%}$is axial strain when the load falls to 85% of the ultimate load in the descending portion of load-experimental curve.

It was reported based on experimental results that the increase in strength of the CFST was influenced by the cross-sectional aspect ratio, material properties, and confining index. The specimen ductility (DI) and confinement (CI) were seen to reduce with an increase in aspect ratio. The experimental load carrying capacity of the specimens was also compared with recommendations of AIJ (1997), EC4 (2004) and Chinese GJB 4142-2000 (2000) codes. The Chinese code was found to give best results for load capacity of stub CFST columns.

Bradford et al. (2002) performed an analytical study and gave the following equation for the elastic local buckling strength (f_{bl}) of circular CFST:

$$f_{bl} = \frac{2E_s}{(1-\nu_s^2)} \frac{1}{(D/t)} \qquad (2.34)$$

The authors noted that filling circular and rectangular hollow tubes filled with concrete show improved elastic local buckling strength, which is 1.73 and 2.67 times respectively that of unfilled tubes.

The cross-sectional slenderness (λ_{cs}) was calculated according to Australian Standard (AS 4100) as:

$$\lambda_{cs} = \left(\frac{D}{t}\right)\left(\frac{f_y}{250}\right) \quad (2.35)$$

It was also recommended that the circular CFST sections may be considered fully effective upto a cross-sectional slenderness value of 125 (instead of 100 as used previously).

Sakino et al. (2004) tested circular and square shaped CFST columns. One hundred fourteen short specimens were manufactured and tested under axial loading condition. Coupons were extracted from the steel plates before manufacturing of the tubes. Tensile tests were performed on these coupons to obtain the stress-strain behaviour of steel tube. The experimental results showed that the peak axial load was greater than the nominal squash load due to confinement in circular CFST specimens. The ultimate capacity observed was however, lower than the nominal squash load CFST specimens for the square specimens of highest D/t ratio. The authors also proposed a linear function (using regression) for the evaluation of difference in experimental load and nominal squash load.

Tan et al. (2013) tested Rectangular concrete columns confined with fiber reinforced polymer (FRP). The FRP was used to improve the poor confinement in rectangular columns with sectional aspect ratio more than 1.5. Based on the experimental results, the authors proposed a new type of "re-profiled" members for rectangular concrete columns which may also be applied to rectangular CFST columns. The re-profiled sections work by adding "semicircular segments" to the shorter sides of steel tubes to increase the confinement of such CFST sections.

2.7 CORE CONFIGURATIONS

2.7.1 General

Different core configurations can be used for construction of CFST columns. The different core configurations serve two major functions; the primary function is to improve the interaction (and hence, the composite action) between steel tube and concrete core. The second reason is to make easier the construction, erection, connection and loading of these columns. A popular new core configuration of CFST consists of stiffening structural members installed inside the steel tube. Various types of stiffeners may be used such as longitudinal stiffeners welded to the inner surface of steel tube (Huang et al., 2002; Abedi et al., 2008), Reinforced Concrete Filled Steel Tubular

(RCC-CFST) columns (Endo et al., 2000; Xiamuxi and Akira , 2012) and Concrete Filled Double Steel Tube (CFDST) columns (El chalakani et al., 2002; Zhao and Grzebieta, 2002).

2.7.2 Reinforced Concrete Filled Steel Tube (RCC-CFST)

Reinforced Concrete Filled Steel Tube (RCC-CFST) columns consist of longitudinal reinforcement provided in addition to the exterior steel tube. These composite members have been found to exhibit better resistance against brittle behaviour of CFST when used in large scale structures (Xiamuxi et al., 2011). They have also been used in zones of high seismic activity due to their higher ductility and improved energy absorption characteristics as compared to traditional CFST columns (Endo et al., 2000). The concrete core in RCC-CFST column is subjected to two different (but simultaneous) confining effects via the outer steel tube and the longitudinal reinforcement.

Very few studies have been performed on RCC-CFST columns due to their recent induction into the construction industry. Endo et al. (2000) performed an experimental study to study the response of RCC-CFST columns and beams and compare the results with normal CFST members. Two types of steel tubes were used; normal steel tubes and ribbed steel tubes. Three types of reinforcement cages were used, viz. i) RCC-CFST with thick concrete cover ii) RCC-CFST with thin concrete cover and iii) RCC-CFST with double reinforcement (i.e. inner longitudinal reinforcement in two concentric cages). Experimental results of column specimens showed higher load capacity and improved confinement in RCC-CFST relative to CFST. Further, specimens with double reinforcement reported best mechanical performance on various parameters like compressive strength, stiffness, and ductility. The cover thickness was found to have no effect on the performance of RCC-CFST, as specimens with both thick and thin cover to reinforcement showed similar behaviour.

Hasegawa and Xiamuxi (2011) tested thin wall steel tubes filled with high strength reinforced concrete. The experimental results of RCC-CFST were compared with those of CFST. The experimental load-displacement curves showed that the post-peak curve of RCC-CFST descends gradually and smoothly. Thus, the RCC-CFST specimens were found to have better energy absorption characteristics (due to larger area under the load-displacement curves) and ductile performance. On the other hand, traditional thin-walled CFST exhibited a rapid rate of descent of load capacity in post-peak response.

An experimental and analytical study was performed by Xiamuxi and Akira (2012) to investigate the mechanical behaviour of circular RCC-CFST columns. The specimens were tested in axial loading condition. The emphasis of the study was on understanding the variation in behaviour of composite columns at different reinforcement ratios. Finite Element analysis was also carried out using ADINA software and validated against experimental results. It was reported that the ultimate strength and ductility of the RCC-CFST were improved due to confining effect of reinforcement bars and steel tube. Further, the loss of load carrying capacity after the point of peak load was found to be negligible in the RCC-CFST columns.

2.7.3 Concrete Filled Double Steel Tube (CFDST)

Concrete Filled Double Steel Tube (CFDST) columns, also known as concrete filled double skin columns, are among one of the more commonly used CFST core configurations. CFDST columns are constructed from two concentric steel tubes with the hollow space between them filled with concrete. The major reason for using such members is to enhance the global and local stability compared to CFST, due to increase in the Moment of inertia in CFDST members (El chalakani et al., 2002). CFDST columns have been used successfully in liquid and gas retaining structures, blast resisting structures, tunnel constructions, and seismic retrofit. CFDST have recently also been used as high rise bridge piers and compression members in elevated expressways in Japan to reduce the structure weight while still maintaining a large energy absorption against seismic loading (Zhao and Grzebieta, 2002). CFDST provide many advantages over traditional CFST such as enhanced bending stiffness, increased section modulus, improved global and local stability, good energy absorption and damping characteristics, light weight. Their superior performance under cyclic and seismic loads also makes them an attractive candidate for use in seismic retrofitting (El chalakani et al., (2002); Zhao and Grzebieta (2002); Tao et al. (2004))

Ultimate strength and ductility of CFDST columns under cyclic loading were studied in the experimental study conducted by Nakanishi et al. (1999). The aim of this study was to develop a new design approach for bridge piers that can withstand serious damage and collapse against severe seismic action in Japan and still transfer less force to the foundations at the same time, since it is quite uneconomical to strengthen existing foundations. The outer steel tubes were manufactured as welded box cross-sections while the inner circular tubes were made of steel or plastic. Low grade concrete of compressive strength around 13 MPa was used to infill the space

between the inner and outer tubes. The experimental results illustrated that the composite columns having hollow steel inner tube at centre showed the best performance against cyclic loads.

El chalakani et al. (2002) performed experimental investigations on CFDST stub columns consisting of outer circular steel tube and inner square steel tube. High strength concrete having compressive strength about 64 MPa was used to fill the annulus between two tubes. The parameters monitored were ultimate strength, ductility and mode of deformation. The results showed that the CFDST columns maintained their load resistance without any significant loss of load carrying capacity even at very large deformations. First local buckles were observed to occur in the outer tube, generally in the bottom one third of the tube length.

Zhao and Grzebieta (2002) investigated the load carrying capacity of stub CFDST columns and moment capacity of CFDST beams. Cold formed square cross-sections were used for outer and inner steel tubes. The space between them was filled with concrete having compressive strength of 58.7 MPa. Hollow steel tubes were also tested in this study as reference specimens. An equation was proposed by the authors for calculating the ultimate load capacity of CFDST columns. The proposed model considered the reduced compressive strength of unconfined concrete as the compressive strength of concrete core (i.e. no confinement effect). The axial capacity obtained from the formula was observed to be in good agreement with the measured values. The mode of deformation of CFDST was defined as outward buckling only of the outer tube, while the inner tube was characterized by both inward and outward buckling.

The effect of hollow section ratio on the response of CFDST was studied in the experimental work conducted by Tao et al. (2004). The inner and outer tubes were of circular cross-section. The hollow space between the tubes was filled with concrete of compressive strength 47.4 MPa and 46.3 MPa. The mode of deformation of the samples was observed. While the outer tube failed by outward local buckling in all column specimens, failure mode of inner tube varied depending on the ratio of outer diameter of inner tube (D_i) to wall thickness of inner tube (t_i), D_i/t_i. The specimens having smaller D_i/t_i showed no local buckling. As the value of D_i/t_i, inward local buckling was observed for inner tube. Results of load compression curve were also compared depending on D_o/t_o (D_o and t_o are outer diameter and wall thickness of outer tube). It was observed that the ductility of the specimen was inversely related to D_o/t_o, i.e. samples with smaller D_o/t_o showed higher ductility and vice-versa.

Tao and Han (2006) experimentally investigated the behaviour of Rectangular CFDST specimens. A total of thirty specimens (i.e. three short columns, three beams, and twenty-four beam columns) were tested in this study. The failure modes and load-deformation behaviour of CFDST specimens were compared with those of CFST members and hollow tube samples. The results showed enhanced strength and ductility for CFDST columns, beams, and beam-columns relative to CFST and hollow tube specimens.

2.8 SLENDERNESS EFFECT

The effect of slenderness ratio on behaviour of axially loaded hollow steel tubes and CFST columns was studied by Knowles and Park (1969). Confining pressure provided by steel tube was studied for circular and square CFST columns having different slenderness ratios. The authors also tested short unconfined control concrete cylinders having approximately the same cross-sectional area of concrete cores. Experimental results of concrete cylinders showed that volume of concrete began to increase corresponding to longitudinal strain of around 0.002. Accordingly, the authors concluded that this increase in volume would cause the steel to provide a confining pressure and increase the strength of the concrete.

Tangent modulus of steel and concrete were also calculated from test results of short specimens of hollow steel tubes and concrete cylinders. All CFST columns tested with hinged ends failed by global buckling and no local buckling was observed. It was observed that the concrete failure occurred only after the peak load was reached in all the cases. Further, the load capacity calculated theoretically using the tangent modulus theory showed good agreement with experimental results for most of the specimens and was conservative for the remaining samples. The authors also reported that the specimens having slenderness ratio less than 44.3 would gain some strength due to confinement. Therefore, theoretical loads calculated using tangent modulus would be conservative. For some of circular short CFST specimens, the strength of unconfined concrete was enhanced to 1.69 times the strength of unconfined concrete for best matching with experimental CFST load values. However, there was little increase due to confinement for short square columns.

Experimental results of Oliveira et al. (2009) showed that the specimens having L/D ratio more than 7 generally showed global buckling prior to beginning of confinement. Such specimens exhibited insufficient radial strain for mobilizing the confinement effect. This may result in lesser enhancement in strength or reduced load carrying capacity.

2.9 NUMERICAL SIMULATIONS

Numerical simulations using Finite Element (FE) method have steadily gained popularity among the researchers as a means of studying complex physical phenomenon. It is an approximate method of analysis (Umar et al., 1994; Umar et al., 1996) and highly sensitive to mesh size and orientation (Umar et al., 1996). From study of simple parameters such as material properties (Partheepan et al., 2008) to complicated problems such as crack behaviour (Choubey et al., 2006) and joint failure (Sridevi and Agrawal, 1991), FE analysis is being used worldwide in solving diverse engineering problems.

Schneider (1998) developed a Finite Element model using ABAQUS software. Suitable constitutive models were adopted for steel tube and concrete core. Eight-node shell element was used for modelling steel tube. Concrete core was modelled using twenty-node solid element. Interface element was used for modelling the contact area between steel and concrete. The proposed model was verified and calibrated with experimental results of the author. A parametric study was then conducted by modelling fifteen circular CFST specimens to study the correlation between large diameter steel tubes on D/t ratio.

Shams and Saadeghvaziri (1999) proposed a Three-dimensional Finite Element model for circular and square CFST under axial loading conditions. ABAQUS software was used to investigate the nonlinear response of such columns. Solid element was used for modelling the concrete core. Shell element was used for modelling the steel tube. The proposed model was validated with experimental results. The load transfer mechanism for circular CFST columns was then investigated using the proposed model. The authors reported that the steel tube resists most of the applied load for initial stage of loading until the steel tube yields. Once the tube yields, load is transferred from steel tube to concrete. Due to this, load carried by concrete increases gradually. Cross-sectional stress distribution for circular and square columns was also investigated in this study. In square sections, it was observed that higher lateral confining pressure was developed at centre and corners as compared to the sides. The lateral stresses at the sides and corner were approximately 35% and 50% of maximum stress at the centre, respectively. It was observed in this study that the confined stress in concrete (f'_{cc}) was about 1.91 times of the unconfined stress (f'_c) in square cross-sections and about 2.4 times in circular cross-sections. Strain corresponding to

maximum stress of confined concrete (ε'_{cc}) was also increased to 4.2 and 3.89 times that of the same in unconfined concrete (ε'_{c}) for circular and square cross-sections, respectively.

Mander et al. (1988) proposed equivalent uniaxial stress-strain relationship to numerically model the stress-strain relationship of concrete confined by steel tube.

Wheeler and Pircher (2002) studied the effect of material properties of circular hollow tube on response of composite sections, with special focus on effect of yield stress on CFST in flexural loading. Both bare and concrete filled steel tubes of varying yield strengths were subjected to four point bending using ABAQUS software. It was observed that the relationship between yield stress of steel tubes and buckling moment is approximately linear. Moreover, higher increase in buckling moment capacity over hollow steel tubes was observed in CFST for higher D/t ratios.

Hu et al. (2003) proposed new material constitutive models for modelling the confined concrete in his numerical investigations. The authors proposed mathematical equation for calculating the confining pressure exerted by steel tube on the concrete core for circular and square CFST as a fraction of the yield strength of steel tube. The confining pressure varied linearly with ratio of D/t of CFST columns.

Ellobody et al. (2006) developed a numerical model for investigating the behaviour of axially loaded circular CFST columns using Finite Element software ABAQUS. Concrete was modelled using stress-strain curve of confined concrete based on the model suggested by Hu et al. (2003). Steel tube was modelled using bilinear stress-strain relationship. A parametric study was carried out using the FE model. Forty specimens were simulated having D/t ranging from 15 to 70 and concrete cube strength 30 to 110 MPa. The results of the parametric study were compared with codal recommendations, which showed that Australian Standards and American Specifications are conservative, while design strengths predicted by Eurocode 4 formulas were unconservative.

Gupta et al. (2007) developed a two dimensional nonlinear finite element model for circular CFST specimens using FEM software ANSYS 8.0. Multilinear elastic material constitutive models were used for steel tube and concrete core. The concrete core was modeled using PLANE42 element. SHELL51 element was used for simulating the steel tube. The proposed model showed good agreement with the load-displacement behaviour and deflected shape of the samples experimentally tested by authors.

CHAPTER THREE

EXPERIMENTAL PROGRAM

3.1 GENERAL

This chapter covers details of experimental program. At the outset, design of concrete mix to be filled in steel tubes is outlined and discussed.

Thereafter, the details of specimen preparations, calculation of material properties and casting and testing of specimens are discussed in the chapter.

3.2 MIX DESIGN FOR INFILL CONCRETE

The CFST specimens to be tested in this study have been filled with normal strength concrete of M30 grade.

Coarse aggregate of 12.5 mm Maximum Size of Aggregate (MSA) were used for making concrete. The aggregate was first carefully sieved through sieve set according to the recommendations of IS 383: 1970 (Reaffirmed 2007). The fines (material passing through 4.75 mm sieve size) were carefully removed. The aggregates were then washed thoroughly and laid to dry for 24 hours (Figure 3.1). The Surface Saturated Dry (SSD) aggregates were packed in bags.

The moisture content and specific gravity of the coarse aggregates were calculated as per IS 2386: Part 3: 1963 (Reaffirmed 2007). The specific gravity and moisture content were obtained as 2.65 and 0.2% respectively.

Natural river sand was used as fine aggregate (FA) for concrete. Sieve analysis of sand was performed as per IS 383:1970 (Reaffirmed 2007). The sand was classified as Zone III FA in accordance with the codal provisions. The aggregates were washed thoroughly and laid to dry for 24 hours (Figure 3.1). The Surface Saturated Dry (SSD) aggregates were packed in bags.

The moisture content and specific gravity of the fine aggregates were calculated as per IS 2386: Part 3: 1963 (Reaffirmed 2007). The moisture content and specific gravity were recorded as 2.68 and 0.5% respectively.

Figure 3.1 Fine and Coarse Aggregate being spread out for drying

The mix design for concrete was done as per IS 10262: 2009 (2009). The target mix strength was 38.25 MPa. The mix design was performed for an expected slump of 25-50 mm. Slump test was used to measure the workability of concrete. Six cubes of 150 mm size and six cylinders of 150 x 300 mm size, i.e., three each for 7 day-strength and 28-day strength were cast and cured. The mix proportions are shown in Table 3.1.

The results of 7-day and 28-day cube and cylinder tests are Specimens were also cast and tested for determining Modulus of Elasticity and splitting tensile strength. The results are shown in Table 3.2.

Table 3.1 Composition of Concrete Mix

Quantity per cubic metre	Normal Concrete (NC)
Cement (kg)	463
Natural River Sand (kg)	769
Natural Coarse Aggregate (kg)	956
Water (kg)	199
Slump (mm)	36

Table 3.2 Compressive strength and mix properties

Mix Property	Cube 1	Cube 2	Cube 3	Cylinder 1	Cylinder 2	Cylinder 3
7-day Compressive Strength (MPa)	33.25	32.47	33.98	26.82	27.45	25.36
28-day Compressive Strength (MPa)	41.54	42.78	39.89	32.87	30.88	31.81
Modulus of Elasticity (GPa)	28.36	29.88	29.23	-	-	-
Split Tensile Strength (MPa)	-	-	-	3.10	2.95	3.04

3.3 CONCRETE FILLED STEEL TUBULAR (CFST) SPECIMENS

A total of 88 CFST specimens have been tested in this study. The samples have been designed so that the effect of various parameters such as change in length, different types of cross-sections and various types of core configurations may be studied on the axial load capacity and ductility of the specimens. Figure 3.2 shows broad classification of type of specimens and parameters under study, which are discussed in the following paragraphs.

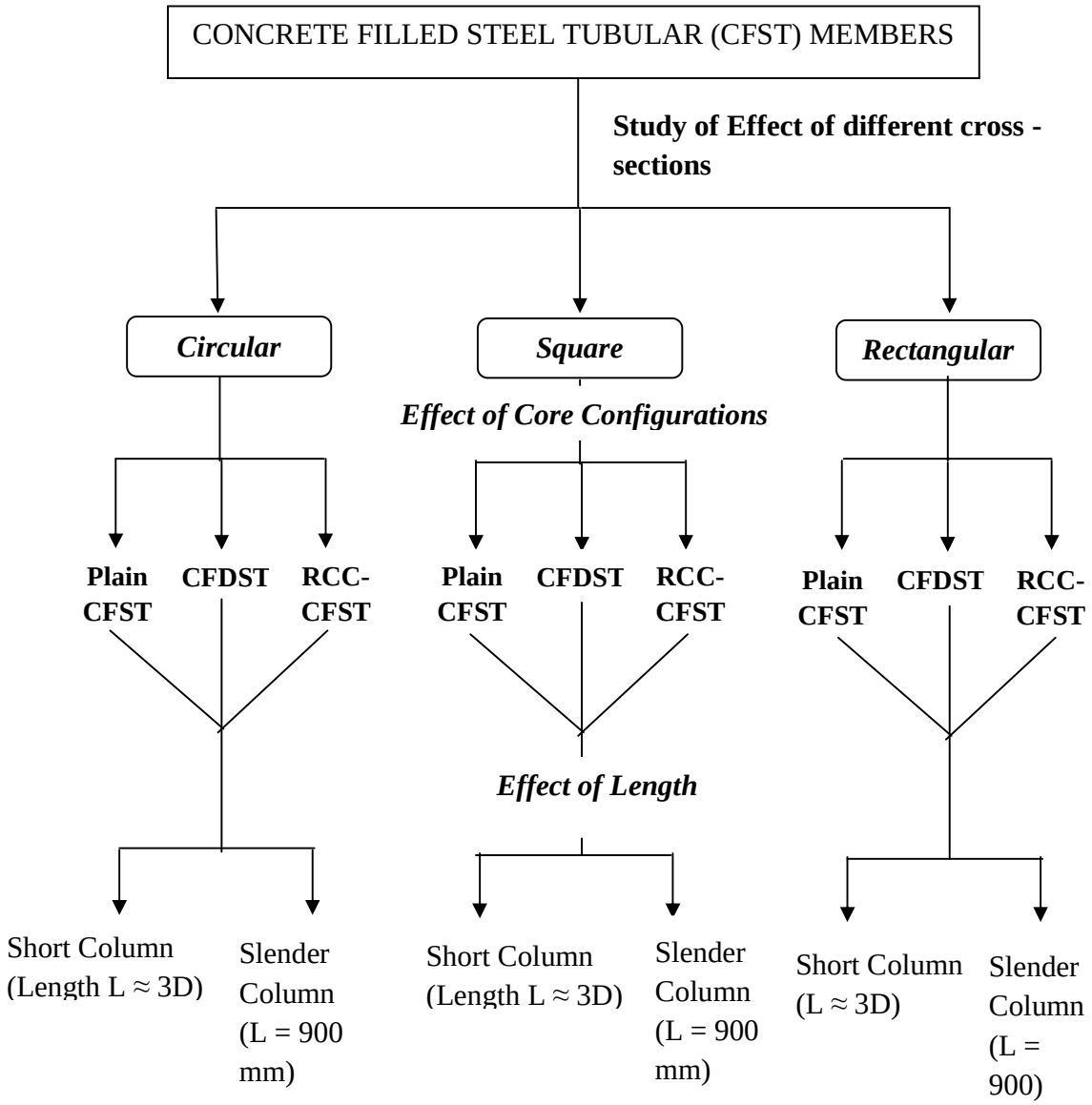

Figure 3.2 A representation of various parameters studied in experimental investigations

Based on Figure 3.2, the outline of the experimental program can be detailed as:

I. **Study of different types of Cross-sections** of CFST has been undertaken in the present research work. Three types of cross-sectional shapes viz. Circular, Square and Rectangular, have been studied.

II. Further, under each category of cross-sections, **three core configurations** have been studied, which are as follows:

1. **Single steel tube filled with plain concrete**: The specimens having such core configuration are labelled as Concrete Filled Steel Tubular (RCFST) columns as shown in Figure 3.3.

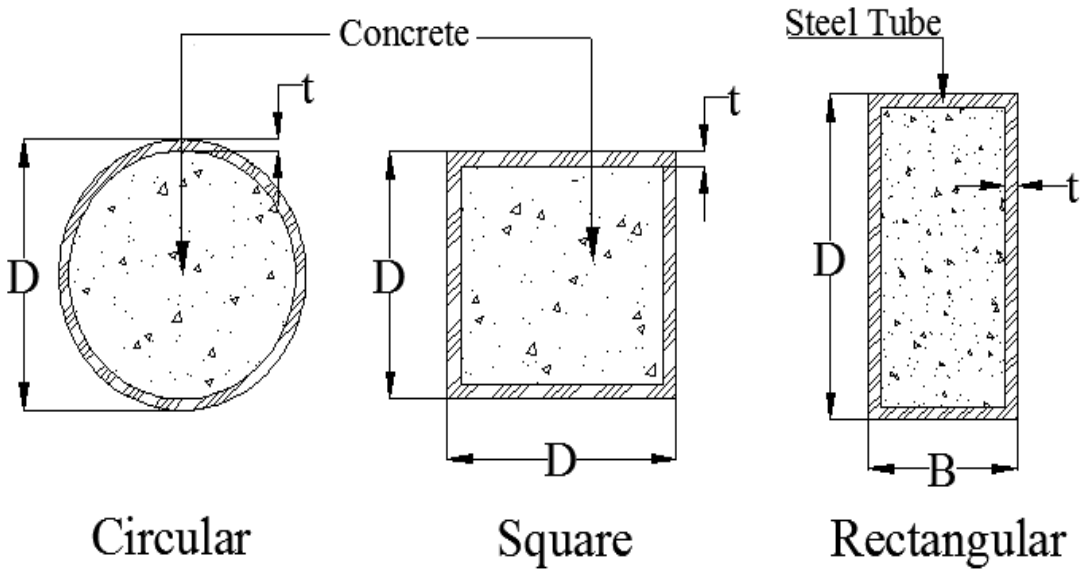

Figure 3.3 Concrete filled steel tubular (CFST) core configuration

2. **Two concentric steel tubes with hollow space between them filled with plain concrete**: The specimens having such core configurations are labelled as Concrete Filled Double Steel tubular (CFDST) columns as shown in Figure 3.4.

3. **Single steel tube filled with reinforced concrete**: The specimens having such core configuration are labelled as Reinforced Recycled Concrete Filled Steel Tubular columns (RCC-CFST) as shown in Figure 3.5.

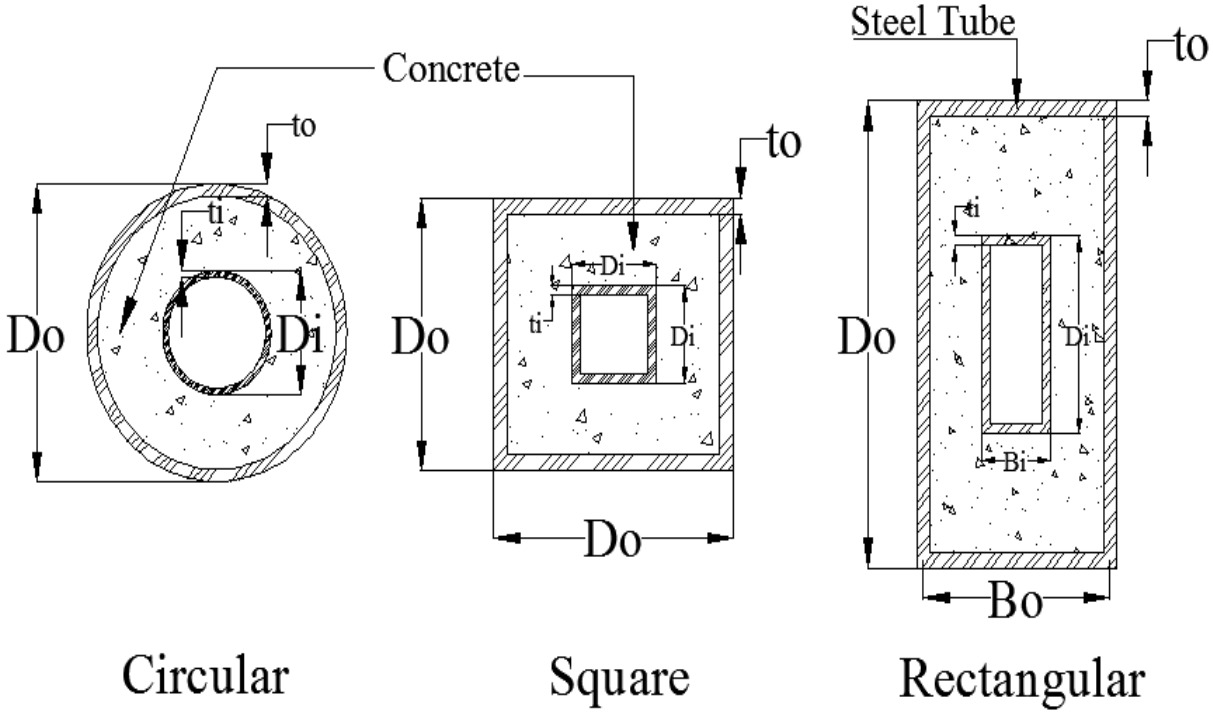

Figure 3.4 Concrete filled double steel tubular (CFDST) core configuration

The amount of reinforcement in RCC-CFST specimens has been chosen in such a way that the sum of area of longitudinal reinforcement and area of steel tube of lower wall thickness is approximately equal to the area of steel provided by a steel tube of higher wall thickness. Such a design criterion was chosen so as to study the effect of change of core configuration (CFST vs RCC-CFST) when the overall area of reinforcing steel is almost same. . It must be noted that a slight difference in the two areas of steel might be observed due to the limits on commercial availability of rebar sizes and steel tube thicknesses. It is often observed that connections between various members are a major problem in CFST. Presence of reinforcing bars such as in RCC-CFST may ease the connections between a CFST column and an existing foundation.

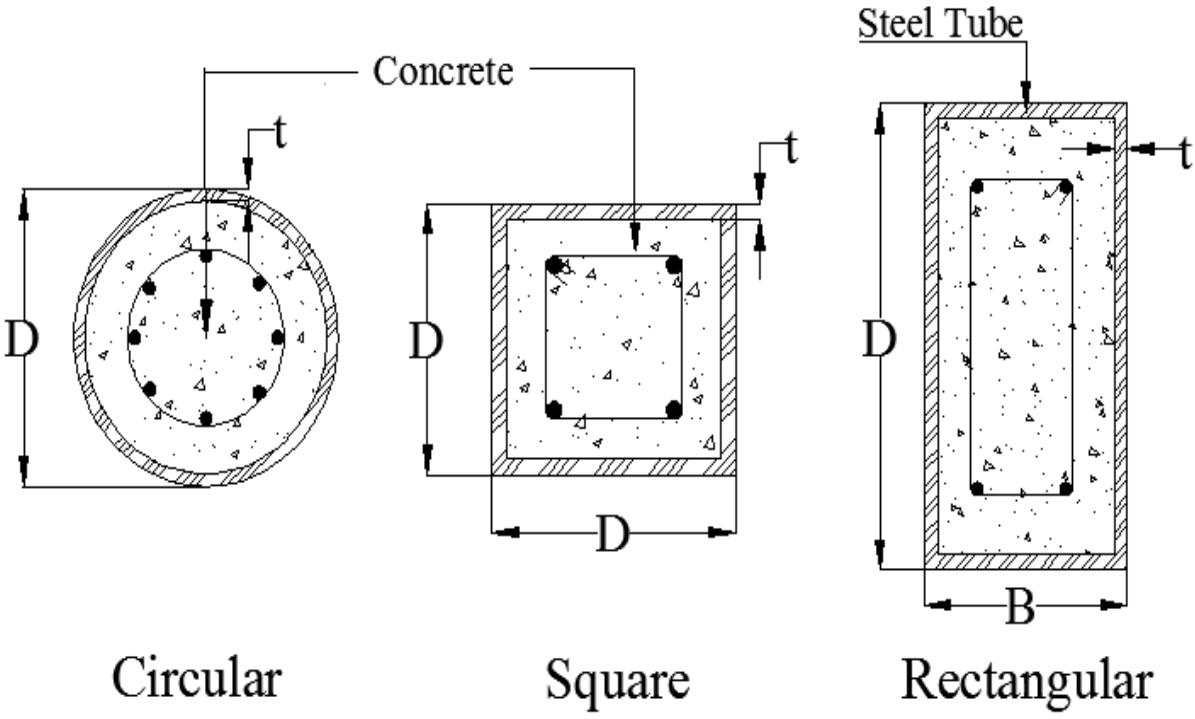

Figure 3.5 Reinforced concrete filled steel tubular (RCC-CFST) core configuration

III. For each core configurations, **two lengths of column** have been tested. The first were short columns with nominal length (L) of three times the tube diameter or tube width. These lengths were selected in such a way that specimens behave as short columns. The second length tested is 900 mm based on the maximum length of specimen that can be installed in the machine. Moreover, in addition to these short and intermediate compression members, some rectangular samples that come under the classification of long columns were also tested.

IV. Finally, different wall thicknesses of steel tube have been tested for different core configurations and lengths of the various cross-sectional shapes. Different thicknesses of steel tube were tested for each outer diameter or width of the sample. Thereafter, the outer dimensions of the steel tube were also varied. This helps in understanding the effect of change in tube thickness and dimensions of the load capacity and ductility of the columns. The thickness of the steel tube was so chosen that the sample did not show local buckling before attaining the ultimate strength.

3.4 PREPARATION OF STEEL TUBES

Steel tubular sections of different cross-sectional shapes and sizes were used in the present research work. The steel tubes were procured from TATA STRUCTURA. These were hot rolled steel sections of 6 m length with a longitudinal seam.

Figure 3.6 Cutting surfacing and smoothing of steel tubes using lathe machine

The steel tubes were then cut into the requisite length using a Lathe machine. Both faces of the tube were then surfaced and smoothened on the Lathe as shown in Figure 3.6.

The final surfaced specimens are shown in Figure 3.7 (a) and (b).

Figure 3.7 Final surfaced (a) Circular specimens and (b) Square Specimens

3.5 CALCULATION OF MATERIAL PROPERTIES

Tensile test specimens were prepared for calculating the yield strength, elongation and tensile strength of the steel tubes. The samples were prepared in accordance with the recommendations of ASTM E8/E8-M (2011). The dimensions of the tensile test specimen are shown in Figure 3.8. The specimens were prepared from the tube face opposite the welded seam face.

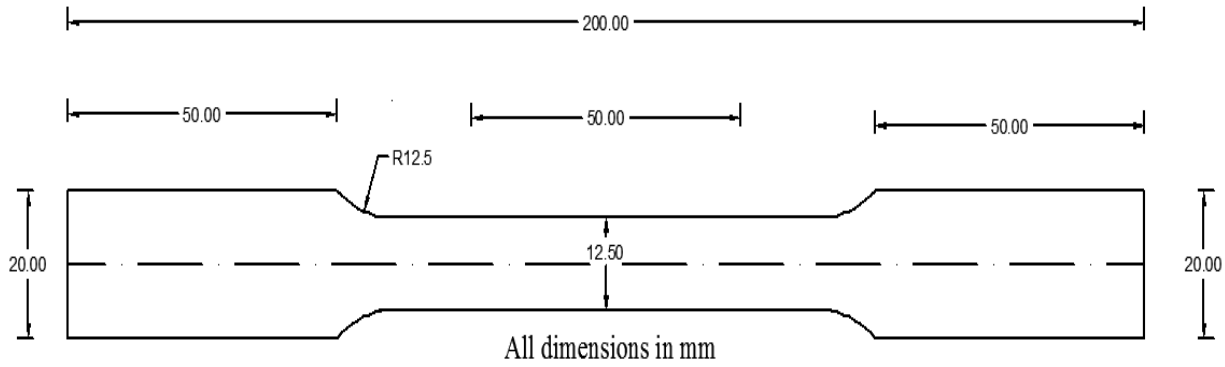

Figure 3.8 Measurements of tensile strength test specimens (ASTM E8/E8M, 2011)

Figure 3.9 shows the location for the tensile test specimen in steel tube and the final prepared specimens.

Figure 3.9 Cut locations of specimens for tensile strength test

Figure 3.10 shows the final prepared specimens. The tested samples are shown in Figure 3.11

Figure 3.10 Final specimens for tensile strength test

Figure 3.11 Tested specimens of tensile strength test

Figure 3.12 shows the test layout of tensile strength test specimens used for testing the material properties of rebars. For reinforcing bars used in RCC-RCFST specimens, the average measured yield stress was 550 MPa and modulus of elasticity was 200,000 MPa.

Figure 3.12 Typical test layout of rebars used for RCC-RCFST specimens

The steel tube manufacturer TATA STRUCTURA supplies the steel tube according to the nominal diameter and thickness. For improved accuracy, diameter and thickness were noted at various locations along the periphery of steel tube, and averaged to get the measured thickness and outer dimensions. These averaged values were then used in calculation of area of steel tube and concrete core. Tables 3.3, 3.4 and 3.5 present material properties of circular, square and rectangular steel tubes used for all tested specimens i.e. CFST, CFDST and RCC-CFST respectively.

Table 3.3 Material properties of circular steel tubes

Outer Diameter (mm)	Nominal Thickness (mm)	Measured Thickness (mm)	Yield Stress (f_y) (MPa)	Tensile Strength (f_u) (MPa)	% Elongation
114.3	3.6	3.4	430	465	30
114.3	4.5	4.2	428	463	31
114.3	5.4	5.06	427	463	32
165.1	4.5	4.28	423	459	36
165.1	5.4	5.03	423	461	37
48.3	3.2	3.04	479	513	28
90	3.2	3	308	361	23.4
90	4	3.75	308	361	23.4
90	4.5	4.5	308	361	23.4

Table 3.4 Material properties of square steel tubes

Outer Width (mm)	Nominal Thickness (mm)	Measured Thickness (mm)	Yield Stress (f_y) (MPa)	Tensile Strength (f_u) (MPa)	% Elongation
150	4	3.75	413	504	22
150	6	5.6	388	478	24
113.5	4.8	4.52	438	474	34
113.5	5.4	5.16	456	492	30
40	3.2	3.02	456	571	23

Table 3.5 Material properties of rectangular steel tubes

Outer Width (mm)	Outer Depth (mm)	Nominal Thickness (mm)	Measured Thickness (mm)	Yield Stress (f_y) (MPa)	Tensile Strength (f_u) (MPa)	% Elongation
100	200	4	3.8	401	490	24
100	200	6	5.68	410	499	22
82	145	4.8	4.65	428	466	36
82	145	5.4	5.15	424	460	35
48	96	4	3.83	452	485	26
40	60	3.6	3.63	458	520	28

3.6 PREPRATION THE SPECIMENS FOR CASTING

Before casting, bottom end of each tube was welded to steel was welded to provide a uniform flat base surface for the CFST specimen. A specially designed setup as shown in Figure 3.13 was used to ensure that the two steel tubes in CFDST were placed concentrically with each other. For RCC-CFST specimens, cages of longitudinal reinforcement confined by lateral ties were prepared. The reinforcing bars were generally cut to a length approximately 1-1.5 cms higher than the length of steel tube. The additional length of rebar was removed by hand grinding prior to testing of the specimens. Figure 3.14 shows the final prepared CFST specimens.

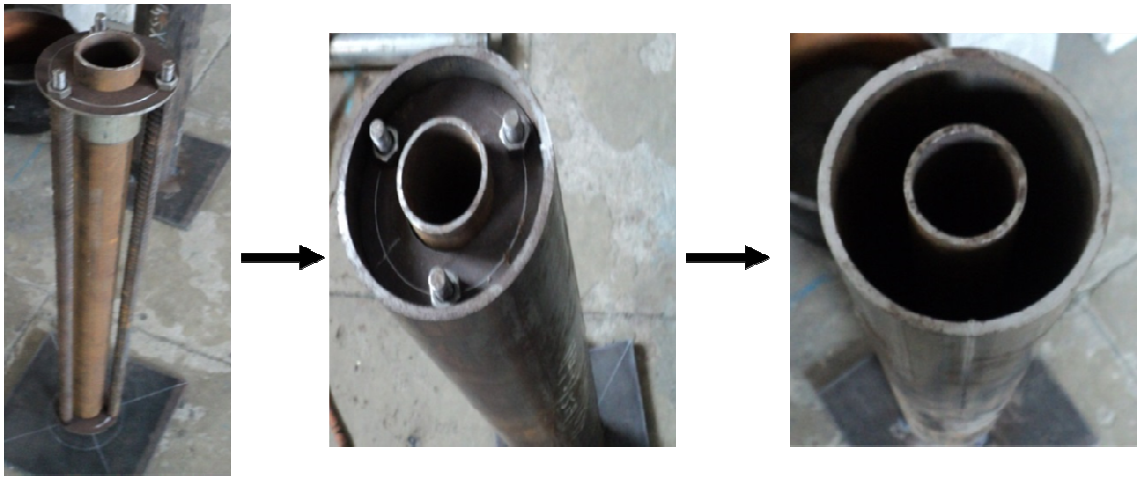

Figure 3.13 Setup used for preparation of circular CFDST specimens

3.7 CASTING

The CFST specimens were filled with normal strength concrete of M30 grade. The concrete mix was prepared in accordance with IS10262:2009 (2009) specifications. Surface Saturated dry (SSD) Coarse and Fine Aggregates and OPC 43 grade cement were used in preparation of concrete mixes. Slump Test was used to check the workability of infill concrete. The mix proportions and slump of the concrete mix are presented in Table 3.1.

The CFST specimens were cast in different batches. The casting was done by pouring concrete manually into steel tubes in 3-5 layers. After each layer was poured, the specimens

were compacted by placing them on a vibrating table for approximately 30 seconds. At the end, an additional layer of concrete 5-10 mm thick above the level of steel tube was left at the top of the specimen for each sample (see Figure 3.15). This was done to compensate for longitudinal shrinkage of concrete, which might otherwise cause the subsidence of concrete below the level of tube when the concrete reaches final setting.

Figure 3.14 RCC-CFST specimens ready for casting

The specimens were allowed to set for 24 hours. Thereafter, the bottom plates were carefully removed using hand grinding. Both ends were sealed using thick polythene sheet and the specimens were kept for dry curing for 28 days as shown in Figure 3.16.

Figure 3.15 Casting of extra concrete at top to avoid effect of longitudinal shrinkage

Figure 3.16 Dry Curing of CFST specimens

After 28 days, the polythene sheets were removed from the top and bottom of the specimens. The top surface of the concrete core was made flush with steel tube using hand grinder (Figure 3.17). This ensures that the load is applied uniformly to the concrete core and steel tube.

Figure 3.17 Finished CFST specimens ready for testing

3.8 TESTING OF SPECIMENS

Two machines available in IIT Roorkee TEST HALL were used to test the CFST specimens based on expected load carrying capacity. Most of the specimens were tested using the four column fully computerized strain controlled INSTRON 8806 UTM available in the laboratory. The hydraulic machine can apply loads upto 2500 KN at user-chosen rate of displacement. In the present study, displacements were applied at the rate of 0.5 mm per minute. Two rigid steel plates 0.5 mm thick made from high strength steel were used to ensure uniform load distribution on entire section.

LVDT were fixed between the two ends of the machine to measure displacement with respect to the fixed bottom end plate of the machine. The INSTRON also captures the reading of platen to platen displacement and the Reaction force on top platen (i.e. Axial Load capacity) at the rate of 1 reading per second.

The samples exceeding load capacity of 2400 KN (practical threshold of INSTRON machine) were tested in the CONTROLS Machine of 5000 KN capacity. The load was displacement controlled at a rate of 0.5 mm per minute. The machine does not have any in-built media for data collection; therefore, the load and displacement data were recorded using external load cell and LVDT.

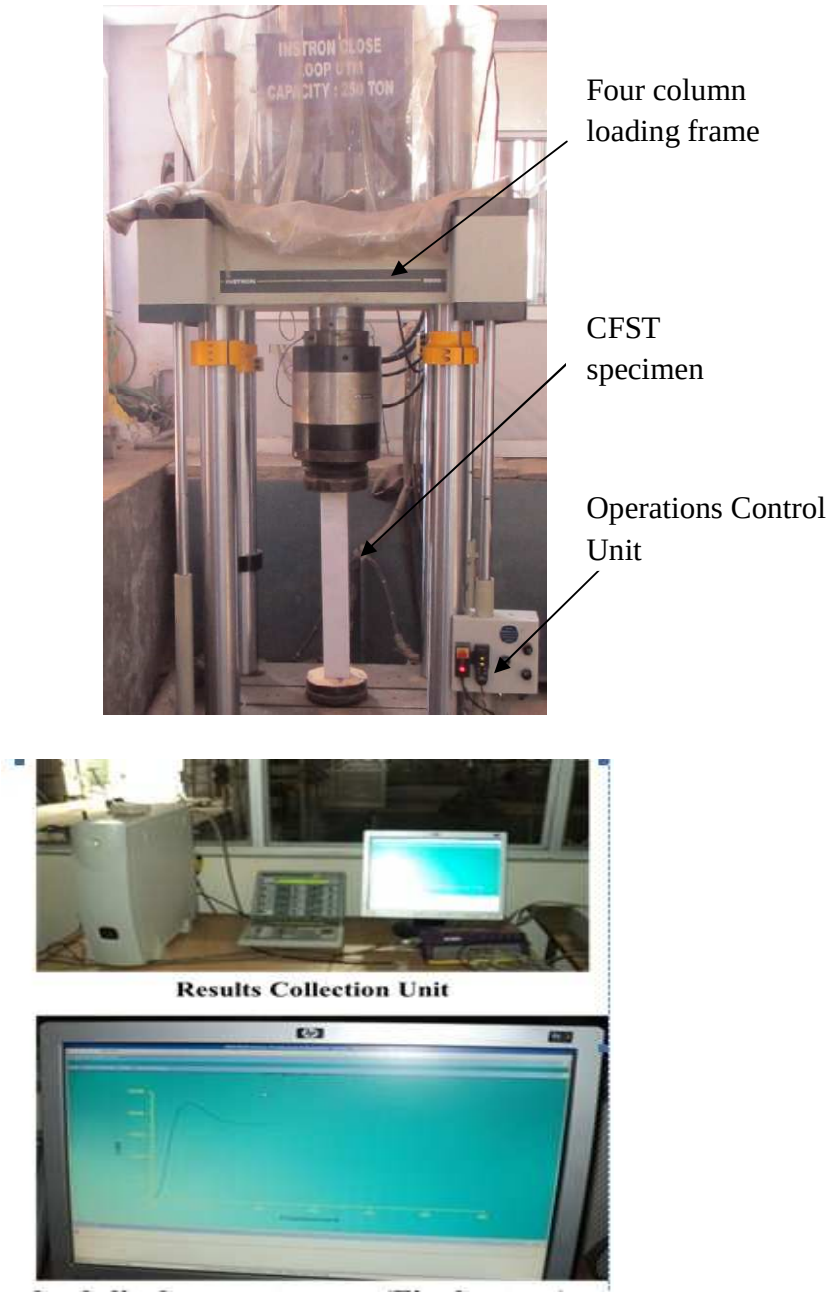

Figure 3.18 INSTRON machine used for testing of tubular specimens

CHAPTER FOUR

NUMERICAL SIMULATIONS - THEORY AND MODELLING

4.1 GENERAL

Full-scale physical testing remains the best method to study the behaviour of structural systems. However, the experimental testing is generally very costly, effort and time consuming, and cumbersome. The complexity involved in such procedures generally rises with the increase in number of parameters to be studied. Further, the application of experimental methods is also dependent upon the commercial availability of materials and testing equipment. These problems impose severe restrictions in the use of experimental methods for exhaustive testing and parametric studies. In such situations, Numerical simulation provides an efficient alternative. Numerical study of any experimental problem affords a researcher complete freedom to explore in detail any number of factors influencing that phenomenon. Finite Element method can be used effectively to simulate the response of different members, materials and systems (Thanoon et al., 2004-a).

An effort has been made in this thesis to provide an alternative to experiments through Finite Element simulations. This chapter covers detailed procedure for modelling axially loaded concrete filled steel tube (CFST) columns having different geometries and core configurations. Three-Dimensional nonlinear Finite Element models have been prepared for different types of sample using ABAQUS 6.8 (2008). The validation of the developed models is also presented to prepare a strong floor for further investigations.

The contact between the steel tube and concrete remains the single most important factor influencing the behavior of the composite columns. This composite action must therefore be very carefully modeled so that it reflects the no-slip condition between the two components. Suitable constitutive models have been adopted for concrete and steel tube to capture the effect of confinement by steel tube to concrete core.

4.2 MODELLING OF CONCRETE CORE

4.2.1 Element

Solid element C3D8R as shown in Figure 4.1 has also been used to model the concrete core. In combination with a suitable constitutive model for concrete, this element is capable of capturing the brittle behavior of concrete, by cracking in tension and crushing in compression

(Abaqus Analysis User Manual, 2008). This element is also capable to model nonlinear material properties of concrete. The geometry of C3D8R element is defined, as shown earlier, as a three-dimensional element and eight nodes having three translational degrees of freedom at each node.

4.2.2 Material Model

Selecting a proper constitutive model for concrete is one of the most important parts of modeling a CFST. The material model for concrete must be capable of representing the effect of confinement provided by steel tube to the concrete core.

Experimental studies carried out on concrete showed that concrete behaves in a highly nonlinear manner in uniaxial compression (Bangash, 2001). With confining pressure provided by steel due to interaction between the steel tube and the concrete core in CFST columns, the nonlinear behaviour of concrete core changes due to triaxial stress state.

Richart et al. (1928) observed that confined concrete showed increased compressive strength, increased stiffness, and extended strain at which the peak stress was reached. As the lateral pressure due to steel-concrete interaction increases, the longitudinal strength and deformation ability also increases. The longitudinal stress at failure was suggested as:

$$f'_{cc} = f'_c + 4.1\, f_l \qquad (4.2)$$

where, f'_{cc} is the uniaxial compressive strength of confined concrete, f'_c is the uniaxial compressive strength of unconfined concrete and f_l is the lateral confining pressure provided by steel tube. f_l was calculated using empirical formulas as:

For circular specimens:

- *CFST and RCC-CFST specimens* (Hu et al., 2003)*:*

$$f_l/f_y = 0.043646 - 0.000832(D/t) \qquad for\ 21.7 \leq D/t \leq 47 \qquad (4.2\ a)$$

$$f_l/f_y = 0.006241 - 0.0000357(D/t) \qquad for\ 47 \leq D/t \leq 150 \qquad (4.2\ b)$$

- *CFDST specimens* (Hu and Su, 2011)

Minimum of:

$$f_l = 8.525 - 0.166(D_o/t_o) - 0.00897(D_i/t_i) + 0.00125(D_o/t_o)^2 + 0.00246(D_o/t_o)(D_i/t_i) - 0.00550(D_i/t_i)^2 \geq 0 \quad (4.3\text{ a})$$

$$f_l/f_{yi} = 0.01844 - 0.00055(D_o/t_o) + 0.00040(D_i/t_i) + 0.00001(D_o/t_o)^2 + 0.00001(D_o/t_o)(D_i/t_i) - 0.00002(D_i/t_i)^2 \quad (4.3\text{ b})$$

$$f_l/f_{yo} = 0.01791 - 0.00036(D_o/t_o) - 0.00013(D_i/t_i) + 0.00001(D_o/t_o)^2 + 0.00001(D_o/t_o)(D_i/t_i) - 0.00002(D_i/t_i)^2 \geq 0 \quad (4.3\text{ c})$$

For square and rectangular specimens (Hu et al., 2003)

- *CFST and RCC-CFST specimens*

$$f_l/f_y = 0.055048 - 0.001885(D/t) \qquad for\ 17 \leq D/t \leq 29.2 \quad (4.4\text{ a})$$

$$f_l/f_y = 0 \qquad for\ 29.2 \leq D/t \leq 150 \quad (4.4\text{ b})$$

- *CFDST specimens*

$$f_l/f_y = 0.055048 - 0.001885(D_o/t_o) \qquad for\ 17 \leq D_o/t_o \leq 29. \quad (4.5\text{ a})$$

$$f_l/f_y = 0 \qquad for\ 29.2 \leq D_o/t_o \leq 150 \quad (4.5\text{ b})$$

where D is the outer diameter of circular steel tube, width of square steel tube, width of broad side of rectangular steel tube, whichever is applicable. t is the wall thickness of steel tube. The subscripts *o* and *i* denote that outer steel tube and inner steel tube, respectively.

The typical equivalent stress-strain curve of confined concrete has been modelled in three parts as shown in Figure 4.4.

The first part defines the linear-elastic behaviour of the confined concrete (from zero stress point up to the proportional limit). The proportional limit stress has been considered as $0.5f'_{cc}$ as recommended by Ellobody et al. (2006). Initial tangent modulus of elasticity was calculated as (ACI 318, 2008):

$$E_{cc} = 4700\sqrt{f'_{cc}} \quad (4.6)$$

Typical Poisson's ratio of concrete was assumed to be as 0.2 as recommended by Bangash (2001).

The second part of the stress-strain curve describes the nonlinear behavior of the concrete core.

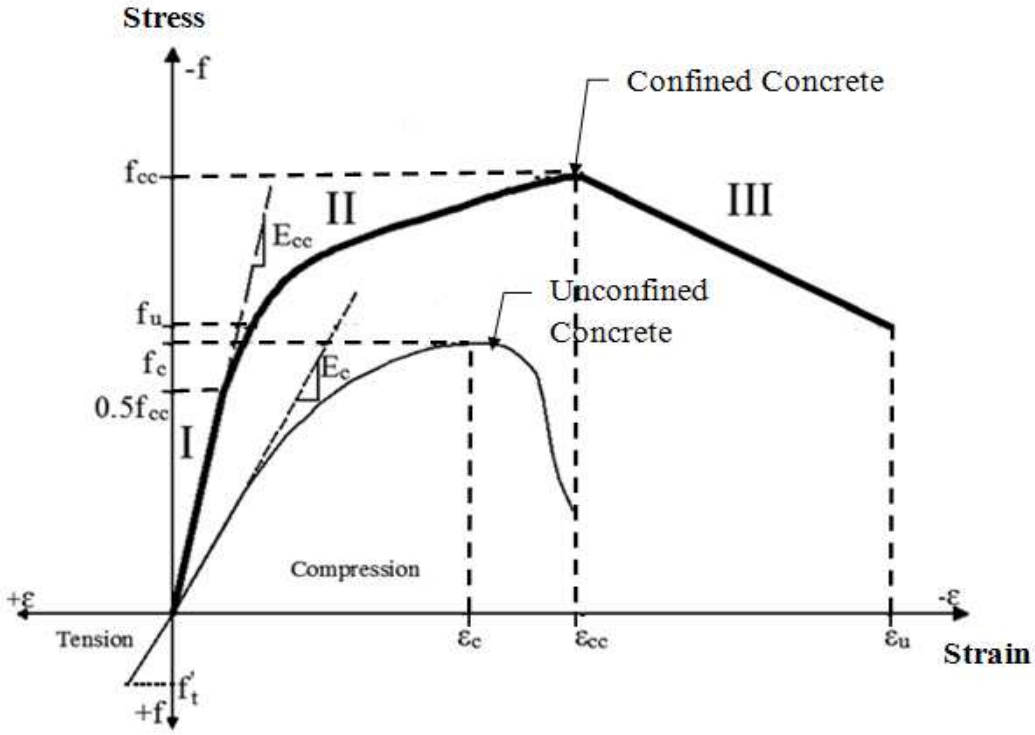

Figure 4.1 Equivalent uniaxial stress-strain curves for confined and unconfined concrete

This part starts from the proportional limit stress,$0.5\,f'_{cc}$, to the maximum strength of the confined concrete, f'_{cc}. This part was modelled using uniaxial compressive stress-strain relationship proposed by Saenz (1964):

$$f = \frac{E_{cc}.\varepsilon}{1+(R+R_E-2)\left[\frac{\varepsilon}{f'_{cc}}\right]-(2R-1)\left[\frac{\varepsilon}{f'_{cc}}\right]^2+R\left[\frac{\varepsilon}{f'_{cc}}\right]^3} \quad (4.7)$$

where R is ratio relation and given as:

$$R = R_E(R_\sigma - 1)/(R_\varepsilon - 1)^2 \quad (4.8\text{ a})$$

in which, R_E is modular ratio which equals to the ratio between initial modulus of elasticity of confined concrete (E_{cc}) to secant modulus at failure ($f'_{cc}/\,'_{cc}$):

$$R_E = E_{cc}.\varepsilon'_{cc}/f'_{cc} \quad (4.8\text{ b})$$

where ε'_{cc} is strain of confined concrete corresponding to f'_{cc} and given as proposed by Richart et al. (1928):

$$\varepsilon'_{cc} = \varepsilon'_c \left[1 + k_2 . \frac{f_l}{f'_c}\right] \quad (4.9)$$

where ε'_c is the failure strain of unconfined concrete corresponding to f'_c and it was considered as 0.003 as recommended by ACI 318 (2008), and $k_1$and k_2 are defined as confining factors, considered as 4.1 and 20.5 ($5k_1$), respectively, as recommended by Richart et al. (1928). R_σ is the stress ratio and given as:

$$R_\sigma = \frac{f'_{cc}}{f_u} \quad (4.10)$$

in which, f_u is the residual ultimate strength of confined concrete and given as:

$$f_u = r k_3 f'_{cc} \quad (4.11)$$

R_ε is the strain ratio given as:

$$R_\varepsilon = \varepsilon'_u / \varepsilon'_{cc} \quad (4.12)$$

where, *r* is a parameter proposed by Dai and Lam (2010) based on numerical simulation results and it was taken as 1.0 for concrete with cube strength of 30 MPa and 0.5 for concrete with cube strength of 100 MPa, and linear interpolation may be used for concrete with strength between 30 and 100 MPa (Dai and Lam, 2010). k_3 may be defined as material degradation parameter and it is given as:

For circular specimens

- *CFST and RCC-CFST specimens* (Hu et al., 2003):

$$k_3 = 1 \qquad for\ 21.7 \le D/t \le 40 \quad (4.13\ a)$$

$$k_3 = 0.0000339(D/t)^2 - 0.0100085(D/t) + 1.3491 \qquad for\ 40 \le (D/t) \le 150 \quad (4.13\ b)$$

- *CFDST specimens* (Hu and Su, 2011):

$$k_3 = 1.73916 - 0.00862(D_o/t_o) + 0.04731(D_i/t_i) + 0.00036(D_o/t_o)^2 + 0.00134(D_o/t_o)(D_i/t_i) - 0.00058(D_i/t_i)^2 \geq 0 \quad (4.14)$$

For square and rectangular specimens

- *CFST and RCC-CFST specimens* (Hu et al., 2003):

$$k_3 = 0.000178(B/t)^2 - 0.02492(B/t) + 1.2722 \qquad for\ 17 \leq B/t \leq 70 \qquad (4.15\ a)$$

$$k_3 = 0.4 \qquad for\ 70 \leq B/t \leq 150 \qquad (4.15\ b)$$

- *CFDST specimens* (Hu et al., 2003)

$$k_3 = 0.000178(B_o/t_o)^2 - 0.02492(B_o/t_o) + 1.2722 \quad for\ 17 \leq B_o/t_o \leq 70 \qquad (4.16\ a)$$

$$k_3 = 0.4 \qquad for\ 70 \leq B_o/t_o \leq 150 \qquad (4.16\ b)$$

ε_u' is the strain corresponding to the residual ultimate strength of confined concrete, f_u', and it was considered as $11_{cc}'$ as recommended by Hu et al. (2003). Moreover, R_σ and R_ε are considered as 4 as recommended by Hu and Schnobrich (1989).

In the modeling of concrete, Drucker Prager (D-P) Hardening Rule has been used. This rule is generally used for materials whose compressive strength is much higher than its tensile strength. The model is suitable for modeling reinforced as well as unreinforced materials in compression hardening.

The input to D-P rule generally consists of two parts:

a) **Elastic Behaviour**: Initial elastic tangent modulus (calculated in Equation 4.6) and Poisson's ratio of concrete are provided in this part. Three more inputs are required, viz. Angle of friction, Flow stress ratio, and Angle of Dilation. The values for these parameters were input as 20 degrees, 0.8 and 20 degrees (Hu et al., 2003)

b) **Plastic Behaviour:** The compression hardening is defined by incorporating the plastic stress-strain behavior of concrete computed using the suitable set of equations chosen

from 4.2 to 4.16 (b). This graphical data is provided in the form of a compressive stress vs plastic strain.

4.3 MODELLING OF STEEL TUBE

4.3.1 Element

In steel tube, the tube thickness is always much smaller as compared to other dimensions. The expected deformation in bare steel tube under an axial compressive load is deformation triggered due to buckling. Shell elements or solid elements can be used to simulate such behaviour in Finite Element analysis. However, use of shell elements significantly reduces number of elements through the thickness of steel tube and limits the accuracy of the analysis. The large shell element size also reduces the total number of elements of the hollow steel tube section, which in turn may significantly affect the simulation accuracy.

Therefore, three-dimensional structural solid element C3D8R Abaqus Analysis User Manual, 2008) is adopted for modelling the steel tube. C3D8R element is defined by eight nodes having three degrees of freedom at each node: translations in the nodal x, y, and z directions as shown in Figure 4.1.

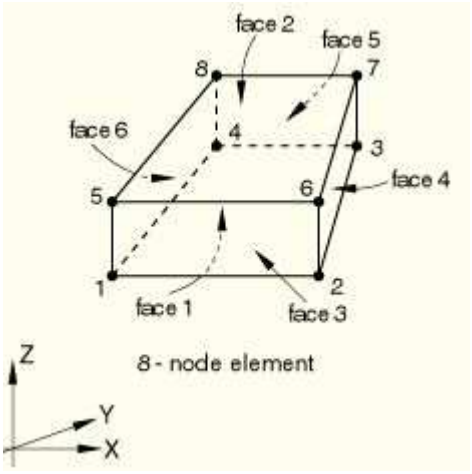

Figure 4.2 Geometry of C3D8R element (Abaqus Analysis User Manual, 2008)

The element supports large strains analysis, plasticity based material models, and large deformations which are necessary to simulate the possibility of local and global buckling.

4.3.2 Material Model

Elastic behaviour of steel tube is modelled using isotropic linear elastic model with initial modulus of elasticity of structural steel as 2 x10^5 MPa and Poisson's ratio 0.3. It is assumed in this study that the proportional limit of steel tube is same of the yield point as the difference can be neglected (ACI 318, 2008).

Plastic behaviour of steel tube is simulated using rate-independent plasticity theory which is characterized by the irreversible straining that occurs in a material once a certain level of stress is reached (Abaqus Analysis User Manual, 2008).

There are three arguments in the rate-independent plasticity theory; yield function, flow rule and the hardening rule. The yield function determines the stress level at which yielding is initiated and subsequent yield surfaces (Hu and Schnobrich, 1988). Standard von Mises yield criterion is the classical yield criterion for steel. The von Mises yield surface is used for initially isotropic materials. It is defined by giving the value of uniaxial yield stress as function of uniaxial equivalent plastic strain (Abaqus Analysis User Manual, 2008).

The flow rule determines the direction of plastic straining and relates the plastic strain increments to stress increments (Hu and Schnobrich, 1988). Flow rule may be defined as associated flow rule when the direction of plastic strains occurs in a direction normal to the yield surface as material is yielding (Abaqus Analysis User Manual, 2008). Associated flue rule is used to model the direction of plastic strains in steel tube.

The hardening rule describes the change of the yield surface with progressive yielding (i.e. defines the motion of the subsequent yield surface during plastic loading stage (Hu and Schnobrich, 1988)) so that the conditions (i.e. stress states) for subsequent yielding can be established. Isotropic Hardening is commonly associated with von mises yielding. In isotropic hardening, the yield surface remains centered about its initial centerline and expands in size as the plastic strains develop assuming that the yield surface expands uniformly without distortion as plastic deformation occurs.

Considering the pressure of concrete core on steel tube in CFST columns, steel tube is subjected to triaxial stress state, which is longitudinal stress due to axial loading (f_{sl}), hoop stress (f_h), and lateral (radial) stress (f_l) (confining stress pressure) as shown in Figure 4.2.

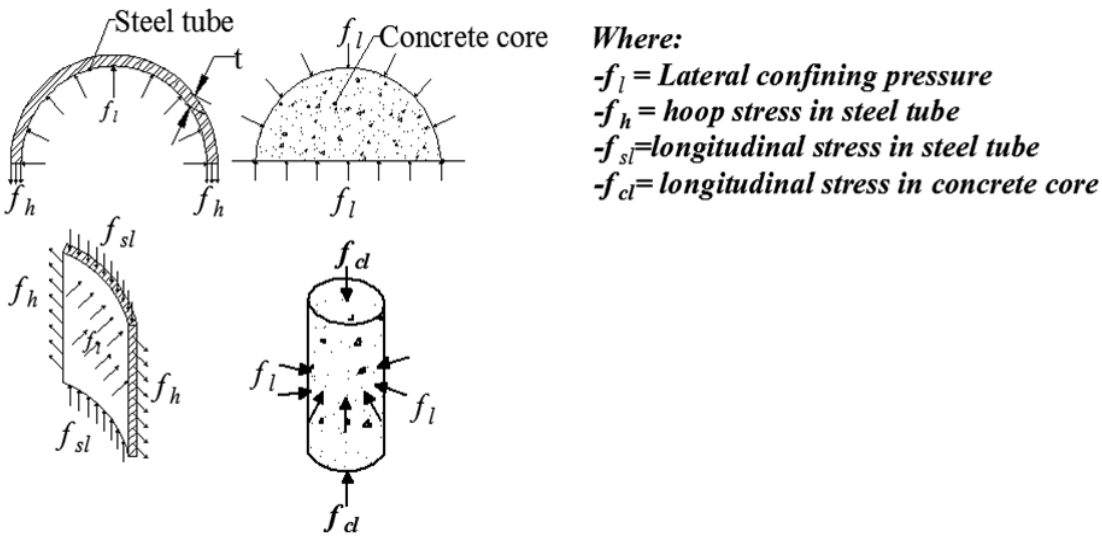

Figure 4.3 Free body diagram of CFST column

When the steel tube is subjected to triaxial stresses, a von Mises yield surface as shown in Figure 4.3 and the criterion *F* is employed to define the elastic limit, which is written (Hu et al., 2003) as:

$$F = \frac{1}{\sqrt{2}}\sqrt{(f_1 - f_2)^2 + (f_2 - f_3)^2 + (f_3 - f_1)^2} = f_y \quad (4.17)$$

Accordingly, the plastic behaviour of steel tube is modelled using a plastic based model bilinear isotropic hardening material model. The required input for this model is equivalent yield stress and tangent modulus. The latter is considered to be zero to simulate the elastic perfectly plastic (elastoplastic) behaviour. This model is used in this study, to simulate the material behaviour of outer steel tube in all core configurations (CFST, RCC-CFST and CFDST), inner steel tube of CFDST specimens, and rebars in RCC-CFST specimens.

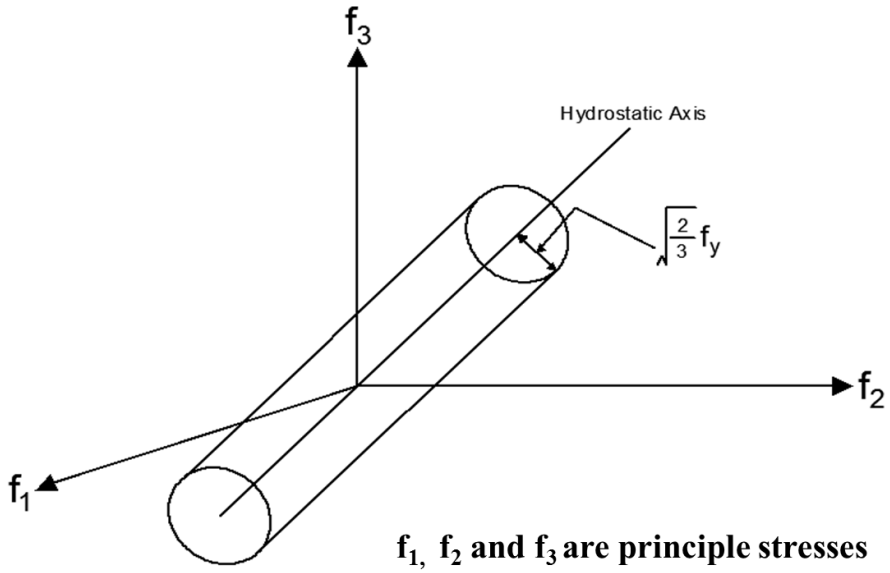

Figure 4.4 von Mises yield surface in the three-dimensional principle stresses

4.4 MODELLING OF REINFORCEMENT

Embedded Constraint is the most commonly used approach for simulating the reinforcement. The rebars can be modelled using link, truss, or beam elements built inside the concrete element in such a way that the rebars will be embedded into the concrete core In this approach, a rebar is embedded into the concrete core using a master-slave approach. The concrete core acts as the master surface; the rebar acts as the slave embedded body. The constraint ensures perfect bond between reinforcement bars and concrete. A typical rebar embedded in a three-dimensional solid element is shown in Figure 4.5. The details of contact and diagrammatic representation of embedded constraint in an actual CFST is provided later in Section 4.6.

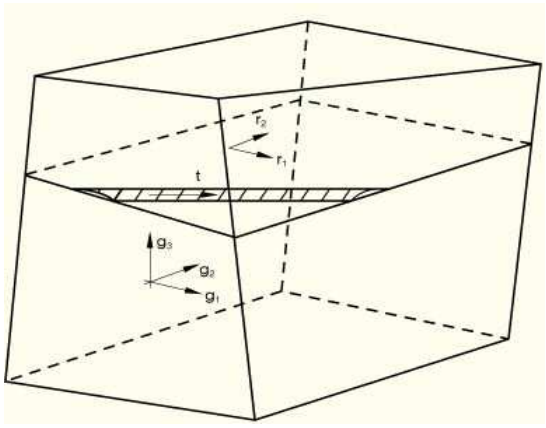

Figure 4.5 A rebar embedded in a typical 3-D solid element (Abaqus Analysis User Manual, 2008)

4.5 MESHING

Meshing involves the discretization of a complex structure into finer elements so that it becomes more easily solvable. In the present study, the steel tube and concrete core in Single Skin CFST were meshed using C3D8R Solid Continuum elements. A single layer of elements was used along the thickness in single skin members. Along the periphery of the circular specimens, there was a one-to-one correspondence between steel and concrete elements, i.e. for every element along the thickness of steel tube, there was a corresponding element of concrete core. The mesh is presented in Figure 4.6.

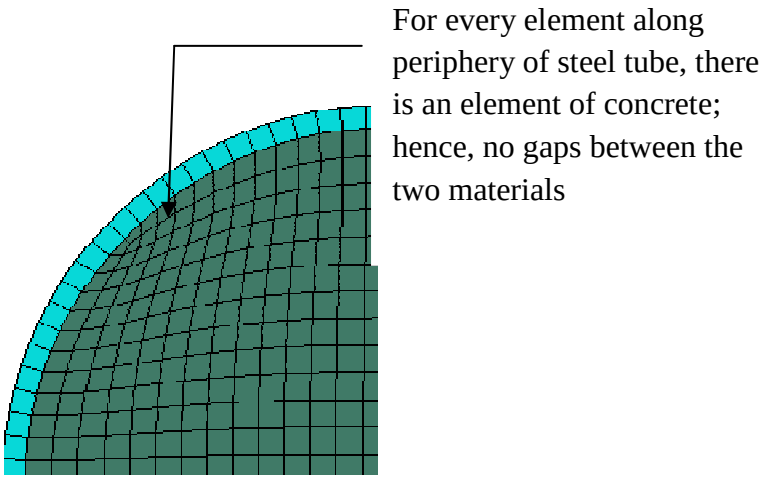

Figure 4.6 Peripheral Mesh for a typical Circular Single Skin Member

However, for all double skin and reinforced CFST members, a mesh with two layers in steel was used due to two reasons:

a) Square and Rectangular Double Skin and Reinforced CFST specimens often suffered from **convergence problems** when a single layer of elements was used in steel tube thickness. For example, the output window of a Square Reinforced CFST with a single layer of elements in steel looks like as in Figure 4.7:

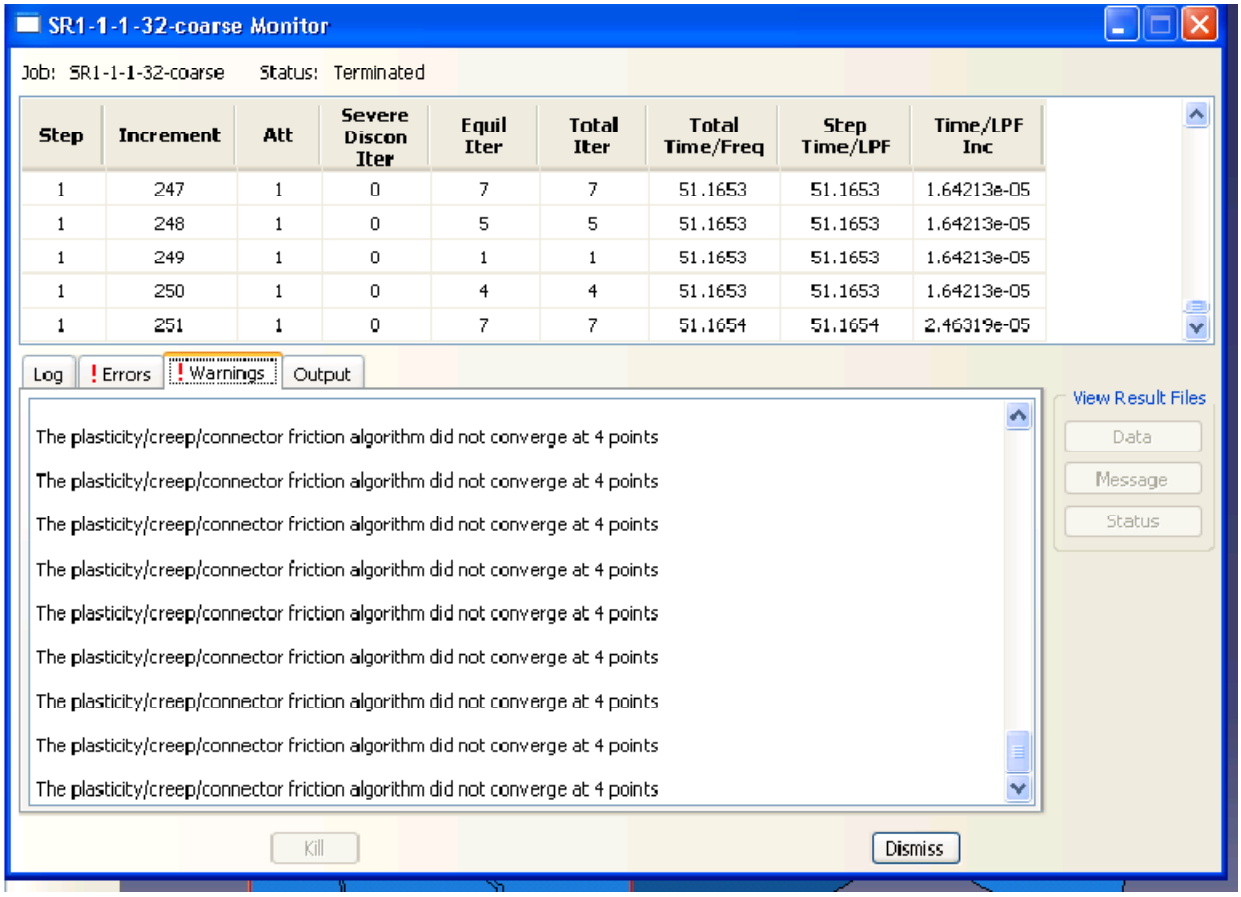

Figure 4.7 Convergence Problems in a Square Reinforced CFST with single layer of elements in wall thickness of steel tube

As can be seen from Figure 4.7, the increment size becomes smaller and smaller, and the analysis ultimately aborts with an error. It must be noted that this was at a very early stage of analysis, corresponding to only about 1.5 mm of axial displacement.

b) Circular Reinforced and Double Skin short columns were found to give very **good matching** with experimental deformed shapes when a double layer of elements was used in thickness (as will be shown in Section 5.2). It must be noted that in both cases a) and b), the meshes along the thickness were quite refined and thus no problems were encountered even when a one-on-on correspondence was not used between steel and concrete.

The meshing along periphery for double skin and RCC-CFST is shown in Figure 4.8.

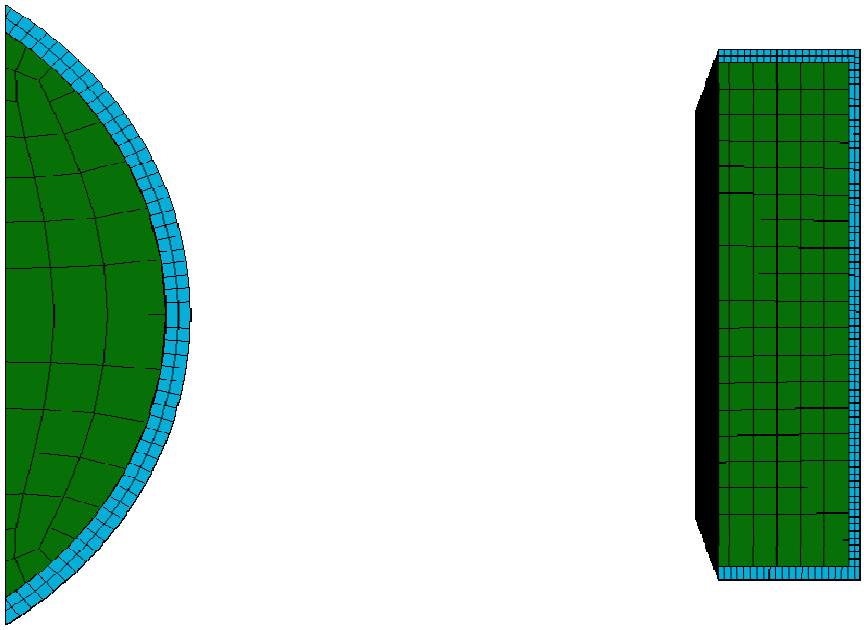

Figure 4.8 Peripheral Mesh for a typical Circular and Square Reinforced CFST

Trials were performed with different mesh densities along the length and thickness of the CFST member. It was found that a relatively coarse mesh with approximately 50 layers along the length of CFST (i.e. a global seed size of 0.02 times the length along the height of the CFST) gave good matching with experimental results.

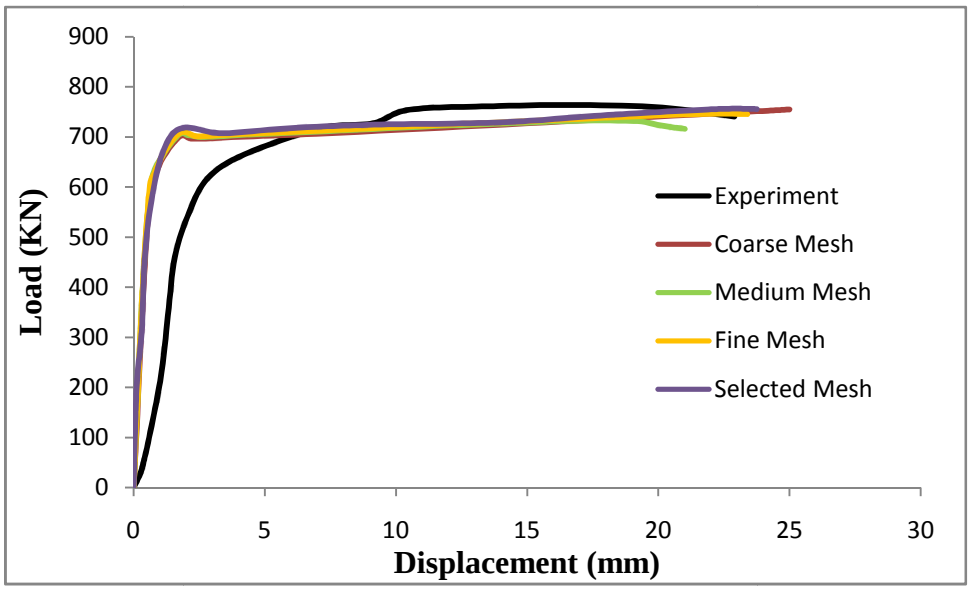

Figure 4.9 Effect of Mesh Density on Load-Deflection Behaviour of CFST

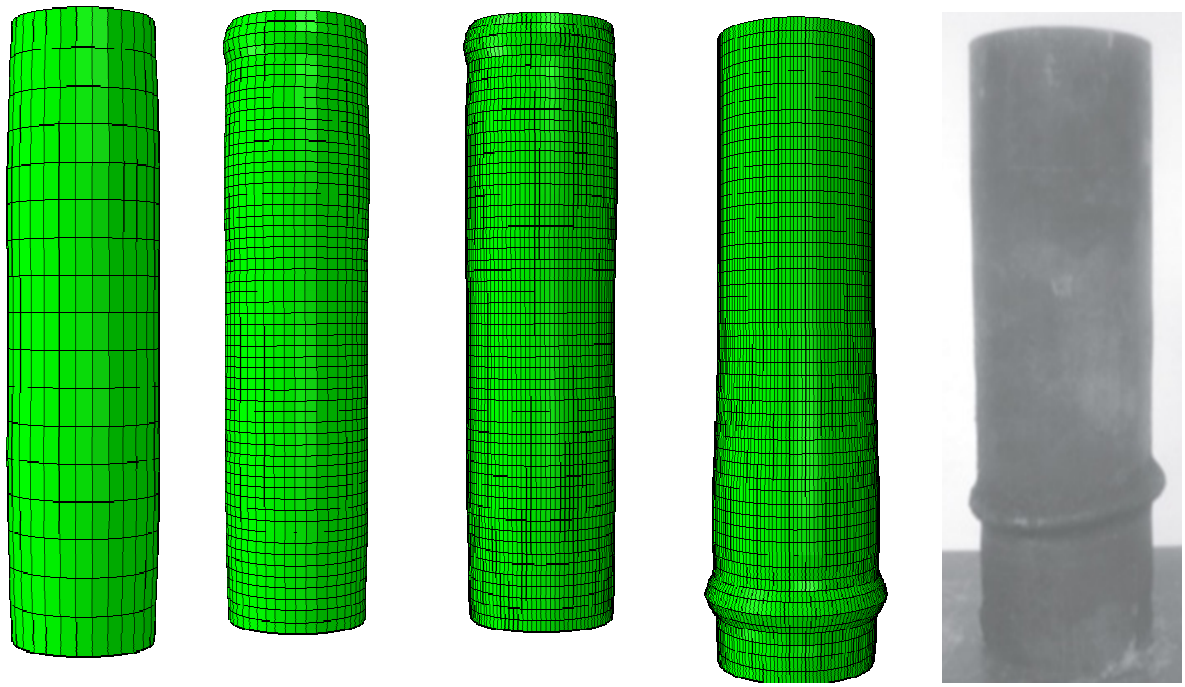

Coarse Mesh **`Medium Mesh** **Fine Mesh** **Selected Mesh** **Experimental Gupta et al. (2007)**

Figure 4.10 Effect of Mesh Density on Deformed Shape of CFST

4.6 MODELLING OF STEEL-CONCRETE INTERFACE

Surface-to- Surface Contact using master-slave approach was adopted to simulate the interface between the steel tube and concrete core in the present study (Abaqus User Manual, 2008). The various contact pairs in CFST are shown in Figures 4.11 (a), (b) and (c).

4.6.1 Contact in Single Skin CFST

In Single Skin CFST specimens, inner surface of steel tube was selected as master, whereas outer surface of concrete core was selected as slave, as shown in Figure 4.11 (a).

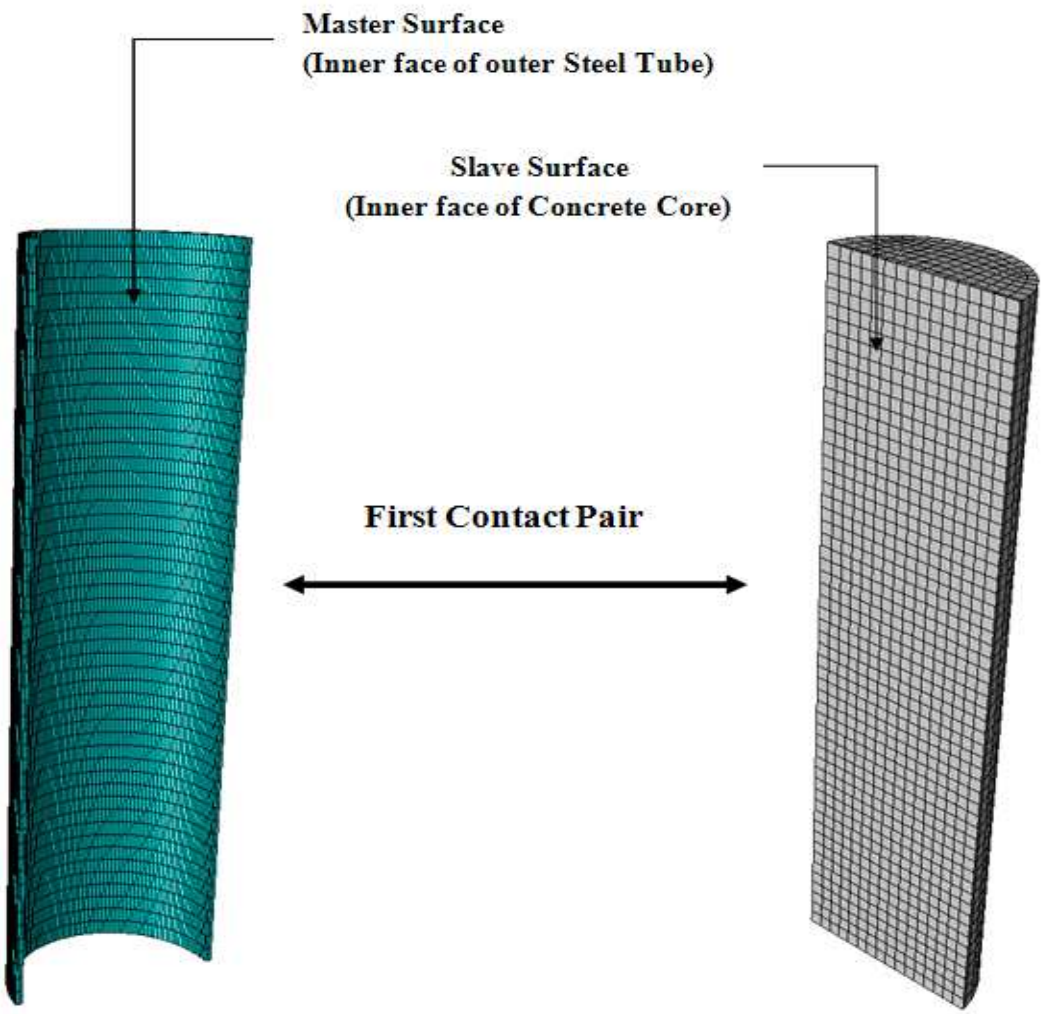

Figure 4.11(a) Contact pair in Single Skin CFST section

4.6.2 Contact in Double Skin CFST (CFDST)

In CFDST specimens, two contact pairs were created. First pair was same as the pair used for CFST and RCC-CFST specimens (i.e. between the outer surface of concrete core as Slave surface and the inner surface of outer steel tube as Master surface). Second contact pair was constructed between inner surface of concrete core (Slave surface) and outer surface of inner steel tube (Master surface). Master and Slave surfaces, and elements are shown in Figure 4.11 (b).

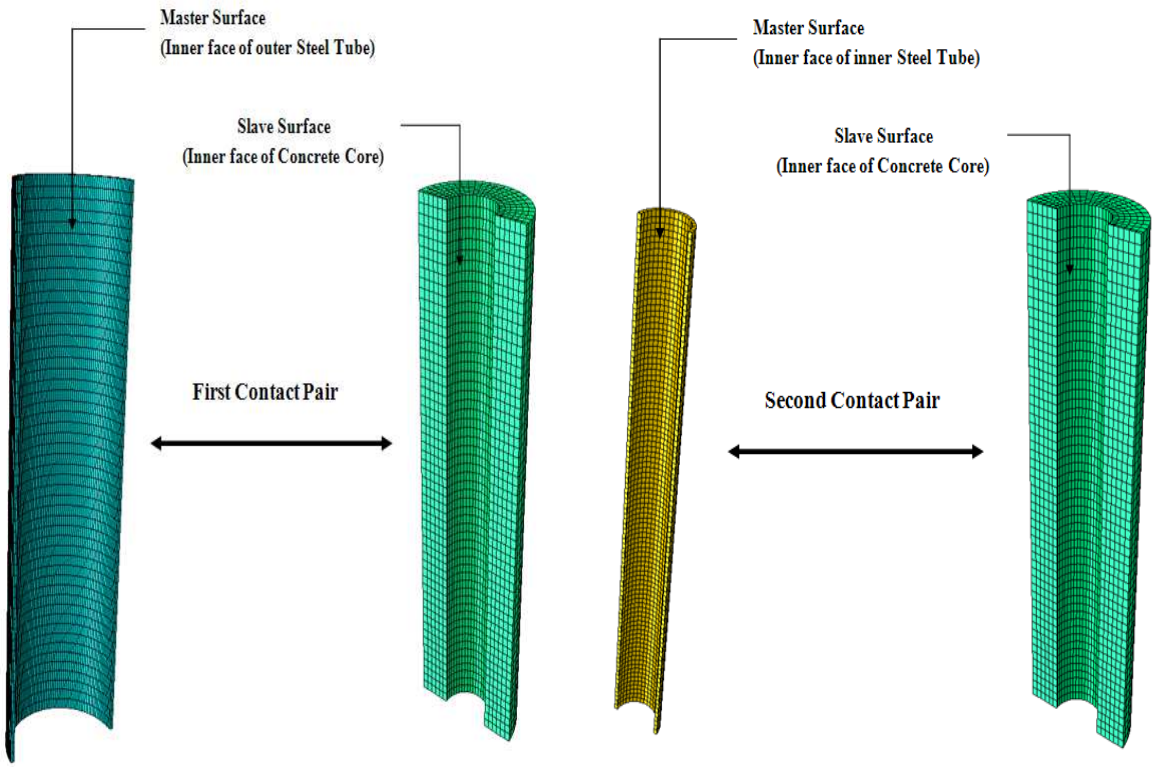

Figure 4.11(b) Contact pairs in Plain CFDST section

4.6.3 Contact in RCC-CFST

One contact pair and one constraint equation have been used in modeling of Reinforced CFST. The contact pair is the same as a Single Skin CFST, having inner face of concrete core as slave surface in contact with inner face of steel tube as master surface, as shown in Figure 4.11 (a). In addition to this, an embedded constraint has been provided for simulating the bond between longitudinal reinforcement cage and the concrete core, as shown in Figure 4.11 (c). The embedded constraint assures a perfect bond at the start between steel and concrete materials. The rebars have been simulated as 1-D truss element, which provides good accuracy in tracking large deformations while simultaneously providing computationally efficient solution.

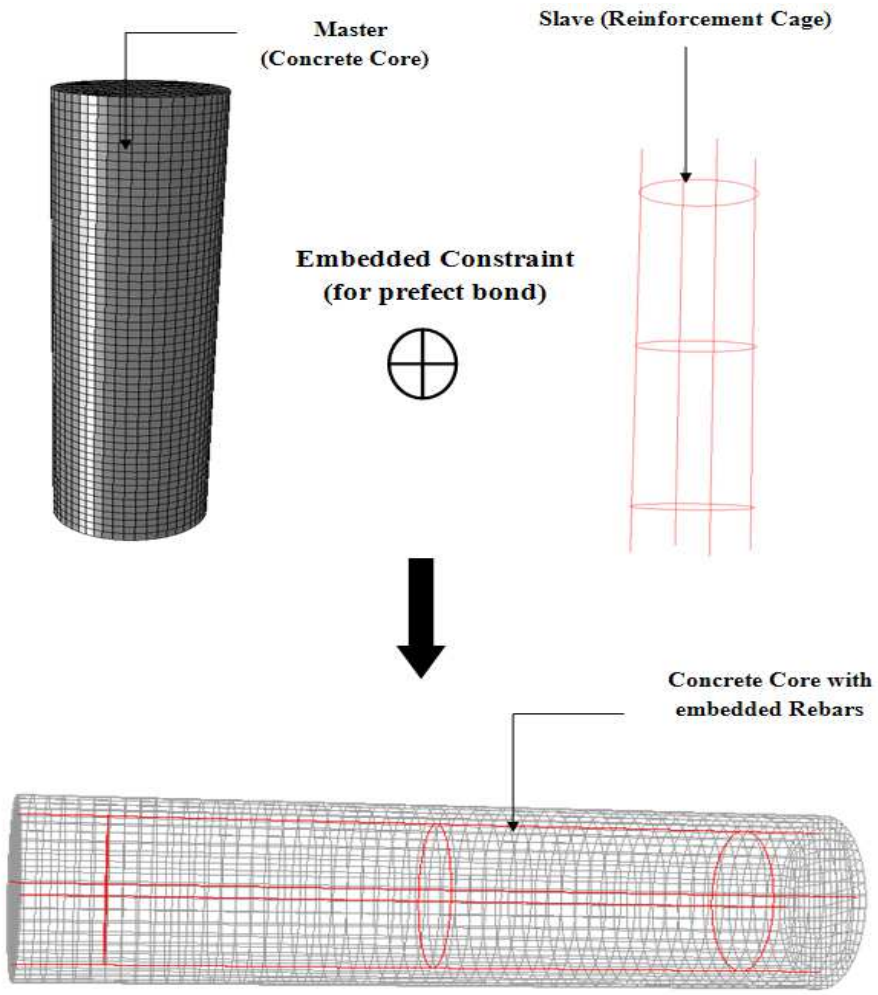

Figure 4.11(c) Embedded Constraint for modeling of Rebars in Concrete core

To define the contact behavior between steel and concrete, Mohr-Coloumb friction criterion was used. A coefficient of friction was provided for transference of load between steel and concrete. The effect of various coefficient of friction between steel and concrete on the behaviour of CFST was studied for a typical specimen CS1-1-1 (short column of outer steel tube dia 114.3 mm, wall thickness 3.4 mm and nominal length three times the outer diameter). Figures 4.12 and 4.13 show the effect of coefficient of friction of load-deflection behaviour and deformed shape of CFST respectively. It is clear from the figures that Mu=0.05 provides the closest agreement with experimental results, and has hence been adopted in further numerical simulations.

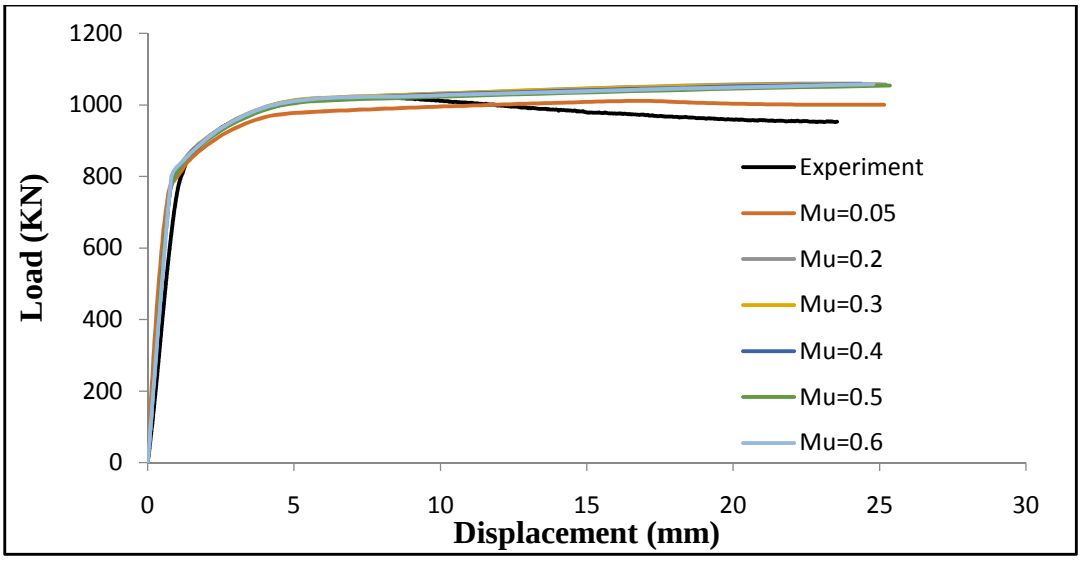

Figure 4.12 Effect of Mu on Load-Deflection Pattern of CFST

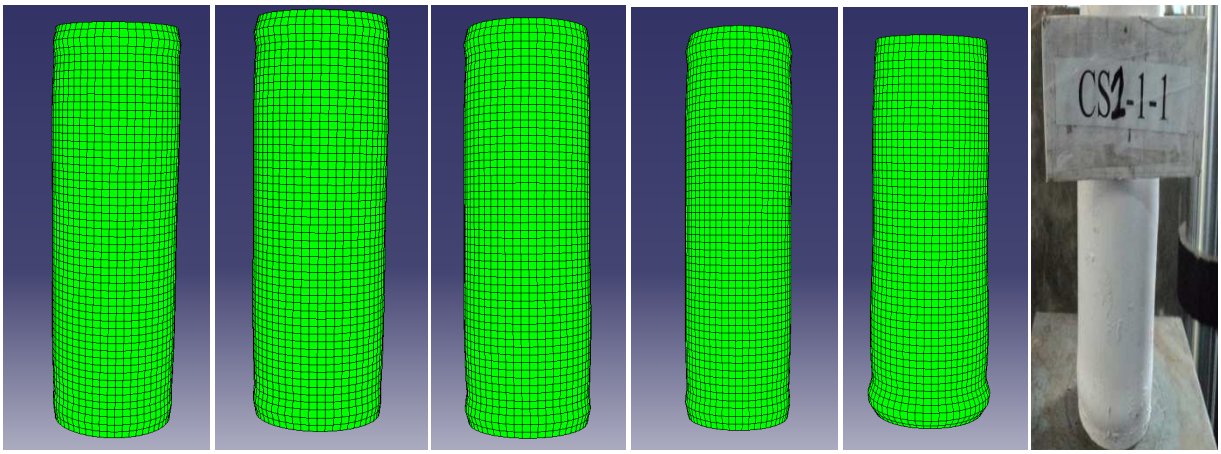

Mu=0.2 **Mu=0.3** **Mu=0.4** **Mu=0.6** **Mu=0.05** **Experiment**

Figure 4.13 Effect of Mu on Deflected shape of CFST

Contact was also provided at the ends between the Rigid platens of the machine and the steel and concrete surfaces in contact with the platen. The Rigid Platen was assumed as the Master surface while the steel (or concrete) face was assumed to be the slave surface. Effect of different coefficient of friction between platen and steel/concrete (f) was also studied. The results are shown in Figure 4.14. As the results show, there is no significant effect of the 'f' parameter on CFST behaviour

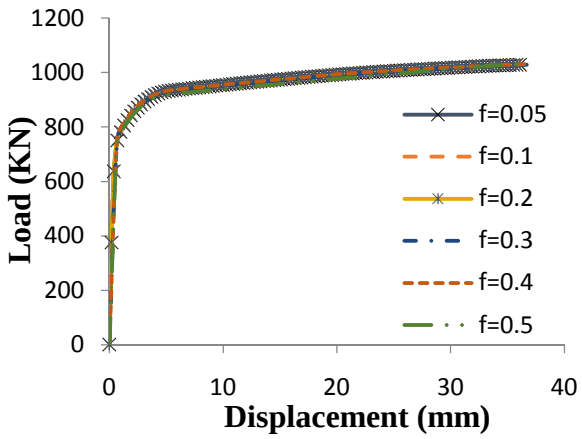

(a) Giakoumelis and Lam (2004)
Sample C3

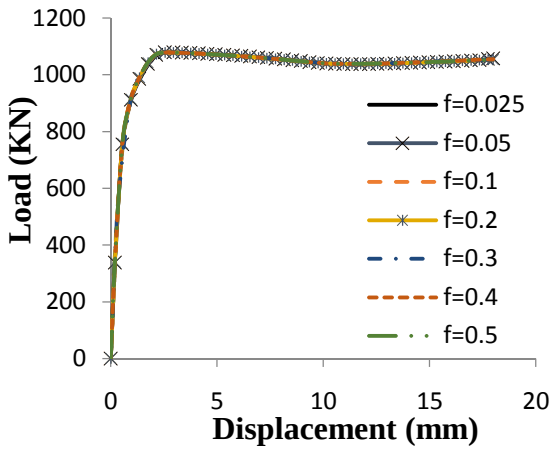

(b) Sakino et al. (2004)
Sample CC4-A-4-1

Figure 4.14 Effect of end friction 'f' on behaviour of CFST

An end friction of 0.2 was thus adopted for the contact between material surfaces and rigid platens.

4.7 STEP TIME AND BOUNDARY CONDITIONS

The step time is a parameter that can be used to define the rate of loading and total test duration of the specimen. The FEM software ABAQUS does not follow any in-built system of units. Therefore, deciding the overall step time is in the hands of the user only. As mentioned in Section 3.8, a loading rate of 0.5 mm per minute was followed in testing in the present experimental study. Therefore, the samples were tested in ABAQUS at this rate only. Figure 4.15 shows a typical step time for the CFST sample tested to 30 mm axial deformation.

Since the rate of loading is 0.5 mm/minute, therefore the total time of test will be equal to 30/0.5 minutes, i.e. 60 minutes (or 3600 seconds). Following the unit of time as second, therefore a step time of 3600 units has been provided. The default loading pattern in ABAQUS is Ramp, i.e. linearly increasing with time, which is suitable for this particular analysis. Fixed Boundary Condition, restraining all the Degrees of Freedom, has been provided at the bottom rigid platen. This imitates the permanently fixed bottom end of the INSTRON testing machine.

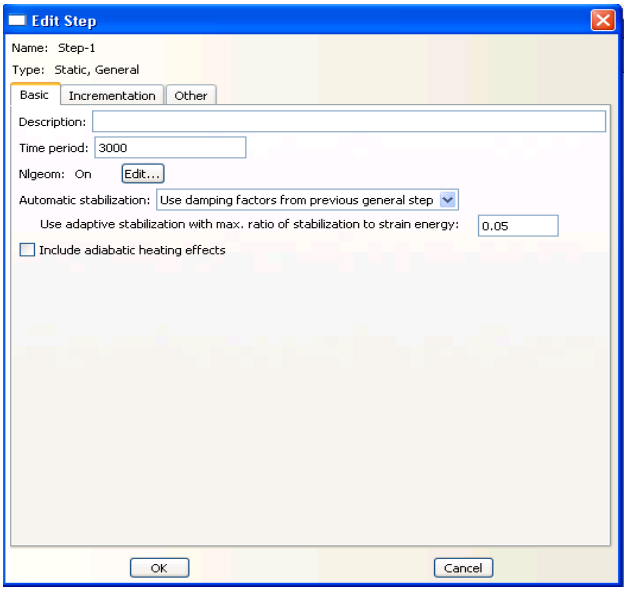

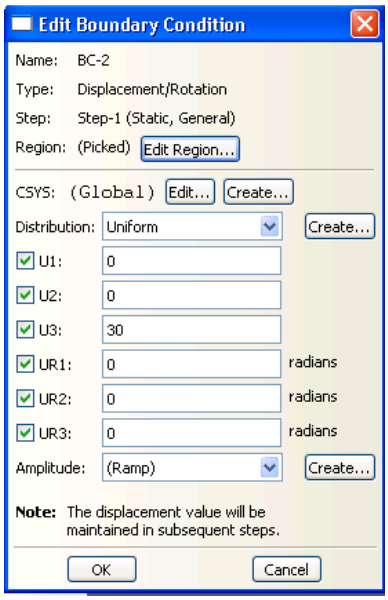

(a) Step Time **(b) Axial Displacement**

Figure 4.15 Defining (a) Step Time and (b) Axial Displacement of 30 mm in ABAQUS for a loading rate 0.5 mm/min

To apply the axial displacement, the top end is allowed to move in downward direction only (as shown by red arrow in Figure 4.16), while restraining all other degrees of freedom at top platen. The concrete core and steel tube are completely unrestrained and free to deform in all directions.

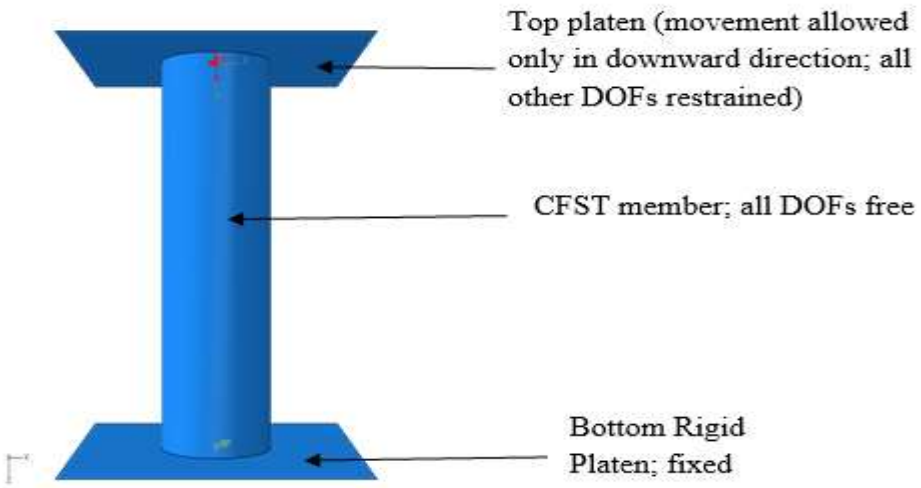

Figure 4.16 Boundary Conditions Applied in CFST member

The final cross-sectional view of the final proposed models is shown in Figures 4.17 to 4.19.

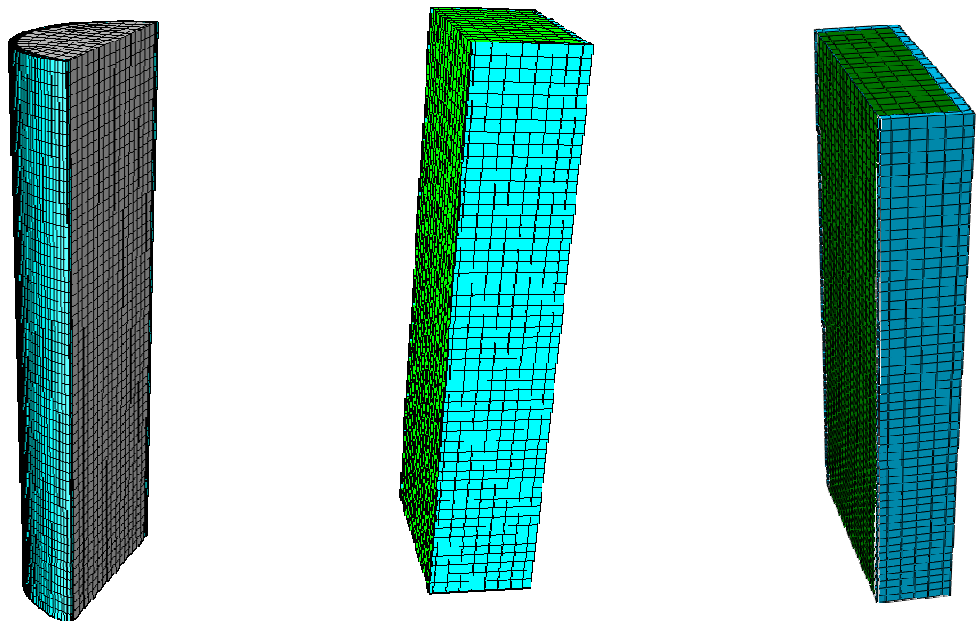

Figure 4.17 Single Skin CFST Members
(Color code: Bluish material is steel tube; concrete is green/grayish)

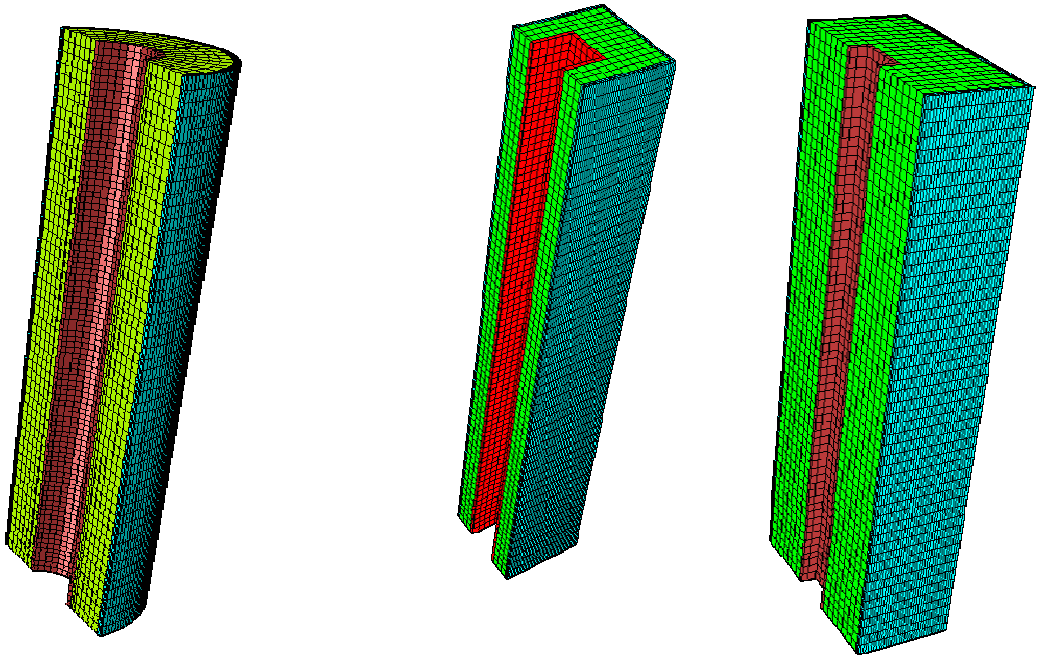

Figure 4.18 Double Skin CFST Members
(Color Code; Bluish: Outer Steel Tube, Green: Concrete, Red: Inner Steel Tube)

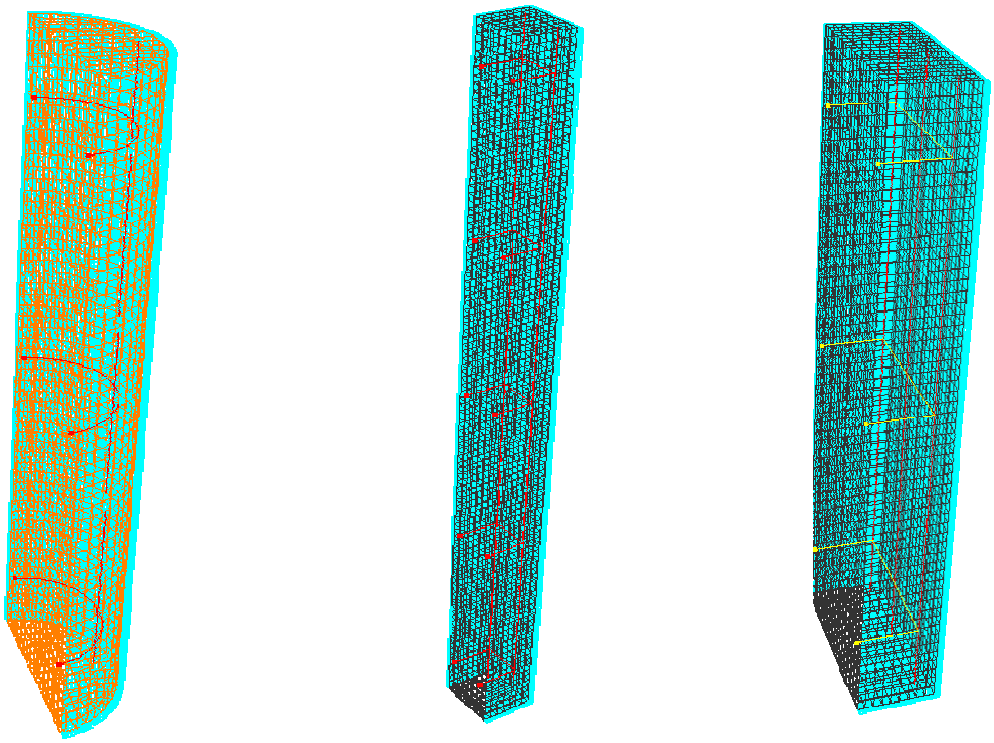

Figure 4.19 Reinforced CFST Members
(Color Code; Bluish: Outer Steel Tube, Black/Orange: Concrete, Red: Rebar cage)

4.8 VALIDATION OF PROPOSED MODEL

Numerical results obtained using proposed model were verified against experimental results selected from available literature. A total of fifty four specimens having different cross-sectional shapes (circular, square and rectangular) were simulated to verify the proposed model. The numerical results in the form of load-displacement curves and ultimate load carrying capacities were compared against corresponding experimental counterparts. This was necessary to ensure that the proposed models are applicable for a wide range of geometry and material configurations. The steel tubes were having different geometric configurations (cross-sectional size, thickness and length) and different material properties (grades of steel yielding stresses and compressive strengths of concrete). The uniaxial compressive strength of concrete cylinder of 150 mm diameter and 300 mm length was considered as compressive strength of concrete core in this study as a For experimental specimens in which the concrete compressive strength was measured using concrete cube of 150 mm size, the equivalent compressive strength was calculated assuming that the compressive strength of concrete cylinders is 80% of compressive strength of concrete cubes as recommended by Neville (2013).

Details of circular specimens simulated for verifying the proposed model are listed in Table 4.1. Numerical load-displacement curves and modes of deformations were compared with corresponding experimental curves in Figure 4.20 (a to g). For some specimens it was not possible to compare modes of deformation as these are not available in concerned literature. It can be concluded based on the Figure 4.20 that the proposed model can predict the structural behaviour (load-displacement curve) of such columns with good accuracy.

It can be concluded from Table 4.1 that the proposed model predicts the ultimate load carrying capacity for specimens having circular cross-sections with good accuracy. The average of the predicted capacities is about 1.01 times the measured values with standard deviation 0.046.

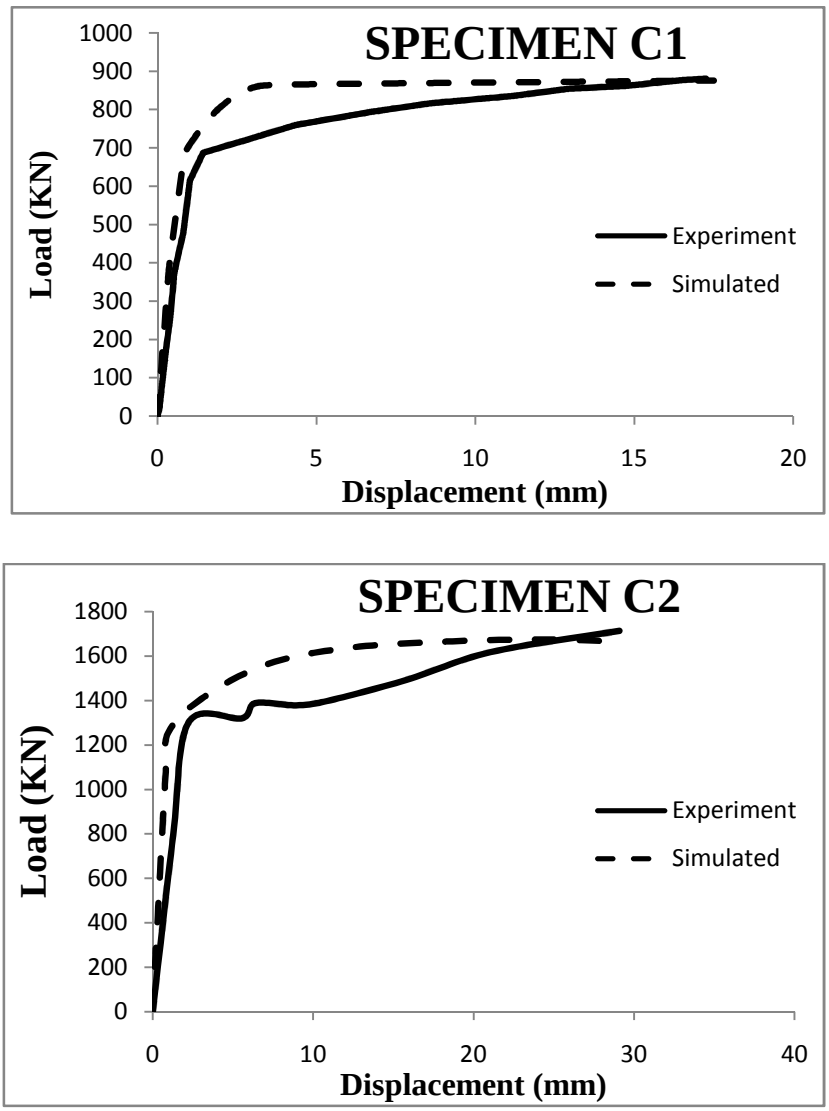

Figure 4.20(a) Schneider et al. (1998)

Table 4.1 Details of simulated circular specimens

Specimen ID	L (mm)	D (mm)	t (mm)	f'_c (MPa)	f_y (MPa)	Ultimate Capacity		Simulated / Experiment	Tested by
						Experimental	Simulated		
C1	605.4	140.8	3	28.18	285	881	875	0.99	Schneider (1998)
C2	608.0	141.4	6.5	23.81	313	1825	1681	0.92	
C3	616	140	6.68	28.18	537	2013	1977	0.98	
CU-040	600	200	5	27.15	265.8	2013	1990	0.99	Huang et al. (2002)
CU-070	840	280	4	31.15	272.6	3025	3024	1.00	
CU-150	900	300	2	27.23	341.7	2180	2151	0.99	
SFE2	650	159	4.8	64.5	433	2170	2167	1.00	Johansson (2002)
SFE4	650	159	5	36.6	390	2040	2177	1.07	
SFE5	650	159	6.8	36.6	402	2860	2742	0.96	
SFE6	650	159	10	36.6	355	3410	3475	1.02	
SFE8	650	159	6.8	93.8	402	3220	3523	1.09	
C3	300.5	114.8	4.91	31.4[2]	343	993	1009	1.02	Giakoumelis and Lam (2004)
C7	300	115.0	4.92	34.7[2]	343	1380	1292	0.94	
C8	300.5	115.0	5.02	104.9[2]	343	1787	1709	0.96	
C11	300	114.3	3.85	57.6[2]	343	1067	1120	1.05	
C14	300	114.5	3.84	98.9[2]	343	1343	1425	1.06	
CC4-A-4-1	447	149	2.96	40.5	308	1064.0	1079	1.01	Sakino et al. (2004)
CC4-C-4-1	900	300	2.96	41.1	279	3277.0	3334	1.02	
CC4-D-4-1	1350	450	2.96	41.1	279	6870.0	6752	0.98	
CC8-C-8	666	222	6.47	77	843	7304	7952	1.09	
D4M3	340	89.32	5.48	37.6	360	650	658	1.01	
D4M4	340	112.4	5.78	37.6	360	764	758	0.99	
C30L3D	342.9	114.3	3.35	32.7	287.33	737	763	1.04	Oliveira et al. (2009)
C60L3D	342.9	114.3	3.35	58.7	287.33	952	971	1.02	
C80L3D	342.9	114.3	3.35	88.8	287.33	1136	1174	1.03	
C100L3D	342.9	114.3	3.35	105.5	287.33	1453	1313	0.90	
Average								1.01	
Standard Deviation								0.046	

[2] Compressive strength of concrete cube; unless this is mentioned, all values of f_c are uniaxial cylinder strength of concrete

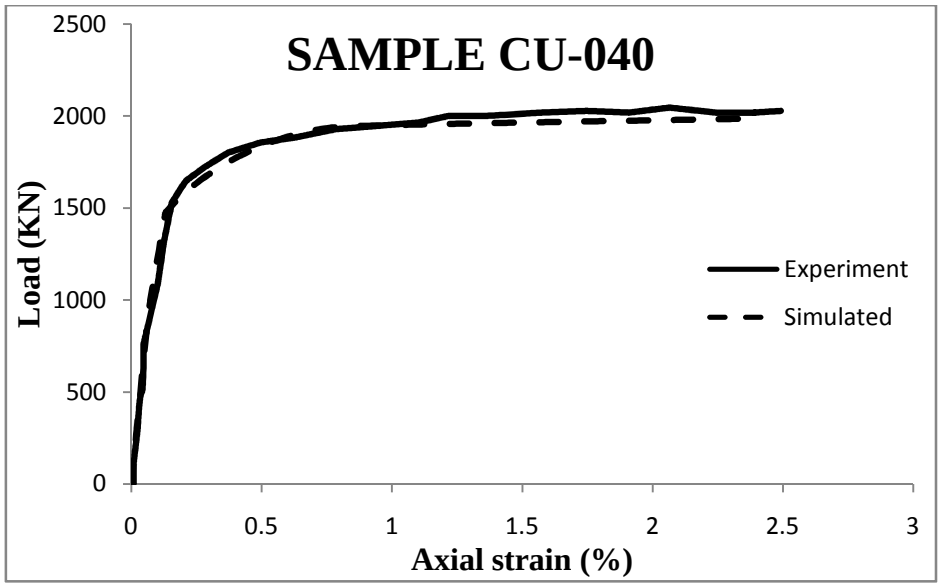

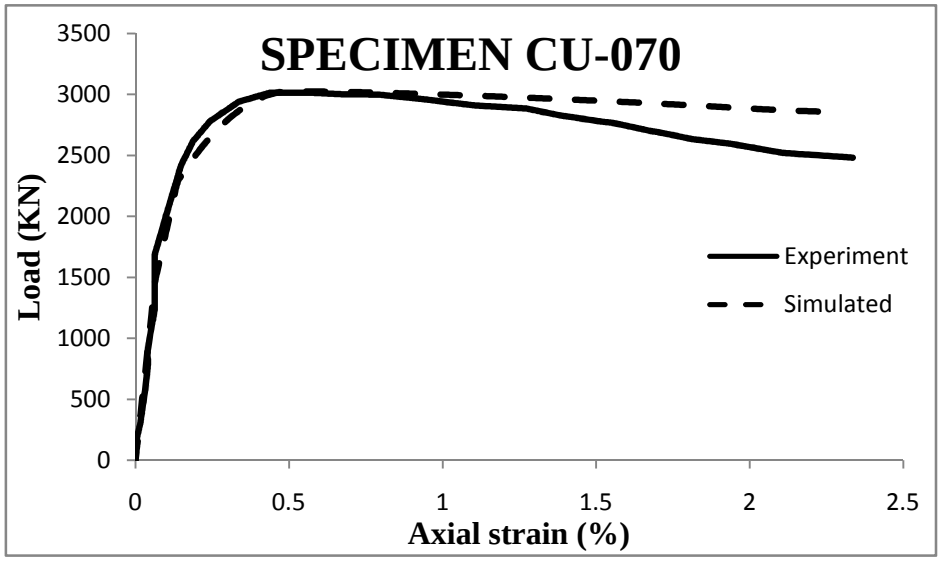

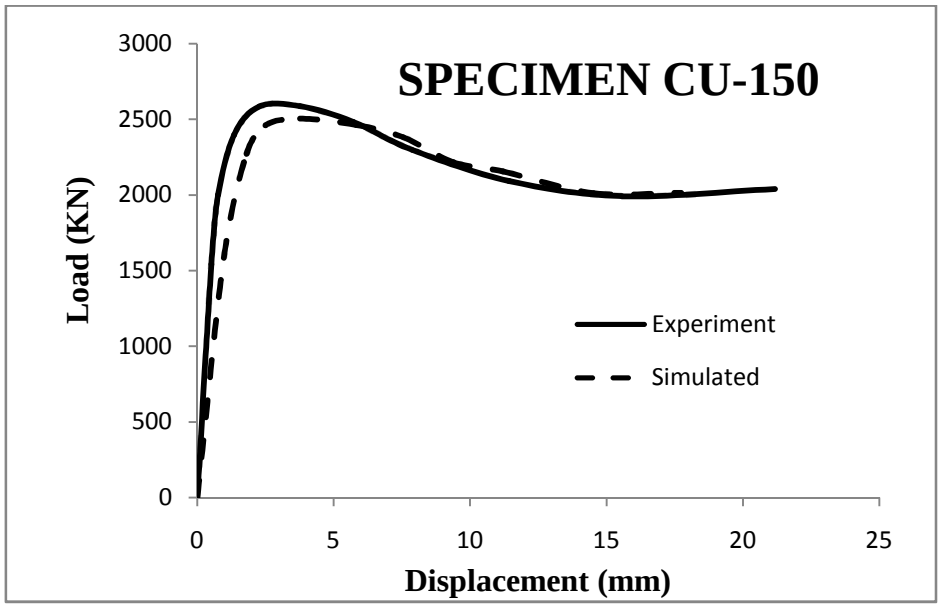

Figure 4.20 (b) Huang et al (2002)

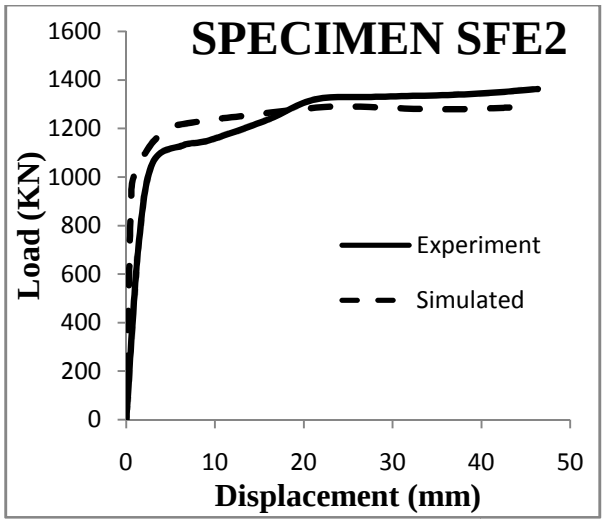

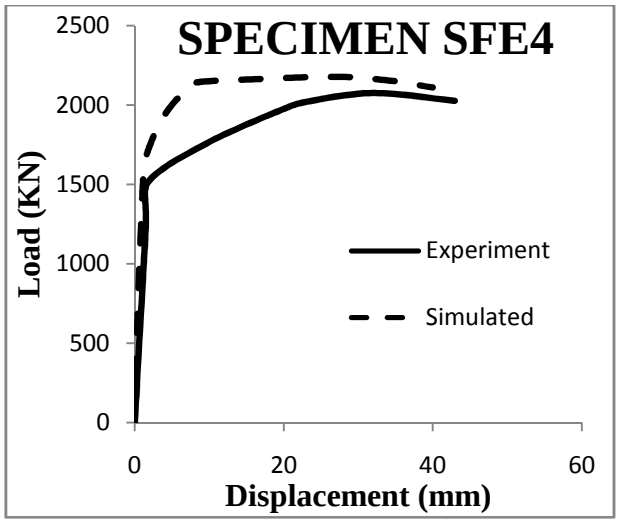

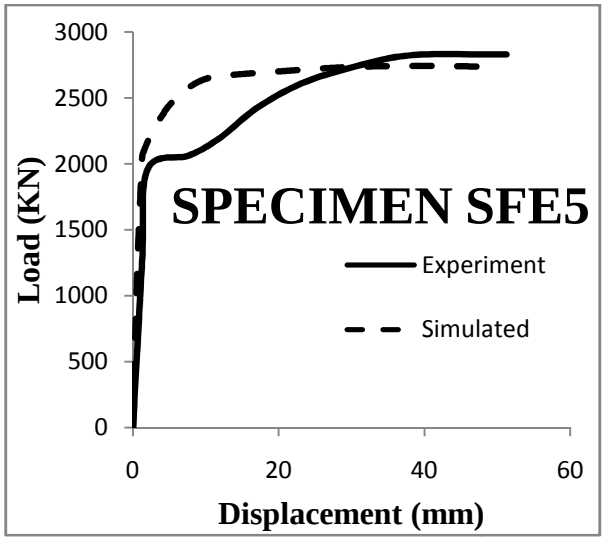

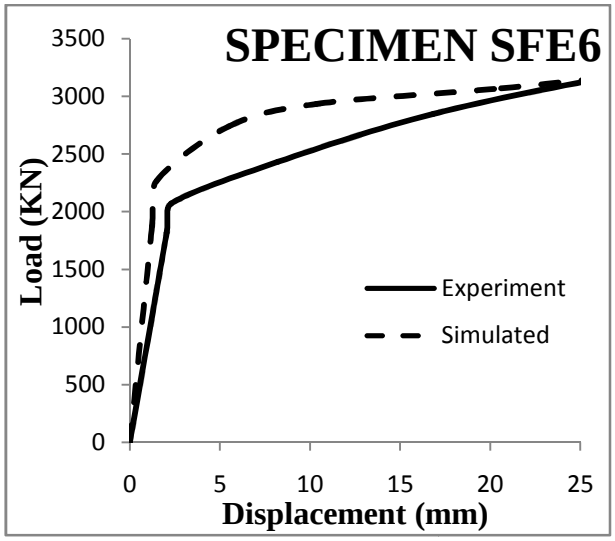

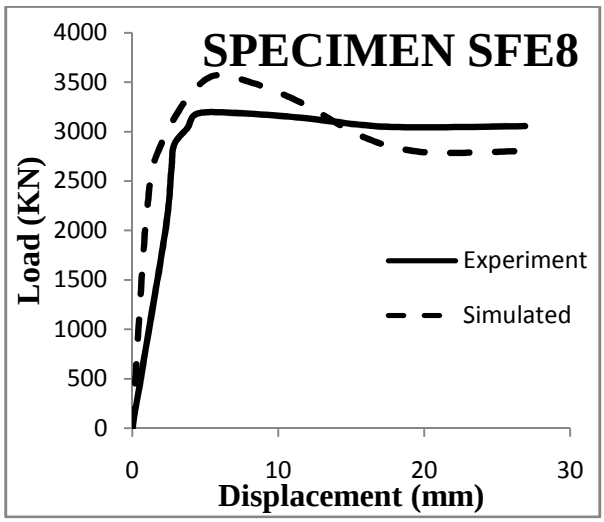

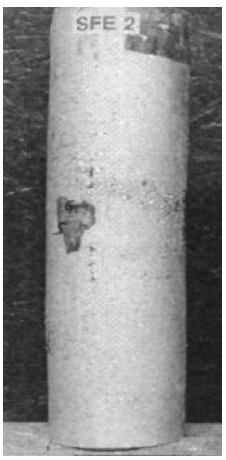

SFE-2 expt. **SFE-2 ABAQUS**

Figure 4.20(c) (Johansson, 2002)

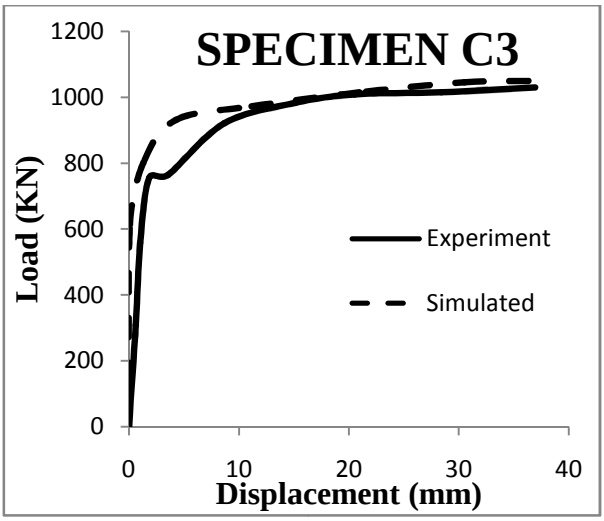

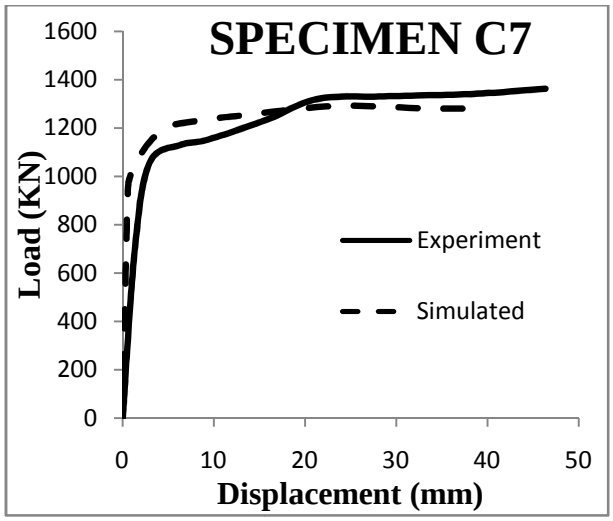

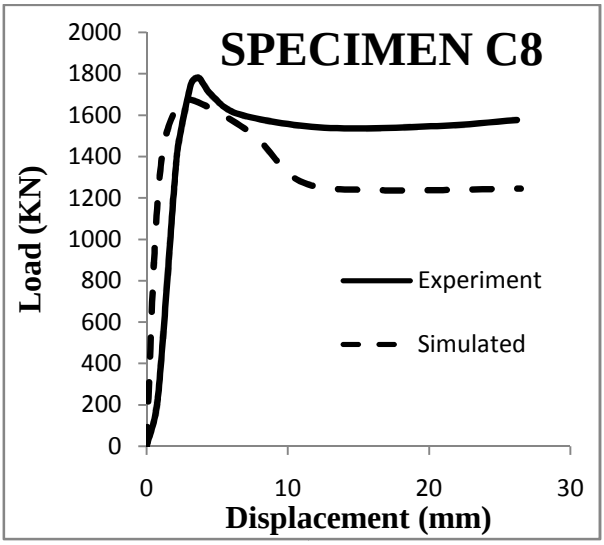

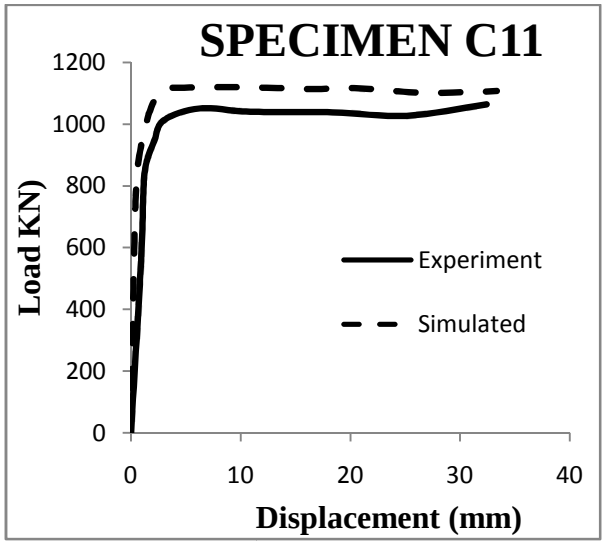

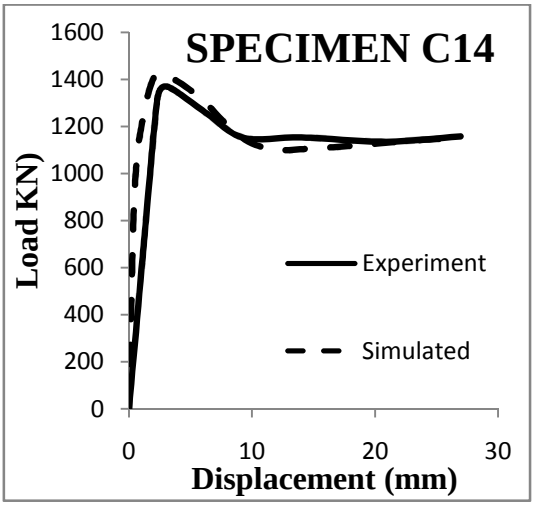

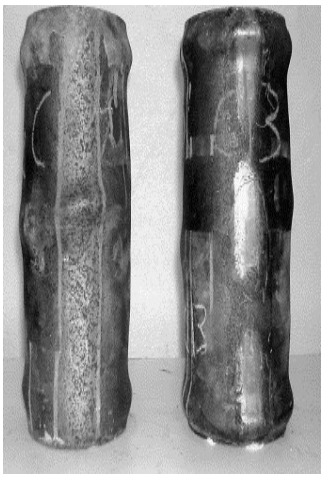

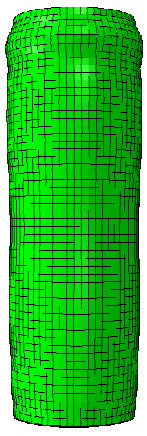

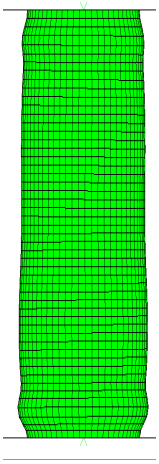

Figure 4.20(d) (Giakoumelis and Lam, 2004)

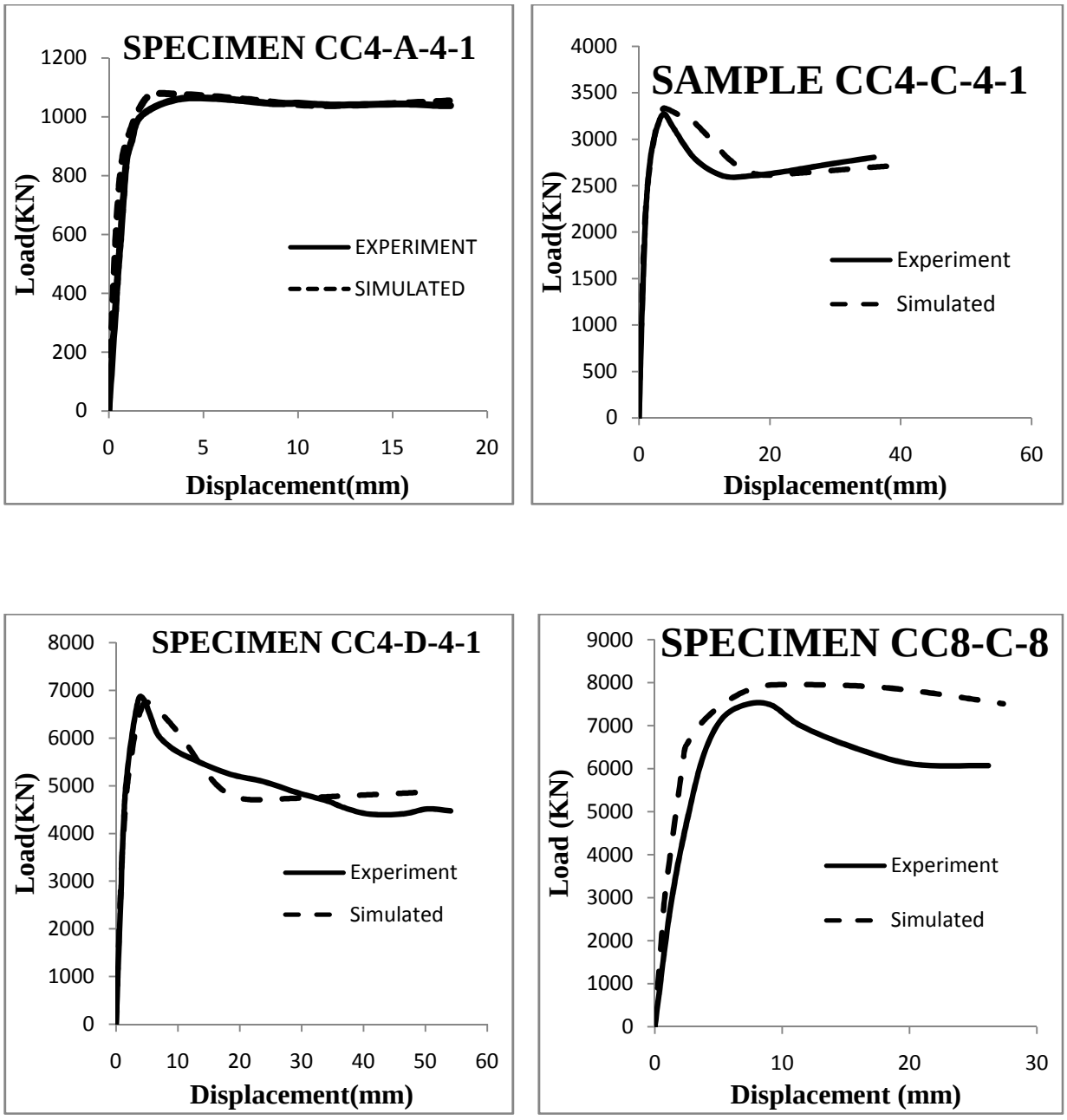

Figure 4.20(e) (Sakino et al., 2004)

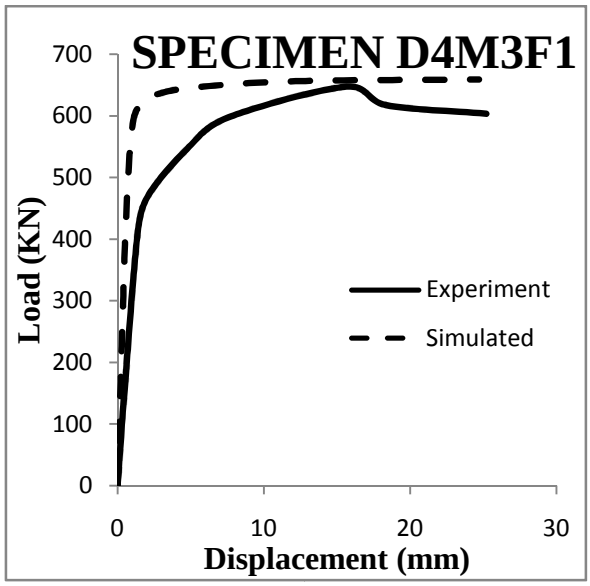

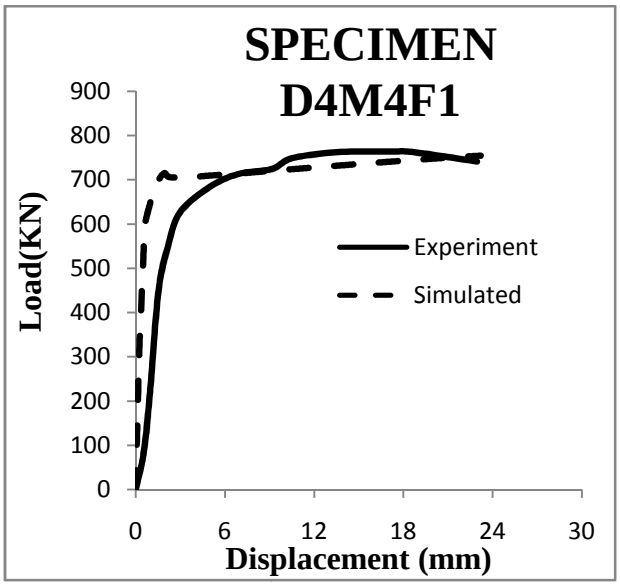

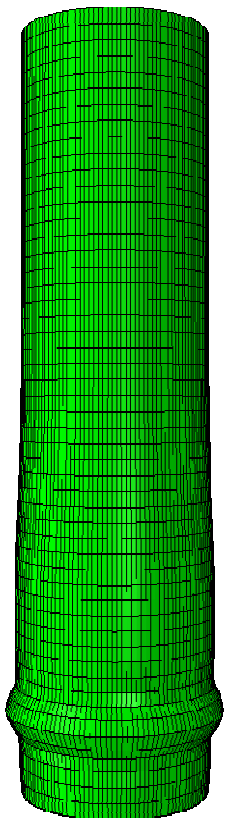

Experiment **Simulated**

Figure 4.20(f) (Gupta et al., 2007)

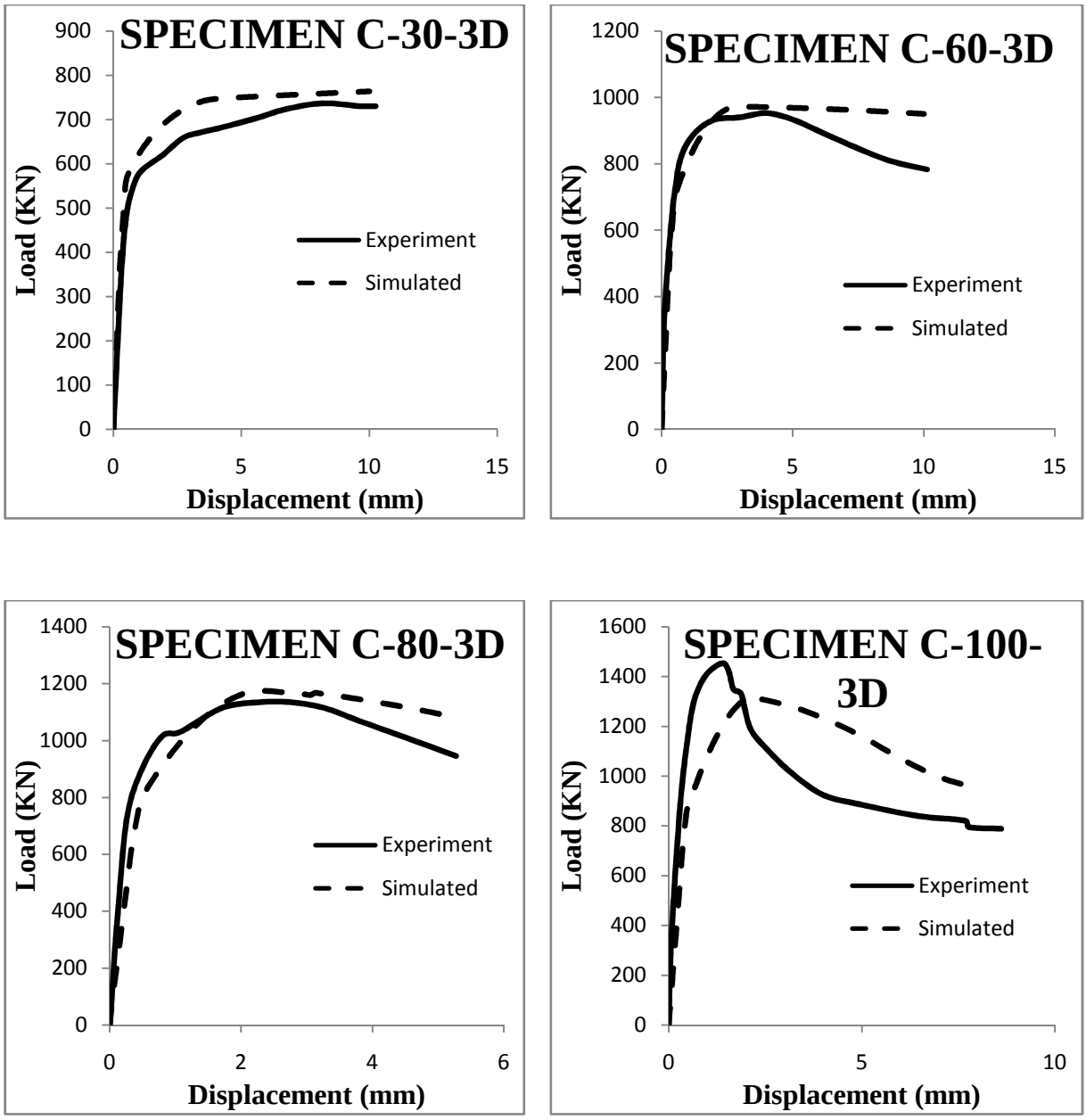

Figure 4.20(g) (Oliveira et al., 2009)

Table 4.2 lists the details of simulated specimens with square cross-sections. It is required to be mentioned here that the fillet on the corners of square as well as rectangular specimens were considered at sharp edges for simplicity. According to Euro Code 3 (EN 1993, 2005), the influence of rounded corners on sectional properties can be ignored if internal radius of fillet r $\leq$ 5t and r $\leq$ 0.15B.

Table 4.2 Details of simulated square specimens

Specimen ID	L (mm)	B (mm)	t (mm)	f'_c (MPa)	f_y (MPa)	Ultimate Capacity (kN)		Simulated / Experiment	Tested by
						Experimental	Simulated		
S1	611.04	127.3x127.3	3.15	30.454	356	917	1012	1.15	Schneider (1998)
S2	609.12	126.9x126.9	4.34	26.044	357	1095	1133	1.03	
S3	611.04	126.9x127	4.55	23.805	322	1113	1108	0.99	
S5	610.52	126.8x127.2	7.47	23.805	347	2069	2081	1.00	
SU-040	600	200x200	5	27.15	265.8	2312	2119	0.87	(Huang et al. (2002)
SU-070	840	280x280	4	31.15	272.6	3401	3520	1.03	
SU-150	900	300x300	2	27.2	341.7	3062	2945	1.03	
CR4-A-4-1	444	148x148	4.38	40.5	262	1414	1458	0.99	Sakino et al. (2004)
CR4-C-4-1	645	215x215	4.38	41.1	262	2424	2415	1.06	
CR4-D-4-1	969	323x323	4.38	41.1	262	4950	5131	0.99	
A1	360	120x120	5.8	83	300	1697	2023	1.19	Liu and Gho (2005)
A2	360	120x120	5.8	106	300	1919	2282	1.18	
Average								1.04	
Standard Deviation								0.091	

Figure 4.21(a to d) shows the load-displacement curves for simulated square specimens against the corresponding experimental specimens. It can be concluded from Figure 4.21 that the proposed model predicts the compression process of square columns with good accuracy. Moreover, it can be concluded from Table 4.2 that the proposed model predicts with good accuracy the ultimate axial capacities of square specimens. The predicted capacities were about 1.04 times, in average, of the measured values with standard deviations of 0.091.

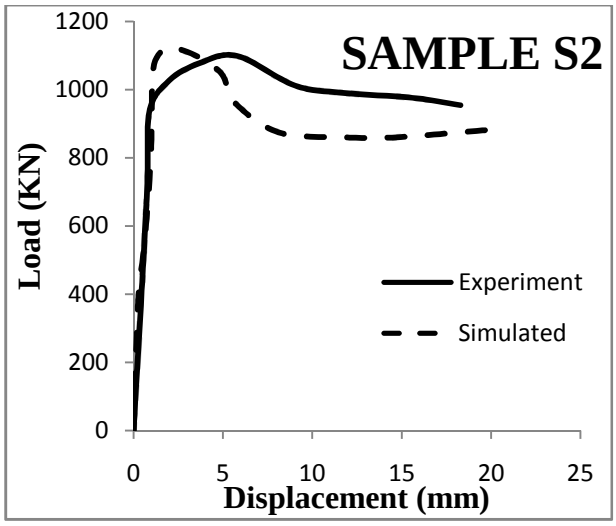

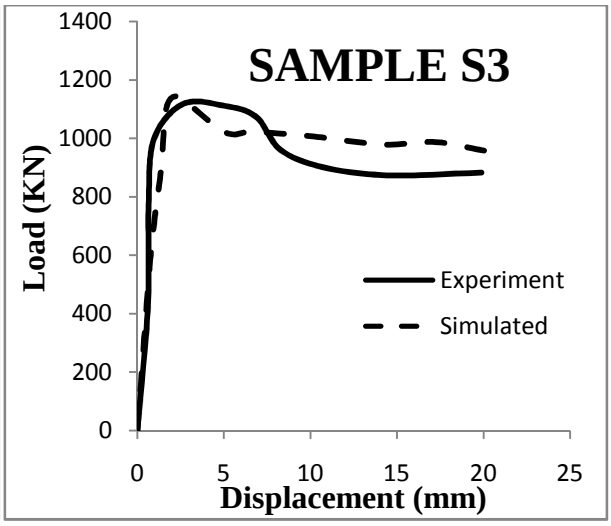

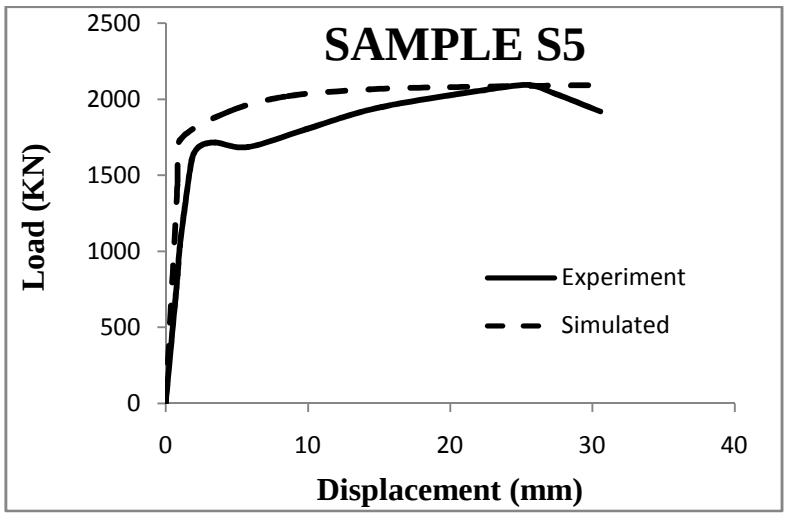

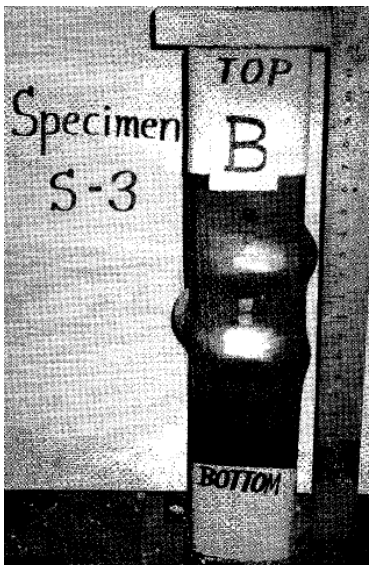

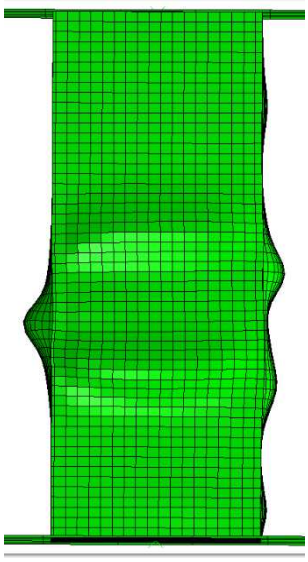

Experimental **Simulated**

Figure 4.21(a) (Schneider,1998)

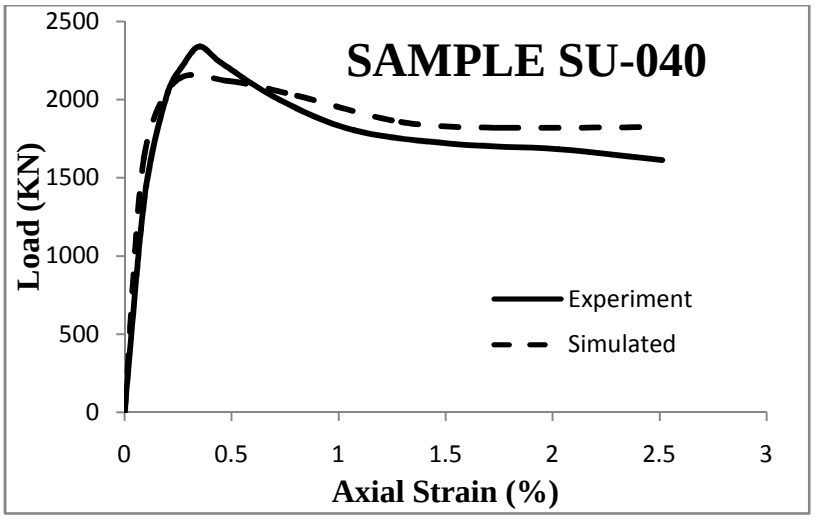

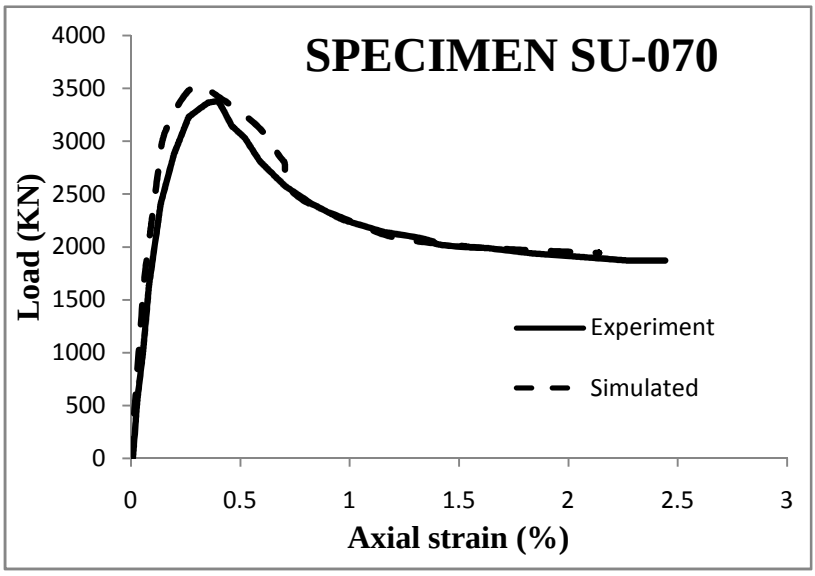

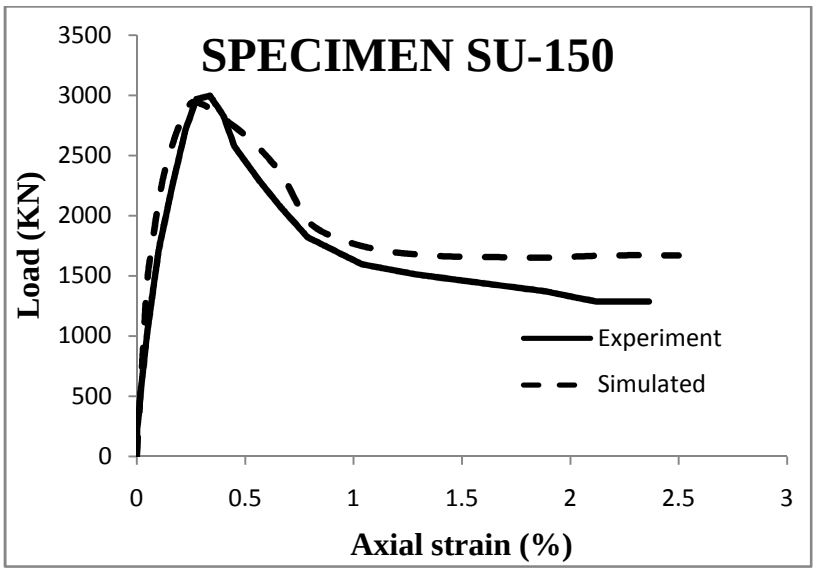

Figure 4.21(b) (Huang et al., 2002)

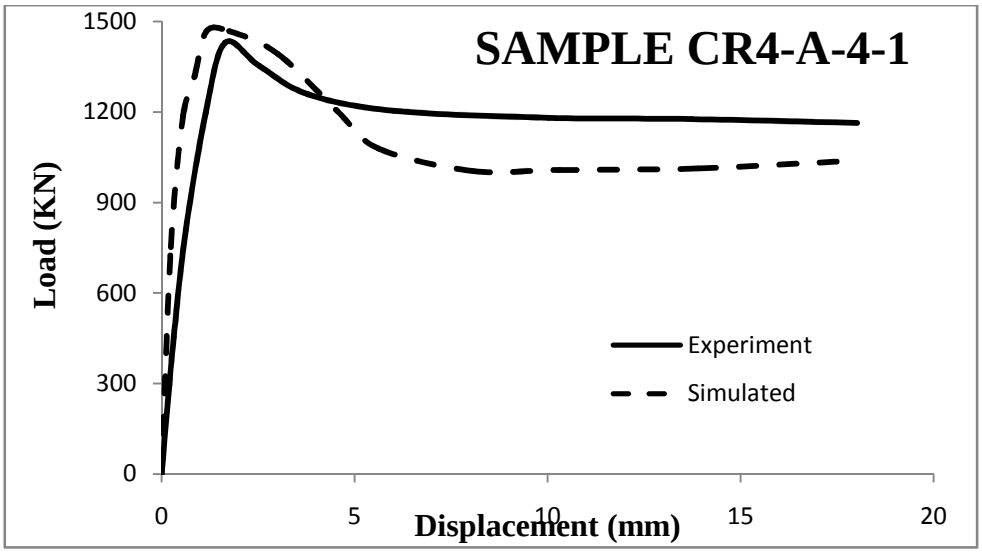

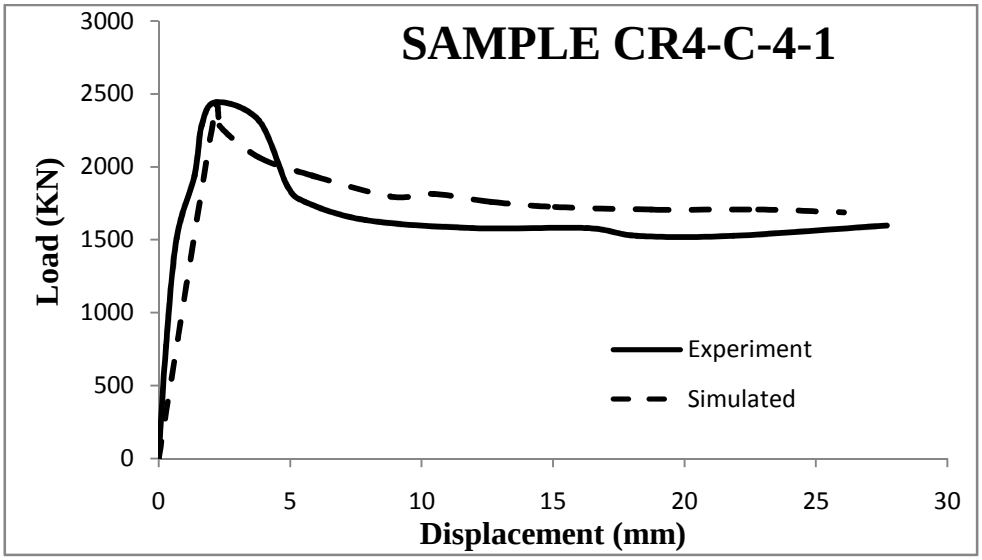

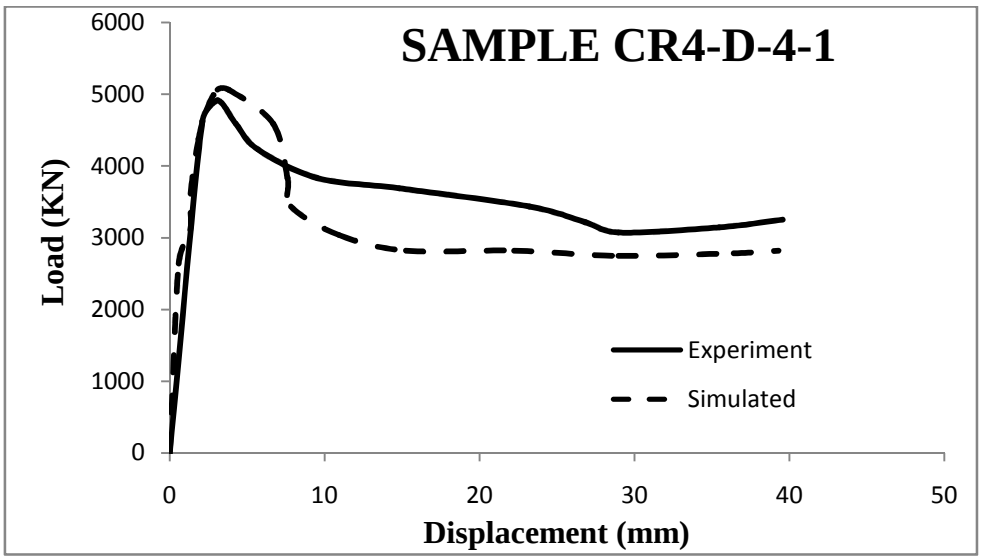

Figure 4.21(c) (Sakino et al., 2004)

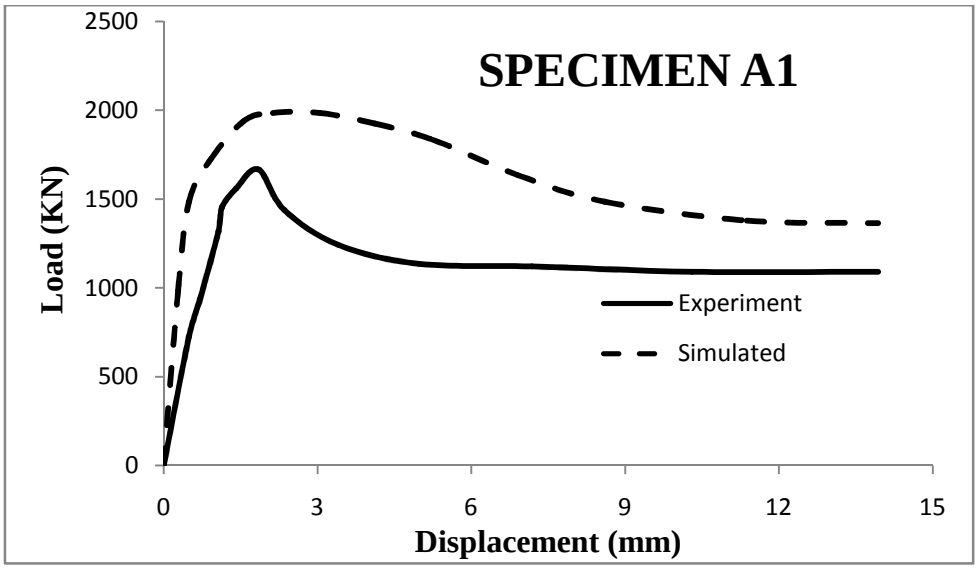

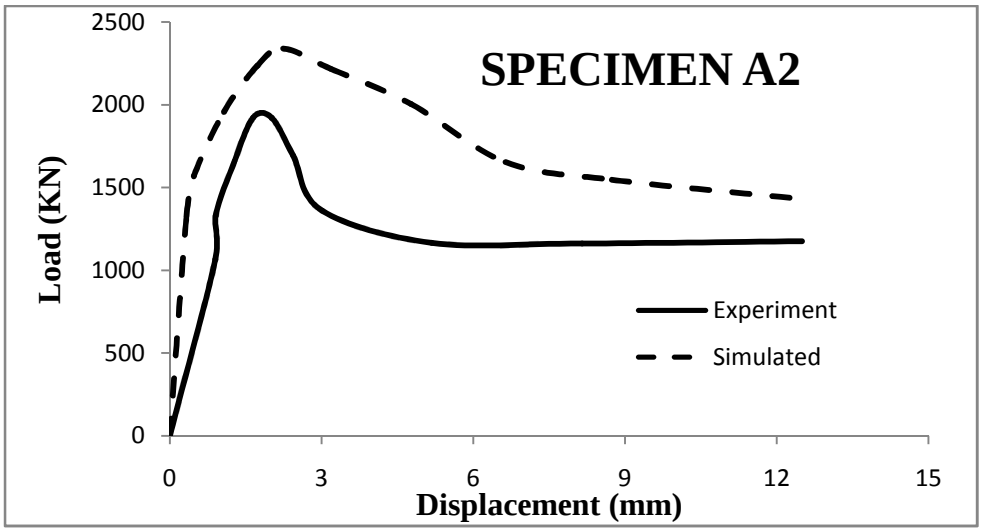

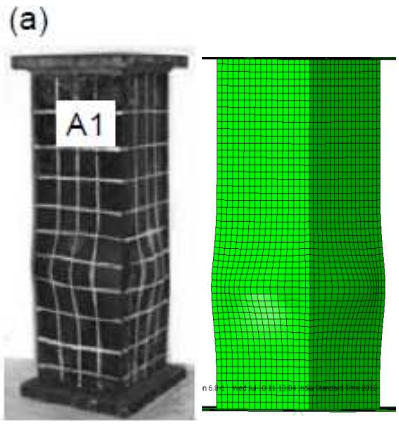

Experimental **Simulated**

Figure 4.21(d) (Liu and Gho, 2005)

Characteristics of simulated specimens with rectangular cross-section are presented in Table 4.3. Numerical load-displacement curves are compared against the experimental curve in Figure 4.22 (a to d). It can be concluded from Figure 4.22 that the proposed model is capable to predict the compression behaviour of rectangular columns with accepted accuracy. However, it can also be concluded from Figure 4.22 and Table 4.3 that the proposed model underestimates the ultimate capacities of rectangular specimens having relatively bigger cross-sections and higher aspect ratios.

Table 4.3 Details of simulated rectangular specimens

Specimen Label	Tested by	B/H	f_c (MPa)	Exp. Peak Axial Load P_{exp} (KN)	ABAQUS Peak Axial Load P_{abq} (KN)	P_{abq} / P_{exp}
R2	Schneider (1998)	2.0	26.044	1006	1022	1.015
R4		1.5	23.805	1224	1164	0.951
R5		1.5	23.805	1335	1307	0.979
R6		1.5	23.805	1691	1630	0.964
rc4-1	Han (2002)	1.1	59.30*	1420	1188	0.837
rc6-1		1.3	59.30*	640	561	0.876
rc8-1		1.3	59.30*	1044	863	0.826
rc10-1		1.3	59.30*	1820	1607	0.883
rc11-1		1.5	59.30*	760	677	0.890
C6-1	Liu et al (2003)	1.5	60.8	1560	1541	0.988
C9-2		2.0	72.1	1820	1758	0.966
A-4-1	Liu et al (2004)	1.3	83	1601	1655	1.034
A-5-1		1.3	106	1854	1903	1.027
A-8-1		1.8	106	2287	2459	1.075
A-10-1		1.5	55	1815	1732	0.954
A-14-1		1.9	55	2038	2060	1.010
Average						0.954
Standard Deviation						0.0733

*Cube compressive strength of concrete; unless mentioned specifically, f_c is cylinder strength of concrete

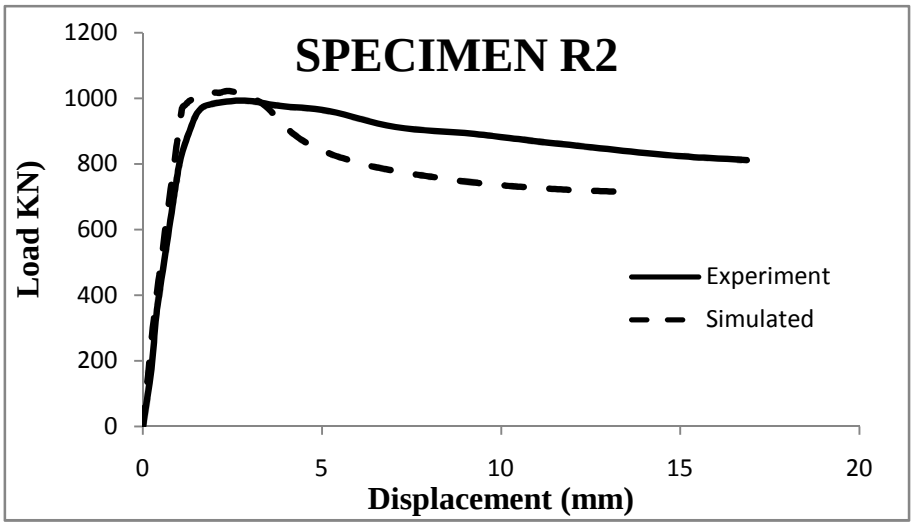

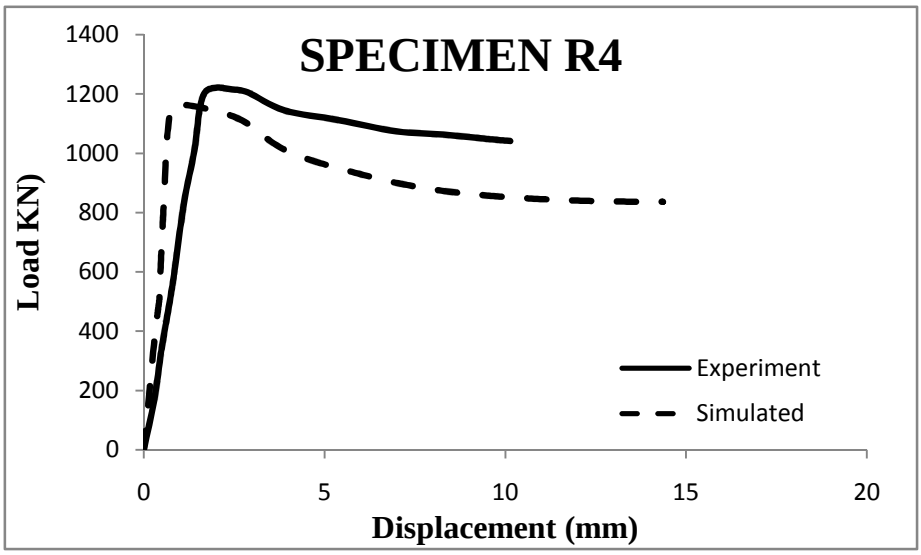

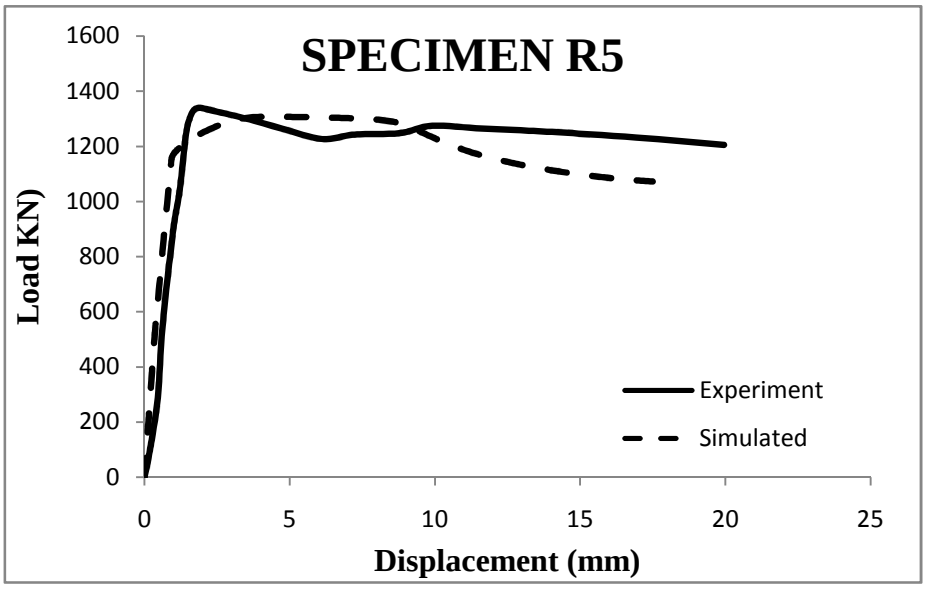

Figure 4.22(a) Schneider et al. (1998)

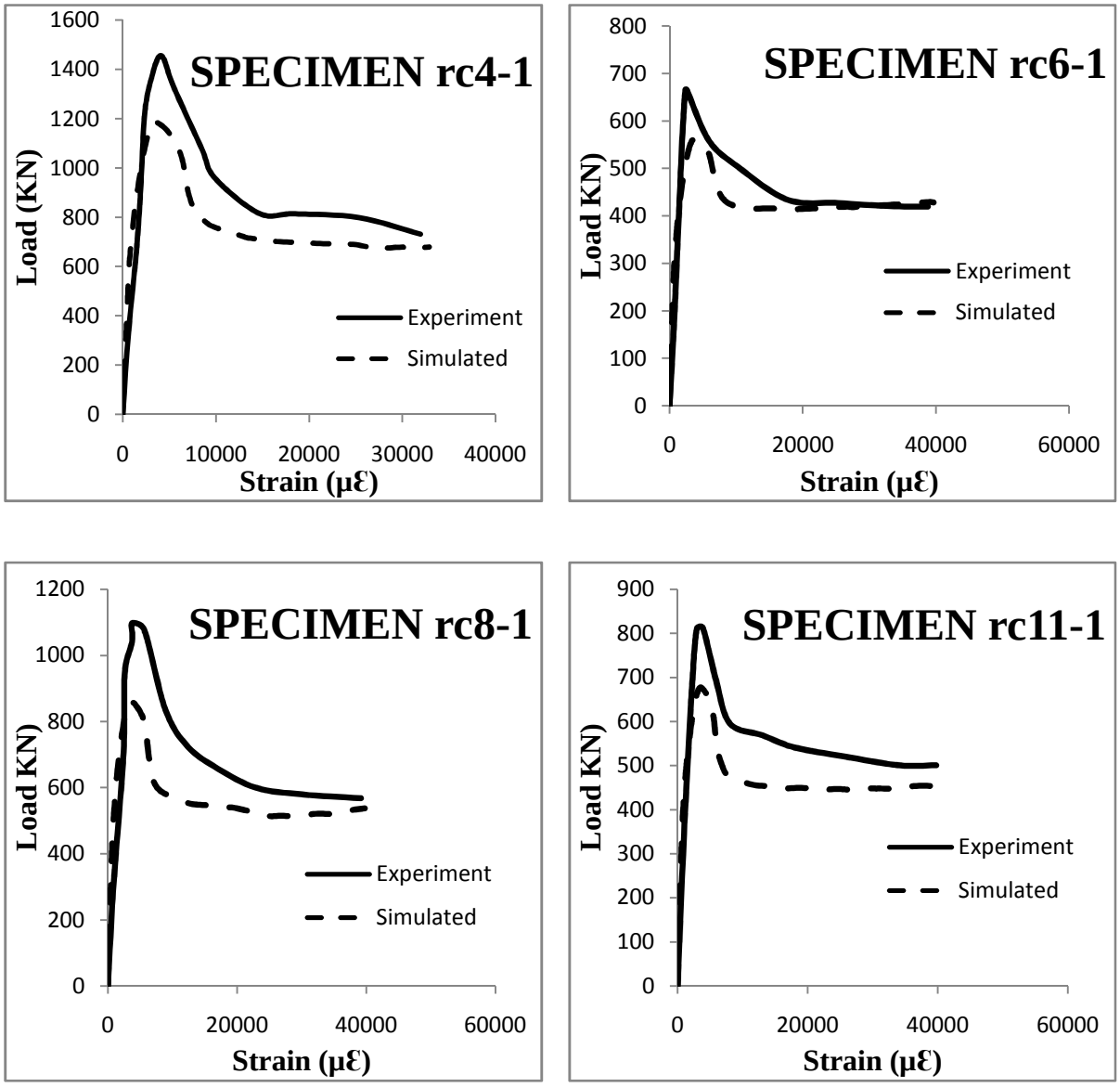

Figure 4.22(b) Han (2002)

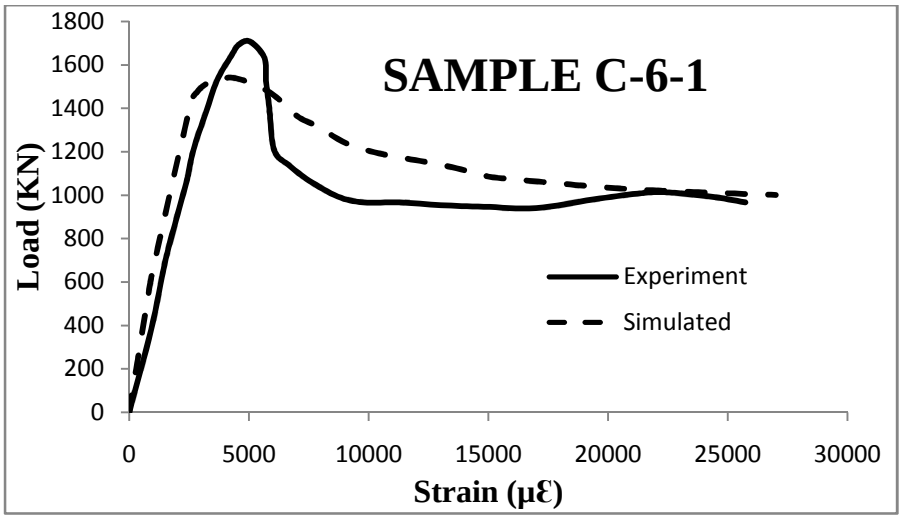

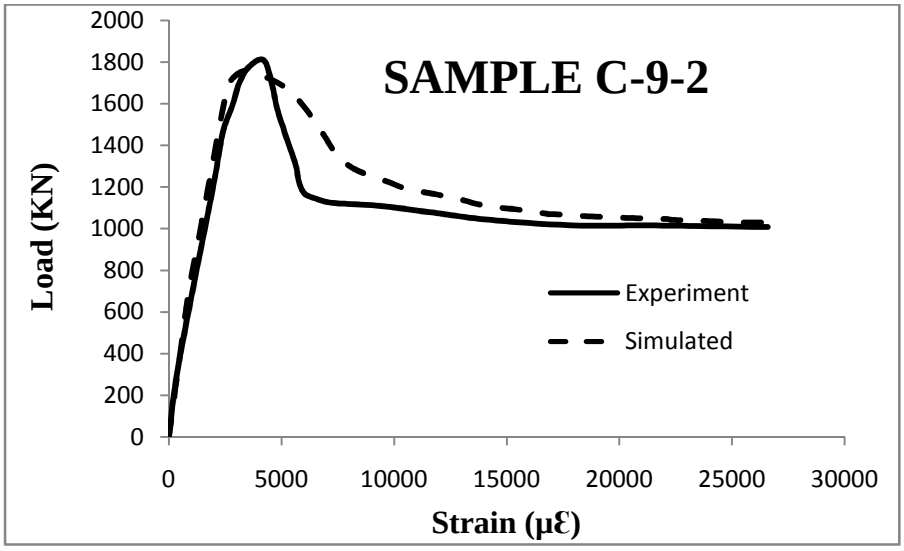

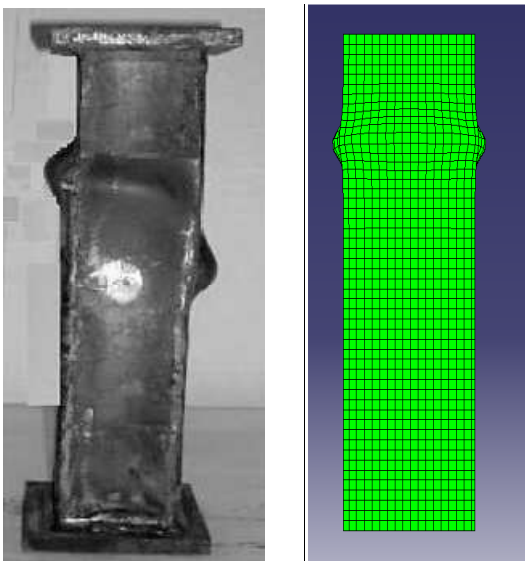

Experimental **Simulated**

Figure 4.22(c) Liu et al. (2003)

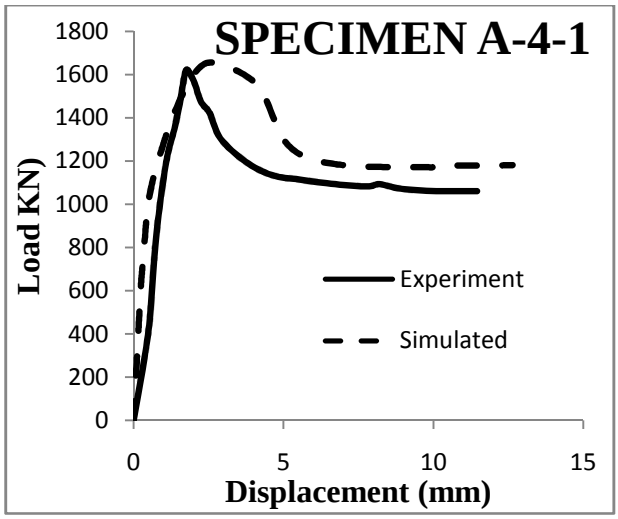

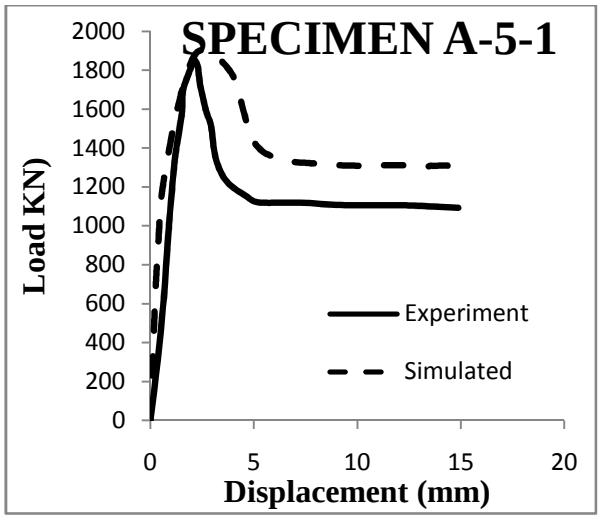

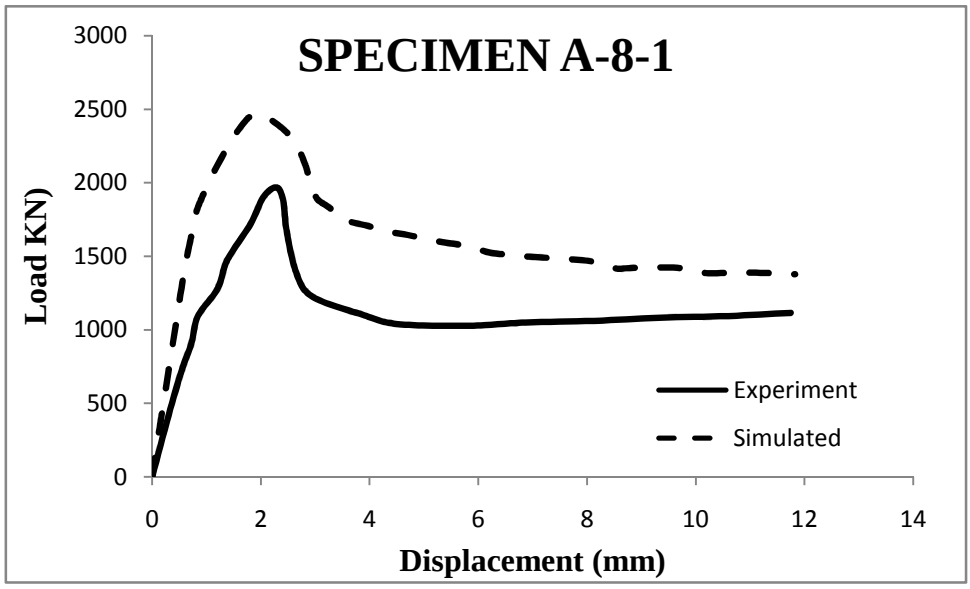

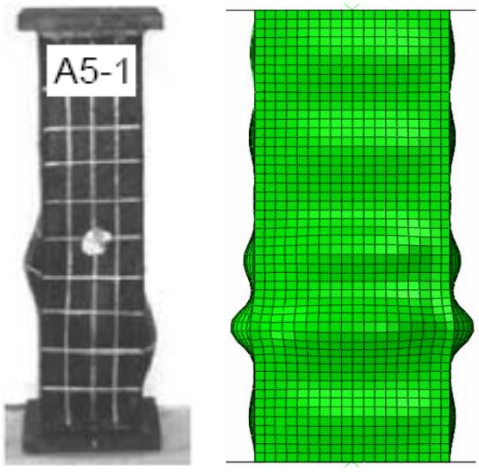

Experimental **Simulated**

Figure 4.22(d) Liu et al. (2004)

4.9 CONCLUSIONS

A three-dimensional nonlinear Finite Element model for simulating the behaviour of circular, square and rectangular Concrete Filled Steel Tube (CFST) columns is presented in this chapter. An effort was made to provide a detailed procedure for Finite Element modelling and simulations of such columns using commercial software package ABAQUS 6.8. Composite action is modeled between concrete core and steel tube. Suitable constitutive models were used for simulating the behaviour of concrete in confinement. The proposed model was then verified by comparing its numerical results with selected experimental results available in literature. Based on the verification of the proposed models, it can be concluded that the proposed model is able to capture the deformation behaviour of such columns. It can also be concluded that the proposed models are capable to predict the load carrying capacity of tubular specimens.

The proposed models will be used to simulate, and investigate the specimens tested in this thesis. In the coming chapters, the models will initially be applied to model single skin CFST members. The proposed models will also be extended to be applicable to simulate the specimens with different core configurations, i.e. RCC-CFST and CFDST.

CHAPTER FIVE

COLUMNS WITH CIRCULAR CROSS-SECTIONS

5.1 GENERAL

The experimental and computational investigations on circular tubes filled with concrete are presented in this chapter. A total of Thirty Seven specimens consisting of three different types; Concrete Filled Steel Tube (CFST) (Figure 3.3); Concrete Filled Double Steel Tube (CFDST) (Figure 3.4) and Reinforced Concrete Filled Steel Tube (RCC-CFST) (Figure 3.5) were cast and tested under axial loading. Specimens with varying outer diameters (D), thicknesses (t) and lengths (L) were tested to study the effect of these parameters on structural response of the tubular columns. The CFST specimens were also modeled using the Finite Element model presented in Chapter 4. The developed model was used to investigate the variation of lateral confining pressure along the height and cross-section of some typical columns. Finally, a novel concept named Digital Image Correlation of experimental specimen has been introduced and compared with results from numerical simulations.

5.2 DETAILS OF SPECIMENS

Circular Composite columns of three different core configurations viz. Nineteen Concrete Filled Steel Tubular (CFST), Thirteen Concrete Filled Double Skin Tubular Columns (CFDST) and Five Reinforced Concrete Filled Steel Tubular Columns (RCC-CFST) were tested in axial loading. Table 3.3 presents the Material properties of circular steel tubes used for preparing the specimens. Labeling of circular specimens used in this chapter is explained in Table 5.1.

Four length categories were used for CFST specimens. From these, two length categories were designed to obtain short specimens. The short specimens have been designated nominally here as L3D and L4D specimens. The two remaining length categories were designed to obtain intermediate specimens which have been designated nominally as L7D and L10D specimens. Moreover, for each of these length categories, three different diameters have been used, with three different thicknesses for every diameter. Geometric Properties of CFST specimens are given in Table 5.2

Table 5.1 Labelling of circular specimens

Typical ID: CPQ-L-M-N		
Character	Denotes	Value
C	Circular specimen	
P	Core configuration	S: CFST
		R: RCC-CFST
		D: CFDST
Q	Length Category	1: L3D and L4D
		2: L7D
		3: L10D
L	Outer diameter of outer steel tube	1: 114.3 mm
		2: 165.1 mm
		3: 90.00 mm
M	Thickness of steel tube with diameter "D"	1: first thickness
		2: second thickness
		3: third thickness
N	Specimen number. with same details	1: first specimen
		2: repeated (second) specimen

For CFDST specimens, two length categories L3D and L7D were designed. Two diameters were used with three different thicknesses for each diameter. The same inner steel tube was used in all the CFDST specimens. Outer diameter and thickness of inner steel tube were 48.3 mm and 3.04 mm. The yield stress and area of steel were 479 MPa and 432 mm^2, respectively. The hollow volume between the two concentric steel tubes was filled with concrete.The inner volume of inner steel tube was kept as hollow to obtain CFDST specimens with lighter weights. Geometric details of CFDST specimens are given in Table 5.3.

Two length categories were used For RCC-CFST specimens,. The first length category was short columns designated nominally as L3D specimens. The second length category was designed to obtain intermediate specimens and designated as L7D specimens. Two different diameters with two different thicknesses for each diameter have been used for the RCC-CFST core configuration. The amount of reinforcement in RCC-CFST specimens were so selected that the sum total of area of steel tube and reinforcement in the specimens with lower wall thicknesses will almost equal the area of steel tube in CFST specimen with higher wall thickness. This was done to maintain a constant total area of steel (area of steel tube plus area of rebars) while examining the effect of redistribution of this area. There was a marginal difference in the total steel areas depending on the commercially available sizes of steel tubes and rebars.

Table 5.2 Details of circular CFST specimens

Length Category		Specimen ID	L (mm)	D (mm)	t (mm)	D/t	L/D	f_y (MPa)
Short specimens	L3D	CS1-1-1-1	380	114.3	3.4	33.62	3.32	430
		CS1-1-2-1	380	114.3	4.2	27.21	3.32	428
		CS1-1-3-1	380	114.3	5.06	22.59	3.32	427
		CS1-2-1	500	165.1	4.28	38.57	3.03	423
		CS1-2-2-1	500	165.1	5.03	32.82	3.03	423
		CS1-2-2-2	500	165.1	5.03	32.82	3.03	423
	L4D	CS1-3-1	360	90	3.0	30.00	4.00	308
		CS1-3-2	360	90	3.8	23.68	4.00	308
		CS1-3-3	360	90	4.5	20.00	4.00	308
Intermediate specimens	L7D	CS2-1-1	900	114.3	3.4	33.62	7.87	430
		CS2-1-2	900	114.3	4.2	27.21	7.87	428
		CS2-1-3-1	900	114.3	5.06	22.59	7.87	427
		CS2-1-3-2	900	114.3	5.06	22.59	7.87	427
		CS2-3-1	630	90	3.0	30.00	7.00	308
		CS2-3-2	630	90	3.8	23.69	7.00	308
		CS2-3-3	630	90	4.5	20.00	7.00	308
	L10D	CS3-3-1	900	90	3.0	30.00	10.00	308
		CS3-3-2	900	90	3.8	23.68	10.00	308
		CS3-3-3	900	90	4.5	20.00	10.00	308

The reason behind such design was to study the difference in behaviour of specimens having same area of steel but two different core configurations (i.e. CFST and RCC-CFST).. Such comparison is useful in two cases;

a) If the required thickness of steel tube is not commercially available, a smaller size of steel tube can be used based on the commercial availability. The remaining area of steel can be provided using longitudinal reinforcement bars to achieve the target area of steel
b) The use of reinforcing bars inside such composite columns helps to facilitate the connections between columns and RCC beams or RCC footings. Table 5.4 gives the details of RCC-CFST specimens.

Table 5.3 Details of circular CFDST specimens

Length Category		ID	L (mm)	D_o (mm)	t_o (mm)	$(D/t)_o$	$(L/D)_o$	f_{yo} (MPa)
Short specimens	L3D	CD1-1-1	380	114.3	3.40	33.62	3.32	430
		CD1-1-2	380	114.3	4.20	27.21	3.32	428
		CD1-1-3	380	114.3	5.06	22.59	3.32	427
		CD1-2-1-1	500	165.1	4.28	38.57	3.03	423
		CD1-2-1-2	500	165.1	4.28	38.57	3.03	423
		CD1-2-2-1	500	165.1	5.03	32.82	3.03	423
		CD1-2-2-2	500	165.1	5.03	32.82	3.03	423
Intermediate specimens	L7D	CD2-1-1-1	900	114.3	3.40	33.62	7.87	430
		CD2-1-1-2	900	114.3	3.40	33.62	7.87	430
		CD2-1-2-1	900	114.3	4.20	27.21	7.87	428
		CD2-1-2-2	900	114.3	4.20	27.21	7.87	428
		CD2-1-3-1	900	114.3	5.06	22.59	7.87	427
		CD2-1-3-2	900	114.3	5.06	22.59	7.87	427

Table 5.4 Details of circular RCC-CFST specimens

Length Category		ID	L (mm)	D (mm)	t (mm)	Reinf. (mm)	D/t	L/D	f_y (MPa)	f_{yr} (MPa)
Short specimens	L3D	CR1-1-1	380	114.3	3.4	8Ø10	33.62	3.32	430	550
		CR1-1-2	380	114.3	4.2	4Ø10	27.21	3.32	428	550
		CR1-2-1	500	165.1	4.28	4Ø12	38.57	3.03	423	550
Intermediate specimens	L7D	CR2-1-1	900	114.3	3.4	8Ø10	33.62	7.87	430	550
		CR2-1-2	900	114.3	4.2	4Ø10	27.21	7.87	428	550

Normal concrete having of M30 grade has been used to fill all the tested samples. The cube strength of infill concrete was 42.16 MPa cube and cylinder strength was 32.05 MPa as presented in Table 5.5. Details of concrete mix proportions are given in Table 3.1.

Table 5.5 Compressive strength (MPa) of concrete core

Group No.	Age (days)	Cube Strength	Average	Cylinder Strength	Average
1	28	39.78	40.15	30.56	30.84
		40.03		31.12	
		40.66		-	
2	48	40.8	41.61	31.72	31.67
		40.91		32.62	
		42.17		-	
3	60	42.65	42.33	32.28	32.50
		41.21		32.72	
		42.87		-	
4	72	43.10	43.65	32.31	32.69
		43.64		33.07	
		44.20		-	
Average			42.16		32.05

5.3 RESULTS

5.3.1 Mode of Deformation

Figures 5.1(a), (b) and (c) show the tested circular single skin (CFST), circular double skin (CFDST) and Reinforced concrete tubular specimens (RCC-CFST) specimens, respectively. Figures 5.2, 5.3 and 5.4 show experimental and numerical deformed shapes for various CFST, CFDST and RCC-CFST and specimens, respectively.

For all core configurations, L3D specimens failed due to local buckling of steel tube followed by crushing of adjoining concrete. On the other hand, global buckling initiated from mid height of the specimens was observed as the primary failure mode in L7D columns.

Figure 5.1(a) Tested circular single skin(CFST) and double skin(CFDST) specimens

Figure 5.1(b) Tested circular RCC-CFST specimens

Experiment **Simulated** **Experiment** **Simulated**

Figure 5.2(a) Comparison of Experimental and Numerical Deflected shapes of short (L3D) 114.3mm diameter CFST columns

Experiment **Simulated**

Figure 5.2(b) Comparison of Experimental and Numerical Deflected shapes of short (L3D) 165.1 mm diameter CFST columns

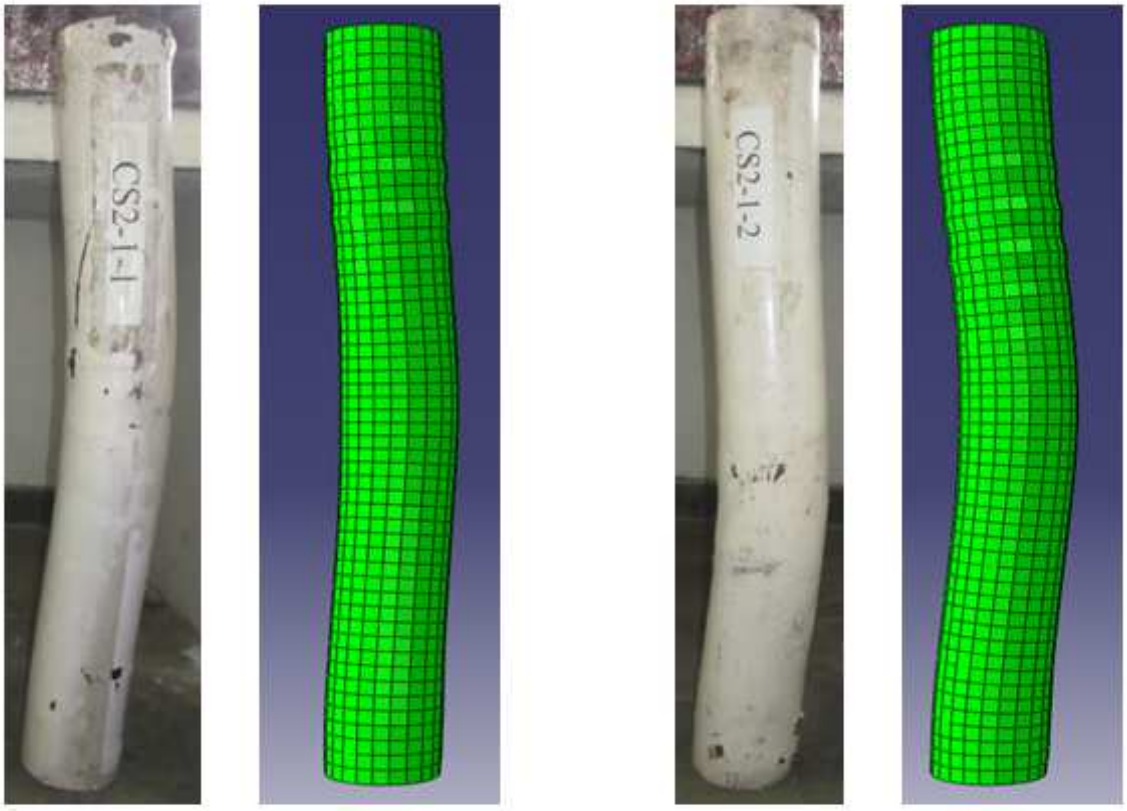

Experiment **Simulated** **Experiment** **Simulated**

Experiment **Simulated**

Figure 5.3 Comparison of Experimental and Numerical Deflected shapes of L7D 114.3 mm diameter CFST columns

Experiment **Simulated** **Experiment** **Simulated**

Experiment **Simulated**

Figure 5.4 Comparison of Experimental and Numerical Deflected shapes of short (L3D) 114.3 mm diameter CFDST columns

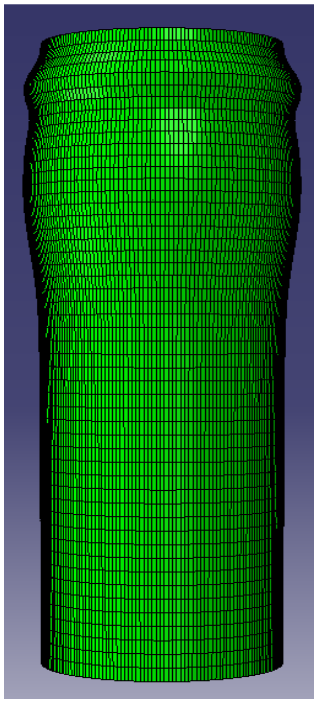

Experiment **Simulated**

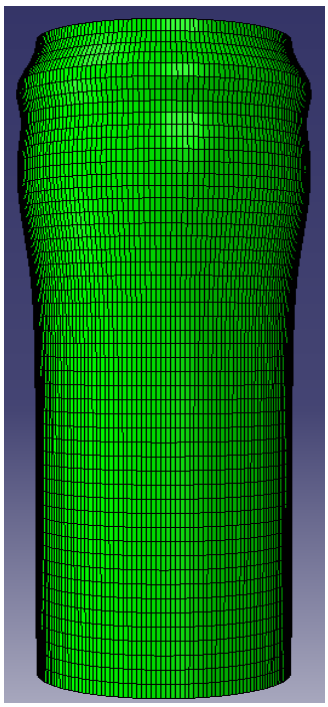

Experiment **Simulated**

Figure 5.5 Comparison of Experimental and Numerical Deflected shapes of short (L3D) 165.1 mm diameter CFDST columns

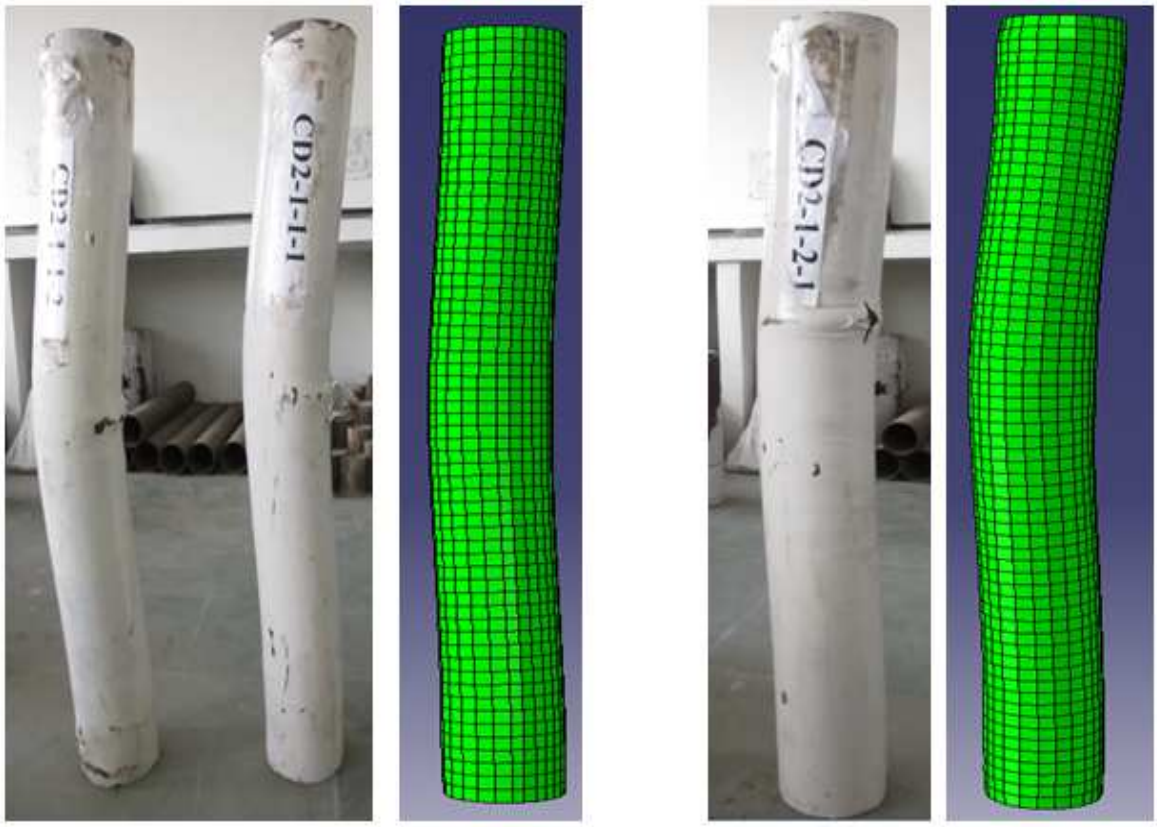

Experiment **Simulated** **Experiment** **Simulated**

Experiment **Simulated**

Figure 5.6 Comparison of Experimental and Numerical Deflected shapes of L7D 114.3 mm diameter CFDST columns

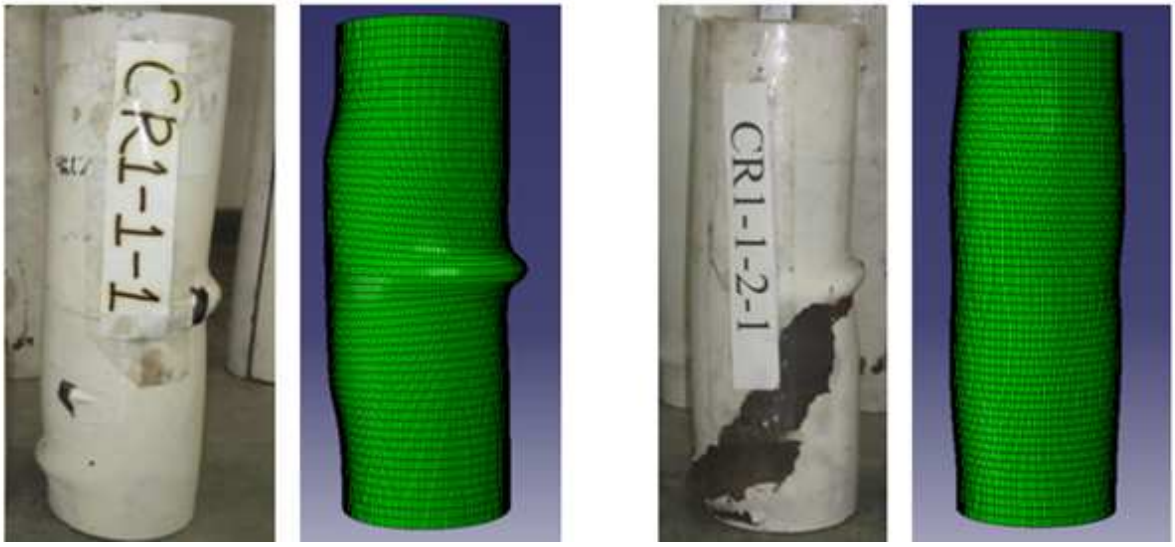

Experiment **Simulated** **Experiment** **Simulated**

Figure 5.7(a) Comparison of Experimental and Numerical Deflected shapes of short (L3D) 114.3 mm diameter RCC-CFST columns

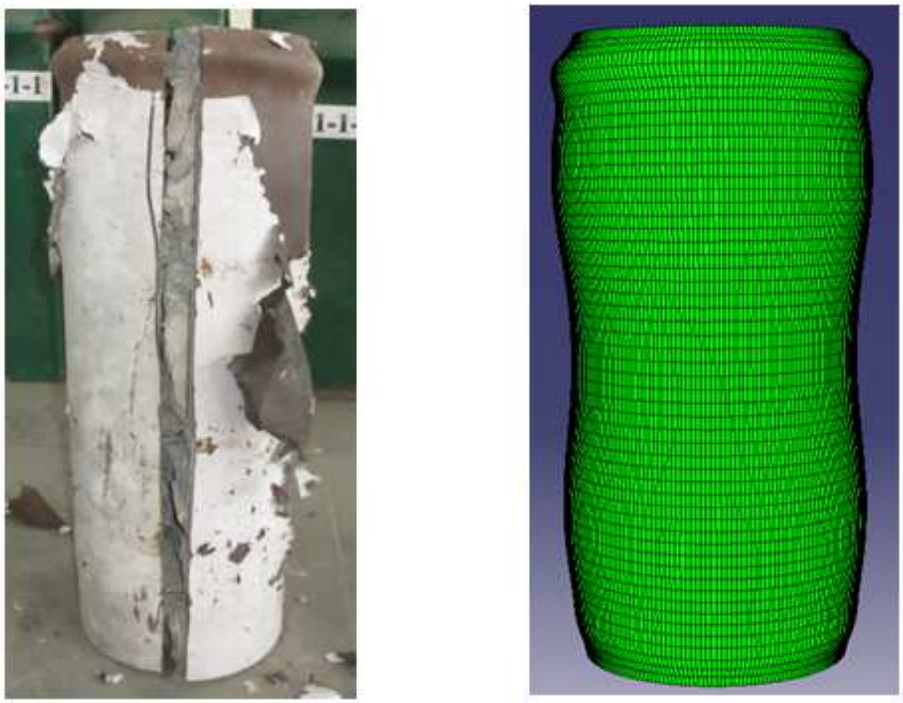

Experiment **Simulated**

Figure 5.7(b) Comparison of Experimental and Numerical Deflected shapes of short (L3D) 165.1 mm diameter RCC-CFST columns

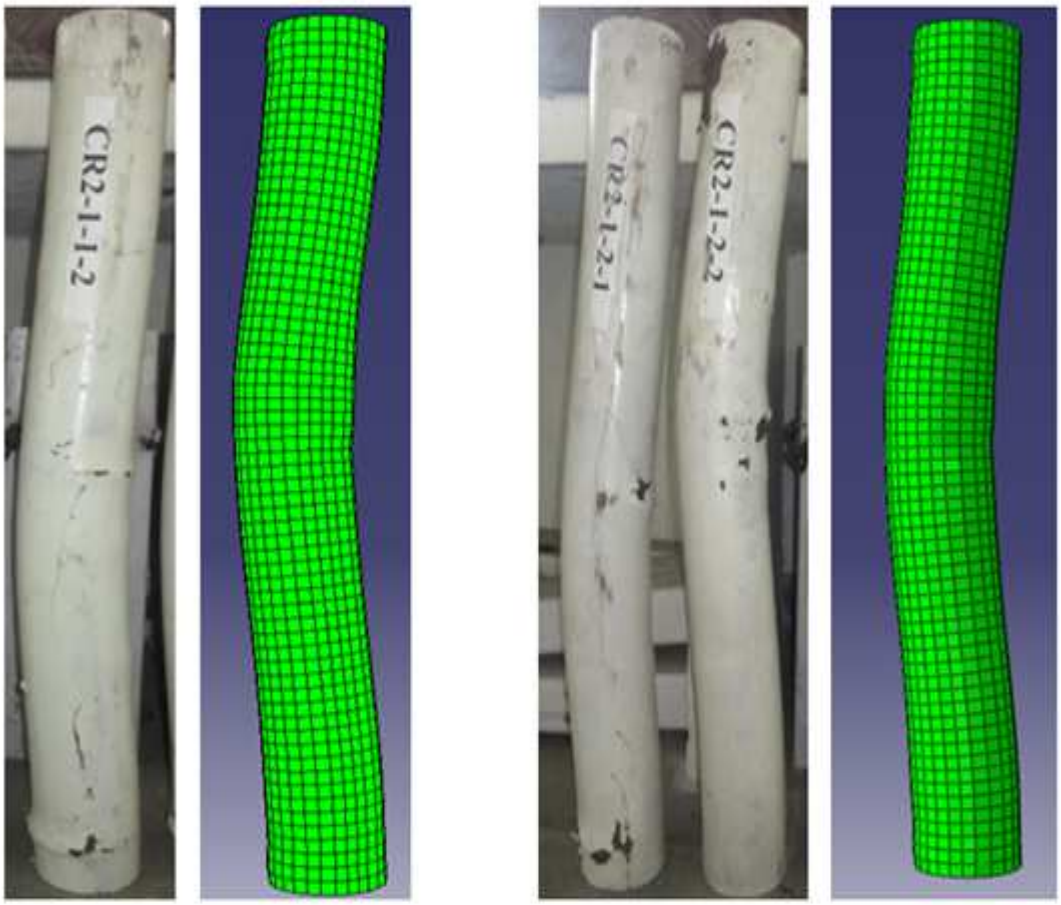

Experiment **Simulated** **Experiment** **Simulated**

Figure 5.8 Comparison of Experimental and Numerical Deflected shapes of L7D 114.3 mm diameter RCC-CFST columns

It can be concluded from Figures 5.2 to 5.8 that the proposed model gives is able to capture the mode of deformation of tubular specimens with different lengths and varying core configurations.

For CFDST specimens with L3D details, the deformed shape was outward local buckling in the outer steel tube (as shown in Figures 5.4 and 5.5) ,while inward local buckling was noticed in the inner steel tube as shown in Figure 5.9 (a).

It was observed that the local buckling generally occurred near the location of tie for RCC-CFST specimens with L3D. To investigate the deformation in the longitudinal reinforcement, steel tube was cut and the concrete was removed carefully using crushing hammer without disturbing the rebars. The deformed shape of rebars was observed to be same of that in RCC columns, i.e. buckling between the ties as observed in Figure 5.9 (b).

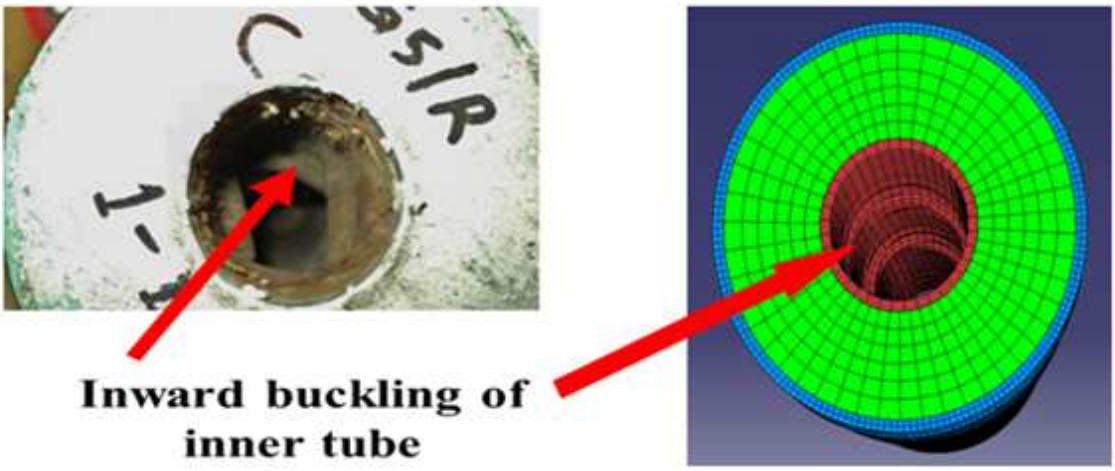

Experiment **Simulated**

Figure 5.9(a) Comparison of Buckling of Inner Tube in CFDST specimens

Buckling of Rebars occurs between the lateral ties

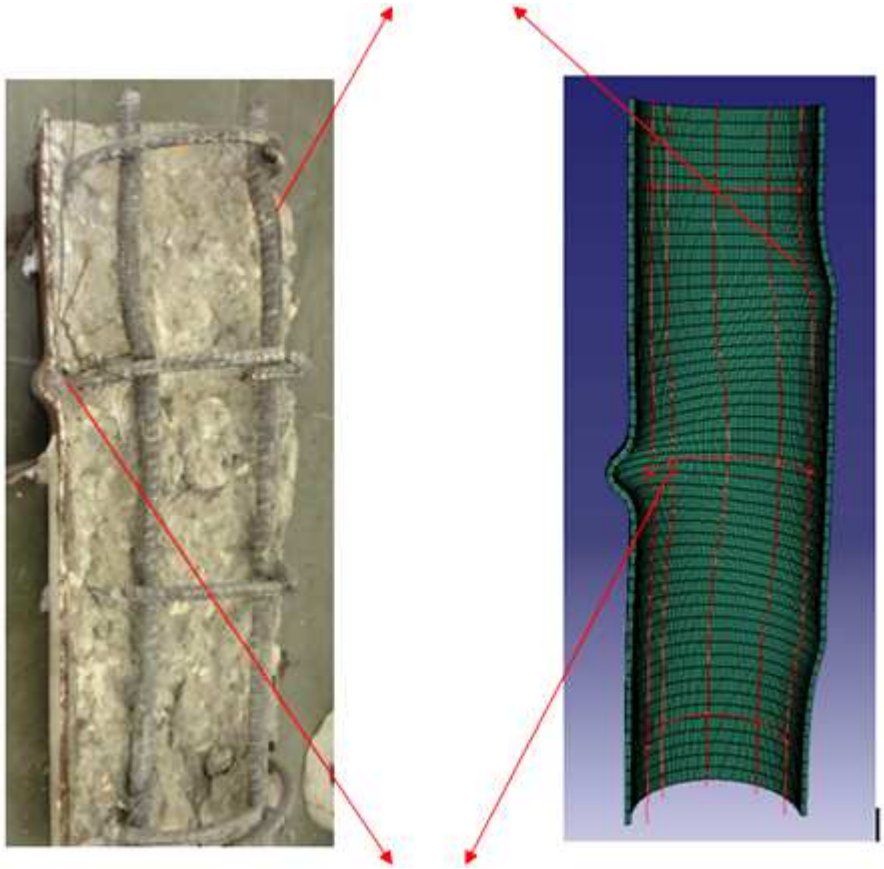

. Figure 5.9(b) Local Buckling of Tube occurs near the Ties in RCC-CFST specimens

5.3.2 Strength

Figures 5.10, 5.11 and 5.12 show experimental and numerical load-displacement curves for CFST, CFDST and RCC-CFST specimens, respectively. It can be concluded from the figures that the axial capacity of specimens increases as the wall thickness of the specimens increases for all diameters, configurations and lengths. It can also be concluded that the proposed model gives acceptable results for load-displacement curves for all specimens and it is applicable to specimens with different lengths and different core configurations.

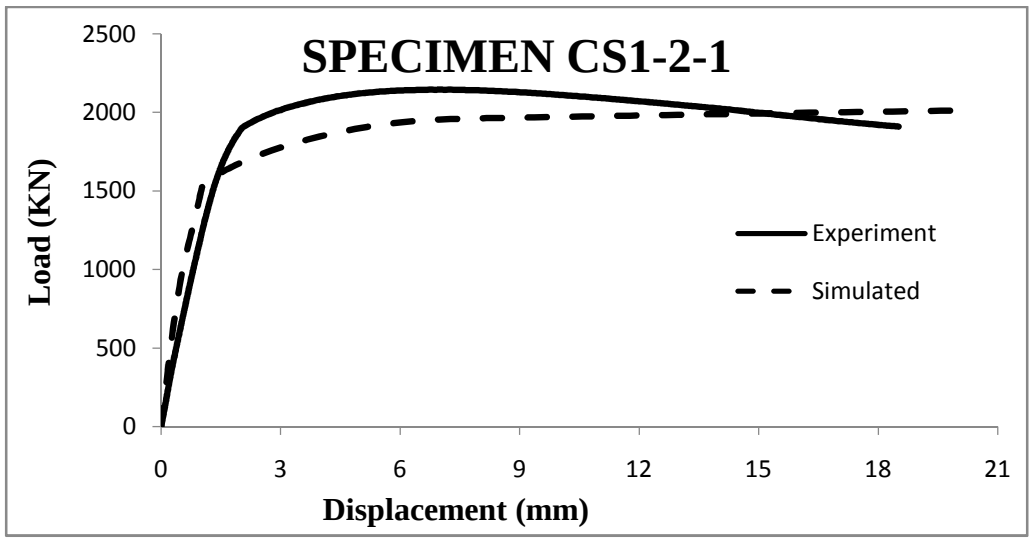

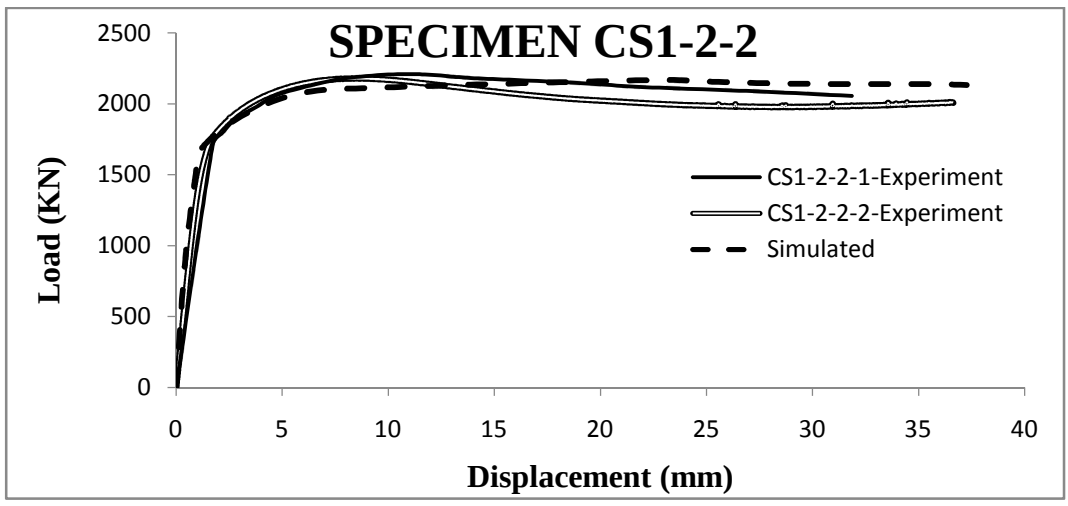

Figure 5.10(a) Comparison of experimental and numerical load-displacement curves for circular L3D CFST specimens, D= 165.1 mm

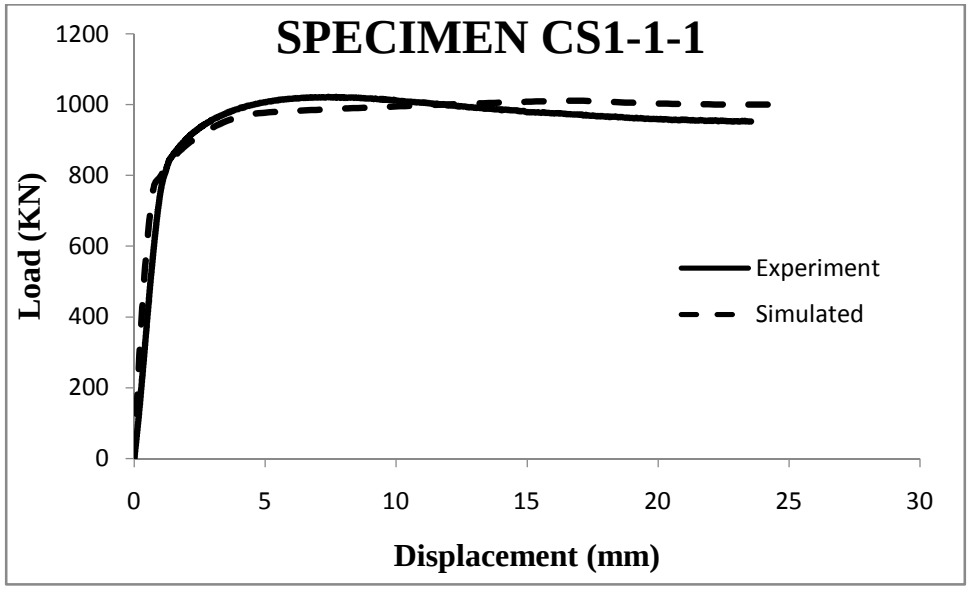

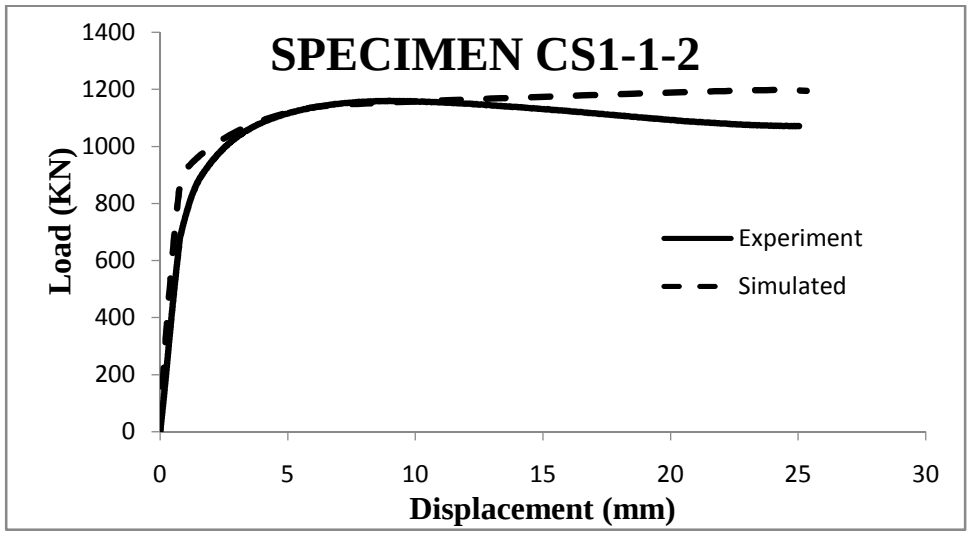

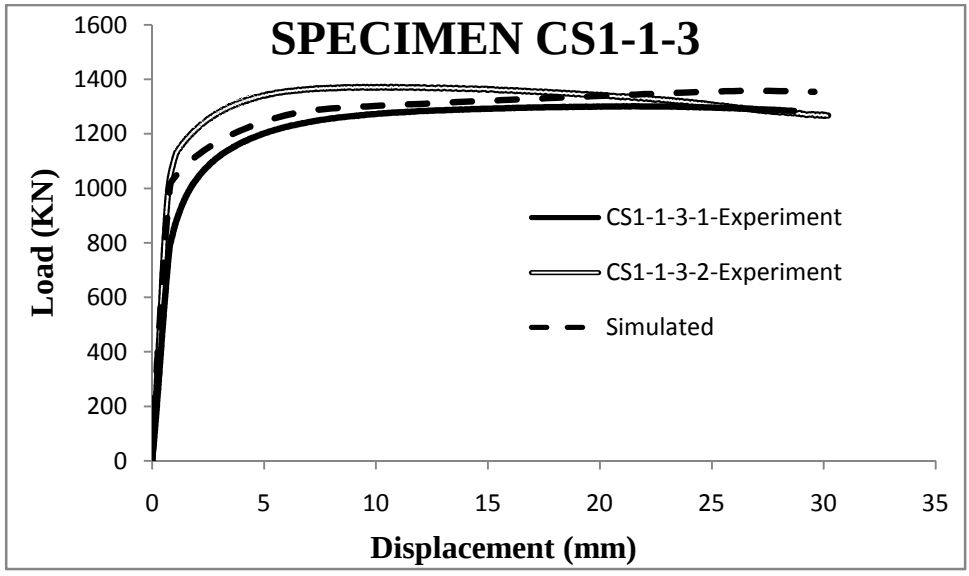

Figure 5.10(b) Comparison of experimental and numerical load-displacement curves for circular L3D CFST specimens, D= 114.3 mm

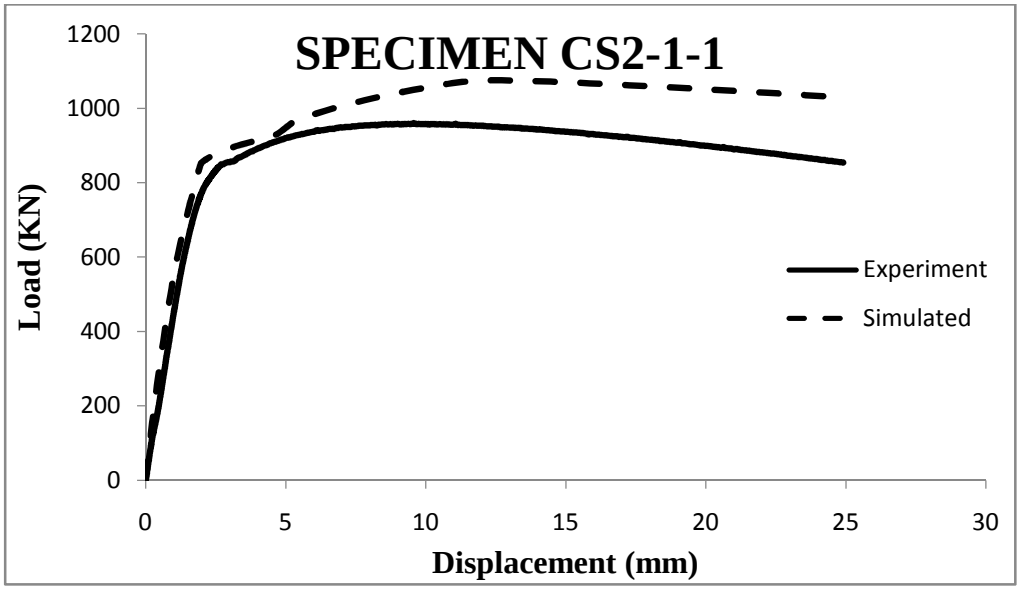

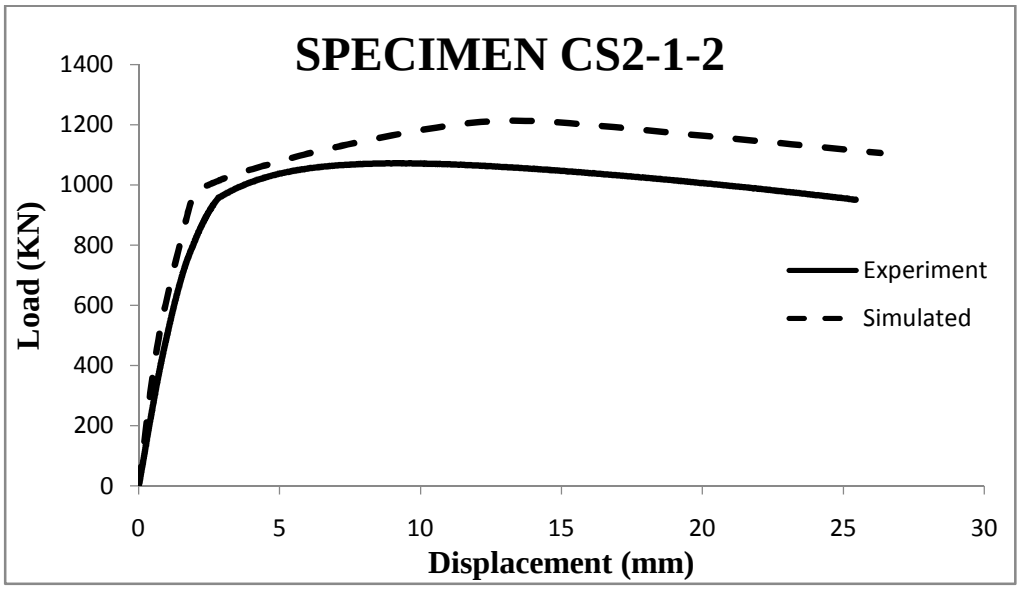

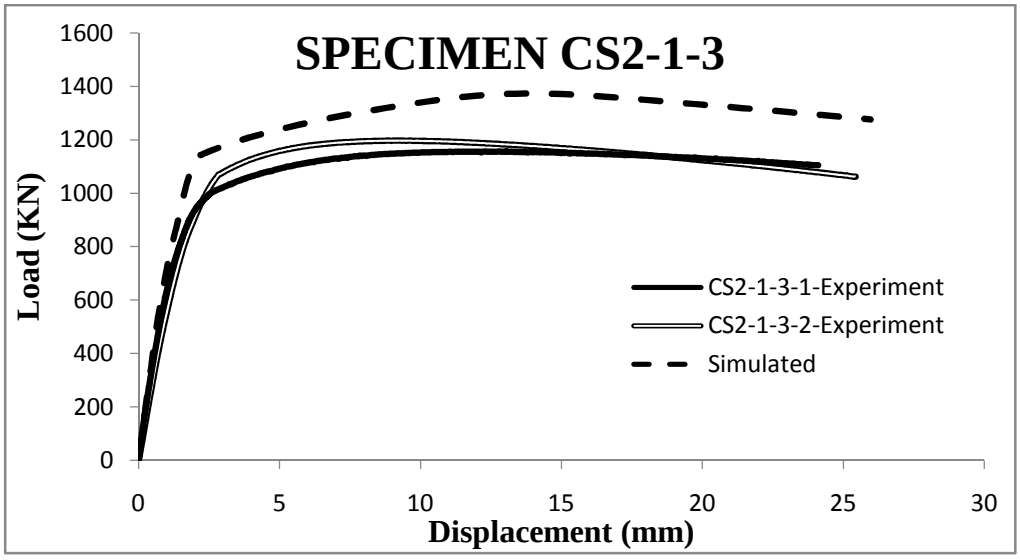

Figure 5.10(c) Comparison of experimental and numerical load-displacement curves for circular L7D CFST specimens, D= 114.3 mm

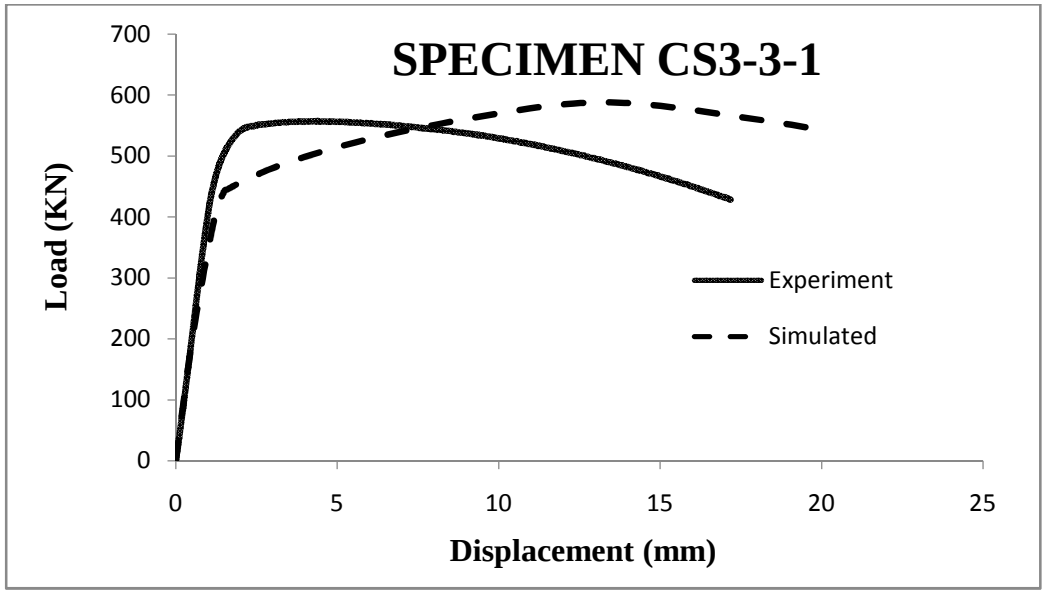

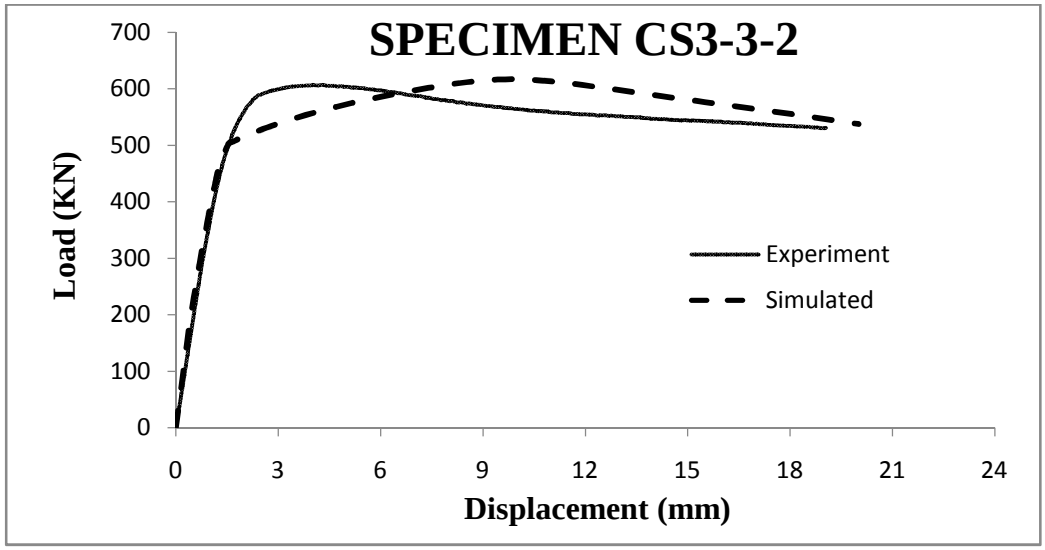

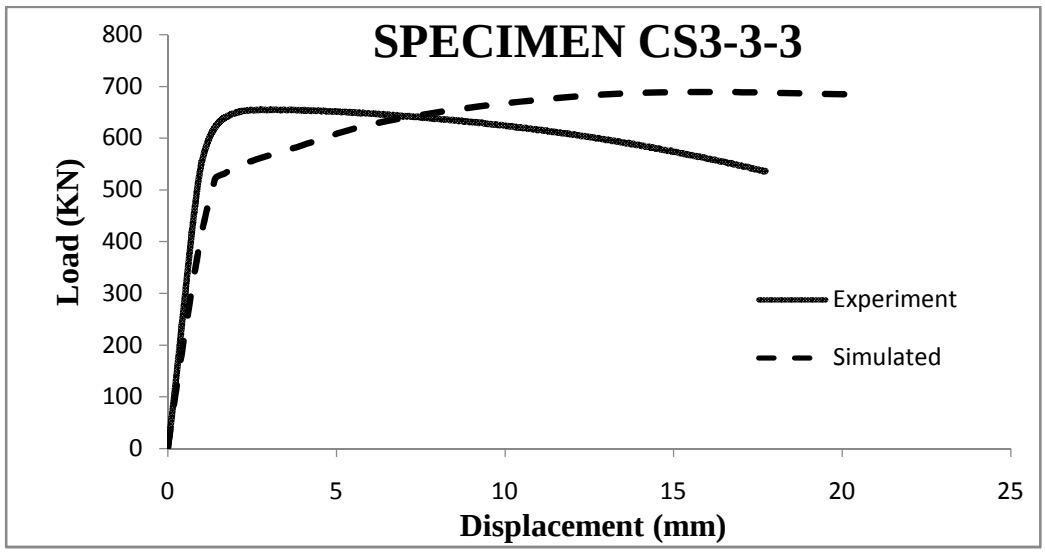

Figure 5.10(d) Comparison of experimental and numerical load-displacement curves for circular L7D CFST specimens, D= 90 mm

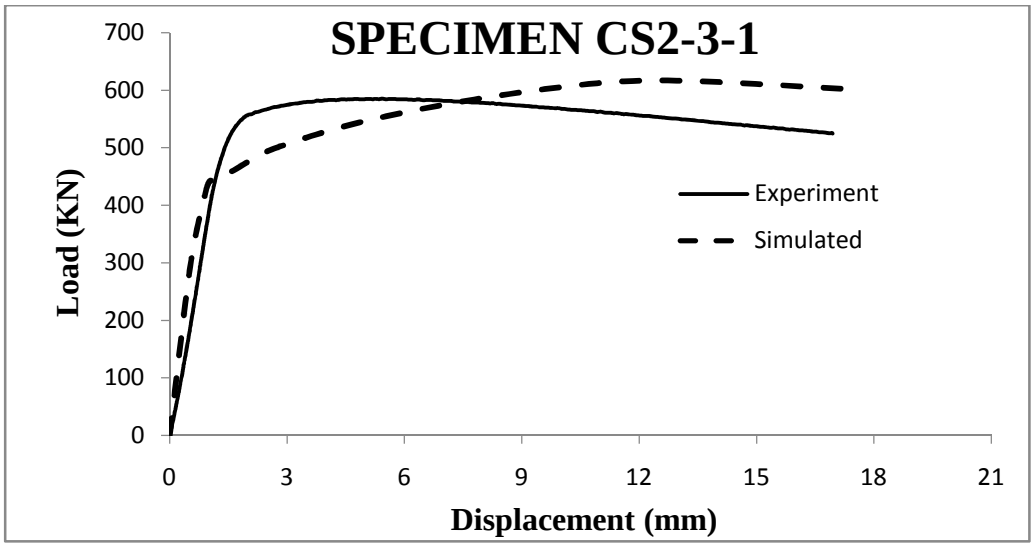

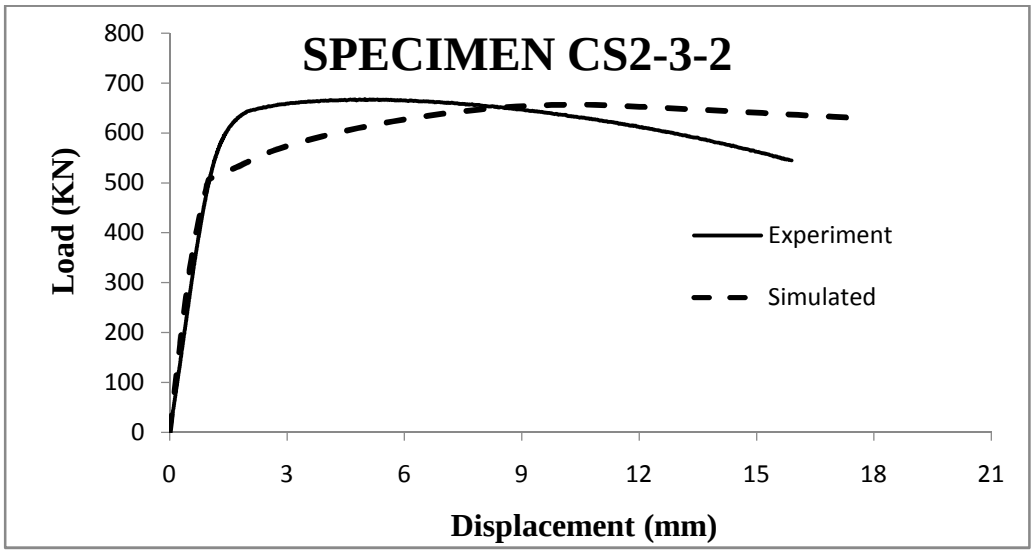

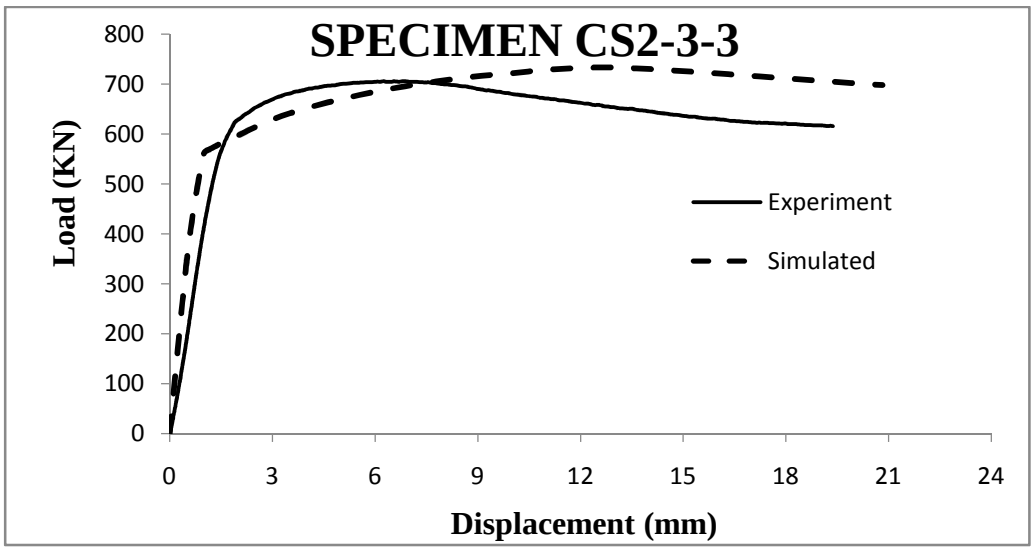

Figure 5.10(e) Comparison of experimental and numerical load-displacement curves for circular L7D CFST specimens, D= 90 mm

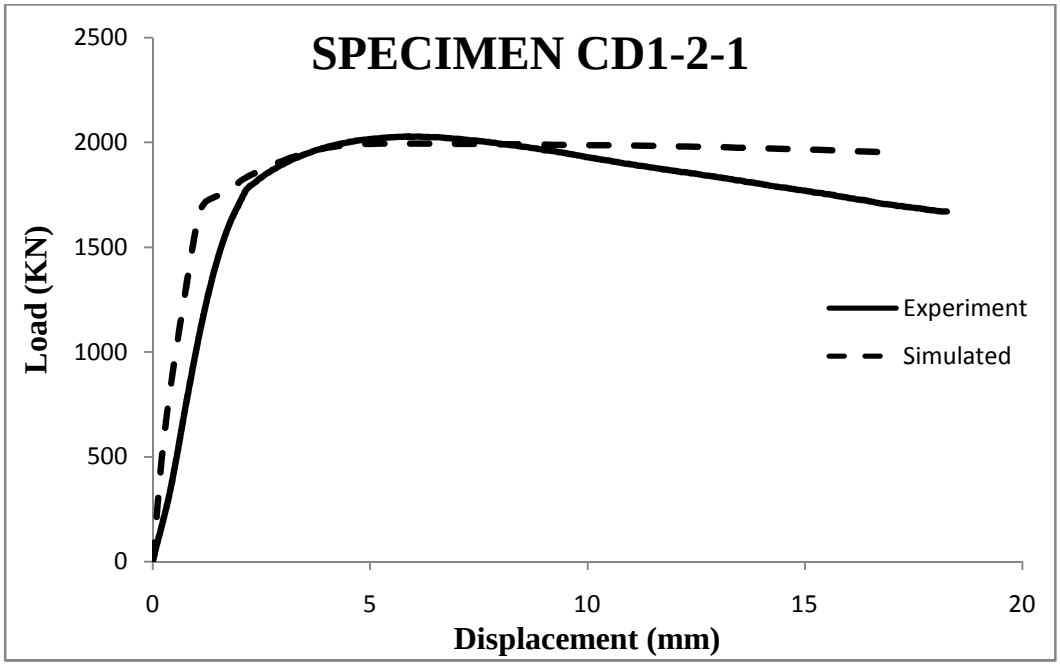

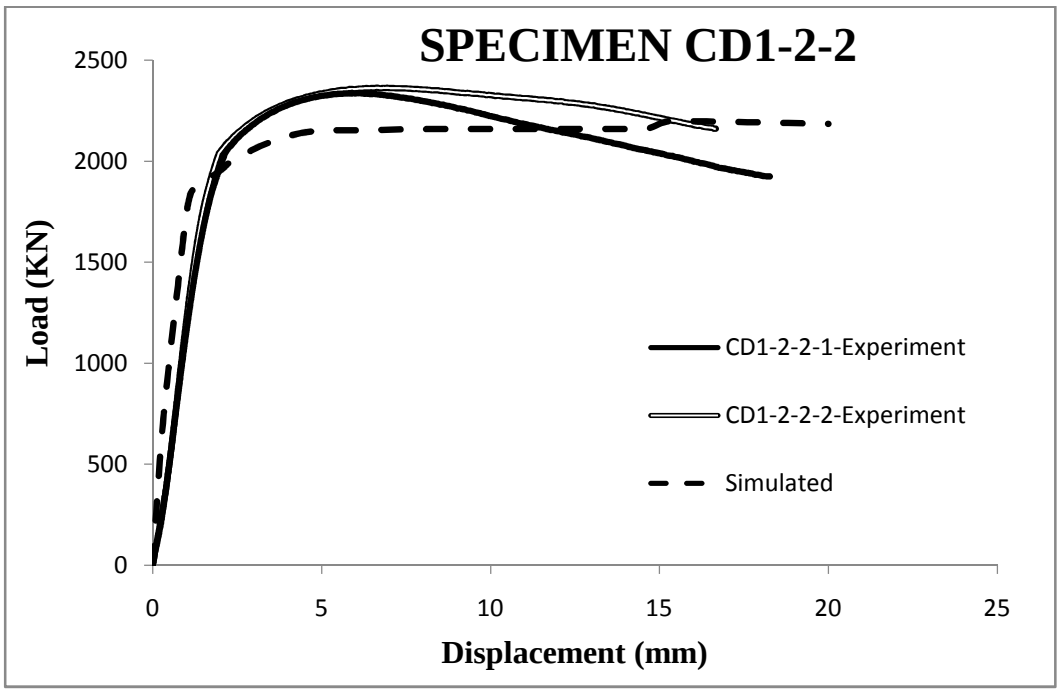

Figure 5.11(a) Comparison of experimental and numerical load-displacement curves for circular L3D CFDST specimens, D = 165.1 mm

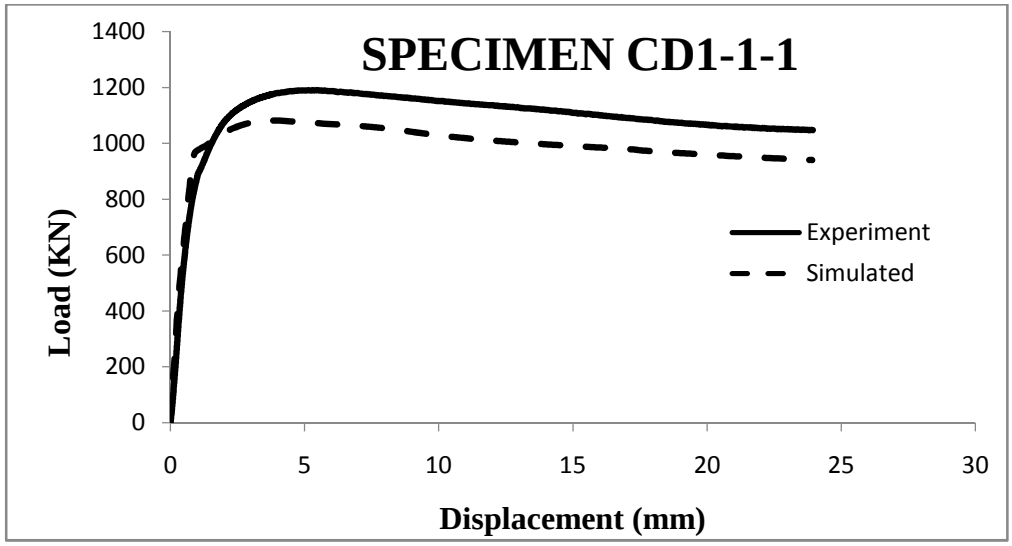

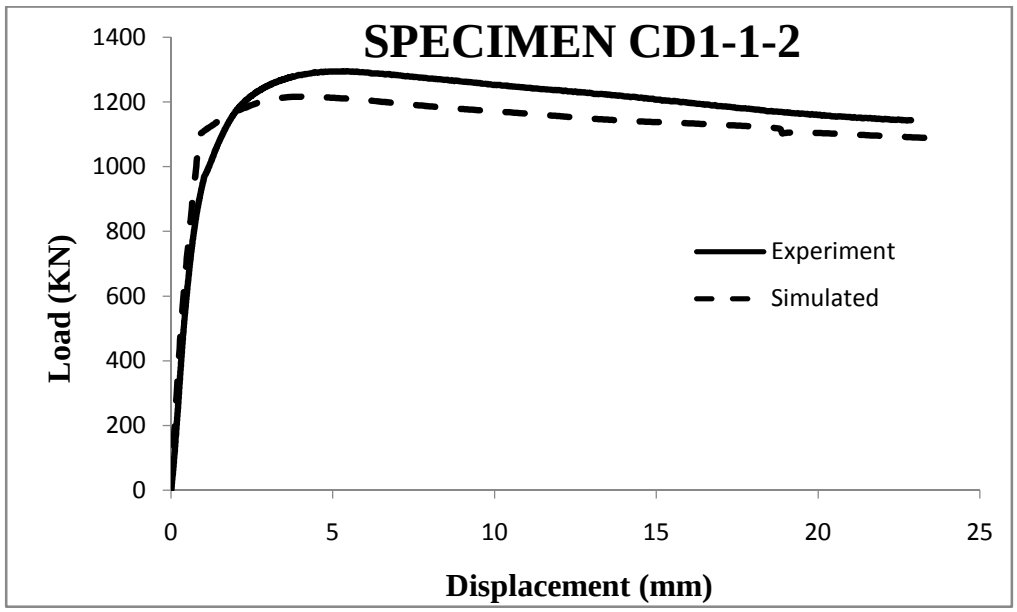

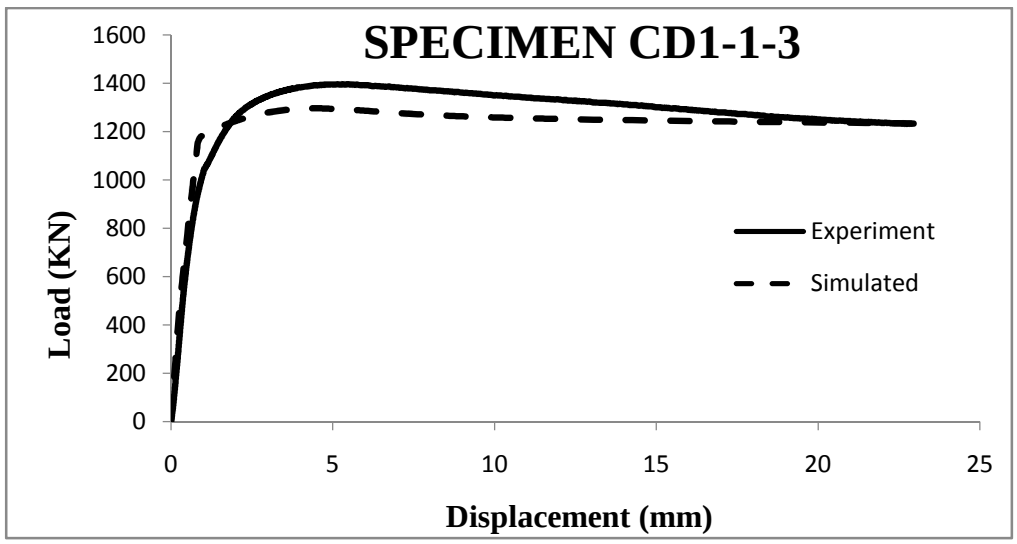

Figure 5.11(b) Comparison of experimental and numerical load-displacement curves for circular L3D CFDST specimens, D = 114.3 mm

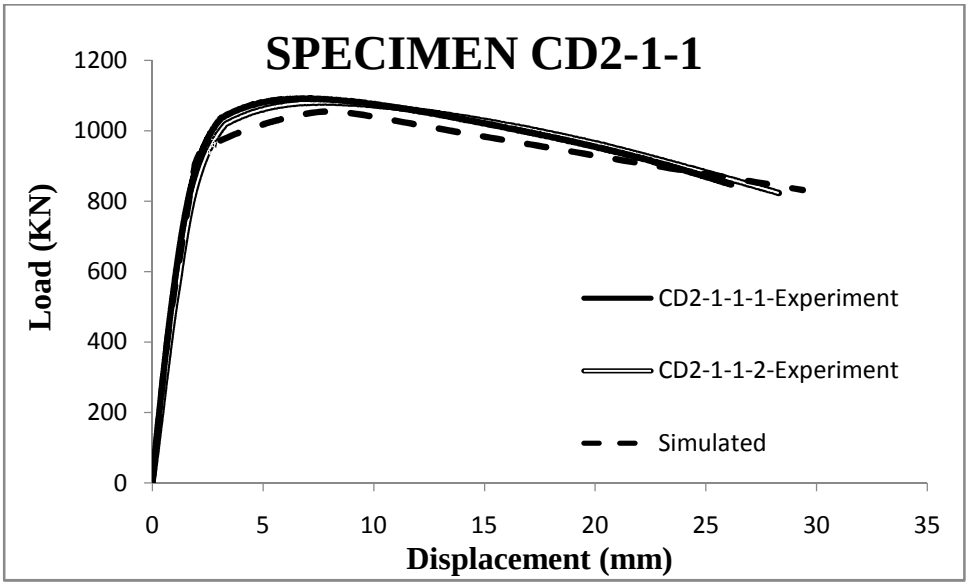

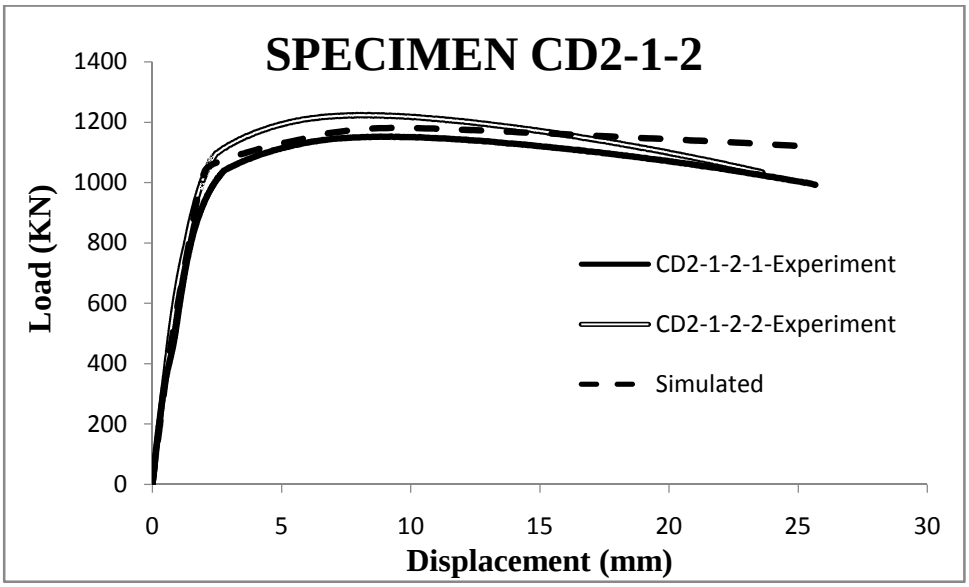

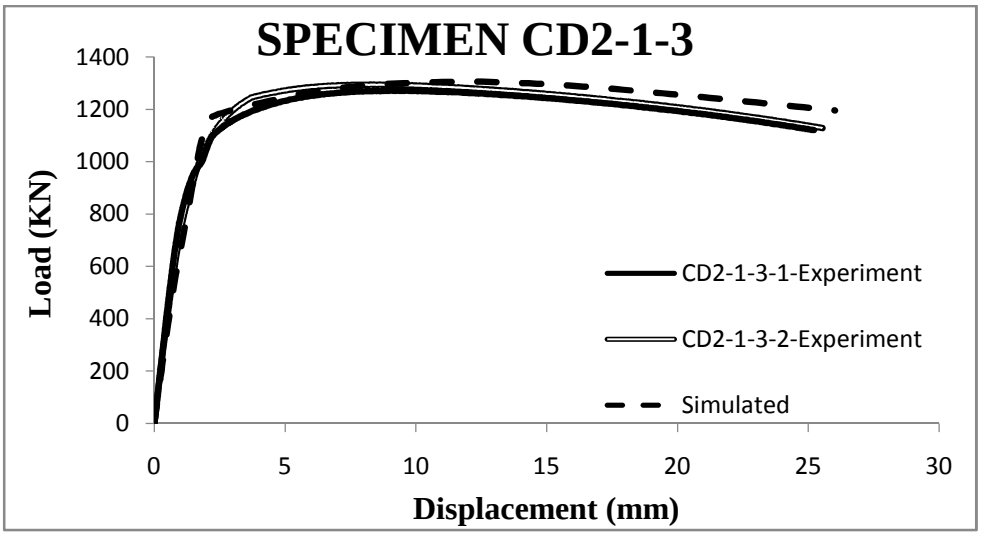

Figure 5.11(c) Comparison of experimental and numerical load-displacement curves for circular L7D CFDST specimens, D = 114.3 mm

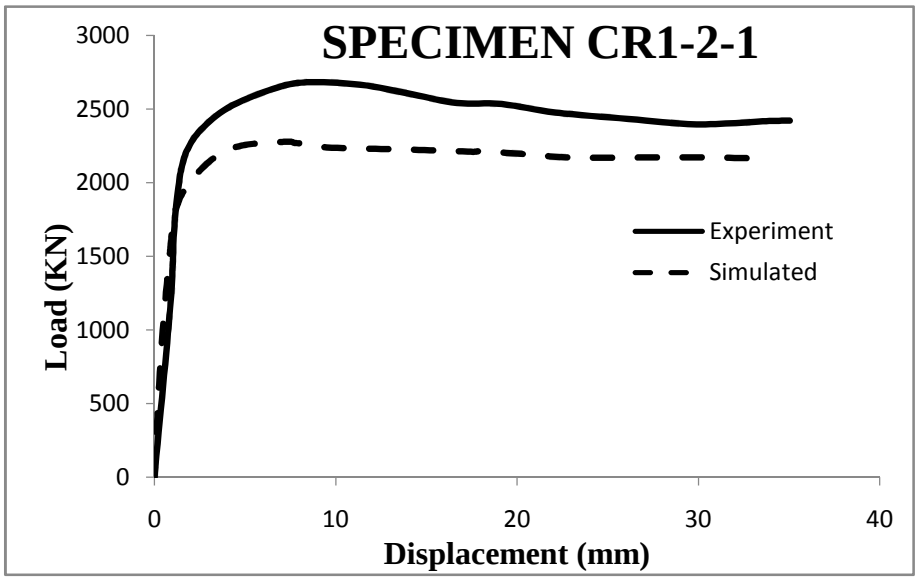

Figure 5.12(a) Comparison of experimental and numerical load-displacement curves for circular RCC-CFST L3D specimens, D=165.1 mm

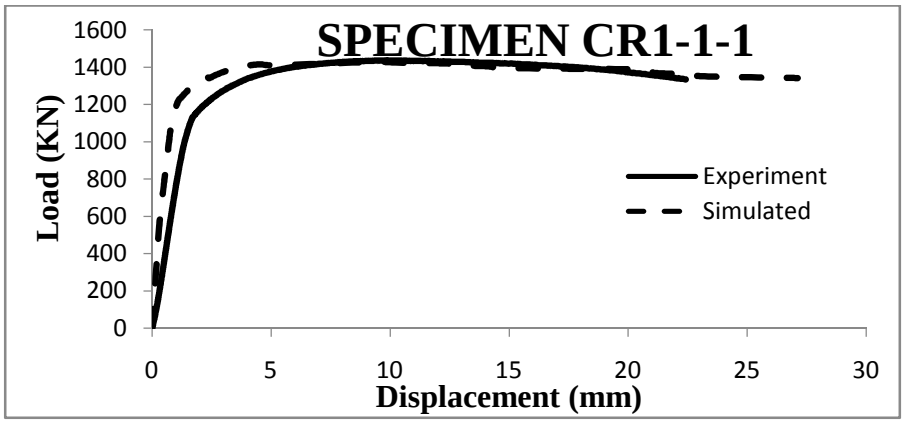

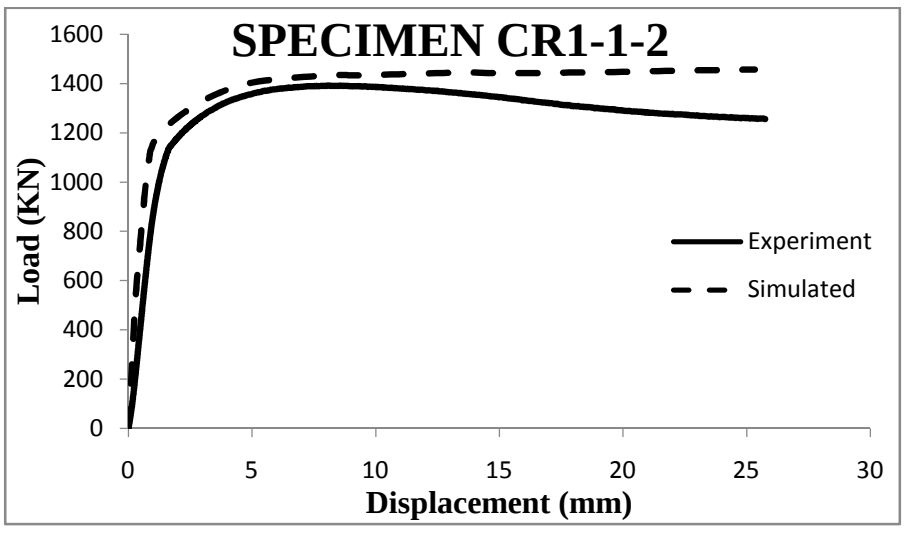

Figure 5.12(b) Comparison of experimental and numerical load-displacement curves for circular L3D RCC-CFST specimens, D = 114.3 mm

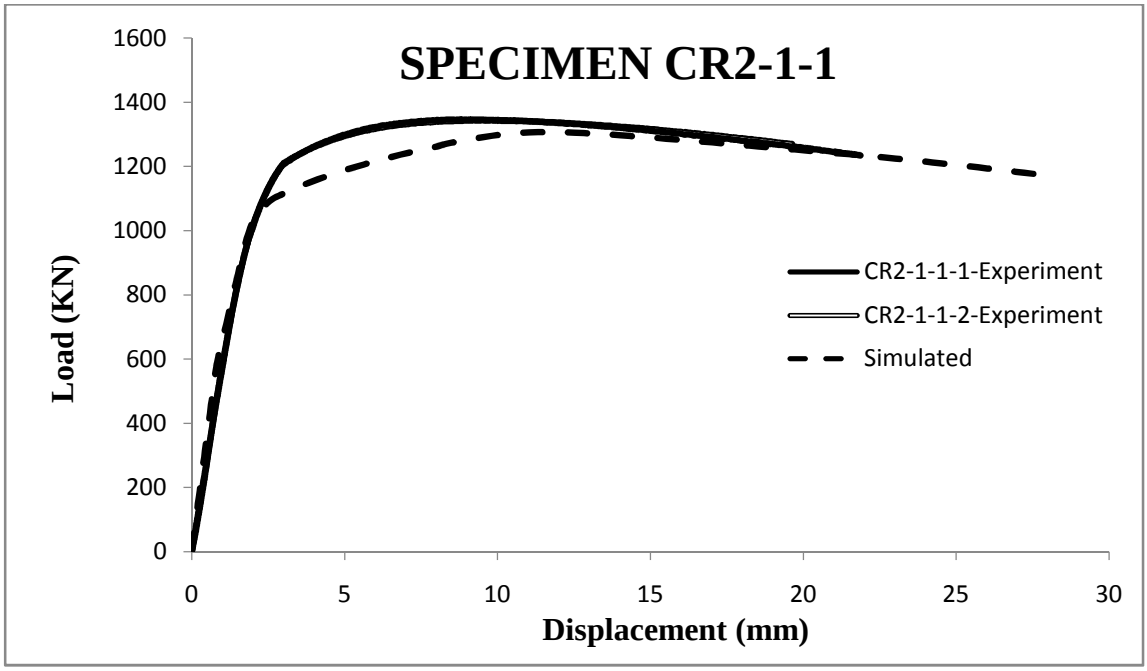

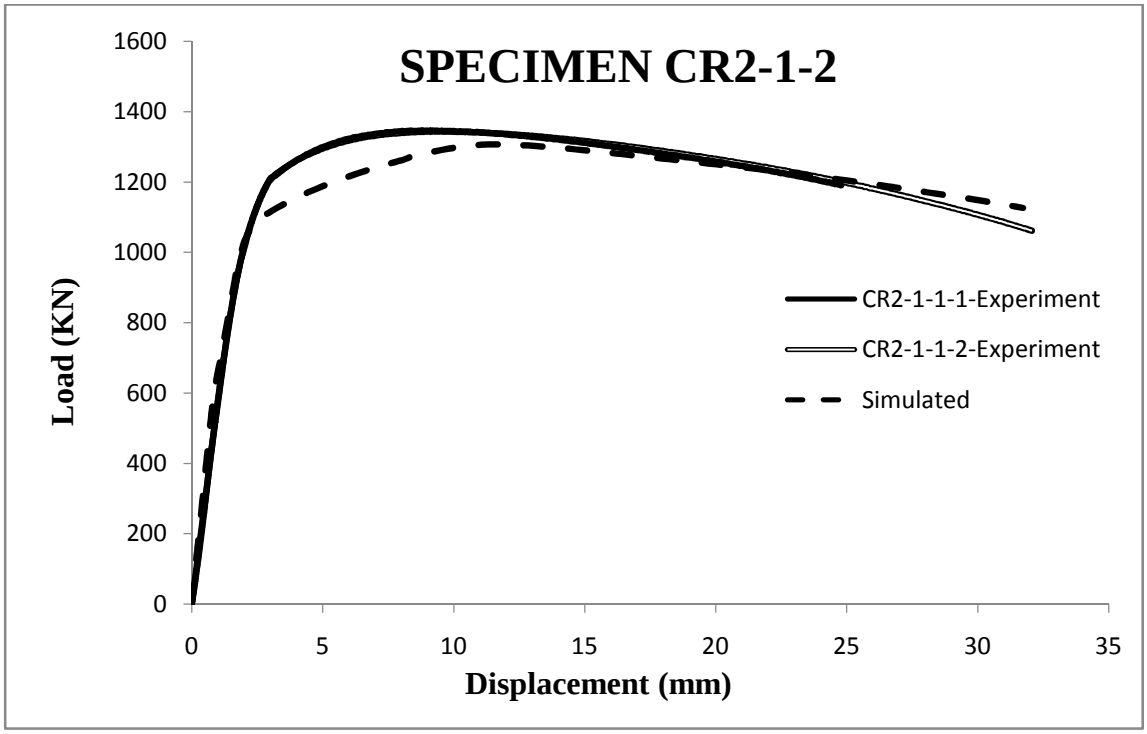

Figure 5.12(c) Comparison of experimental and numerical load-displacement curves for circular L7D RCC-CFST specimens, D = 114.3 mm

Ultimate capacity (strength, P_u) is defined as the maximum axial load observed in load-displacement curve. The nominal capacity was calculated based on the ultimate strength of the materials of the cross-section. The nominal capacity, P_n, is calculated as:

$$P_n = A_s f_y + A_c f_c' \quad \text{For CFST specimens} \quad (5.1\ a)$$

$$P_n = A_{so} f_{yo} + A_{si} f_{yi} + A_c f_c' \quad \text{For CFDST specimens} \quad (5.1\ b)$$

$$P_n = A_s f_y + A_{sr} f_{yr} + A_c f_c' \quad \text{For RCC-CFST specimens} \quad (5.1\ c)$$

where A_s, A_c, and A_{sr} are the cross-sectional area of steel tube, concrete core, and reinforcement bars, respectively. f_y, and f_c' are the uniaxial yield strength of steel tube and uniaxial compressive strength of concrete core (unconfined strength), respectively. f_{yr} is the yield stress of rebars. A_{so}, f_{yo}, A_{si}, and f_{yi} are the cross-sectional area and yield strength of outer and inner steel tube, respectively. 0.2% strain offset method was used to calculate the Yield load (P_y) for specimens. The calculated nominal and ultimate load as well as experimental yield load and ultimate load, and yield displacement for CFST, CFDST and RCC-CFST are given in Tables 5.6 to 5.8, respectively.

The ultimate capacities, P_u have been normalized with respect to the corresponding nominal capacities P_n to investigate the enhancement in strength. The ratio of the two capacities is identified as "Strength Index, SI ". The parameter SI is defined as:

$$SI = \frac{P_u}{P_n} \quad (5.2)$$

P_n has been calculated using Equation 5.1. The values of strength index for various specimens presented in Tables 5.6 to 5.8 clearly indicate that a significant increase over the nominal capacity is observed for all specimens due to composite action. Even in the longer L7D specimens, nominal capacities were always achieved or exceeded (i.e. SI $\geq$1.0).

Table 5.6 Experimental and numerical results of circular CFST specimens

Length Category	Specimen ID	P_n (KN)	Δ_y (mm)	P_y (KN)	P_{5y} (KN)	P_u (kN)		SI	DI
						Experiment	Simulated		
L3D	CS1-1-1-1	799.40	1.89	873.11	990.36	1021.11	1011.22	1.25	1.13
	CS1-1-2-1	916.33	1.88	931	1159.70	1161.32	1198.77	1.27	1.25
	CS1-1-3-1	1017.64	1.72	1002.6	1261.20	1337.67	1357.62	1.31	1.26
	CS1-2-1	1514.40	2.59	1976.2	2049.00	2144.48	2019.70	1.42	1.04
	CS1-2-2-1	1677.05	2.06	1786	2132.00	2206.31	2267.28	1.31	1.19
	CS1-2-2-2	1677.05	2.35	1870	2142.23	2179.22	2267.28	1.30	1.15
L4D	CS1-3-1	434.16	1.10	471.90	571.20	612.32	621.34	1.41	1.21
	CS1-3-2	469.72	1.16	554.55	653.25	667.66	688.32	1.37	1.18
	CS1-3-3	547.33	1.20	652.23	750.82	788.61	792.54	1.44	1.16
L7D	CS2-1-1	799.40	3.77	883.20	908.50	960.11	1061.35	1.21	1.03
	CS2-1-2	916.33	3.86	1004.40	1012.36	1072.32	1218.66	1.20	1.01
	CS2-1-3-1	1017.64	3.48	1044.00	1143.00	1185.55	1254.45	1.17	1.09
	CS2-1-3-2	1017.64	3.17	975.48	1082.79	1196.64	1254.45	1.15	1.11
	CS2-3-1	435.46	2.68	570.82	571.32	586.53	616.32	1.34	0.96
	CS2-3-2	491.33	2.50	593.48	571.60	650.67	653.63	1.33	0.93
	CS2-3-3	513.54	2.95	654.55	582.60	708.33	733.32	1.38	0.90
L10D	CS3-3-1	435.46	3.10	559.20	489.22	558.99	588.60	1.19	0.96
	CS3-3-2	491.33	2.50	522.60	506.67	606.6	616.84	1.09	0.96
	CS3-3-3	513.54	2.86	665.30	642.33	655.89	678.22	1.06	0.97

Table 5.7 Experimental and numerical results of circular CFDST specimens

Length Category	Specimen ID	P_n (kN)	Δ_y (mm)	P_y (kN)	P_{5y} (KN)	P_u (kN)		SI	DI
						Experiment	Simulated		
L3D	CD1-1-1	960.90	1.63	1018.71	1175.52	1190.36	1155.19	1.24	1.09
	CD1-1-2	1066.61	1.62	1106.23	1271.33	1295.22	1294.60	1.21	1.11
	CD1-1-3	1179.27	1.81	1232.11	1361.50	1396.42	1406.33	1.18	1.11
	CD1-2-1-1	1699.28	2.51	1834.22	1864.66	2030.64	1994.50	1.23	1.02
	CD1-2-2-1	1845.41	2.62	2133.13	2110.59	2337.64	2160.85	1.27	0.99
	CD1-2-2-2	1845.41	2.78	2176.21	2228.11	2362.14	2160.85	1.27	1.02
L7D	CD2-1-1-1	960.90	3.23	1039.40	1006.22	1092.18	1057.32	1.13	0.97
	CD2-1-1-2	960.90	3.19	1011.39	1016.11	1080.24	1057.32	1.13	1.00
	CD2-1-2-1	1066.61	3.04	1050.63	1098.45	1152.31	1181.39	1.11	1.04
	CD2-1-2-2	1066.61	3.38	1142.88	1145.88	1223.29	1181.39	1.15	1.00
	CD2-1-3-1	1179.27	3.25	1172.65	1219.32	1271.06	1305.18	1.08	1.04
	CD2-1-3-1	1179.27	3.42	1227.00	1239.21	1294.59	1305.18	1.10	1.01

Table 5.8 Experimental and numerical results for circular RCC-CFST specimens

Length Category	Specimen ID	P_n (KN)	Δ_y (mm)	P_y (KN)	P_{5y} (KN)	P_u (KN)		SI	DI
						Experimental	Simulated		
L3D	CR1-1-1	1137.17	2.33	1212.95	1432.65	1427.54	1449.8	1.26	1.18
	CR1-1-2	1077.41	2.10	1191.98	1419.31	1391.28	1461.3	1.29	1.19
	CR1-2-1	1780.97	3.46	2088.65	2629.58	2665.57	2279.08	1.50	1.26
L7D	CR2-1-1	1137.17	4.00	1250.62	1295.88	1368.28	1368.50	1.14	1.04
	CR2-1-2	1077.41	4.01	1260.00	1265.47	1346.56	1346.33	1.19	1.00

The effect of core configuration on enhancement in load carrying capacity has been investigated plotting the variation of SI for specimens with different core configurations. For more clarity, the specimens have been categorized based on L/D ratio. The SI for L3D and L7D specimens are shown in Figure 5.13 (a) and 5.13 (b), respectively.

It can be concluded from Figure 5.13 that RCC-CFST specimens showed the maximum SI out of all three core configurations for L3D and L7D specimens. This is due to the fact that the concrete core is confined by reinforcing bars which are further confined in turn with the confined concrete core (by steel tube). Strain hardening behaviour is thus the expected response for such members.

CFDST specimens showed lesser SI as compared with other core configurations for L3D and L7D specimens. This may be attributed to:

a) The improvement in strength is primarily due to the confinement of concrete core. The cross-sectional area of confined concrete is comparatively lower in case of CFDST specimens and accordingly the concrete enhancement is expected to be lower

b) Based on free body diagram of CFDST specimens (Figure 5.14), the concrete annul is confined by inner steel tube and outer steel tube. Since the same inner steel tube is used for all CFDST specimens, the confining pressure provided by inner steel tube is same in all specimens. This confining pressure significantly decreases the load carried by outer steel tube as stress redistribution occurs due to multiaxial stress state according to von Mises failure criterion. Hence, increasing thickness of outer tube without changing thickness of inner tube will lead to increase the nominal capacity of cross-section without significant increase in ultimate capacity. Hence, SI decreases as D/t ratio of outer tube decreases.

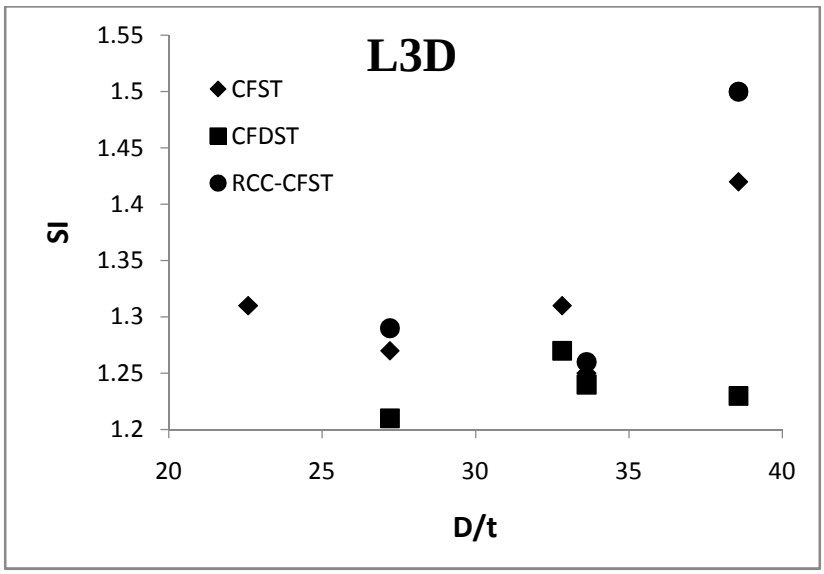

Figure 5.13(a) Strength index for L3D circular specimens with different core configurations

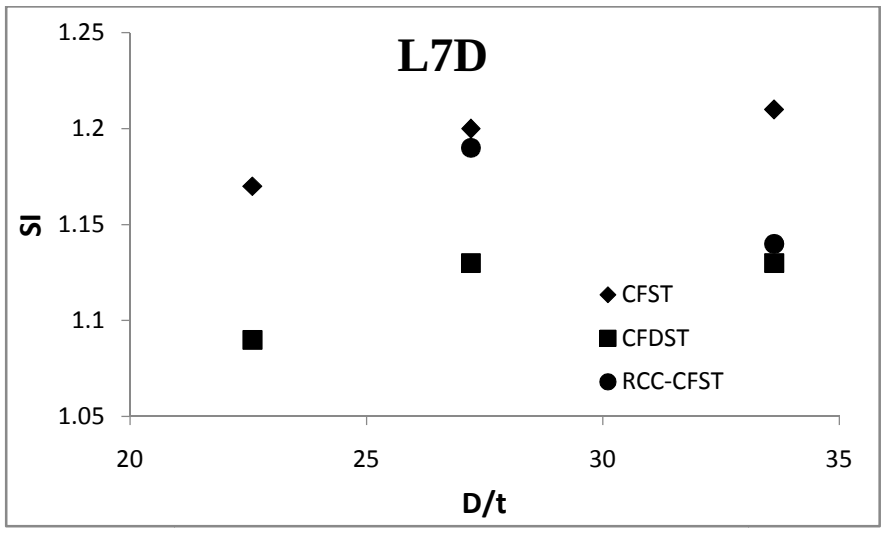

Figure 5.13(b) Strength index for L7D circular specimens with different core configurations

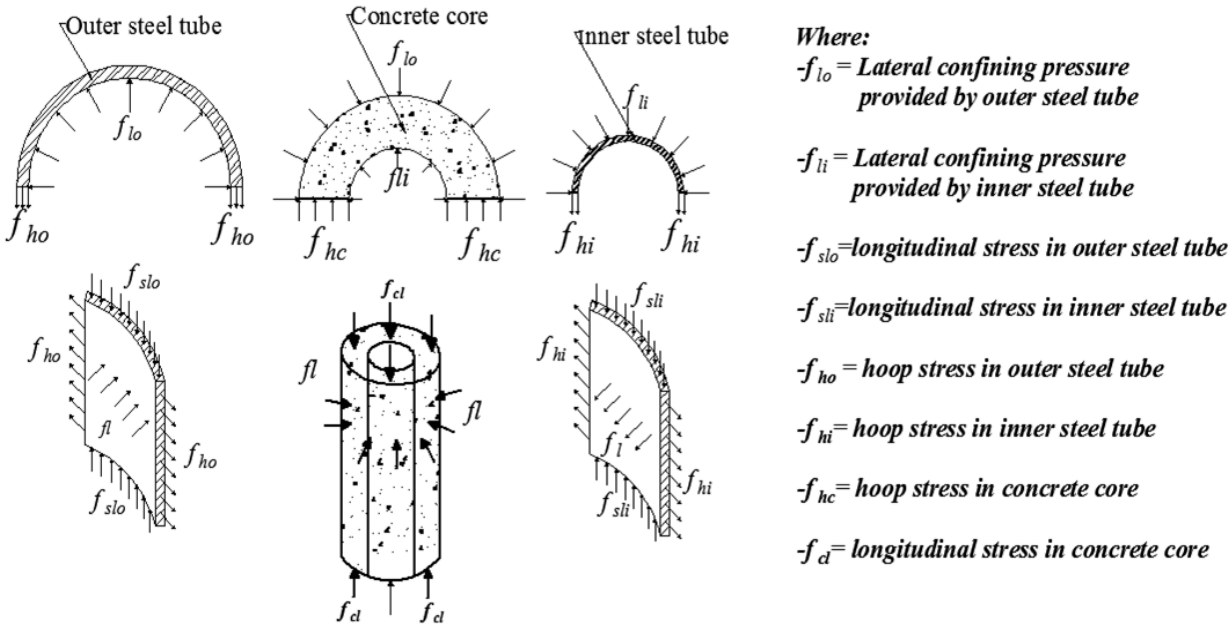

Figure 5.14 Free body diagram for columns with CFDST core configuration

5.3.3 Ductility and Post Yield Behaviour

Ductility of a structural member might be defined as "the ability to undergo large plastic deformation without significant degradation in strength" (Liang and Fragomeni, 2009). It is expected that CFST specimens may display highly ductile behaviour due to confinement provided by steel tube,. To investigate the effect of different core configurations on ductility, Ductility Index, DI, has been calculated for all specimens as (Johansson, 2002):

$$DI = \frac{P_{5y}}{P_y} \tag{5.3}$$

where P_{5y} is the load corresponding to five times yield displacement, $5\Delta_y$. The composite specimens are classified on the basis of their DI value as follows:

a) If DI exceeds 1.0, it will be classified as **Strain hardening** behaviour.
b) **Elastic-perfectly-plastic** behaviour will be the classification if specimen has DI as 1.0.
c) **Strain softening** behaviour is the characterized as having DI less than 1.0.

The effect of core configurations on DI is shown for L3D specimens in Figure 5.15. It can be concluded from Figure 5.11 that the DI was greater for RCC-CFST specimens and smaller for CFDST specimens. This is due to the fact that the rebars in RCC-CFST specimens are confined by concrete core and could sustain the applied load carrying well beyond the yield point. It can also be concluded that the the DI decreased for all core configurations with increase in D/t ratio. However, trend of reduction of DI was more pronounced in CFDST specimens as compared to RCC-CFST specimens.

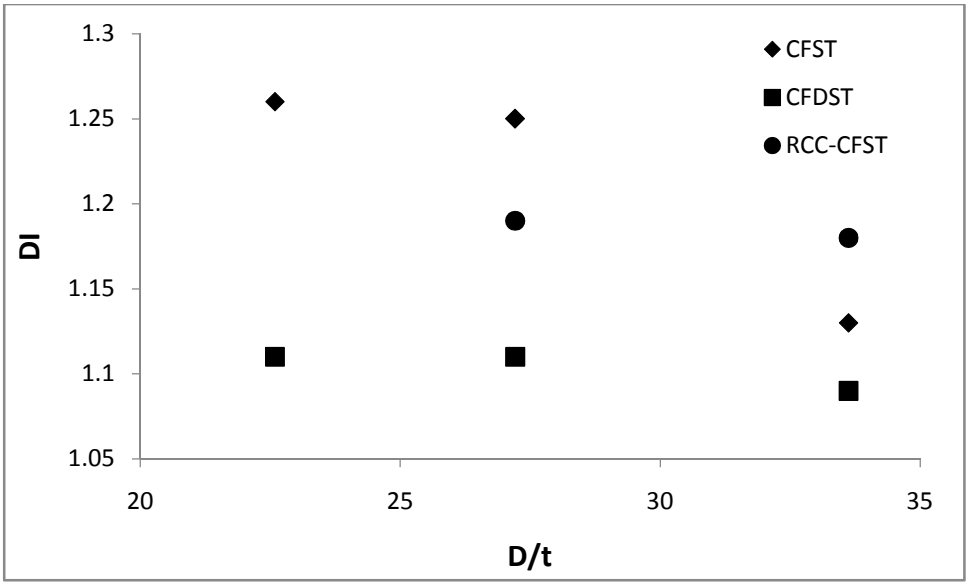

Figure 5.15 Ductility index for circular specimens with different core configurations

5.3.4 Length Effect

The results of L7D and L10D have been compared with corresponding L3D specimens (Figure 5.16) as a function of D/t ratio to study the effect of length on load carrying capacity of CFST specimens,. SI has been calculated for investigating the normalized ultimate capacities. It can be concluded from Figure 5.16 that increase in D/t ratio significantly decreases the SI for L3D and L4D specimens, whereas SI generally increased for L7D and L10D specimens as D/t ratio increased. This indicates that the specimens with higher tube thickness undergo greater reduction due to increased length as compared to specimens with smaller tube thickness. It is due to the fact that the concrete contribution is greater in smaller thickness specimens than the higher tube thickness specimens. The higher axial stiffness of concrete results in increased concrete contribution which increases the axial stability of specimens.

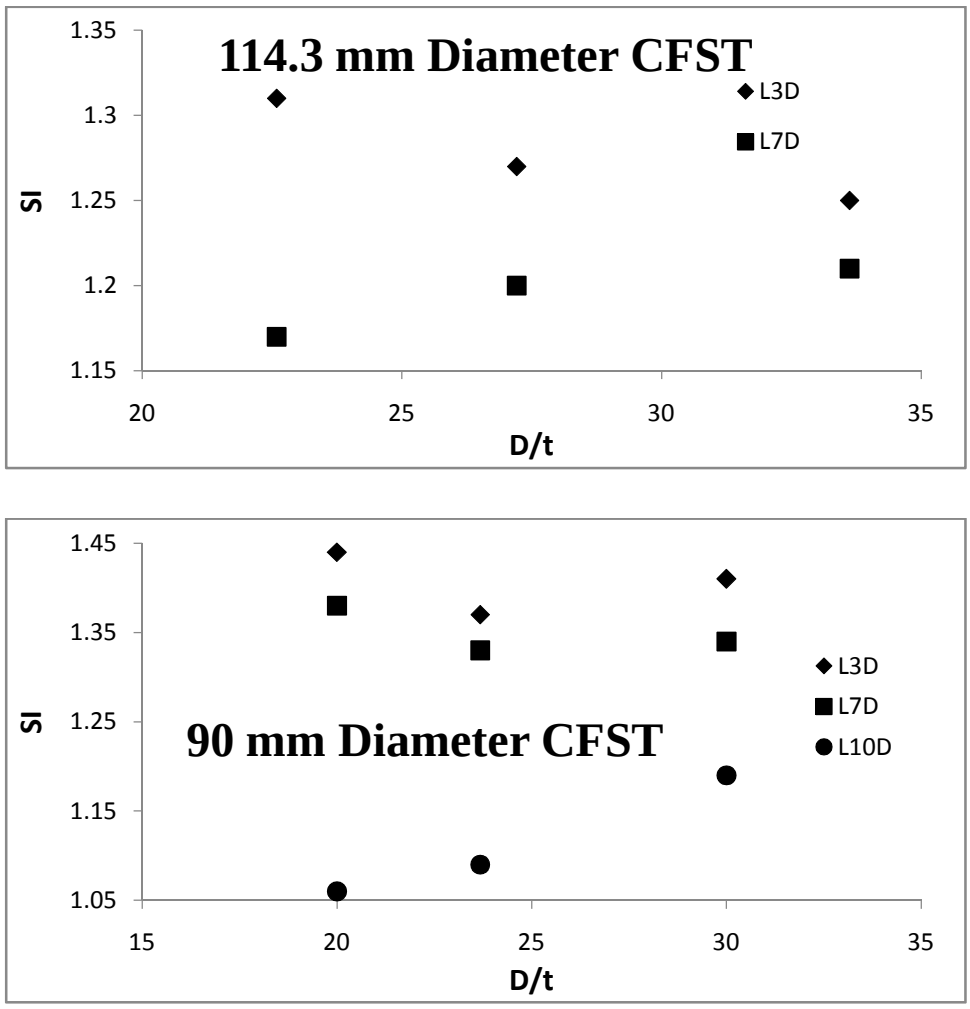

Figure 5.16 Effect of length on strength index of circular CFST specimens

Reduction in load carrying capacities due to increased length has also been investigated for specimens with different core configurations. Load carrying capacities of L7D specimens and corresponding L3D specimens have been compared for every core configuration. The reduction in load carrying capacity due to increase in length is shown in Figure 5.15. It can be concluded from the figure that for the specimens with greater thickness (i.e. lower D/t ratio), lower reduction due to increased length was observed for all configurations. This is due to the fact that the specimens with greater tube thicknesses provide greater lateral confining pressure for concrete core. This decreases the maximum longitudinal stress the steel tube can bear due to its triaxial state of stress (in accordance with von Mises criteria). Therefore, as shown in Figure 5.17 that the specimens with D/t=33.62 showed the lowest reduction for all core configurations as compared to other D/t ratios.

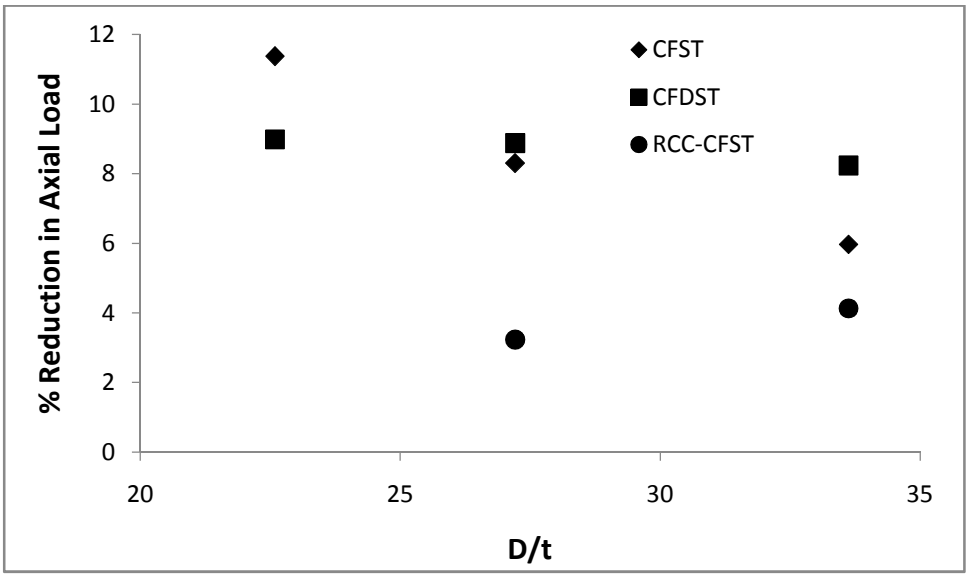

Figure 5.17 Effect of increase in length on load carrying capacity of circular specimens with different core configurations

5.3.5 Equivalent Area of Steel

Details of the specimens with L3D and L7D were considered to investigate the effect of use of equivalent cross-sectional area of steel in composite columns having two different core configurations (i.e. CFST and RCC-CFST). Details of specimens are listed in Table 5.6. In this Table, results of CFST specimens with greater thickness were compared with RCC-CFST specimens with smaller thickness. The difference in area of steel was compensated by adding rebars. Due to difference in yield stress between steel tubes and the rebars as well as marginal difference in area of steel due to commercial availability of the steel tubes and rebars, the axial

load was normalized with respect to nominal cross-sectional capacity of each specimen. The nominal cross-sectional capacities were calculated using Equation 5.1. The normalized load-displacement curves are shown in Figure 5.18. Strength index (SI) and ductility index were also calculated for each specimen using. It can be concluded from Table 5.9 that for specimens with 114.3 mm diameter the enhancement in strength of RCC-CFST specimens was slightly lesser than that of CFST specimen for L3D and L7D details. Moreover, the enhancement in strength of CR1-1-2 and CR2-1-2 specimens was reduced as compared to the corresponding CFST specimens (i.e. CS1-1-3-1 and CS2-1-3-1) since rebars cannot provide same confining pressure provided by a continuous and uniform steel tube . This indicated that the RCC-CFST specimens which contain lesser compensated area of steel exhibit similar amount of enhancement in strength as obtained for CFST specimens.

RCC-CFST specimen with D=165.1 mm (CR1-2-1) showed quite greater value of SI (SI=1.50) as compared to its corresponding CFST specimen (CS1-2-2) (SI=1.31). This indicates that greater diameter may reflect the greater enhancement in load carrying capacity. Hence, it can be concluded that using specimens with bigger diameter and smaller thickness is more feasible than using smaller diameters with greater thicknesses. In general, enhancement in SI of RCC-CFST L3D and L7D specimens indicates that use of equivalent area of steel in terms of rebars has almost similar effect of using thicker tubes..

Variation of ductility index for L3D specimens with 114.3 mm and 165.1 mm diameters was almost having same trend as strength index. The ductility index was slightly decreased for RCC-CFST specimens with higher compensated area of steel, whereas specimens with lower compensated area of steel showed significantly enhanced ductility index

Table 5.9 Comparison of circular specimens with equivalent area of steel but different core configurations

Specimen ID	L (mm)	D (mm)	t (mm)	L/D	D/t	A_s (mm^2)	A_{sr} (mm^2)	A_s (Total) (mm^2)	f_y (MPa)	SI	DI
CS1-1-3-1	**380**	**114.3**	**5.06**	**3.32**	**22.59**	**1736**	**0**	**1736**	**427**	**1.31**	**1.26**
CR1-1-1	380	114.3	3.40	3.32	33.62	1184	628	1812	430	1.26	1.18
CR1-1-2	380	114.3	4.20	3.32	27.21	1452	314	1766	428	1.29	1.19
CS2-1-3-2	**900**	**114.3**	**5.06**	**7.87**	**22.59**	**1736**	**0**	**1736**	**427**	**1.15**	**1.11**
CR2-1-1	900	114.3	3.40	7.87	33.62	1184	628	1812	430	1.14	1.04
CR2-1-2	900	114.3	4.20	7.87	27.21	1452	314	1766	428	1.19	1.00
CS1-2-2-1	**500**	**165.1**	**5.03**	**3.03**	**32.82**	**2528**	**0**	**2528**	**423**	1.31	1.19
CR1-2-1	500	165.1	4.28	3.03	38.57	2161	452	2613	423	1.50	1.26

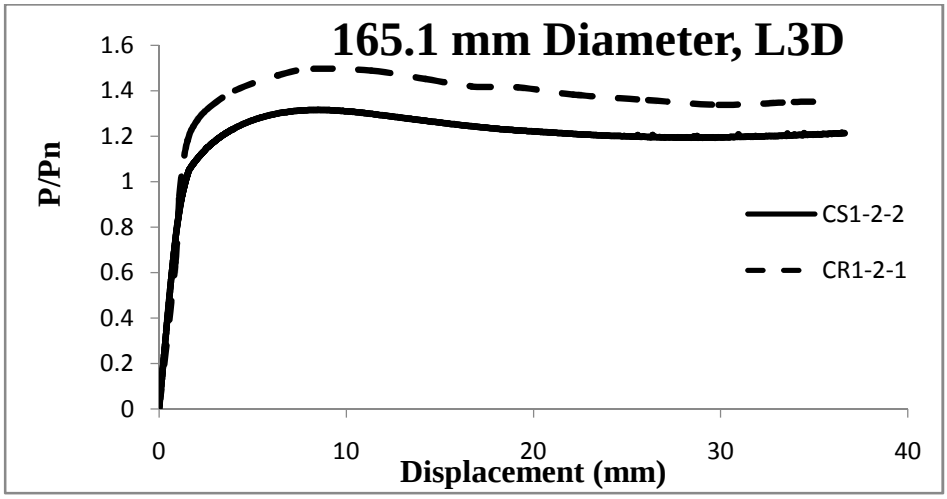

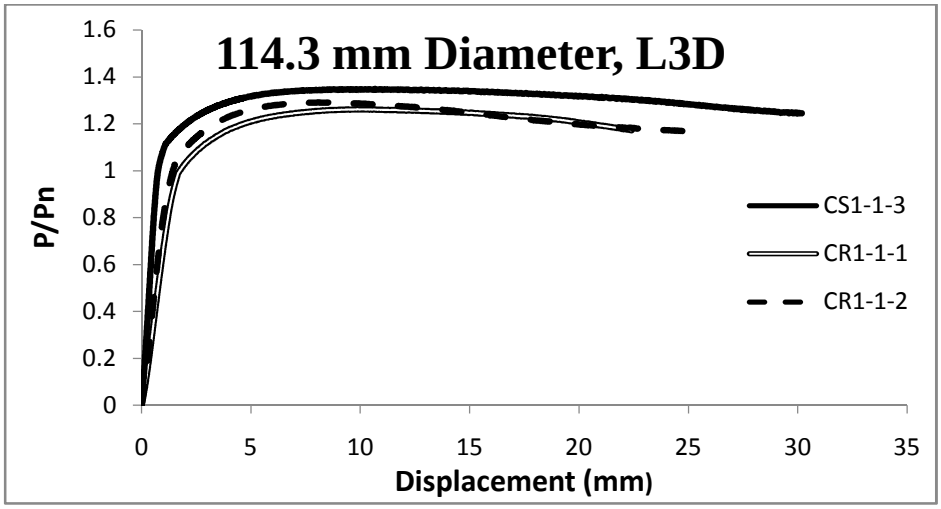

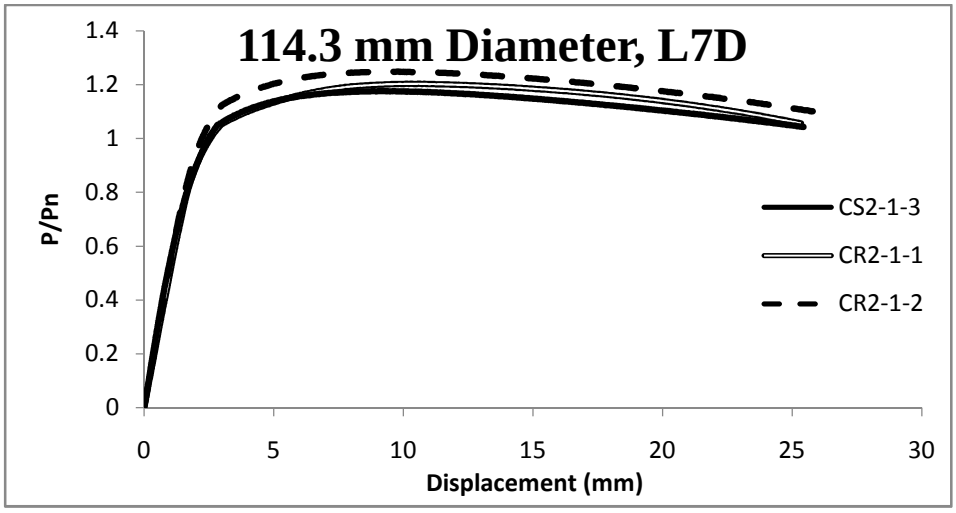

Figure 5.18 Comparison of load-displacement curves of circular CFST and RCC-CFST specimens

5.4 CODAL RECOMMENDATIONS

Provisions from eight International Codes are used to predict the axial load capacity of the tested specimens. The obtained capacities are compared with the measured strengths. The employed codes used are: ACI 318 (2008), ANSI/AISC 360 (2010), British Standard 5400 (BS 5400, 2005), Canadian Standard S016 (CSA) (S016, 2001), two Chinese Standards; CECS 28 (1990) (Zhang et al., 2007) and GJB and DL/T 4142 (2000) (Han, 2002), Euro Code 4 (EC4) (EN 1994, 2004) and Japanese Standard AIJ (2001) (Morino and Tsuda, 2003). In all these codes the ultimate strength is calculated as the sum of the strength of individual components. However, in some of them (EN 1994, 2004; BS 5400, 2005; Canadian Standard S016, 2001) the strength of concrete core is increased to account for the confinement effect. The formulas and, detailed procedures of these codes are given in following sections.

5.4.1 American Concrete Institute (ACI 318, 2008)

Building Code Requirements of Reinforced Concrete ACI 318 (2008) considers all members reinforced longitudinally with structural steel shapes, pipe or tubes with or without longitudinal reinforcement as ordinary reinforced concrete (RCC) members. This code predicts the load carrying capacity of CFST columns with same limiting conditions applicable to RCC members. Concrete confinement effect has been neglected in this code. Thickness of steel tube has been limited to prevent local buckling and the limitation is based on achieving yield stress in a hollow steel tube under monotonic axial loading. The strength of CFST column is given in this code as:

$$P_u = 0.85A_c f_c^{'} + A_s f_y \tag{5.4}$$

The limitations for using steel tubes in this code are:

$$t \geq D\sqrt{\frac{f_y}{8E_s}} \tag{5.5}$$

5.4.2 American National Standards Institute/ American Institute of Steel Construction (ANSI/AISC360, 2010)

The plastic stress distribution method provided in ANSI/AISC360 (2010) is used for calculating the nominal strength of composite columns. In this procedure, the nominal strength of the composite section is computed based on plastic strength of steel and concrete without allowing for confinement. In other words, the load carrying capacity of short CFST is

calculated assuming that the steel components have attained the yield stress either in tension or compression and concrete components in compression have reached crushing stress. Crushing stress of concrete core is defined as 0.95 $f_c^{'}$ for circular cross-section to account for the effects of concrete confinement provided by steel tube. The cross-section area of steel should be at least 1% of the total area of composite cross-section for it to qualify as a CFST column.

The plastic stress distribution method is recommended for use in the cross-sections which are uniform (as in the present study). Based on the cross-sectional slenderness (D/t), the code classified CFST columns subjected to compression into three categories: compact, non-compact or slender sections.

Compact sections:

Compact section is defined as the section "capable of developing a fully plastic stress distribution and possessing a rotation capacity of approximately three before the onset of local buckling". For compact sections:

$$\frac{D}{t} \leq 0.15 \frac{E_s}{f_y} \tag{5.6}$$

Non-compact sections:

Non-compact section is defined as the section "that can develop the yield stress in its compression elements before local buckling occurs, but cannot develop a rotation capacity of three" as in case of compact section. The maximum D/t ratios for section to be classified as non-compact section are:

$$\frac{D}{t} \leq 0.19 \frac{E_s}{f_y} \tag{5.7}$$

Slender sections

If a section is "possessing plate components of sufficient slenderness such that local buckling in the elastic range will occur", it is referred to as a slender section. The maximum D/t ratios for section to be classified as slender are:

$$\frac{D}{t} \leq 0.31 \frac{E_s}{f_y} \tag{5.8}$$

The nominal compressive strength for axially loaded composite columns should be determined for the limit state of flexural buckling based on column cross-sectional slenderness and global slenderness.

When $\frac{P_n}{P_{cr}} \leq 2.25$

$$P_u = P_n \left[0.658^{\left(\frac{P_n}{P_{cr}}\right)}\right] \quad (5.9)$$

When $\frac{P_n}{P_{cr}} > 2.25$

$$P_u = 0.877\, P_{cr} \quad (5.10)$$

where P_{cr} is elastic Euler buckling load calculated as:

$$P_{cr} = \frac{\pi^2}{(KL)^2}(EI)_{eff} \quad (5.11)$$

$$(EI)_{eff} = E_s I_s + E_r I_r + C_3 E_c I_c \quad (5.12)$$

$$C_3 = 0.6 + 2\left(\frac{A_s}{A_c + A_s}\right) \leq 0.9 \quad (5.13)$$

P_n is the nominal cross-sectional capacity based on material strength calculated as:

For compact sections

$$P_n = P_{n1} = A_s f_y + \emptyset f_c^{'}\left(A_c + A_r \frac{E_s}{E_c}\right) \quad (5.14)$$

where $\emptyset$ is strength reduction factor considered as 0.85 for rectangular sections and 0.95 for circular sections.

For non-compact sections

$$P_n = P_{n2} = P_{n1} - \frac{P_{n1} - P_y}{(\lambda_r - \lambda_p)^2}\left(\lambda_m - \lambda_p\right)^2 \quad (5.15)$$

where λ_m is the maximum cross-sectional slenderness permitted to be used and calculated as

$$\lambda_m = 0.31\frac{E_s}{f_y} \quad (5.16)$$

λ_r is the maximum cross-sectional slenderness permitted to be classified as non-compact section and that is :

$$\lambda_r = 0.19\frac{E_s}{f_y} \tag{5.17}$$

λ_p is the maximum cross-sectional slenderness permitted to be classified as a compact section and that is

$$\lambda_p = 0.15\frac{E_s}{f_y} \tag{5.18}$$

$$P_y = A_s f_y + 0.7f_c^{'}\left(A_c + A_r\frac{E_s}{E_c}\right) \tag{5.19}$$

For slender sections

$$P_n = P_{n3} = A_s f_{bl} + 0.7f_c^{'}\left(A_c + A_r\frac{E_s}{E_c}\right) \tag{5.20}$$

where f_{bl} is the local buckling strength of steel tube calculated based on simplified Bryan's formula as (Galambos, 1998):

$$f_{bl} = \frac{0.72f_y}{\left(\left(\frac{D}{t}\right)\frac{f_y}{E_s}\right)^{0.2}} \tag{5.21}$$

5.4.3 British Standard (BS 5400, 2005)

British standard (BS 5400, 2005) considers the composite action between steel and concrete for designing such composite columns in circular CFST. The method for designing the composite columns in this standard as follows:

Steel Tube

The thickness of steel tube should follow the constraint

$$t \geq D\sqrt{\frac{f_y}{8E_s}} \tag{5.22}$$

Concrete core

The strength of core concrete measured by concrete cubes should not be less 20 MPa and the density of concrete should be 2300 kg/m^3 at least.

The code limits the concrete contribution factor (P_c) to be within a specified range to permit the use of this approach for composite columns design. The columns having P_c lower than the minimum limit should be designed as RCC columns and the columns having P_c higher than the maximum limit should be designed as steel columns. Where:

$$P_c = \frac{0.45 A_c f_{cc}^{'}}{P_n} \tag{5.23}$$

Where, $P_c$is the concrete contribution factor ($f_{cu}^{'}$) is the compressive strength of concrete cubes, and $f_{cc}^{'}$is the enhanced characteristics strength of concrete core calculated as:

$$f_{cc}^{'} = f_{cu}^{'} + C_1 \frac{t}{D} f_y \tag{5.24}$$

P_n is the ultimate load carrying capacity of CFST column calculated as:

$$P_n = 0.95 A_s f_y^{'} + 0.87 A_r f_{yr} + 0.45 A_c f_{cc}^{'} \tag{5.25}$$

$$f_y^{'} = C_2 f_y \tag{5.26}$$

The constants C_1 and C_2 are given in Table 3 of the code as a function of slenderness ratio of column.

If the ratio L/D does not exceed 12, the code classifies CFST column as short column and limits the ultimate limit state of load carrying capacity at failure to:

$$P_u = 0.85\ P_n \tag{5.27}$$

The factor 0.85 is a reduction factor to allow the moments due to constructions. Columns having L/D ratio greater than 12 may be considered as long columns. In this case the capacity of the column should be calculated considering bending moment not less than 0.03 B.

5.4.4 Canadian Standard (S016, 2001)

Full composite resistance is specified in Canadian Standard S016 (2001) for hollow steel tubes completely filled with concrete. The limitations for using such columns in this code are:

$$\frac{D}{t} \geq \frac{28000}{\sqrt{f_y}} \tag{5.28}$$

Grade of concrete should be between 20 MPa and 40 MPa for CFST columns. This code predicts the factored compressive strength of CFST columns by increasing the strength of concrete core due to confinement effect and reduces the strength of steel tube.

$$P_u = \left(\tau \emptyset_s A_s f_y + \tau' 0.85 \emptyset_c A_c f_c'\right)\left(1 + \bar{\lambda}^{2n}\right)^{-1/n} \quad (5.29)$$

where,$\tau = \tau' = 1$ for circular columns having L/D ≥ 25. For circular CFST columns having L/D < 25:

$$\tau = \frac{1}{\sqrt{1+\rho+\rho^2}} \quad (5.30\text{ a})$$

$$\tau' = 1 + \left(\frac{25\rho^2\tau}{D/t}\right)\left(\frac{f_y}{0.85 f_c'}\right) \quad (5.30\text{ b})$$

where

$$\rho = 0.02(25 - L/D) \quad (5.31)$$

$$\overline{\lambda} = \sqrt{\frac{P_n}{P_e}} \quad (5.32)$$

P_n and P_e are nominal cross-sectional capacity and Euler buckling load, respectively calculated as

$$P_n = \tau A_s f_y + \tau' 0.85 A_c f_c' \quad (5.33)$$

$$P_e = \frac{\pi^2}{(KL)^2}(EI)_{eff} \quad (5.34)$$

$$(EI)_{eff} = E_s I_s + \frac{0.6 E_c I_c}{1+(C_{fs}/C_f)} \quad (5.35)$$

$$E_c = \left(3300\sqrt{f_c' + 6900}\right)\left(\frac{w_c}{2300}\right)^{1.5} \quad (5.36\text{ a})$$

For concrete having compressive strength between 20 MPa to 40 MPa, E_c can be calculated as:

$$E_c = 4500\sqrt{f_c'} \quad (5.36\text{ b})$$

Here $\bar{\lambda}$ is the relative slenderness parameter and w_c is the density of concrete. C_{fs} is defined as the sustained axial load on the column while C_f is the total axial load on the column. The ratio

of C_{fs}/C_f is taken as 1.0 for short-term loading condition. The constant n has been considered as 1.8 as recommended by the code. $\emptyset_s$ and $\emptyset_c$ are the nominal resistance factors for steel and concrete respectively and have been considered as 1.0.

5.4.5 Euro Code 4 (EN 1994, 2004)

There are two methods for designing composite columns in Euro Code 4 (EC4) (EN 1994, 2004). The first method is "Simplified Design Method". This method is used for doubly symmetrical columns with uniform cross-section over the length of the column. In this method, the plastic strength of concrete is modified by enhancement factor for concrete strength to include the confining effect provided by steel tube to the concrete core. The strength of steel tube is also reduced by a suitable factor to include the effect of biaxial stress state. The ultimate load carrying capacity of the column is then expressed as a function of the modified concrete and steel tube strengths. The second method is "General Design Method". This method is used for composite columns with non-symmetrical or non-uniform cross-section over the column length. In the present study, all the columns are satisfying the requirements of the first method. Therefore, this method is explained and adopted for capacity calculations. The limits of applicability of this method are:

The steel contribution ratio, P_s, must be $0.2 \leq P_s \leq 0.9$. If P_s is less than 0.2, the column may be designed as a reinforced concrete column. If P_s is larger than 0.9, the concrete contribution is ignored and the column is designed as a steel column. Where P_s is defined as:

$$P_s = \frac{A_s f_y}{P_{ud}} \tag{5.37}$$

where P_{ud} is design nominal plastic resistance of concrete filled steel tube (design nominal squash load) calculated as:

$$P_{ud} = \eta_s A_s f_y + A_r f_{yr} + \left[1 + \eta_c \frac{t}{D}\frac{f_y}{f_c'}\right] A_c f_c' \tag{5.38}$$

where A_r is the area of reinforcement bars, if any, f_{yr} is design yield stress of reinforcement bar, λ_s and λ_c are confinement parameters for steel tube and concrete core. η_s reduces the strength of steel section due to biaxial stress state. η_c enhances the strength of concrete section due to confinement. η_s and η_c depend on relative slenderness ratio $\bar{\lambda}$. $\bar{\lambda}$ is calculated as:

$$\bar{\lambda} = \sqrt{\frac{P_n}{P_{cr}}} \tag{5.39}$$

P_n is the plastic resistance of the composite cross-section to compression calculated using the nominal yield strength of steel tube and reinforcement bars and nominal compressive strength of concrete cylinder:

$$P_n = A_s f_y + A_r f_{yr} + A_c f_c^{'} \tag{5.40}$$

P_{cr} is the critical buckling load:

$$P_{cr} = \frac{\pi^2 EI_{eff}}{L^2} \tag{5.41}$$

EI_{eff} is the effective elastic flexural stiffness of the composite column calculated as:

$$EI_{eff} = E_s I_s + E_r I_r + 0.6 E_{cm} I_c \tag{5.42}$$

E_r and I_r are modulus of elasticity and yield stress of reinforcement bars and E_{cm} is the mean secant modulus of elasticity for structural concrete calculated as:

$$E_{cm} = 22000 \left[\frac{f_{cm}}{10}\right]^{0.3} \tag{5.43}$$

where f_{cm} is mean compressive strength of concrete at 28 days age and calculated as:

$$f_{cm} = f_c^{'} + 8\ (MPa) \tag{5.44}$$

For columns having e/d <10:

$$\lambda_s = 0.25\left(3 + 2\overline{\lambda}\right) \leq 1.0 \tag{5.45}$$

$$\lambda_c = 4.9 - 18.5\overline{\lambda} + 17\overline{\lambda}^{\,2} \geq 0 \tag{5.46}$$

The squash load of composite columns in axial compression is calculated as:

$$P_u = \chi\, P_{u1} \tag{5.47}$$

where P_u is the ultimate load carrying capacity of CFST columns and χ is reduction factor to account buckling effect.

$$\chi = \frac{1}{\Phi + \left(\Phi^2 - \overline{\lambda}^2\right)^{0.5}} \tag{5.48}$$

$$\Phi = 0.5 * (1 + \alpha(\overline{\lambda} - 0.2) + \overline{\lambda}^2) \quad (5.49)$$

where α is imperfection factor and has been taken as 0.34 as recommended by Hicks et al. (2002). The code imposes the following limitations for design the CFST columns:

- The relative slenderness $\overline{\lambda}$ of the composite column shall not exceed 2.
- The maximum amount of longitudinal reinforcement that can be considered in the analysis is 6% of the concrete area. i.e. $\frac{A_r}{A_c} \leq 0.06$
- To prevent premature local buckling, the ratio between the width to the wall thickness of steel tube cross-section in compression must satisfy the following limits:

$$D/t \leq 90 \times \frac{235}{f_y} \quad (5.50)$$

5.4.6 Architectural Institute of Japan (AIJ)

Architectural Institute of Japan (AIJ) has published Standard for Structural Calculations of Steel Reinforced Concrete Structures (2001) and Recommendations for Design and Construction of Concrete Filled Steel Tubular Structures (1997) in Japanese language. However, the details for calculating the allowable and ultimate compressive strength of CFST columns are given by Morino and Tsuda (2003). AIJ code classifies the circular CFST column into three categories:

a) Short if KL/D ≤ 4: The axial load carrying capacity for short CFST columns is calculated by superimposing the strength of steel column and concrete column. The confining effect is considered by incorporating a multiplication factor of 1.27 for strength of concrete column.

b) Long if KL/D > 12: The ultimate compressive strength of the long CFST columns is calculated as the summation of critical buckling loads of concrete column and steel column.

c) CFST columns having 4 < KL/D ≤ 12 are classified as Intermediate columns. Linear interpolation is used to calculate the compressive strength of intermediate CFST columns.

The details of calculating the load carrying capacity are:

For KL/D ≤ 4

$$P_{u1} = 1.27\, P_{uc} + P_{us} \quad (5.51)$$

where P_{u1} is the axial load carrying capacity of RCFST column having KL/D ≤ 4, P_{uc} is the ultimate axial compressive load carried by concrete column, and $P_{us}$is the ultimate axial compressive load carried by steel column.

$$P_{uc} = 0.85 f_c^{'} A_c \tag{5.52}$$

$$P_{us} = f_y A_s \tag{5.53}$$

For 4 < KL/D ≤ 12

$$P_{u2} = P_{u1} - 0.125\left(P_{u1} - P_{u3,12}\right)\left(\frac{KL}{D} - 4\right) \tag{5.54}$$

Here P_{u2} is the load carrying capacity of column having 4 < KL/D ≤ 12 and$P_{u3,12}$ is the load carrying capacity of a virtual CFST column having same cross-section but with KL/D =12

For KL/D > 12

$$P_{u3} = A_c f_{crc} + A_s f_{crs} \tag{5.55}$$

where f_{crc} and $f_{crs}$are critical buckling stress of concrete column and steel column, respectively.

For $\overline{\lambda}_c \leq 1.0$

$$f_{crc} = \frac{2}{1+\sqrt{\overline{\lambda}_c^{\,4}+1}} 0.85 f_c^{'} \tag{5.56}$$

For $\overline{\lambda}_c$>1.0

$$f_{crc} = 0.83 \times e^{\left(c_c\left(1-\overline{\lambda}_c\right)\right)} 0.85 f_c^{'} \tag{5.57}$$

where:

$$\overline{\lambda}_c = \frac{\lambda_c}{\pi}\sqrt{\varepsilon_{uc}} \tag{5.58}$$

$\overline{\lambda}_c$ is the relative slenderness parameter of concrete column and $\lambda_c$is the slenderness parameter of concrete column calculated as:

$$\lambda_c = \frac{KL}{r_c} \tag{5.59}$$

where r_c is the radius of gyration of concrete column and ε_{uc} is the ultimate axial strain of concrete column calculated as:

$$\varepsilon_{uc} = 0.93(0.85f_c^{'})^{1/4} \times 10^{-3} \tag{5.60}$$

C_c is an empirical parameter calculated as:

$$C_c = 0.568 + 0.00612\ f_c^{'} \tag{5.61}$$

For $\overline{\lambda}_s$ ***< 0.3***

$$P_{crs} = f_y A_s \tag{5.62 a}$$

For 0.3 ≤ $\overline{\lambda}_s$ ***< 1.3***

$$P_{crs} = \left(1 - 0.545\left(\overline{\lambda}_s - 0.3\right)\right) f_y A_s \tag{5.62 b}$$

For $\overline{\lambda}_s$ ***≥ 1.3***

$$P_{crs} = \frac{P_{es}}{1.3} \tag{5.62 c}$$

$$\overline{\lambda}_s = \frac{\lambda_s}{\pi}\sqrt{\frac{f_y}{E_s}} \tag{5.63}$$

$\overline{\lambda}_s$ is the relative slenderness parameter of steel column, $\lambda_s$is the slenderness parameter of steel column calculated as:

$$\lambda_s = \frac{KL}{r_s} \tag{5.64}$$

r_s is the radius of gyration of steel tube and P_{es} is the Euler buckling load of steel column calculated as:

$$P_{es} = \frac{\pi^2 E_s I_s}{(KL)^2} \tag{5.65}$$

5.4.7 Chinese Codes

There are four codes in China for designing CFST members. These codes are published in Chinese language and the code methodologies are also discussed in Han (2002), Zhang et al., (2007), Hatzigeorgiou (2008), and Lu and Zhao (2010). The codes are:

- DL/T 5085:1999, Codes for design of steel-concrete composite structures, issued by Chinese State Economic and Trade Commission.
- GJB 4142:2000, Technical Specifications for early-strength model composite structure used for navy port emergency repair in war time, Military code
- JCJ 01:89, Specification for design and construction of Concrete Filled steel tubular structures, issued by Chinese National Structural Materials and Industry Bureau.
- CECS 28:90 and CECS 104:99, Specification for design and construction of Concrete Filled steel tubular structures and Specification for design and construction of high-strength concrete structures, respectively, issued by Association of Chinese Engineering Construction Standardization.

The capacity of short CFST column in JCJ and CECS codes is calculated based on confinement theory. In this theory, the separate cross-sectional strength of steel tube and concrete core are calculated separately and then added to get the strength of composite cross-section. The details of these codes, as presented in Han (2002) and Zhang et al. (2007) are as follows:

CECS 28:90 code:

$$P_u = A_c f_{ck}\left(1 + \xi + \sqrt{\xi}\right) \tag{5.66}$$

Where:

$$\xi = \frac{A_s f_y}{A_c f_{ck}} \tag{5.67}$$

Here ξ is the confining factor. The value of ξ must lie between 0.03 and 3.0.

Other limitations for using this code are: f_{ck}= 30-80 MPa, f_y = 235-420 MPa, D/t = 20-$90\sqrt{235/f_y}$.

The DL/T and GJB codes work on the principle of unified theory i.e. A heterogeneous CFST cross-section consisting of concrete and steel is converted to an equivalent single composite

cross-section. The procedure for calculating the load carrying capacity as per these codes is given as:

GJB 4142:2000 (Han, 2002) ***and DL/T 5085:1999*** (Lu and Zhao, 2010)

$$P_u = f_{scy} A_{sc} \tag{5.68}$$

f_{scy} and A_{sc} are the equivalent stress and area of new composite cross-section.

$$f_{scy} = (1.212 + B\xi + C\xi^2) f_{ck} \tag{5.69}$$

where B and C parameters are given (Lu and Zhao, 2010) for circular CFST columns as:

$$B = 0.1759 \frac{f_y}{235} + 0.794 \tag{5.70}$$

$$C = -0.1038 \frac{f_{ck}}{20} + 0.0309 \tag{5.71}$$

$$A_{sc} = A_s + A_c \tag{5.72}$$

The value of f_{ck} (characteristics compressive strength of concrete core) is obtained using 67% of the compressive strength of concrete cubes as recommended by Han (2002).

It can be seen from the above equations that none of the codes give any formulas for prediction of load carrying capacity of Double skin concrete filled steel tubes (CFDST). Hence, while calculating the load capacity for the CFDST, the inner tube in CFDST specimen was considered in a similar way as the outer steel tube. The load carrying capacities calculated from the different codes are shown in Table 5.7. The ratio of codal to experimental values is also shown in the table. It can be seen in this table that all of the codes give conservative results with most conservative results being obtained from the AISC and ACI codes. Further, it is also observed from that the Canadian code (CSA) and Chinese code (CECS) give best estimations of the capacities with average of capacities of all specimens as 0.98 of tested capacity. The next best estimates were obtained from Euro code (EC4), with average predicted capacity of all samples as 92% of the experimental results.

.

Table 5.10 Results of different International Codes used for predicting the axial capacities of circular tested specimens

Core	Length	Sample	$P_{u\text{-}EC4}$ (kN)	$\frac{EC4}{EXP}$	$P_{u\text{-}AISC}$ (kN)	$\frac{AISC}{EXP}$	$P_{u\text{-}ACI}$ (kN)	$\frac{ACI}{EXP}$	$P_{u\text{-}BS}$ (kN)	$\frac{BS}{EXP}$	$P_{u\text{-}CSA}$ (kN)	$\frac{CSA}{EXP}$	$P_{u\text{-}AIJ}$ (kN)	$\frac{AIJ}{EXP}$	$P_{u\text{-}CECS}$ (kN)	$\frac{CECS}{EXP}$	$P_{u\text{-}GJB}$ (kN)	$\frac{GJB}{EXP}$
RCFST	L3D	CS1-1-1	1034.8	1.01	780.3	0.76	755.9	0.74	932.1	0.91	1074.1	1.05	905.1	0.89	1104.0	1.08	844.9	0.83
		CS1-1-2	1185.8	1.01	883.9	0.76	860.9	0.74	1085.4	0.93	1237.7	1.07	1039.3	0.90	1240.3	1.07	934.5	0.81
		CS1-1-3	1328.8	1.02	994.3	0.76	964.9	0.74	1233.6	0.95	1407.2	1.08	1174.3	0.90	1371.1	1.05	1009.3	0.78
		CS1-2-1	1994.6	0.93	1491.7	0.70	1437.5	0.67	1748.3	0.82	2034.9	0.95	1709.2	0.80	2116.2	0.99	1631.3	0.76
		CS1-2-2	2207.2	1.02	1635.1	0.75	1582.7	0.73	1967.2	0.90	2268.1	1.04	1896.4	0.87	2311.4	1.06	1766.4	0.81
	L4D	CS1-3-1	539.1	0.88	417.9	0.68	403.1	0.66	429.4	0.70	548.6	0.90	478.3	0.78	594.45	0.97	450.1	0.74
		CS1-3-2	620.3	0.93	475.6	0.71	461.8	0.69	513.8	0.77	637.2	0.96	555.6	0.83	672.4	1.00	503.5	0.75
		CS1-3-3	687.9	0.93	525.1	0.71	512.2	0.70	575.1	0.78	711.0	0.96	621.9	0.84	736.8	0.95	543.4	0.74
	L7D	CS2-1-1	856.9	0.89	759.2	0.79	755.9	0.79	818.4	0.85	940.4	0.98	854.1	0.89	911.1	0.96	845.8	0.88
		CS2-1-2	971.3	0.91	860.4	0.80	860.9	0.80	950.3	0.89	1079.2	1.01	978.1	0.91	1024.1	0.98	934.5	0.87
		CS2-1-3	1083.1	0.94	967.7	0.83	964.9	0.83	1078.6	0.93	1224.0	1.06	1100.1	0.95	1132.1	0.82	1009.3	0.87
		CS2-3-1	478.4	0.82	414.2	0.71	403.1	0.69	413.1	0.69	662.6	1.14	448.5	0.77	476.3	0.84	450.1	0.77
		CS2-3-3	607.6	0.86	519.3	0.74	512.2	0.73	540.0	0.73	773.8	1.10	577.4	0.82	590.1	0.76	503.5	0.77
	L10D	CS3-3-1	424.3	0.76	405.1	0.73	403.1	0.73	399.7	0.73	546.8	0.98	417.6	0.75	426.9	0.80	543.4	0.81
		CS3-3-2	484.2	0.80	461.0	0.76	461.8	0.76	450.1	0.76	538.7	1.00	479.6	0.79	482.9	0.81	503.6	0.83
		CS3-3-3	534.1	0.82	508.3	0.78	512.2	0.79	502.3	0.79	599.1	0.98	532.8	0.93	529.2	1.08	543.8	0.83
RCC-RCFST	L3D	CR1-1-1	1370.3	0.95	914.1	0.64	1101.0	0.77	1232.4	0.86	1318.0	0.94	1343.7	0.82	1553.2	1.09	1108.7	0.77
		CR1-1-2	1350.7	0.97	951.0	0.68	1034.5	0.74	1236.6	0.89	1345.5	0.99	1259.4	0.94	1462.8	1.10	1059.7	0.76
		CR1-2-1	2227.0	0.85	1591.0	0.60	1657.5	0.62	1940.0	0.72	2229.1	0.83	2024.2	0.90	2414.2	1.14	1661.5	0.62
	L7D	CR2-1-1	1186.5	0.87	895.2	0.65	1101.0	0.80	1119.7	0.82	1216.1	0.89	1255.7	0.76	1283.1	1.07	1108.7	0.81
		CR2-1-2	1134.5	0.84	928.1	0.69	1034.5	0.77	1100.5	0.82	1221.4	0.91	1179.2	0.92	1208.1	0.97	1059.7	0.77
RCFDST	L3D	CD1-1-1	1082.1	0.91	929.9	0.78	902.1	0.76	1014.0	0.85	1084.8	0.91	1116.1	0.88	1283.1	0.95	916.2	0.74
		CD1-1-2	1215.1	0.94	1033.5	0.80	1002.4	0.77	1149.5	0.89	1227.2	0.95	1250.1	0.94	1409.1	1.00	956.5	0.69
		CD1-1-3	1352.8	0.97	1136.1	0.81	1122.5	0.80	1278.2	0.92	1364.6	0.98	1384.1	0.97	1530.2	1.08	968.6	0.86
		CD1-2-1	2051.2	1.01	1641.7	0.70	1595.2	0.79	1842.7	0.91	2052.1	1.01	1920.2	0.99	2311.2	1.05	1747.0	0.80
		CD1-2-2	2254.3	0.97	1785.1	0.76	1740.6	0.75	2048.3	0.88	2272.4	0.97	2106.2	0.95	2496.4	1.06	1862.2	0.80
	L7D	CD2-1-1	923.7	0.86	901.6	0.83	902.1	0.74	924.1	0.85	989.2	0.91	1039.3	0.95	1059.1	0.90	916.2	0.84
		CD2-1-2	1029.9	0.89	1002.3	0.87	1002.4	0.83	1042.2	0.85	1114.1	0.91	1164.5	0.95	1163.0	0.94	956.5	0.78
		CD2-1-3	1141.5	0.90	1109.5	0.87	1122.5	0.82	1157.4	0.91	1157.4	0.97	1287.1	1.01	1269.1	0.90	968.6	0.76
Average				0.92		0.75		0.76		0.84		0.98		0.88		0.98		0.79
Standard Deviation				0.06		0.07		0.06		0.08		0.07		0.07		0.10		0.06
Coefficient of Variation				7.61		9.33		7.89		9.53		7.14		7.95		9.87		7.59

5.5. CONCLUSIONS

Mode of deformation:

a. The primary mode of deformation in L3D specimens was observed to be combination of local buckling in steel tube accompanied by crushing in concrete core for all core configurations (Figures 5.2, 5.4, 5.5 and 5.7). The L7D and L10D specimens were observed to fail by global buckling (Figures 5.3, 5.6 and 5.8).

b. The deformed shape for RCC-CFST specimens was observed to be local buckling near the location of ties. The deformation of the reinforcing bars was observed to be buckling between the ties (Figure 5.9 (b)).

Strength:

a. Increase in strength due to composite action was observed for all tested specimens as compared to the nominal capacity calculated based on the plastic strength of the materials. The enhancement in strength was lower for specimens with smaller tube thickness (Table 5.4).

b. The increase in load carrying capacity was observed to be greatest in RCC-CFST specimens among the three core configurations. It was the least for CFDST specimens (Figure 5.13).

Ductility:

a. Most of the specimens exhibited strain-hardening behaviour. However, the L7D and L10D specimens of small diameter single skin sections (CFST 90 mm diameter) showed strain softening behaviour (Tables 5.5 to 5.7).

b. The lowest ductility was observed in the case of CFDST specimens, while the CFST single skin specimens generally showed the maximum ductility (Figure 5.15).

Length effect:

a. The L7D and L10D specimens showed lower load carrying capacity was lower for all specimens as compared to the corresponding L3D details due to length effect.

Further, reduction in load carrying capacity was more in the specimens having greater thicknesses as compared to specimens having smaller thicknesses (Figure 5.17).

b. RCC-CFST specimens reported the lowest reduction in the axial load due to increase in length among all tested specimens. (Figure 5.17).

Equivalent area of steel:

Steel rebars can be used with specimens having smaller wall thickness as compensation for getting similar results of CFST specimens with greater wall thickness. However, as the compensated area increases the enhancement in strength and ductility decreases (Table 5.9).

Codal recommendations:

Among eight International Codes, the Canadian code S016 (CSA) and Chinese (CECS) code give closest estimation for strength with average predicted capacity (of all samples) as 98% of average experimental capacity. The next best estimate is given by Euro Code, with average predicted strength being approximately 8% lesser than the measured capacities (Table 5.10).

5.6. STUDY OF CONFINEMENT PRESSURE

5.6.1 General

The improved structural performance of CFST members is due to the radial confining pressure (f_{cp}) exerted by the steel tube on the concrete, which enhances the compressive strength and ductility of concrete. Estimating the correct value of this parameter is pivotal to finding the load resistance of CFST member under any given type of loading. However, the experimental measurement of the value of confining pressure at any section is very difficult and requires sophisticated equipment. Hence, the proposed FEM model has been used to study its variation along the height and the circumference of the specimen.

5.6.2 Procedure of Measurement of Confining Pressure

The sample CC4-A-4-1 from Sakino et al., 2004 is taken as an example to understand the procedure. It is a circular single skin CFST with diameter of outer tube as 149 mm. The height of the specimen is 447 mm.

The estimation of the radial pressure at any cross-section requires defining a circumferential path at that section. Figs. 5.19 (a) and 5.19 (b) show the cross-section under consideration (at 70 mm from top surface of CFST) and the circumferential path at that cross-section in sample CC4-A-4-1. Figure 5.20 (a) shows the confining pressure distribution for the path shown in Figure 5.19. The negative value of the confining pressure implies a compressive confining pressure on concrete.

It is expected that since in axial compression, concrete expands laterally in all directions, the confining pressure should be nearly constant at all points of any particular cross section in concrete. This is evident from Figure 5.20 (b), where it is observed that at any section (i.e. any Z-value), the radial confining pressure is more or less constant throughout the path.

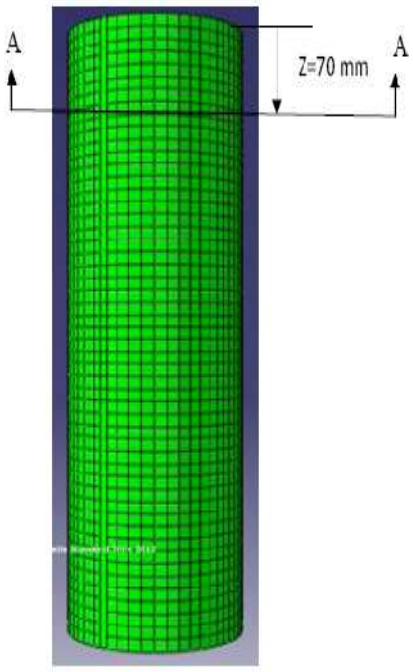

Figure 5.19(a) A section AA cut in CFST at 70 mm from top surface

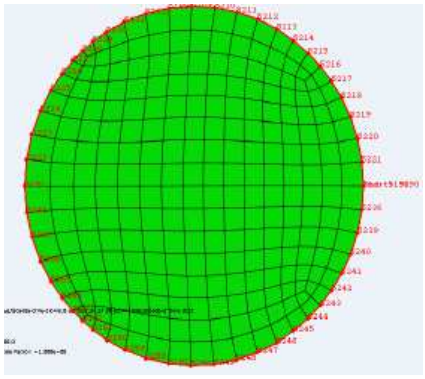

Figure 5.19(b) A circumferential path defined at 70 mm from top

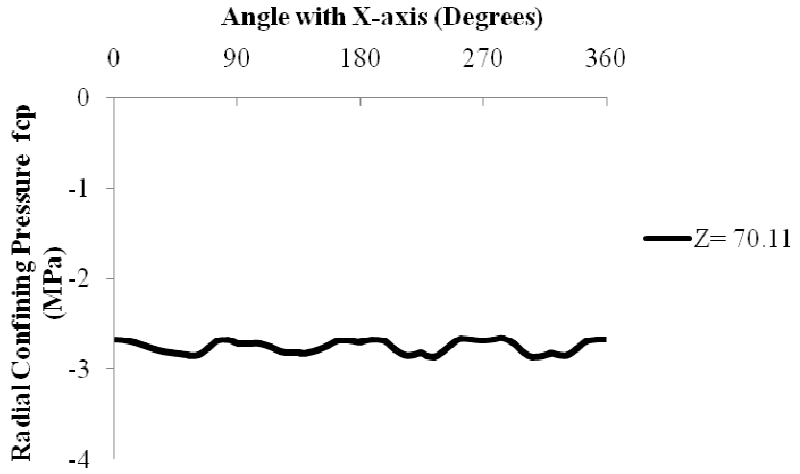

Figure 5.20(a) Radial confining pressure distribution along the circumference (at a cross-section 70 mm from top in Sakino CC4-A-4-1)

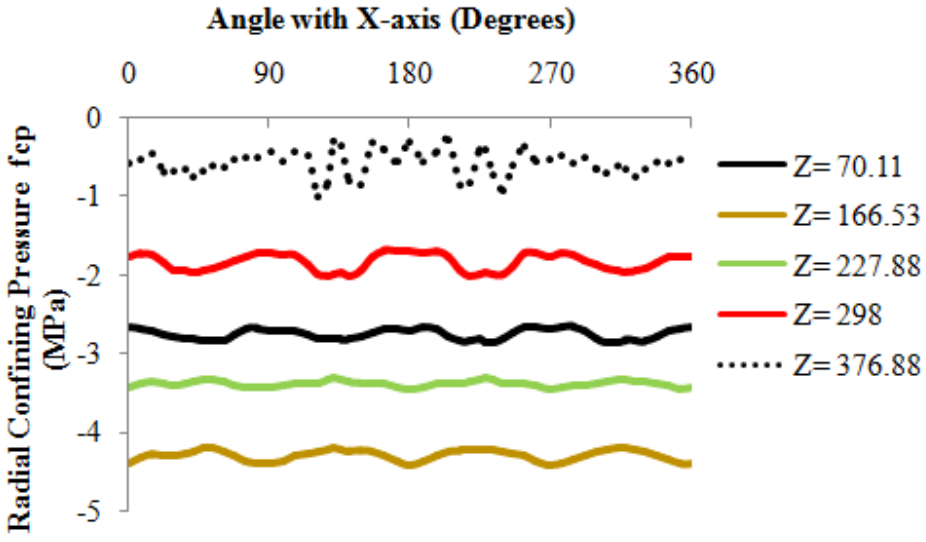

Figure 5.20(b) Radial confining pressure distribution for different sections along the height of Sakino CC4-A-4-1

Consider the same procedure for another sample. The sample chosen is C3 (Giakoumelis and Lam, 2004). The length of the sample is 300 mm. The distribution of circumferential confining pressure is drawn at different cross-sections at varying distance (Z-values) from the top. This is shown in Figure 5.19 (a). It is seen from this figure at Z=52 mm and Z=247 mm from the top, there are large variations in confining pressure around the circumference. This is due to the effect of end friction near the test machine platens, which offers an additional restraint to the CFST.

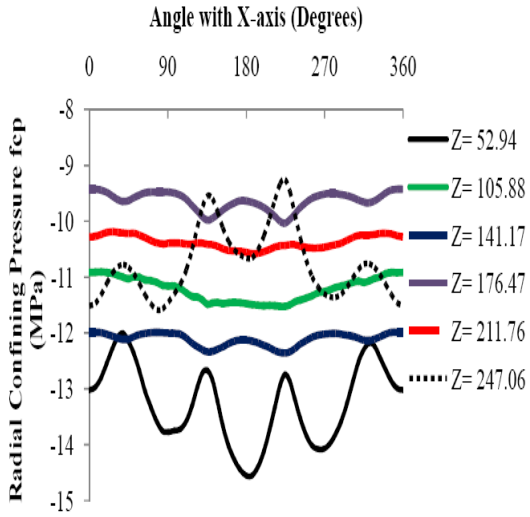

Figure 5.21(a) Radial confining pressure at different cross-sections along the length of specimen C3

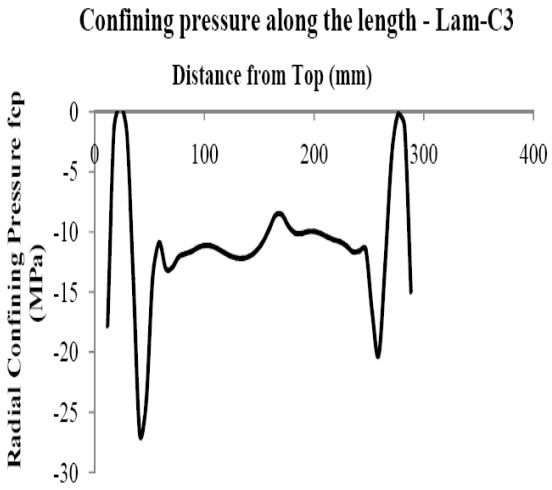

Figure 5.21(b) Variation of confining pressure along the length of specimen C3

The variation in the lateral confining pressure along the length of sample has also been drawn. since confining pressure at all points on any horizontal cross section is approximately same, any vertical can be chosen. The variation is shown in Figure 5.19 (b). It is evident from this figure that It can be observed that the confining pressure in the areas adjacent to top and bottom of machine platens is much higher than the corresponding values in the remaining length of the specimen.

5.6.3 Confining Pressure in 114.3 mm Diameter circular specimens

The procedure of obtaining confining pressure has then been applied to the circular specimens tested by the author. Circular specimens of 114.3 mm steel tube diameter have been analysed. The variation of confining pressure was obtained along the full length of the specimen. This operation was performed for different axial displacements on the numerical load-displacement curve of the sample.

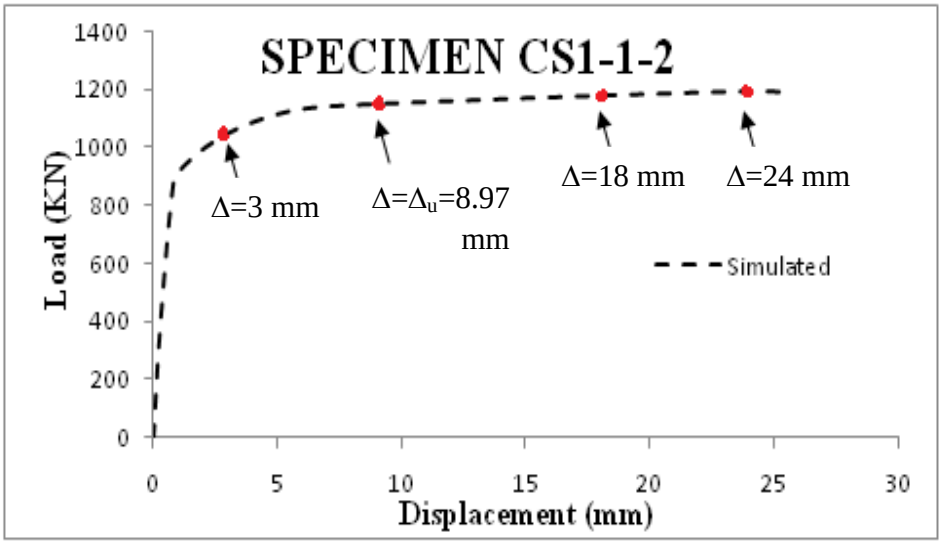

Figure 5.22 Different displacements chosen along short column CS1-1-2 for obtaining confining pressure

For instance, consider a typical short (L3D) CFST single skin specimen of 114.3 mm dia and 4.5 mm thickness. Four displacement levels, as shown in Figure 5.22, have been chosen for obtaining the variation of confining pressure along the length of the specimen. Figure 5.23(a) shows the confining pressure distribution at these times.

It can be seen from Figure 5.23(a) that the pressure distribution over the length of the specimen is fairly constant at any given displacement level (except at the end regions). Therefore, excluding the end regions (the parts with abnormally high values), the values of confining pressure can be averaged from the remaining part to get a single value for f_{cp} at this displacement. The averaged value of confining pressure has been noted for the point of maximum load in simulated curves for different specimens.

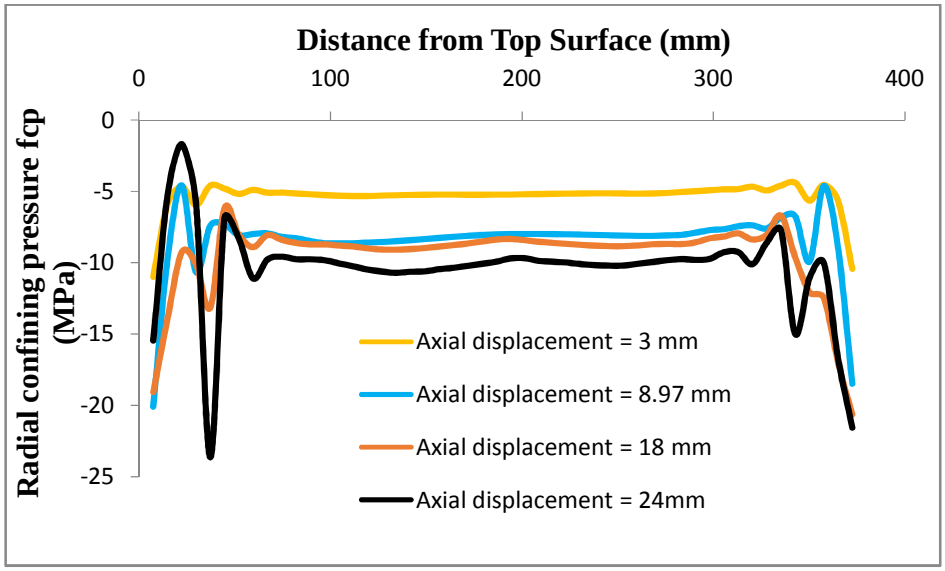

Figure 5.23(a) Confining pressure distribution in specimen CS1-1-2 along the length

the end regions (the parts with abnormally high values), the values of confining pressure can be averaged from the remaining part to get a single value for f_{cp} at this displacement. The averaged value of confining pressure has been noted for the point of maximum load in simulated curves for different specimens (Please note that the confining pressure distribution at displacement corresponding to maximum load is shown by a solid black line in Figures 5.23 to 5.28). These values can then be compared with the confining stress from theoretical equation in literature (see Equations 4.2 and 4.3, Chapter 4).

Figure 5.23(b) shows a comparison of numerical and experimental debonding between the steel tube and concrete core at the location of local buckling of the CFST. Further, the variable CPRESS (contact pressure between steel and concrete) shows a zero value at this location, thereby indicating a loss of confinement at this location.

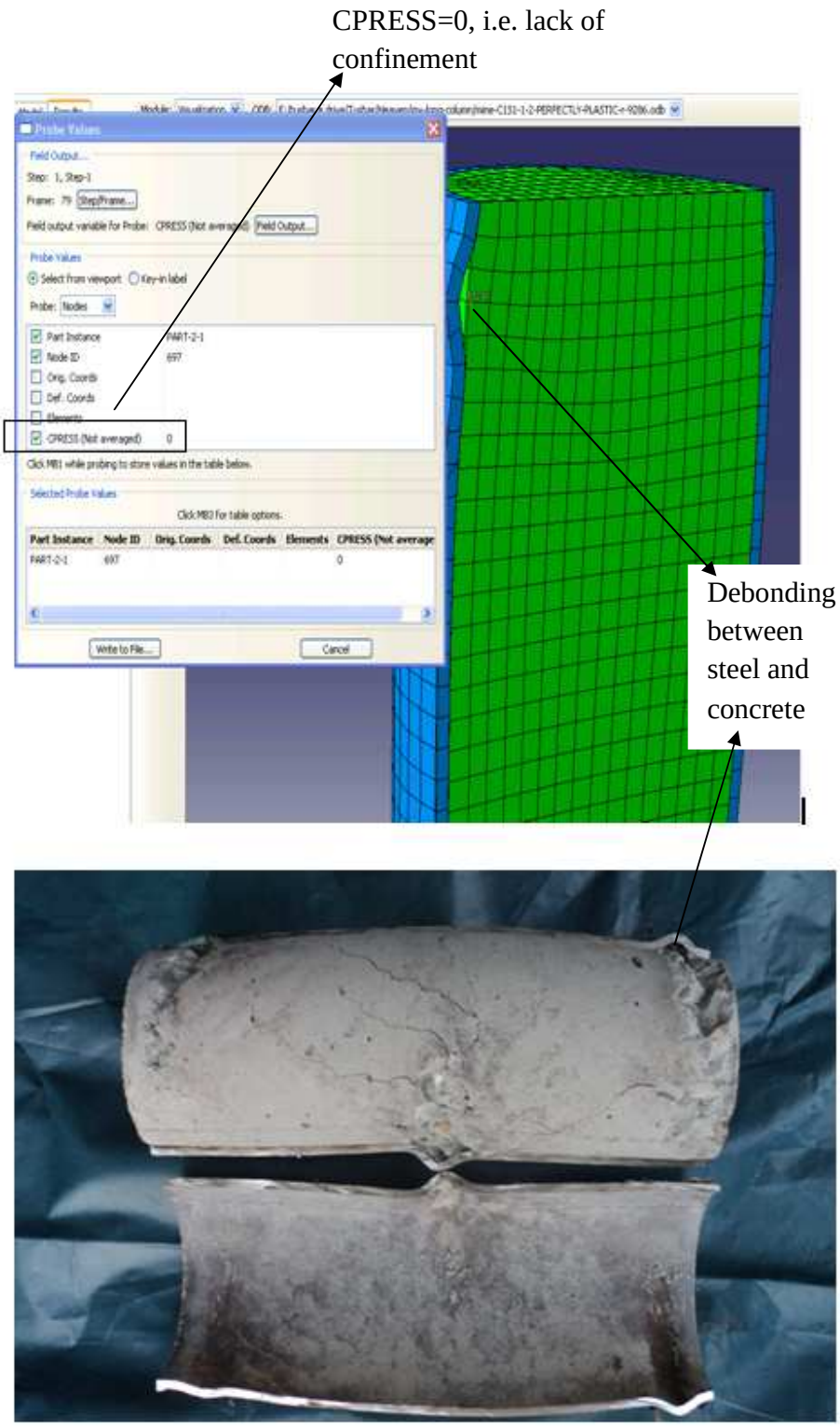

Figure 5.23(b) Debonding and loss of confinement in a typical short CFST specimen CS1-1-2

On the same lines, Figure 5.24(a) shows the values of displacements chosen for obtaining the confining pressure on the numerical (obtained from ABAQUS) load-deflection curve of typical intermediate specimen (L7D) CS2-1-2. Figure 5.24(b) shows the location of the path (shown as connection of red dots with the node numbers) along which the confining pressure distribution along the height has been reported. The path has been chosen so as to be quite close the location of maximum global buckling. The confining pressure distribution of single tube column along this path CS2-1-2 is also shown in Figure 5.24(b).

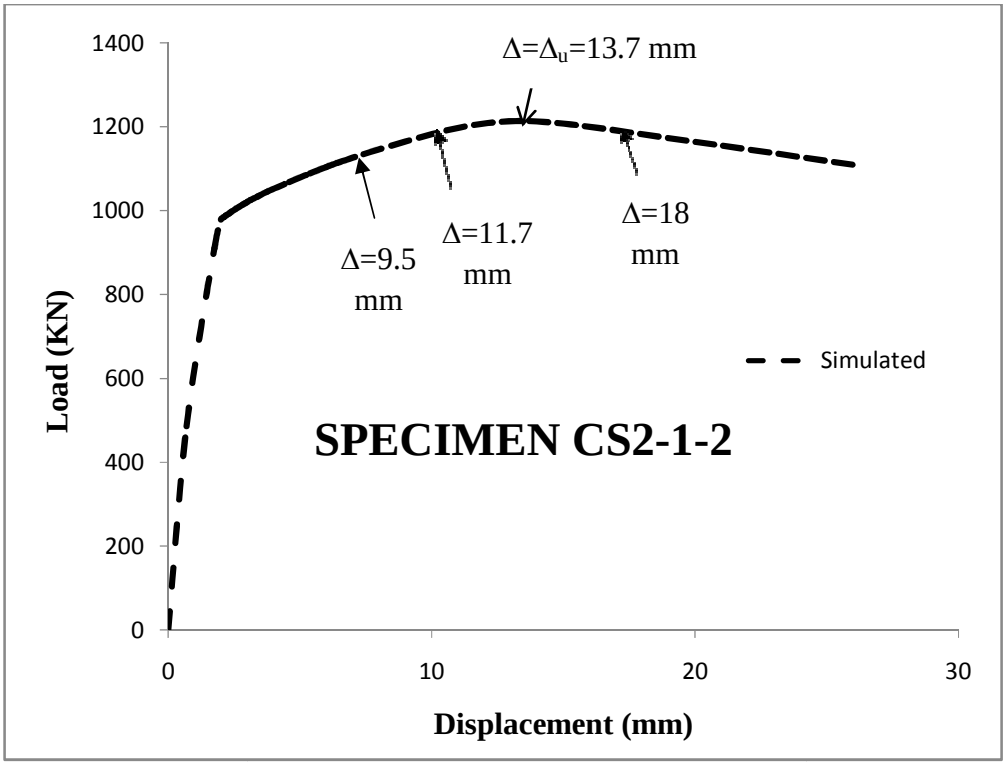

Figure 5.24(a) Different displacements chosen along intermediate column CS2-1-2 for obtaining confining pressure

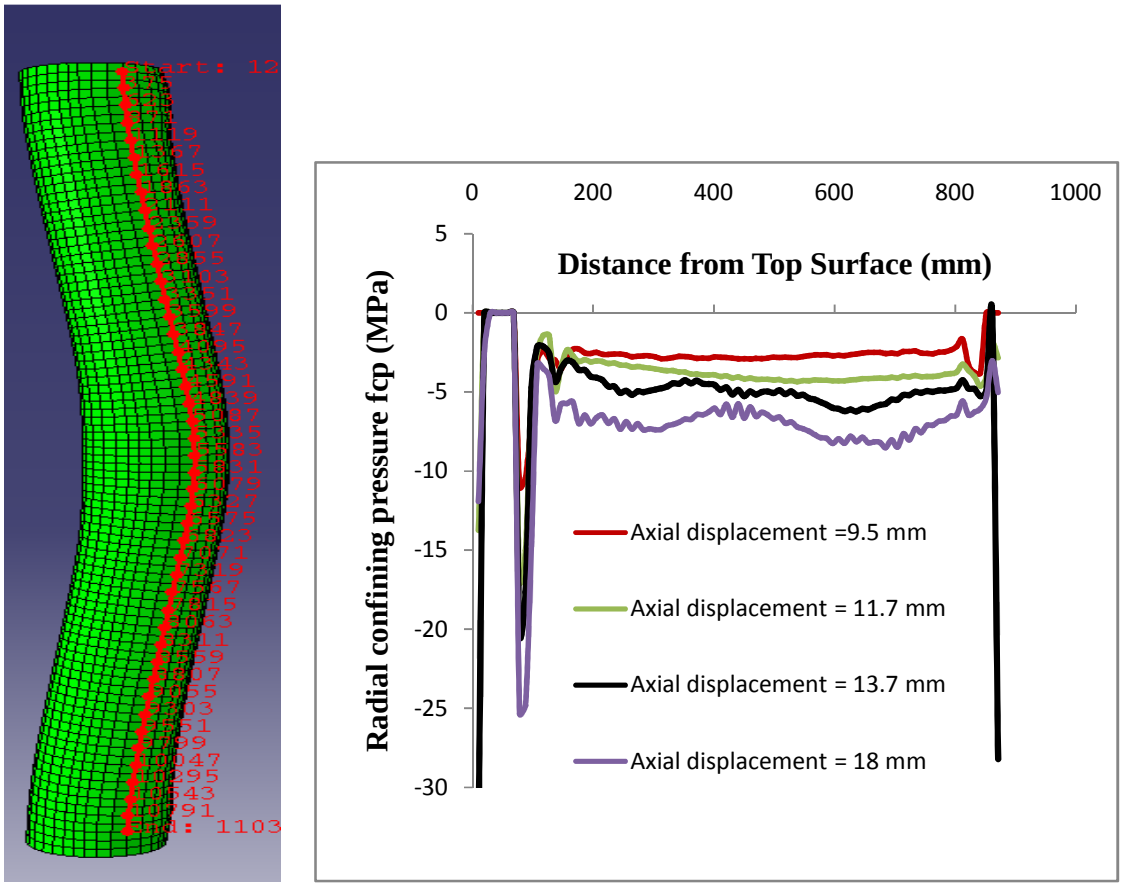

Figure 5.24(b) Location of path and confining pressure distribution in specimen CS2-1-2 along the chosen path

Table 5.11 Comparison of confining pressure values for 114.3 single skin specimens

Specimen ID	L/D (nominal)	f_{cp} (MPa)	f_l from theoretical model (MPa) of Hu et al. (2003) (see Equation 4.2, Chapter 4)
CS1-1-1	3.00	7.83	6.74
CS1-1-2	3.00	9.83	8.99
CS1-1-3	3.00	11.74	10.61
CS2-1-1	7.00	5.19	6.74
CS2-1-2	7.00	4.88	8.99
CS2-1-3	7.00	4.35	10.61

Table 5.10 compares the result from theoretical equation and numerical simulations for all single skin specimens of 114.3 mm outer diameter. It is clear from the table that the numerical confining pressure agrees well with the theoretical values for short L3D columns. However, the theoretical model overestimates the confining pressure value for specimens of higher length (L7D).

On the same lines, the path (shown as a connection of line connecting the red dots) for checking the confining pressure in short double skin specimen CD1-1-2 (Double Skin short column of 114.3 mm outer diameter) is shown in Figure 5.25The confining pressure distribution also shown for this path. From Figure 5.25, it is clear that the path has been chosen near the critical region of local buckling.

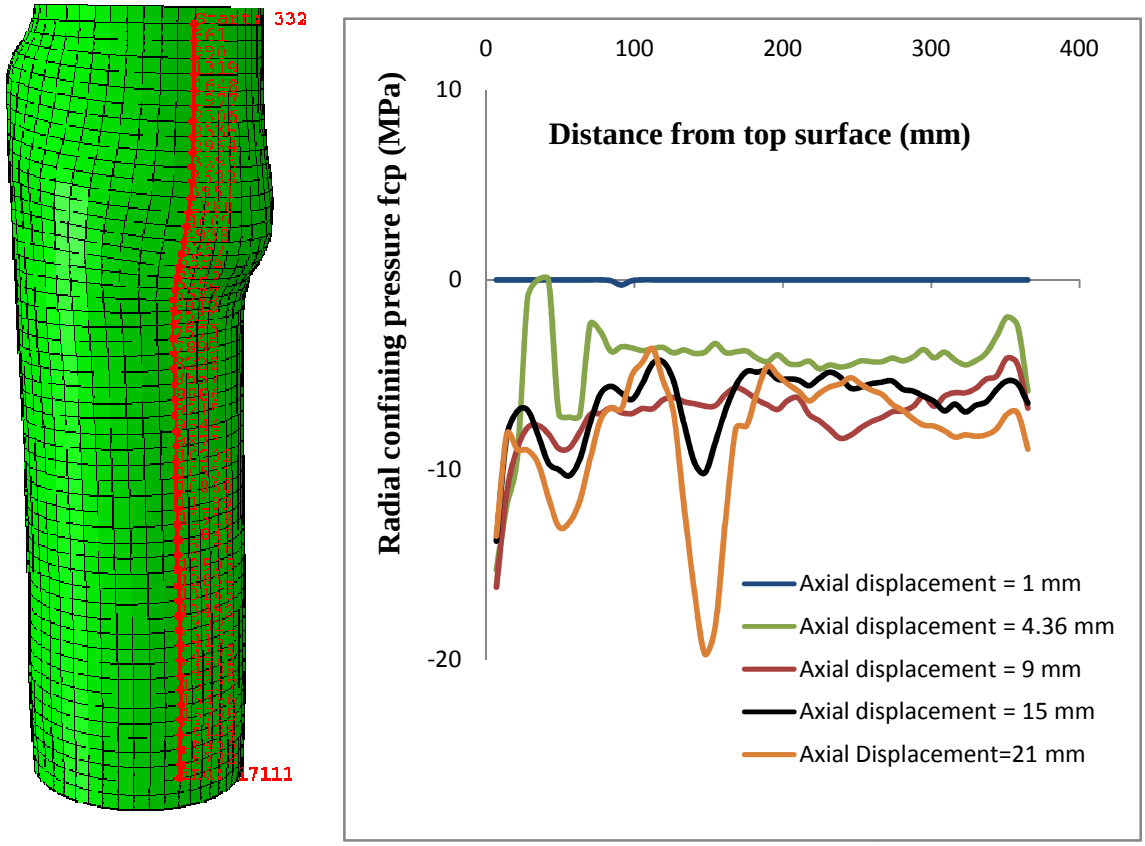

Figure 5.25 Location of path and confining pressure distribution in specimen CD1-1-2 along the path

Figure 5.26(a) shows the location of displacements used for obtaining the confining pressure on numerical load-deflection curve of CD2-1-2 (Double skin specimen of 114.3 mm diameter and 4.5 mm outer steel tube thickness).

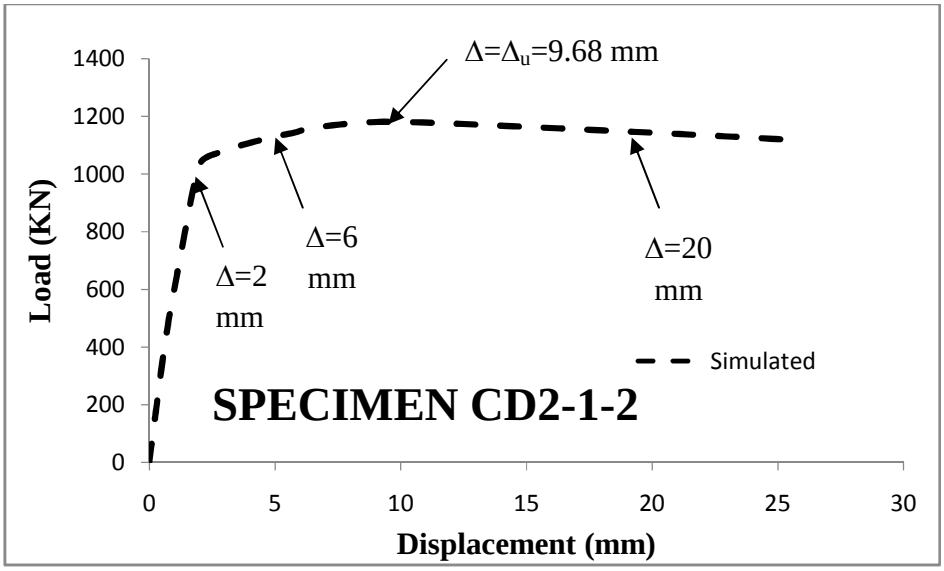

Figure 5.26(a) Different displacements chosen along short column CD2-1-2 for obtaining confining pressure

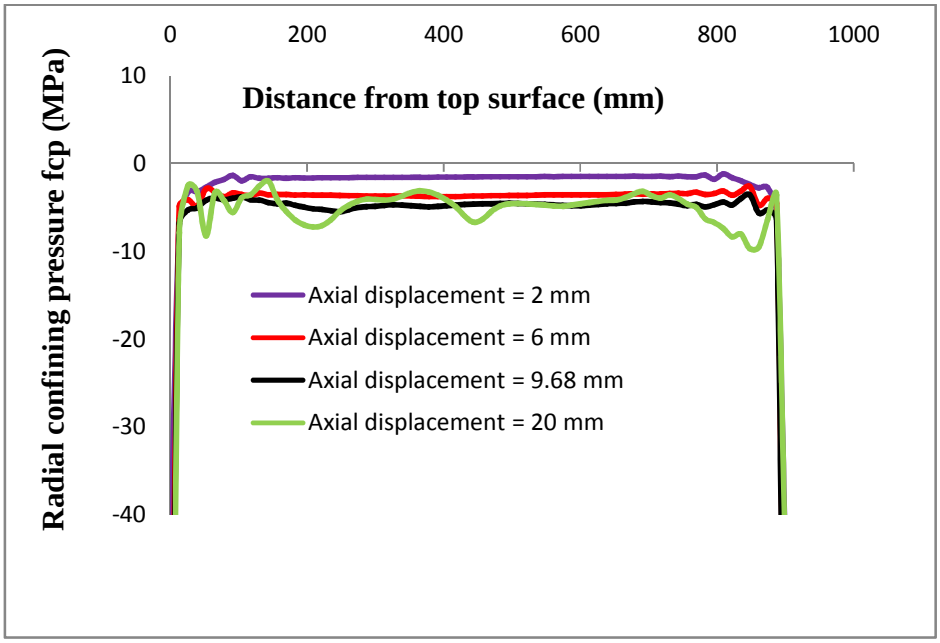

Figure 5.26(b) Confining pressure distribution in specimen CD2-1-2 along the length

It is clear from Figures 5.25 and 5.26(b) the CFDST specimens show appreciable variation in the confining pressure distribution even in the central region of the specimen (area excluding the end regions) as compared to Single skin specimens. This variation is even more pronounced at higher levels of axial displacement. However, the peak loads are seen to occur at lower levels of displacement, where the values of numerical confining pressure have been averaged and compared with theoretical values in Table 5.11.

Table 5.12 Comparison of confining pressure values for 114.3 mm diameter Double skin specimens

Specimen ID	L/D (nominal)	f_{cp} (MPa)	f_l from theoretical model (MPa) of Hu and Su (2011) (see Equation 4.3, Chapter 4)
CD1-1-1	3.00	3.63	6.74
CD1-1-2	3.00	3.97	8.99
CD1-1-3	3.00	4.95	10.61
CD2-1-1	7.00	2.14	6.74
CD2-1-2	7.00	3.68	8.99
CD2-1-3	7.00	4.67	10.61

It is clear from Table 5.11 that the values from software are lower than the theoretical values.

Figures 5.27 and 5.28 show the confining pressure distribution for samples CR1-1-2 and CR2-1-2 (114.3 diameter RCC-CFST on L3D and L7D respectively). It can be seen from the Figures that the confining pressure is quite large near the location of lateral ties, which is also the location of local buckling of the steel tube. The confining pressure is relatively much lower between the ties, where the reinforcing bars buckle.

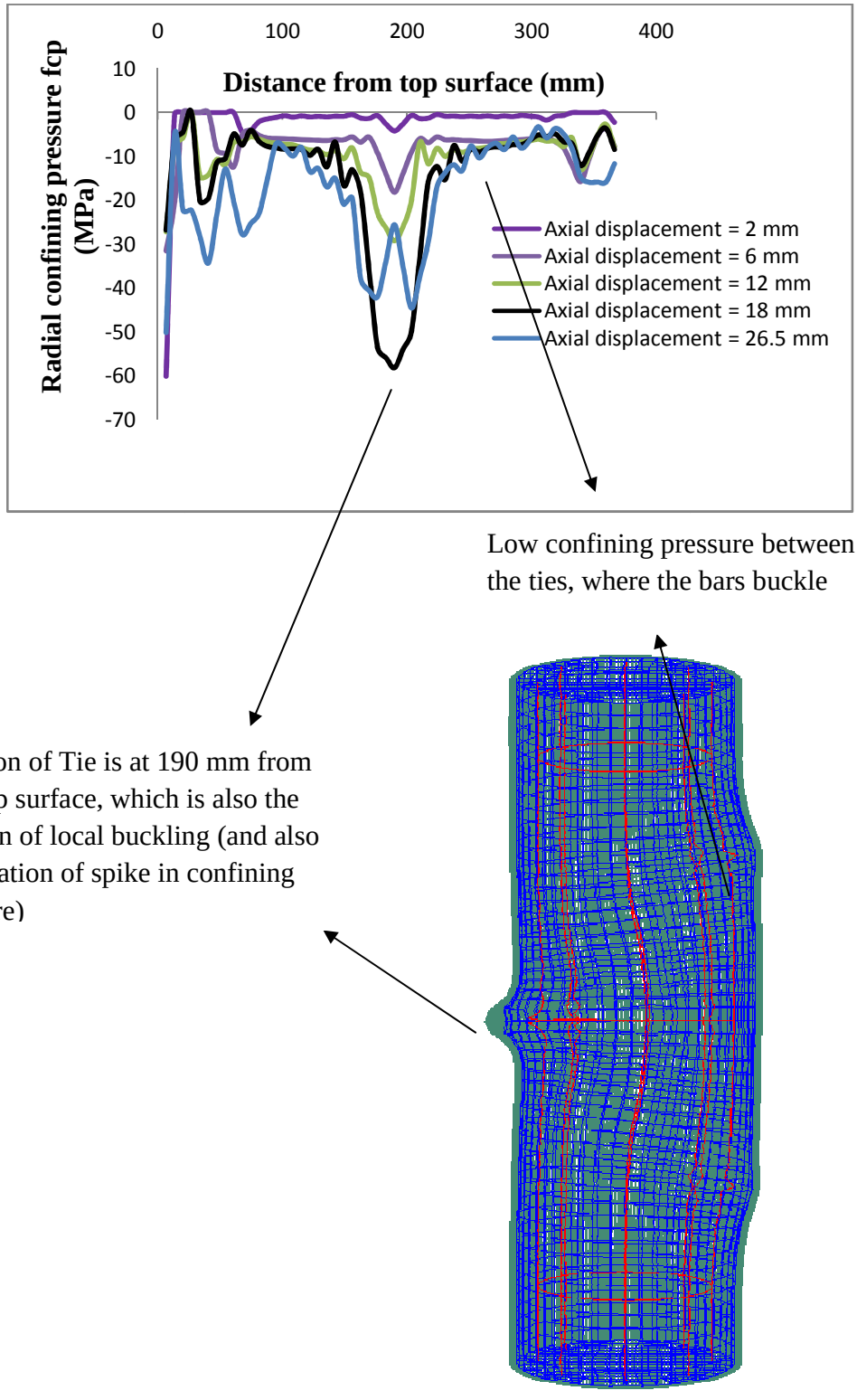

Figure 5.27 Confining pressure distribution in specimen CR1-1-2 along the length (Rebars are red colored lines)

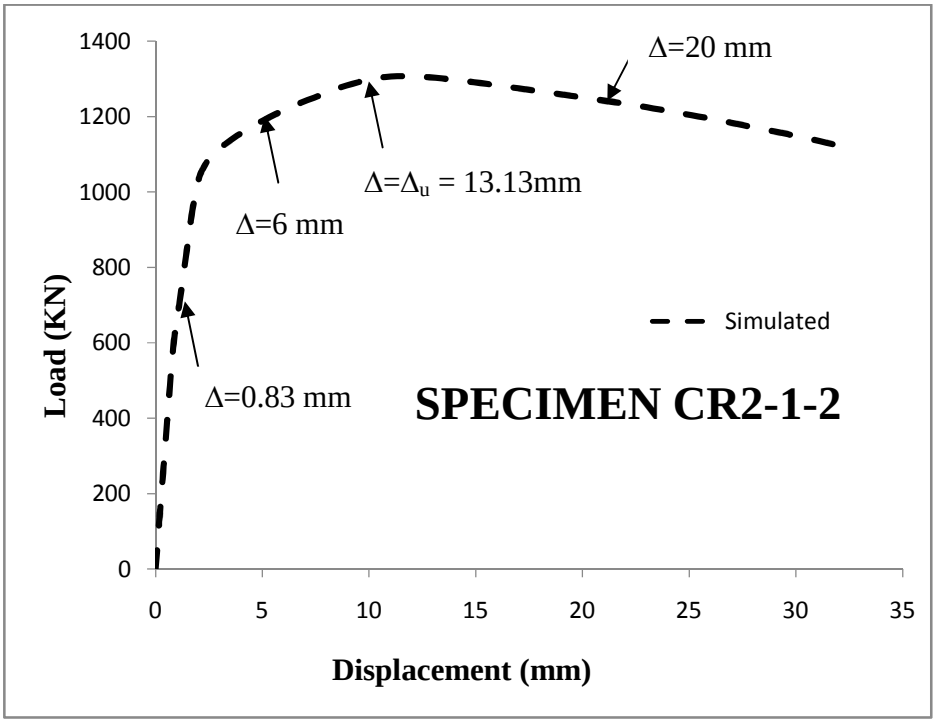

Figure 5.28(a) Different displacements chosen along intermediate column CR2-1-2 for obtaining confining pressure

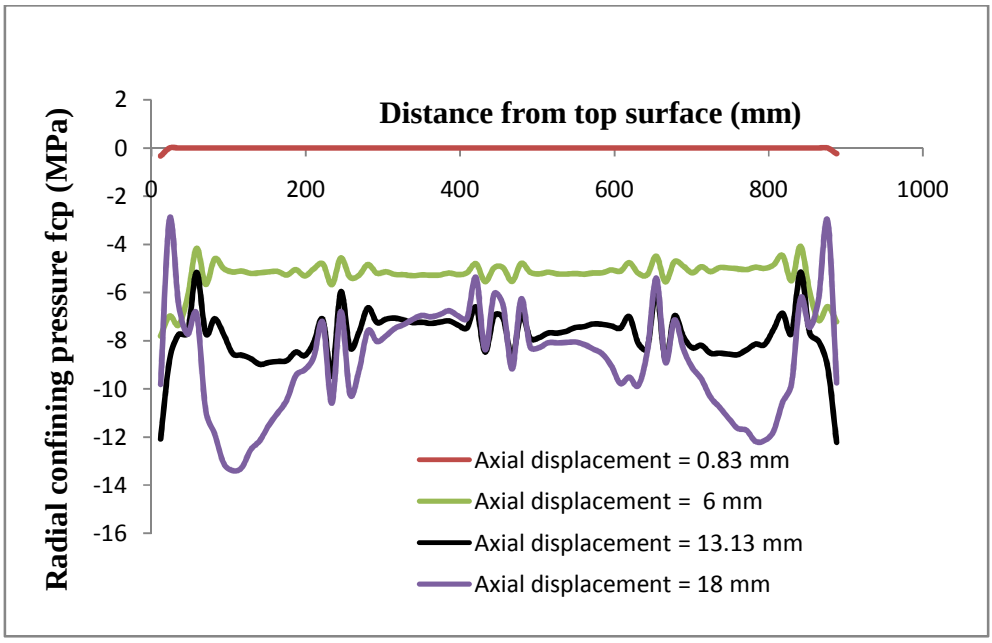

Figure 5.28(b) Confining pressure distribution in specimen CR2-1-2 along the length

The same behaviour is seen in long CFST columns also, as the sudden peaks in confining pressure correspond to location of ties.

5.6.4 Conclusions

A new concept involving the study of confinement pressure in Circular concrete filled tubular columns using the proposed FE model has been introduced in this section. Circular Tubular columns of 114.3 mm outer diameter of three different core configurations have been analyzed using this method. The distribution of confinement pressure along the length of the column has been obtained. The following conclusions can be drawn from this study:

a. The confining pressure values at the end regions of the CFT section are unusually high due to the end restraint applied by machine platens.

b. In the region of the sample away from the machine platens, the confining pressure is almost constant for CFST i.e. Single Skin Specimens. However, in CFDST columns, there is appreciable variation in confining pressure even in this middle region.

c. The confinement pressure values obtained from the numerical model have been compared with the corresponding values from theoretical models from literature. It is observed that the theoretical models generally overestimate the value of confining pressure for specimens of higher length.

d. For RCC-CFST specimens, large jump in values of confining pressure was observed near the region of lateral ties (which is also the location of local buckling of steel tube). Further, the region between the ties was seen to give relatively much lower values of confining pressure.

5.7. MEASUREMENT OF STRAIN USING DIGITAL IMAGE CORRELATION (DIC)

5.7.1 General

Strain gauge or LVDT can be used to obtain the strain field at specific location in the test specimen. However, for complex investigations, strain values may be required at a large number of locations on the specimen surface to study the behaviour of material. A new technology called Digital Image Correlation (DIC) has been used to provide a strain map over the entire surface of specimen. First introduced by a group of researchers at the University of South Carolina in 1980s

(Salmanpour and Mojsilović, 2013), the DIC system can be a very useful tool to study the actual strains in a specimen during the testing. In this chapter, DIC system is explained and the strains obtained from analysis using DIC are compared with strains obtained from simulations. The work presented in this chapter was done after the proposed work of PhD was finished. When author came to know about the procurement of DIC system in the Department of Civil Engineering, IIT Roorkee, he tested a previously extra specimen to get the strain maps at different loading stages using the DIC system.

5.7.2 Digital Image Correlation Techniques

Digital image correlation (DIC) is an optical technique in which a mathematical correlation analysis is used to examine digital images taken at the time of testing of specimen (Correlated Solutions, 2011). In this technique, a number of images are captured at periodic intervals with digital camera during the deformation process of specimen to evaluate the change in surface characteristics of material. To apply this technique, a random speckle pattern is created on the surface of specimen (Figure 5.22). An image is then taken before loading the specimen (reference image). A number of images are captured at pre-decided intervals (10 seconds for this sample) during the deformation process. A software is then used to analyse the change in speckle pattern between various DIC images and the reference image by correlating all the pixels of both the images. The software converts this correlation to the strain values. In this way, the strain distribution can be obtained over the surface of the specimen.

5.7.3 Digital Image Correlation Apparatus

This apparatus consists of computer software and two digital cameras mounted on a tripod frame (Figure 5.29). Two lamps are required for providing the proper lighting to specimens to get good images. During the test, the images are captured by the digital cameras. The software analyzes the images to calculate axial, transverse and shear strains.

5.7.4 Preparation of Specimen And Operation Of Equipment

The strain analysis of a typical sample CS3-3-3 (details in Table 5.2) has been performed using the DIC apparatus. It is a CFST single skin specimen with 90 mm dia outer steel tube and length 10 times the diameter (L10D). The surface of specimen to be examined is carefully cleaned before using DIC apparatus. The speckle pattern is applied with white and black paint on the

surface of specimen (Figure 5.30). A thin layer of white paint is applied first on the surface followed by black spray paint which is used to create dots. After this speckle pattern is created on surface, the specimen is tested in Universal testing machine.

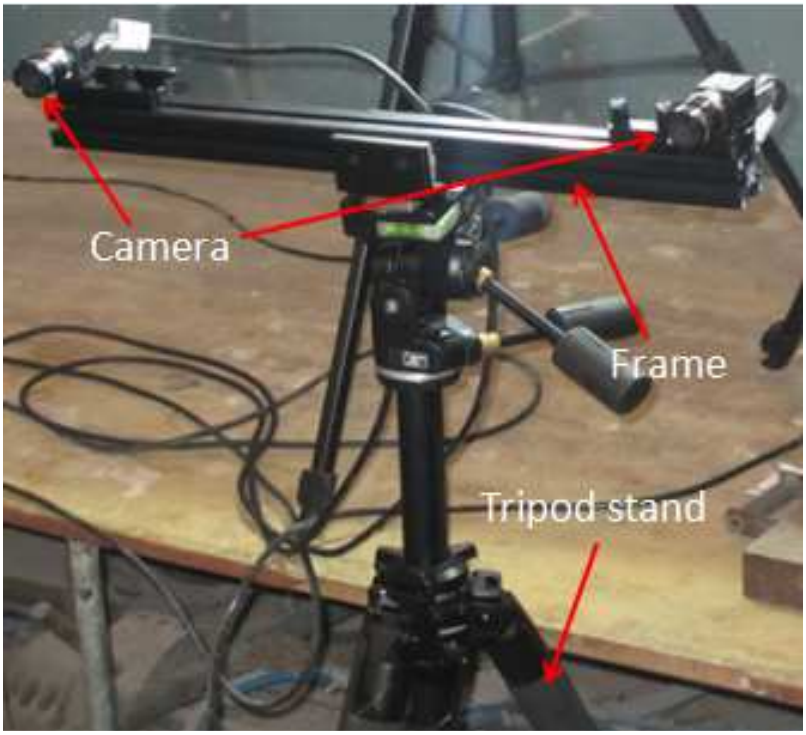

Figure 5.29 Digital Cameras mounted on a frame with tripod

The tripod with digital cameras is fixed in an accessible position. Focal length of lens of cameras is adjusted unless clear images are obtained. Two electric lamps kept near the machine provide proper lighting to the specimens. The set-up for Digital Image Correlation is shown in Fig. 5.31. Prior to the main test, the DIC system has to be calibrated (so that the pixels from the images can later be converted to strains by the software). A standard grid (size-28mm) having 14 black dots along length and 10 black dots along width is used for calibration (Fig. 5.32). The process of calibration is shown in Fig. 5.33.

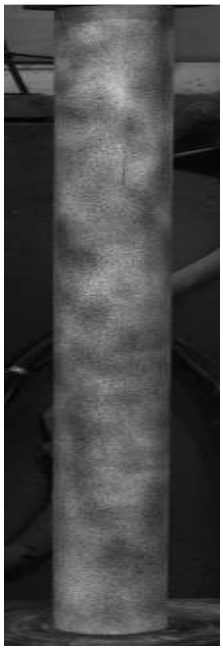

Figure 5.30 Speckle pattern

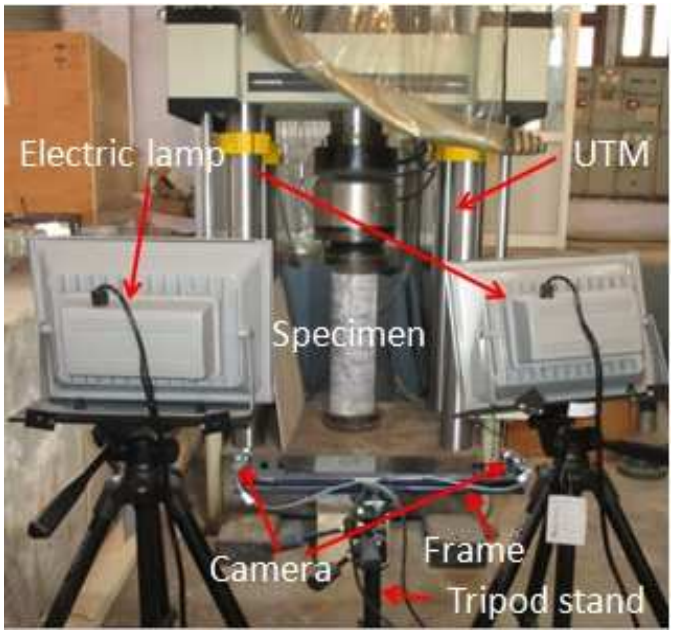

Figure 5.31 Setup for Digital Image correlation

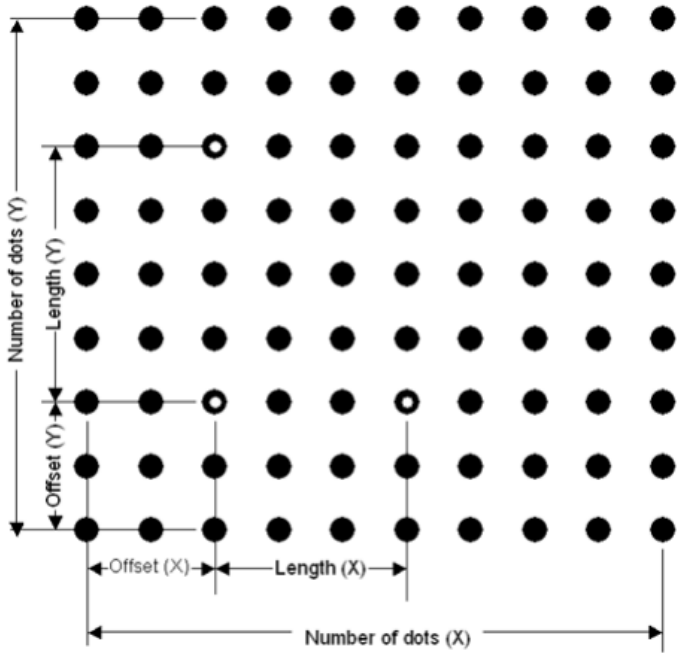

Figure 5.32 Grid (28 mm) used for calibration

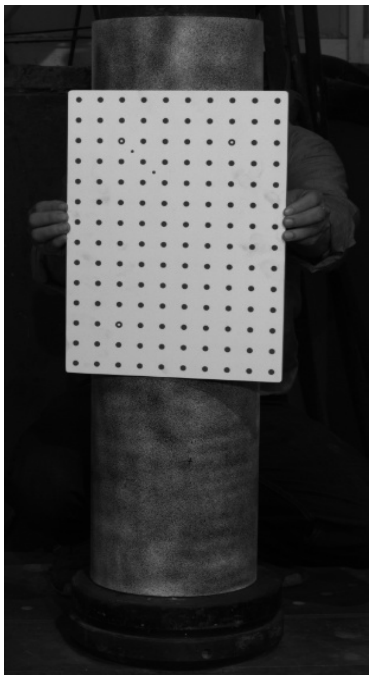

Figure 5.33 Calibration process

5.7.5 Results and Discussion

The prepared sample is tested in UTM under axial compression. The tripod-mounted cameras take images at every 10 seconds during the deformation process. The recorded digital images are processed using Vic-3D commercial code to obtain strain map. In this code, an area of interest is

selected initially by the user and a guess point is given (Figure 5.34). The software then analyses the data from the images to obtain the strain field over the surface of the sample. Four points are taken over the sample surface and the results from DIC at these points are compared from the results on numerical ABAQUS model. The location of points is shown in Figure 5.35. Two points are selected a horizontal line at the cross-section of maximum global buckling. The two remaining points are selected near the specimen edges and are mirror images of each other. The strains from DIC and ABAQUS are then compared at intervals of 10 % of the maximum applied displacement. The comparison of lateral strain e_{xx} between DIC and ABAQUS is shown in Table 5.12. These strain values are presented graphically in the Figures 5.36.

Figure 5.34 Marking the Area of Interest

Fig. 5.35 Location of the four points selected for comparison between DIC and ABAQUS

Table 5.13 Comparison of lateral strain e_{xx} between DIC and ABAQUS

% of Maximum applied displacement	Location P0		Location P1		Location P2		Location P3	
	DIC	ABAQUS	DIC	ABAQUS	DIC	ABAQUS	DIC	ABAQUS
10	0.0005	0	0.0003	0	0.001	0.00273	0.00082	0.000197
20	0.0023	0.00151	0.0023	0.001587	0.0019	0.00477	0.00191	0.00118
30	0.00357	0.00341	0.00348	0.0032	0.00165	0.00661	0.00322	0.00277
40	0.01	0.00525	0.0056	0.00472	0.0017	0.00789	0.0041	0.004
50	0.017	0.0071	0.0066	0.00641	0.00131	0.00911	0.00671	0.00518
60	0.025	0.0105	0.007	0.00725	0.00188	0.01081	0.00926	0.00621
70	0.033	0.01508	0.0081	0.00781	0.00147	0.0121	0.011898	0.0071
80	0.042	0.02085	0.0086	0.00813	0.001	0.014	0.01417	0.0093
90	0.056	0.026	0.0096	0.0086	0.00077	0.0165	0.01591	0.0124
100	0.07	0.0317	0.01	0.009096	0.00032	0.0188	0.01696	0.0173

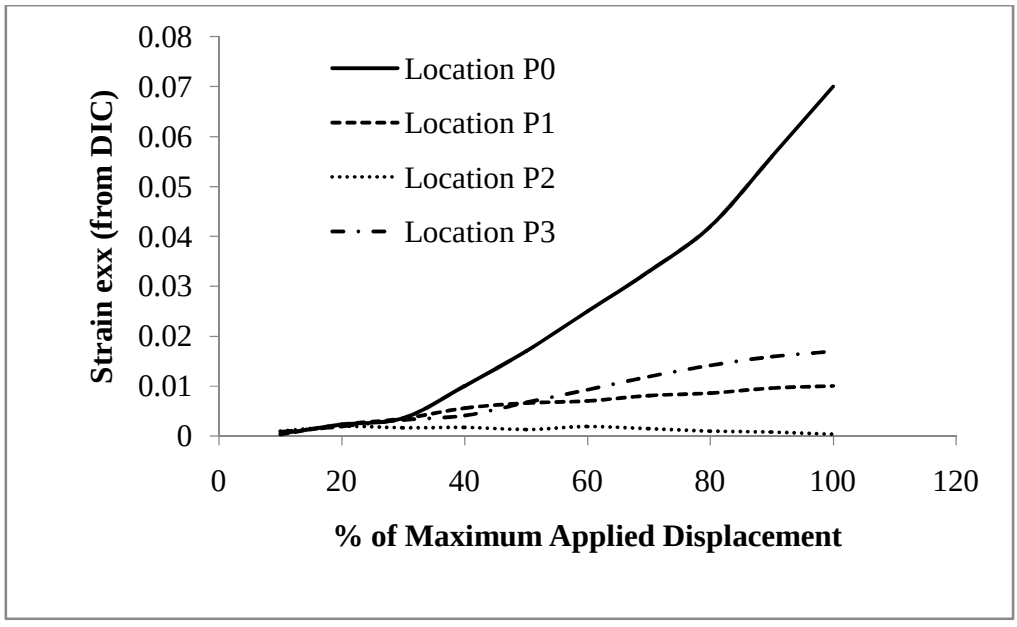

Figure 5.36 Strain values obtained from DIC at select locations along the sample

Figures 5.37 shows the comparison of strain e_{xx} batewwn DIC and ABAQUS at different locations. It can be noted from these figures that the values from the proposed model are in acceptable agreement with the values from DIC.

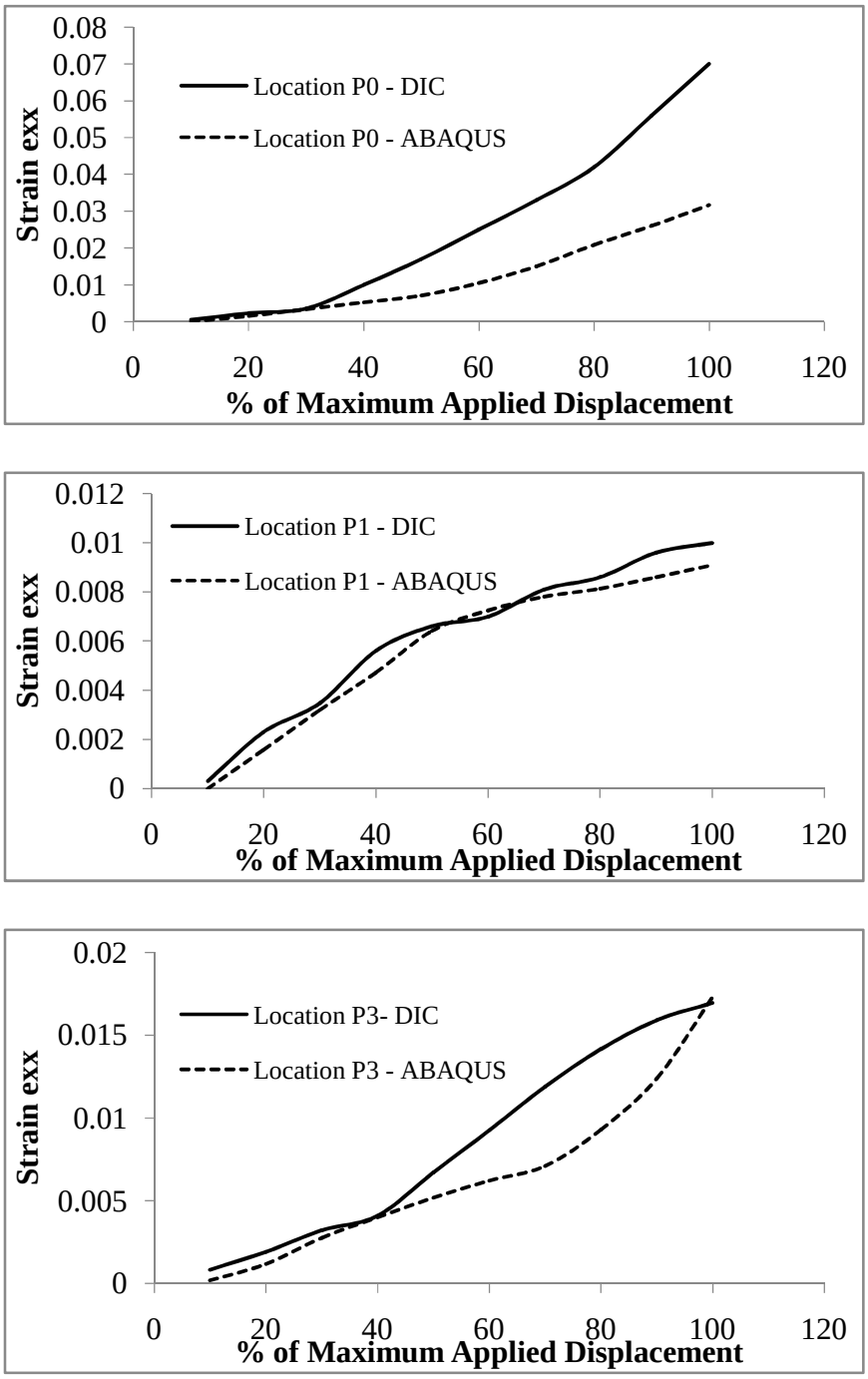

Figure 5.37 Comparison of e_{xx} strain values from DIC and ABAQUS

Table 5.14 Comparison of lateral strain e_{yy} between DIC and ABAQUS

% of Maximum applied displacement	Location P0		Location P1		Location P2		Location P3	
	DIC	ABAQUS	DIC	ABAQUS	DIC	ABAQUS	DIC	ABAQUS
10	-0.001	-0.00304	-0.0006	-0.00325	-0.00107	-0.0052	-0.00099	-0.0004
20	-0.0038	-0.00675	-0.00296	-0.00704	-0.003	-0.0092	-0.00259	-0.0024
30	-0.01	-0.00996	-0.004	-0.00978	-0.00349	-0.0124	-0.0043	-0.0062
40	-0.018	-0.01384	-0.00654	-0.0135	-0.00352	-0.0148	-0.0066	-0.0088
50	-0.026	-0.01812	-0.0085	-0.01564	-0.0035	-0.0168	-0.0099	-0.0112
60	-0.0346	-0.0321	-0.01	-0.0165	-0.00346	-0.0195	-0.0134	-0.0134
70	-0.044	-0.0432	-0.012	-0.01742	-0.003	-0.0218	-0.0169	-0.0162
80	-0.054	-0.05076	-0.014	-0.01858	-0.00232	-0.025	-0.02	-0.0202
90	-0.064	-0.0617	-0.016	-0.0197	-0.00165	-0.026	-0.0228	-0.032
100	-0.075	-0.0681	-0.017	-0.0202	-0.00094	-0.032	-0.00241	-0.041

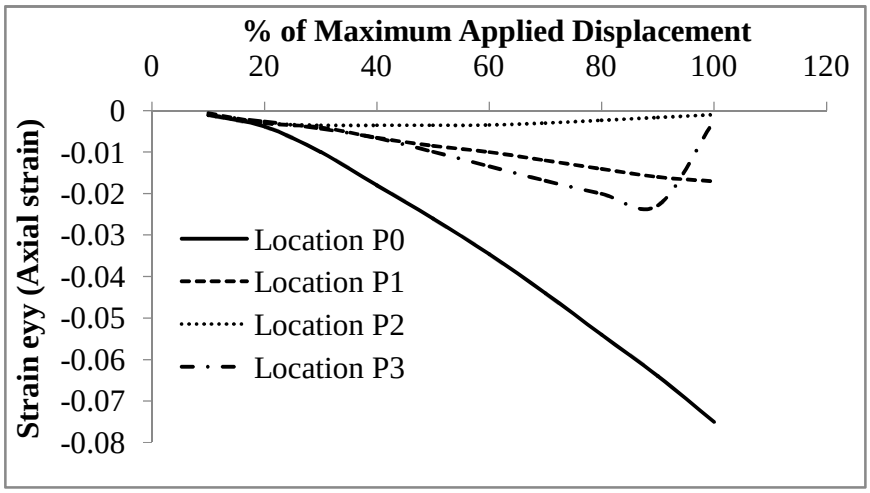

Figure 5.38 Strain values obtained from DIC at select locations along the sample

Figures 5.39 shows the comparison of strain e_{xx} batewwn DIC and ABAQUS at different locations. It can be noted from these figures that the values from the proposed model are in acceptable agreement with the values from DIC.

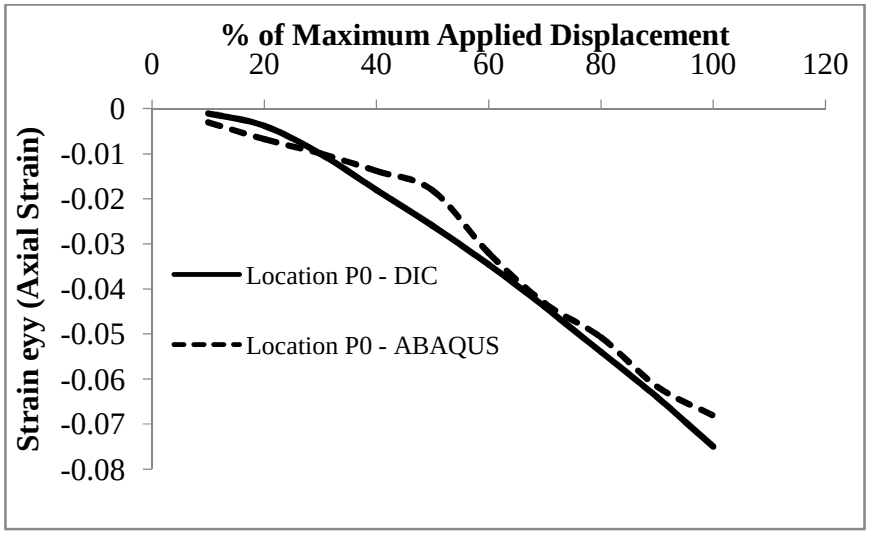

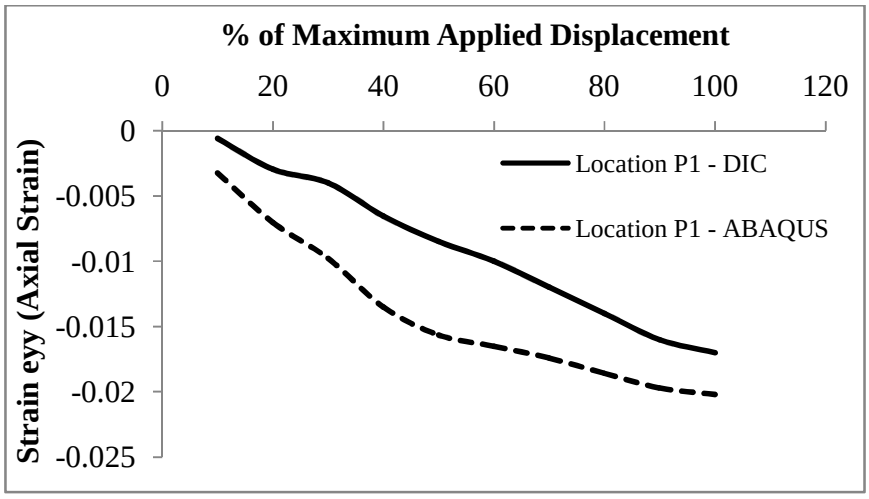

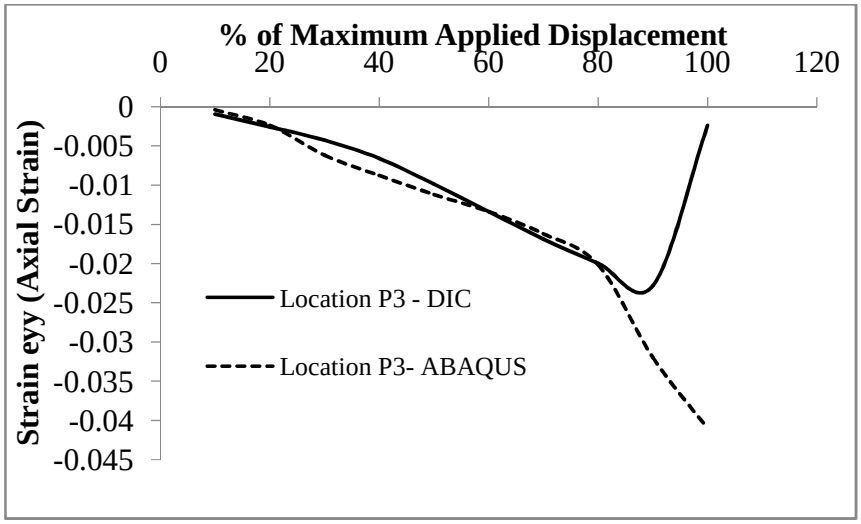

Figure 5.39 Comparison of e_{yy} strain values from DIC and ABAQUS

5.7.6 Conclusions

Digital Image Correlation System can be used to get the in-situ behaviour of the sample during the actual testing procedure. The images recorded from the apparatus at periodic intervals were calibrated to give material strains and the results compared with proposed numerical model. The results from numerical model were found in acceptable agreement with DIC results. This might be attributed to the axi-symmetric nature of the Euler Buckling deformed shape. More specimens, especially those where deformed shape is expected to be non-axisymmetric, must be tested, so that the method can be used further to propose mechanics of deformation of the sample.

CHAPTER SIX

COLUMNS WITH SQUARE CROSS-SECTIONS

6.1 GENERAL

The experimental and computational investigations on square tubes filled with concrete are presented in this chapter. A total of fifteen specimens consisting of three different types; Concrete Filled Steel Tube Columns (CFST) (Figure 3.3); Concrete Filled Double Steel Tube Columns (CFDST) (Figure 3.4) and Reinforced Concrete Filled Steel Tube Columns (RCC-CFST) (Figure 3.5) were cast and tested under axial loading. Specimens with varying outer widths (B), thicknesses (t) and lengths (L) were tested to study the effect of these parameters on structural response of the tubular columns. The effect of change in core configurations on the strength and ductility of the square CFST columns was also studied. The CFST specimens were then modeled using the Finite Element model presented in Chapter 4. The results from numerical simulations were compared with the experimental results.

6.2 DETAILS OF SPECIMENS

Square Composite columns of three different core configurations viz. Six Concrete Filled Steel Tubular (CFST), Six Concrete Filled Double Skin Tubular Columns (CFDST) and Three Reinforced Concrete Filled Steel Tubular Columns (RCC-CFST) were tested in axial loading. Table 3.4 presents the Material properties of square steel tubes used for preparing the specimens. Labeling of square specimens used in this chapter is explained in Table 6.1.

Two length categories were used for CFST specimens. The first category was the short column specimens, nominally designated as L3D specimens. The other length category wase designed to obtain intermediate specimens which have been designated nominally as L7D specimens. Moreover, a single cross-section with two different thicknesses (of the steel tube) has been used for each length category of every core configuration. Geometric Properties of square CFST specimens are given in Table 6.2.

Table 6.1 Labelling of square specimens

Typical ID: SPQ-L-M-N		
Character	Denotes	Value
S	Square specimen	
P	Core configuration	S: CFST
		D: CFDST
		R: RCC-CFST
Q	Length Category	1: L3B
		2: L7B
L	Outer dimension D of outer steel tube	1: 150 mm
		2: 113.5 mm
M	Thickness of steel tube with width "D"	1: first thickness
		2: second thickness
N	Specimen number. with same details	1: first specimen
		2: repeated (second) specimen

The same inner steel tube was used in all the CFDST specimens. Outer dimensions and thickness of inner steel tube were 40 x 40 mm and 3.02 mm. The yield stress and area of steel were 456 MPa and 447 mm^2, respectively. The hollow volume between the two concentric steel tubes was filled with concrete. The inner volume of inner steel tube was kept as hollow to obtain CFDST specimens with lighter weights. Geometric details of CFDST specimens are given in Table 6.3.

Table 6.2 Details of square CFST specimens

Length Category		Specimen ID	L (mm)	D (mm)	t (mm)	D/t	L/D	f_y (MPa)
Short Specimens	L3D	SS1-1-1	450	150x150	3.75	40.00	3.00	413
		SS1-1-2-1	450	150x150	5.60	26.79	3.00	388
		SS1-1-2-2	450	150x150	5.60	26.79	3.00	388
Intermediate Specimens	L7D	SS2-1-1	900	113.5x113.5	4.52	25.11	7.93	438
		SS2-1-2-1	900	113.5x113.5	5.16	22.00	7.93	456
		SS2-1-2-2	900	113.5x113.5	5.16	22.00	7.93	456

The square RCC-CFST specimens were designed in the same way as circular RCC-CFST samples. The amount of reinforcement in RCC-CFST specimens were so selected that the sum total of area of steel tube and reinforcement in the specimens with lower wall thicknesses will almost equal the area of steel tube in CFST specimen with higher wall thickness. This was done to maintain a constant total area of steel (area of steel tube plus area of rebars) while examining the effect of redistribution of this area. There was a marginal difference in the total

steel areas depending on the commercially available sizes of steel tubes and rebars. The sample details are given in Table 6.4.

Table 6.3 Details of square CFDST specimens

Length Category		Specimen ID	L (mm)	D_o (mm)	t_o (mm)	$(D/t)_o$	$(L/D)_o$	f_{yo} (MPa)
Short Specimens	L3D	SD1-1-1-1	450	150x150	3.75	40.00	3.00	413
		SD1-1-1-2	450	150x150	3.75	40.00	3.00	413
		SD1-1-2-1	450	150x150	5.60	26.79	3.00	388
		SD1-1-2-2	450	150x150	5.60	26.79	3.00	388
Intermediate Specimens	L7D	SD2-1-1	900	113.5x113.5	4.52	25.11	7.93	438
		SD2-1-2	900	113.5x113.5	5.16	22.00	7.93	456

Table 6.4 Details of square RCC-CFST specimens

Length Category		Specimen ID	L (mm)	D (mm)	t (mm)	Reinf. (mm)	D/t	L/D	f_y (MPa)
Short Specimens	L3D	SR1-1-1-1	450	150x150	3.75	4Ø10+4Ø16	40.00	3.00	413
Intermediate Specimens	L7D	SR2-1-1-1	900	113.5x113.5	4.52	4Ø10	25.11	7.93	438
		SR2-1-1-2	900	113.5x113.5	4.52	4Ø10	25.11	7.93	438

Normal concrete having of M30 grade has been used to fill all the tested samples. The cube strength of infill concrete was 42.16 MPa cube and cylinder strength was 32.05 MPa. Details of concrete mix proportions are given in Table 3.1.

6.3 RESULTS

6.3.1 Mode of Deformation

Figure 6.1 shows the tested square single skin (CFST), square double skin (CFDST) and Reinforced concrete tubular specimens (RCC-CFST) specimens, respectively. Figures 6.2 to 6.7 show experimental and numerical deformed shapes for various square CFST, CFDST and RCC-CFST and specimens, respectively.

For all core configurations, L3D specimens failed due to local buckling of steel tube followed by crushing of adjoining concrete. On the other hand, local buckling in the top one-third of the

specimen and originating near the top of the sample was observed as the primary failure mode in L7D columns.

Figure 6.1 All tested square specimens

Experiment **Simulated** **Experiment** **Simulated**

Figure 6.2 Comparison of Experimental and Simulated Deflected Shape of L3D 150 mm Square CFST

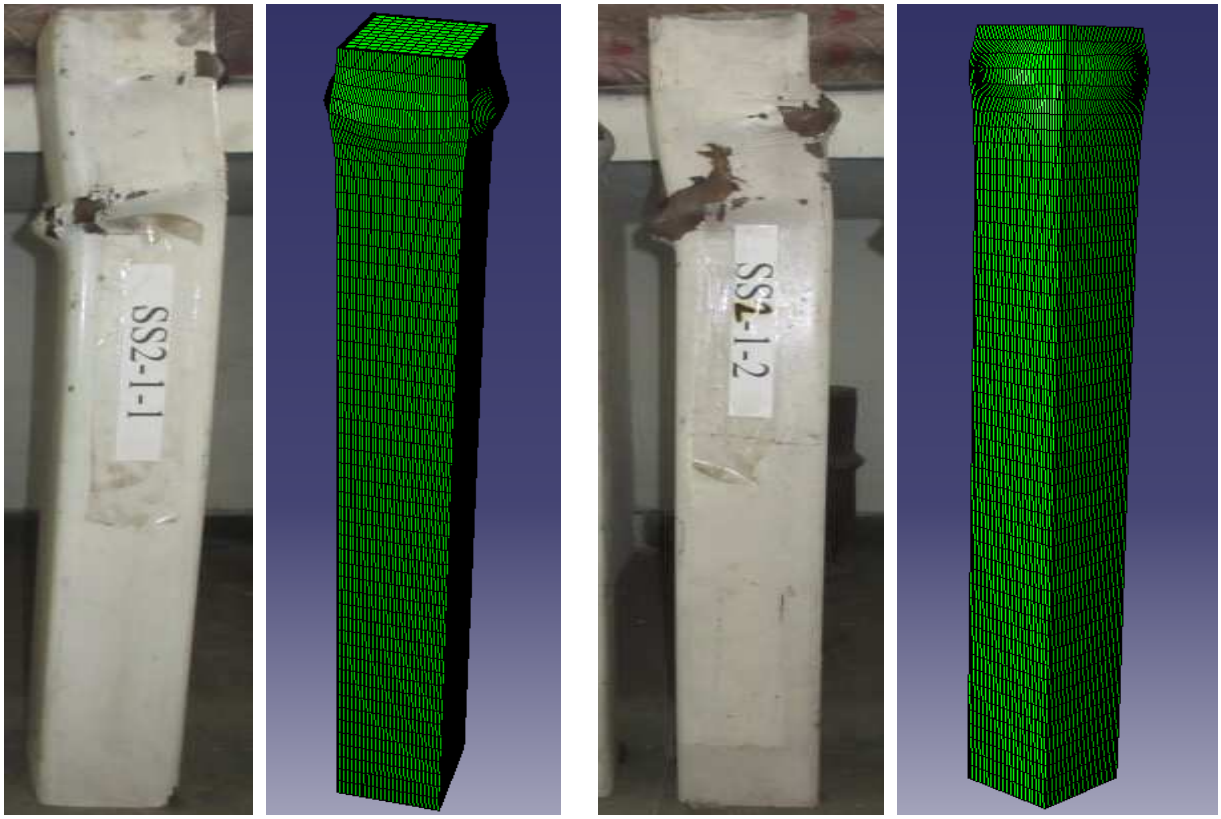

Experiment **Simulated** **Experiment** **Simulated**

Figure 6.3 Comparison of Experimental and Simulated Deflected Shape of L7D 113.5 mm Square CFST

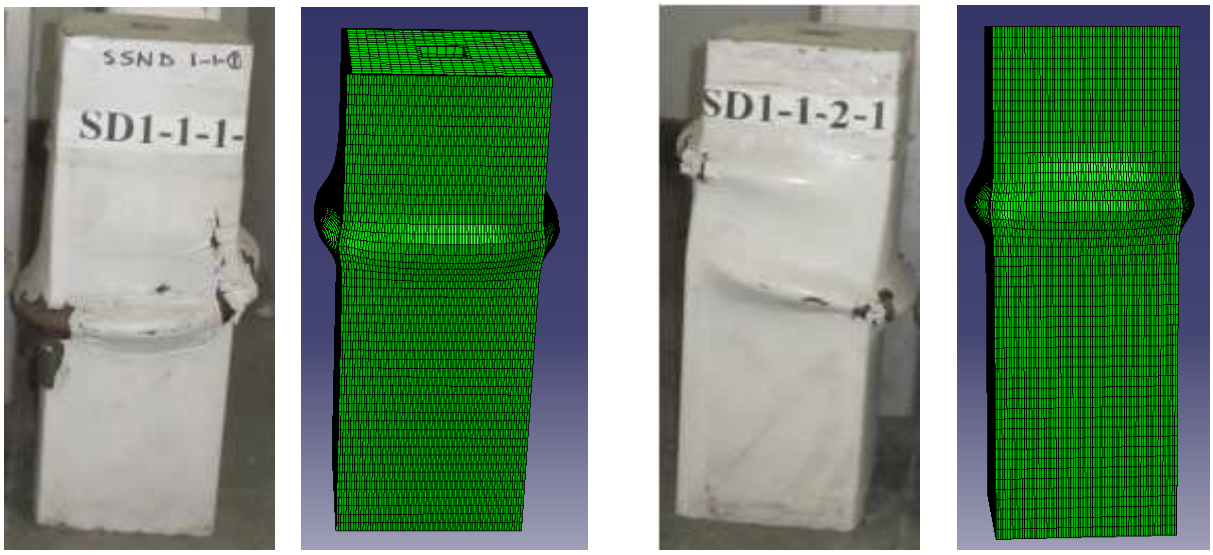

Experiment **Simulated** **Experiment** **Simulated**

Figure 6.4 Comparison of Experimental and Simulated Deflected Shape of L3D 150 mm Square CFDST

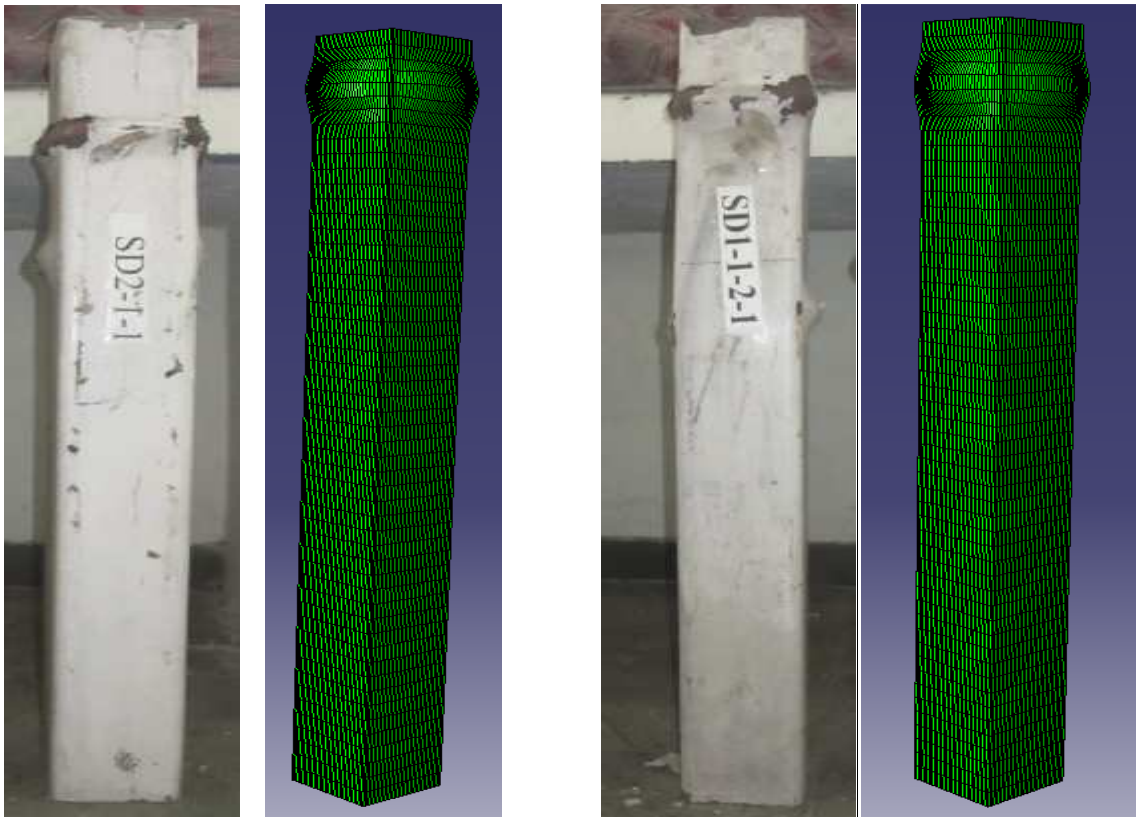

Experiment **Simulated** **Experiment** **Simulated**

Figure 6.5 Comparison of Experimental and Simulated Deflected Shape of L7D 113.5 mm Square CFDST

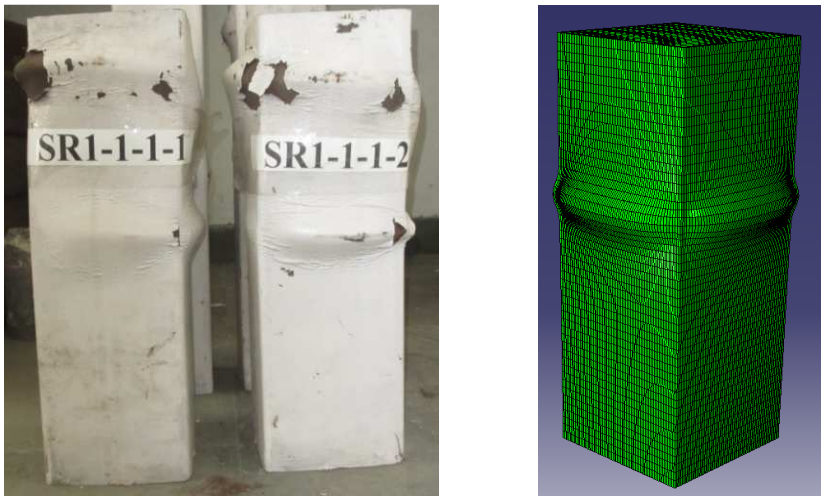

Experiment **Simulated**

Figure 6.6 Comparison of Experimental and Simulated Deflected Shape of L3D 150 mm Square RCC-CFST

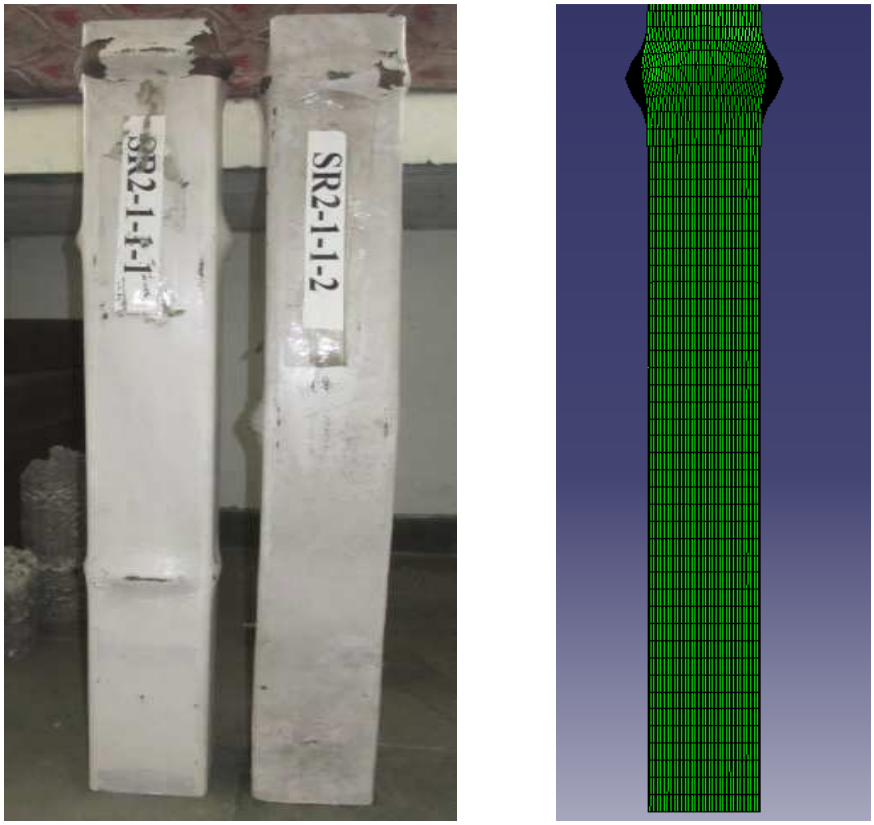

Experiment **Simulated**

Figure 6.7 Comparison of Experimental and Simulated Deflected Shape of L7D 113.5 mm Square RCC-CFST

Outward local buckling was reported in all the specimens. At these locations, separation between steel tube and concrete core occurred. It was also observed that in square CFST of smaller thickness, the cross-sectional local buckling occurred around the central portion of the edge, thereby maintaining the contact between the tube and concrete core near the corners. However, as seen in Figure 6.8, the thicker square CFST had a tendency to lose this contact near the corners also, at advanced stages of loading (At small deformations around 10 mm, where testing of SS1-1-1-2 was aborted due to machine problems, there was still some contact at corners between the tube and concrete.

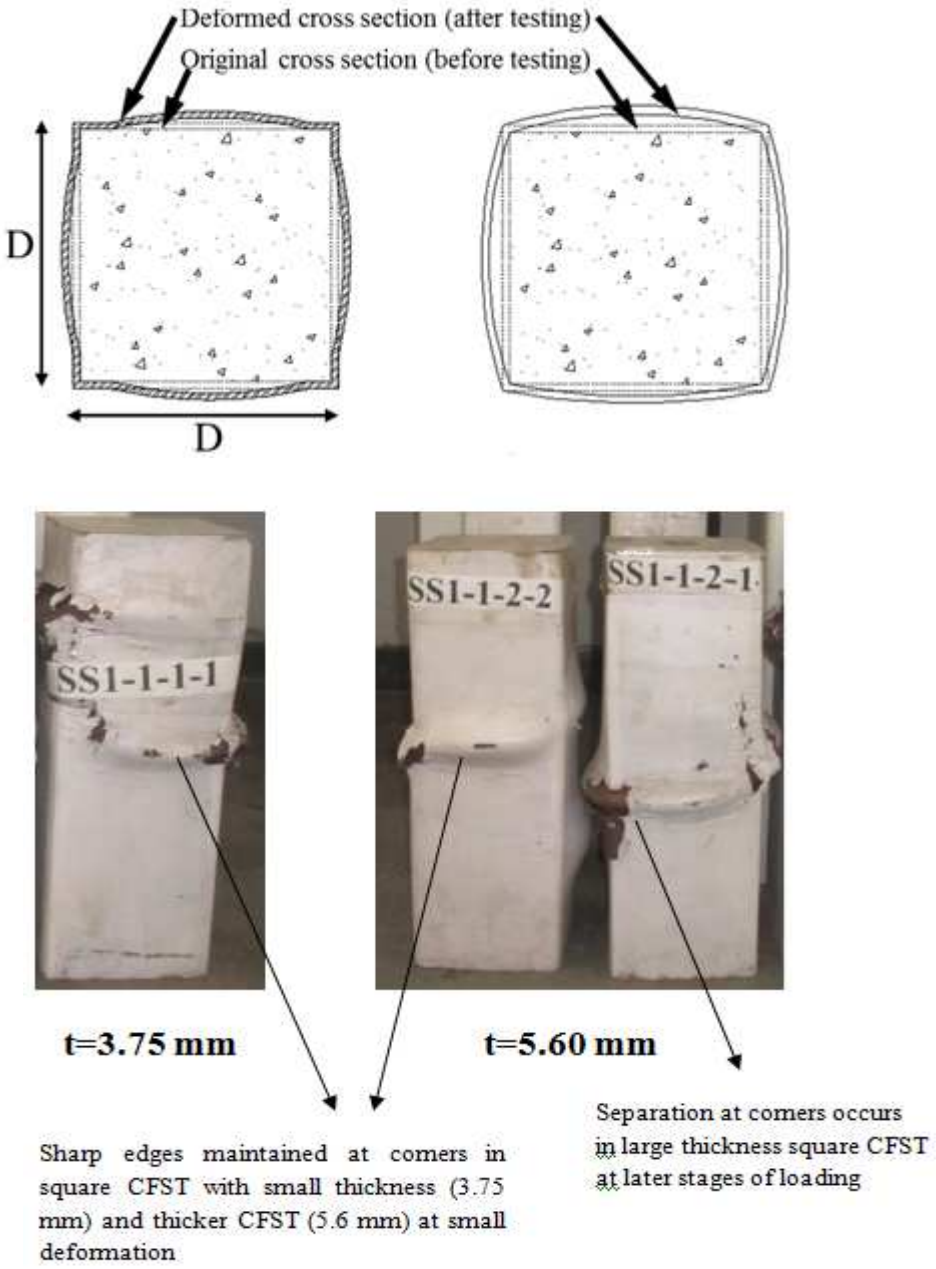

Figure 6.8 Typical deformation in square CFST column

6.3.2 Strength

Figures 6.9, 6.10 and 6.11 show experimental and numerical load-displacement curves for CFST, CFDST and RCC-CFST specimens, respectively. It can be concluded from Figures 6.9 to 6.11 that the axial capacity of specimens increases as the wall thickness of the specimens increases for all diameters, configurations and lengths. It can also be concluded that the proposed model gives acceptable results for load-displacement curves for all specimens and it is applicable to specimens with different lengths and different core configurations. (Please note

that specimen SS2-1-2-2 had to be aborted due to problem in test machine; hence the sudden fall in load capacity in the graph).

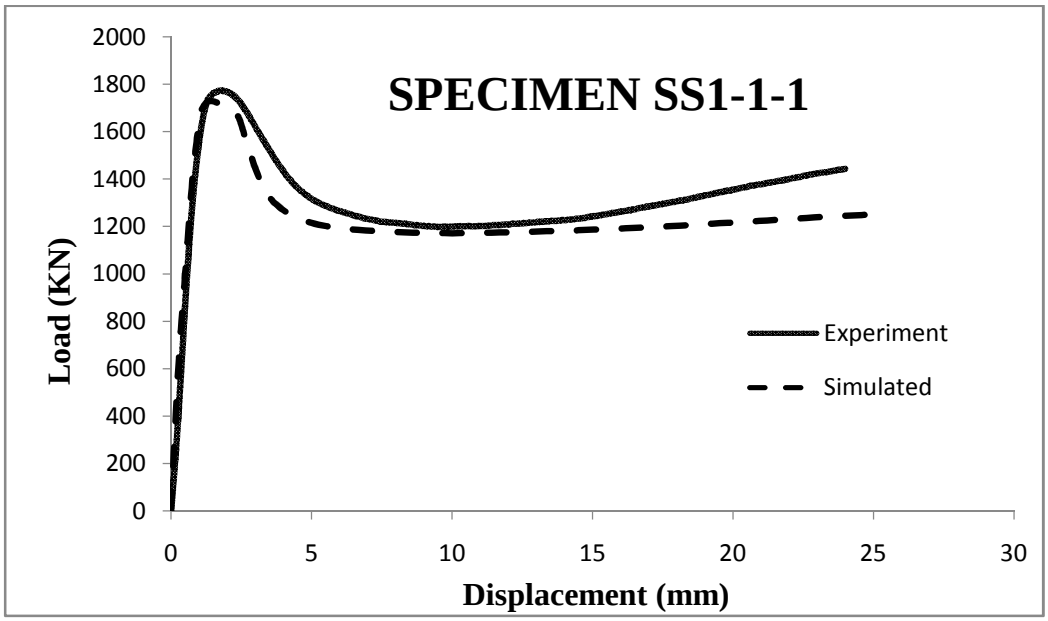

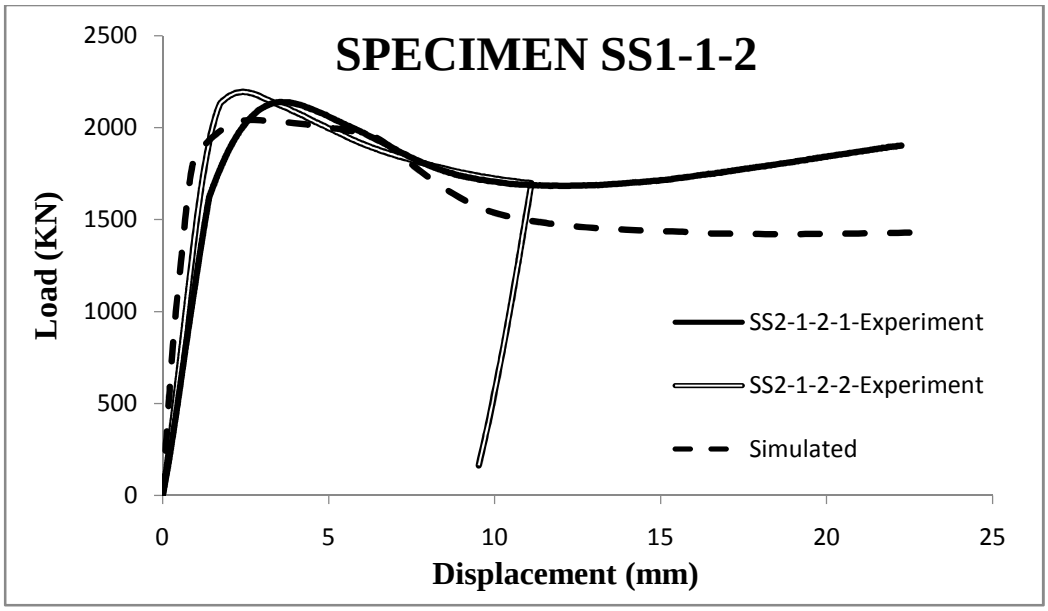

Figure 6.9(a) Comparison of experimental and numerical load-displacement curves for L3D square CFST specimens, B=150 mm

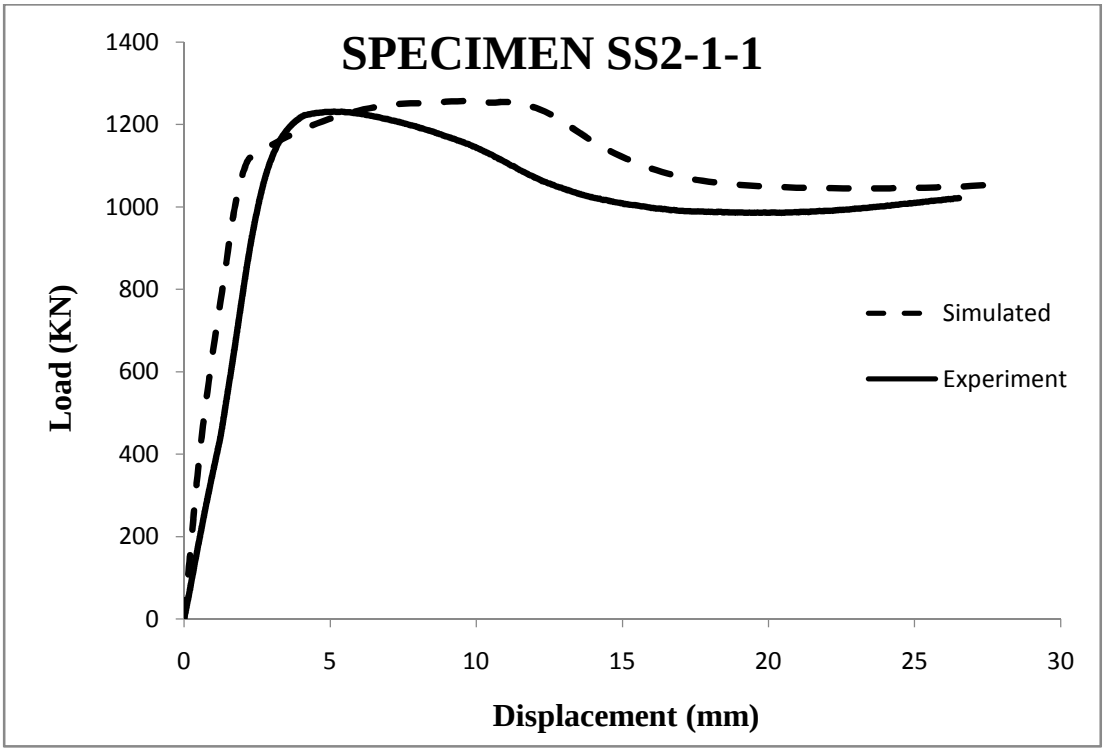

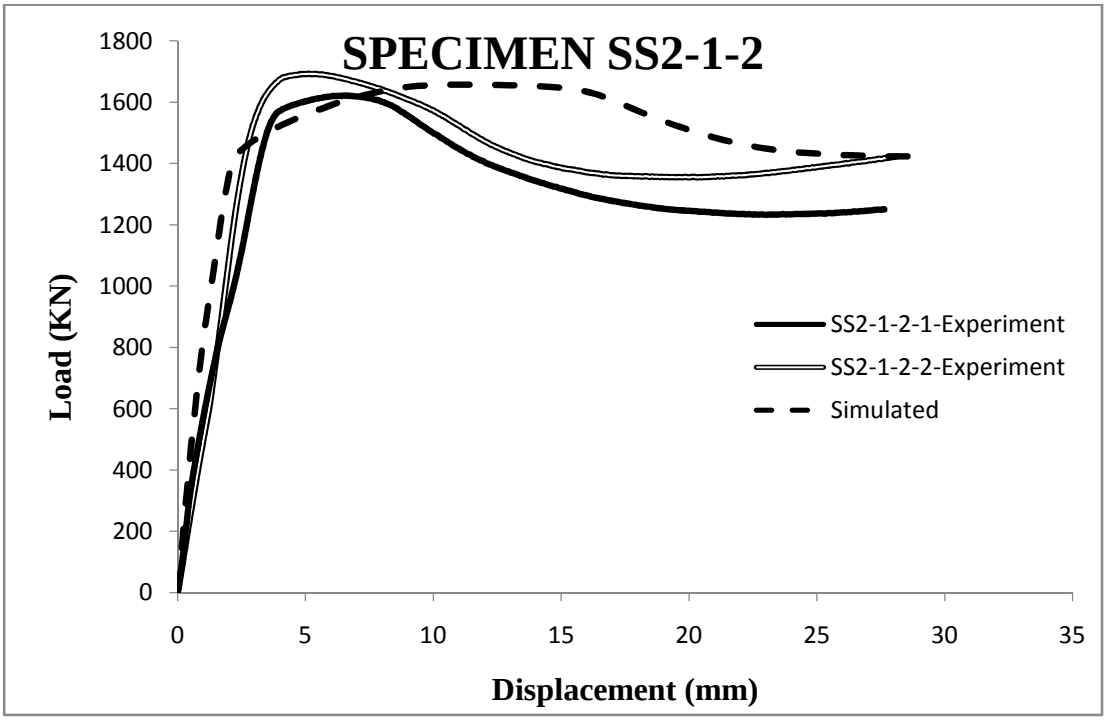

Figure 6.9(b) Comparison of experimental and numerical load-displacement curves for L7D square CFST specimens, B=113.5 mm

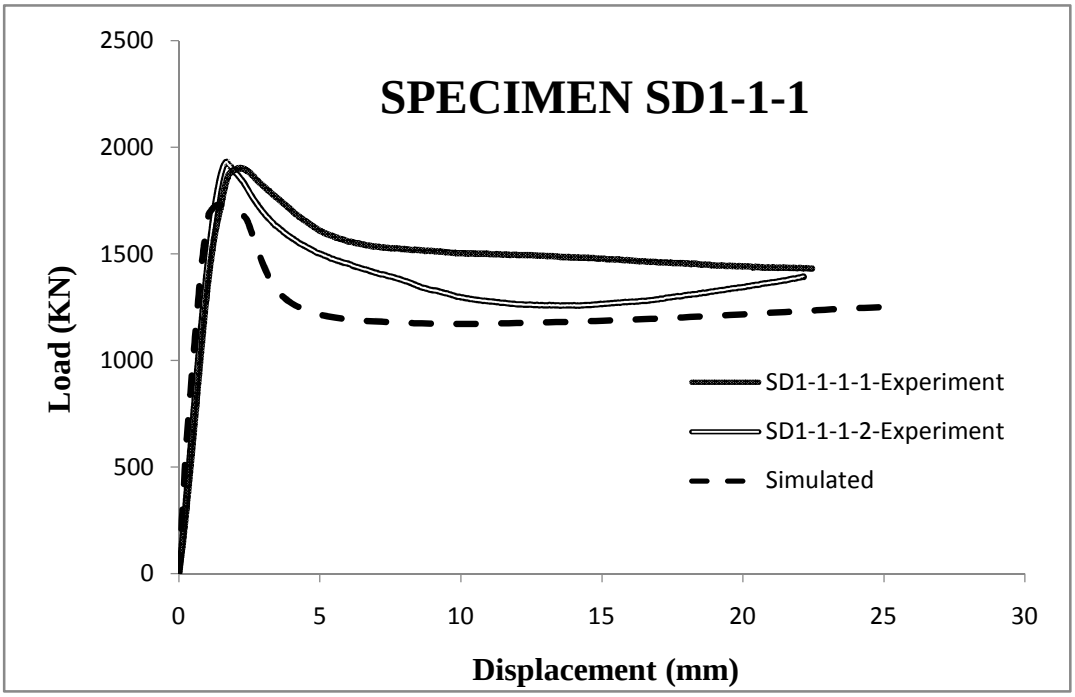

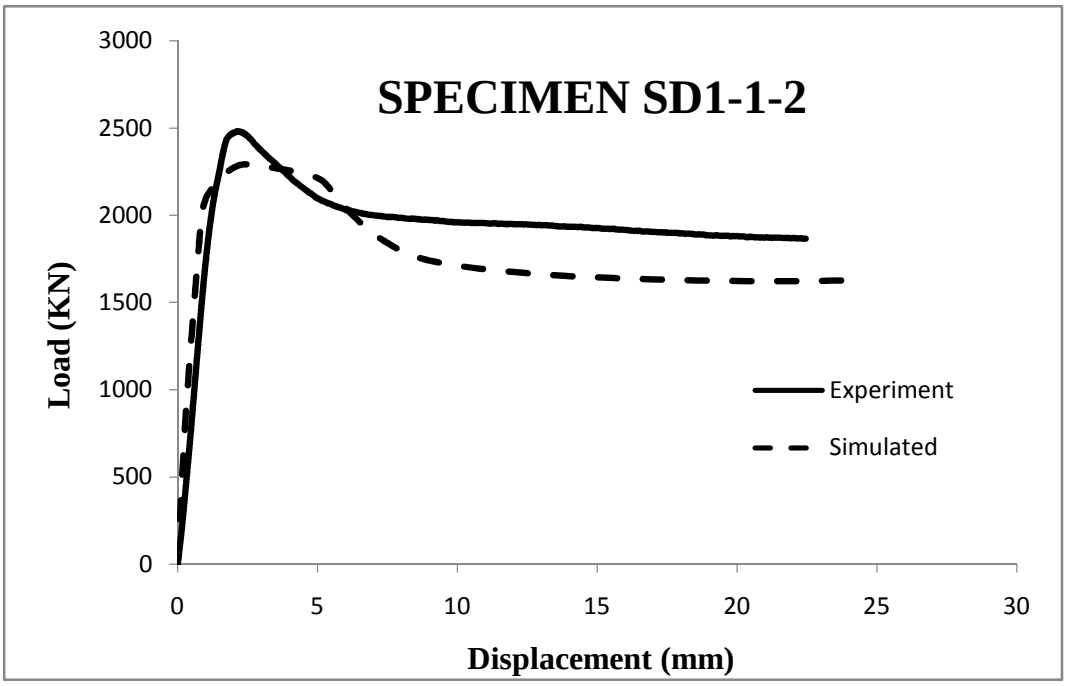

Figure 6.10(a) Comparison of experimental and numerical load-displacement curves for L3D square CFDST specimens, B=150 mm

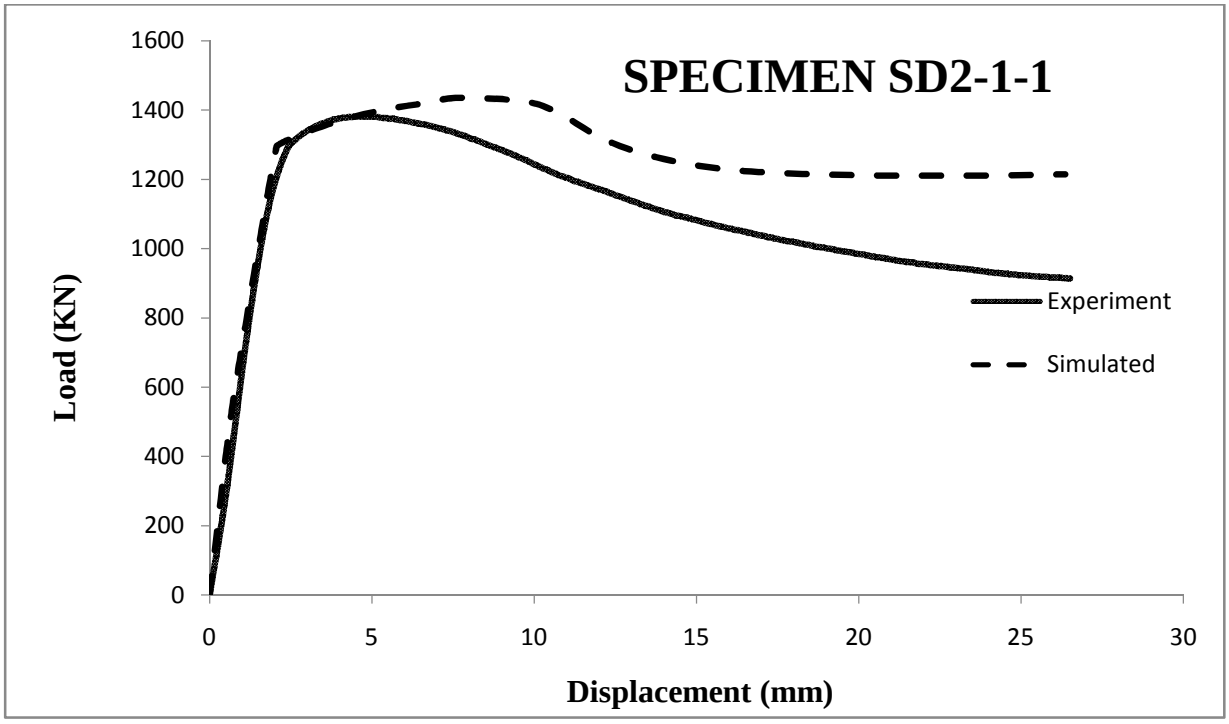

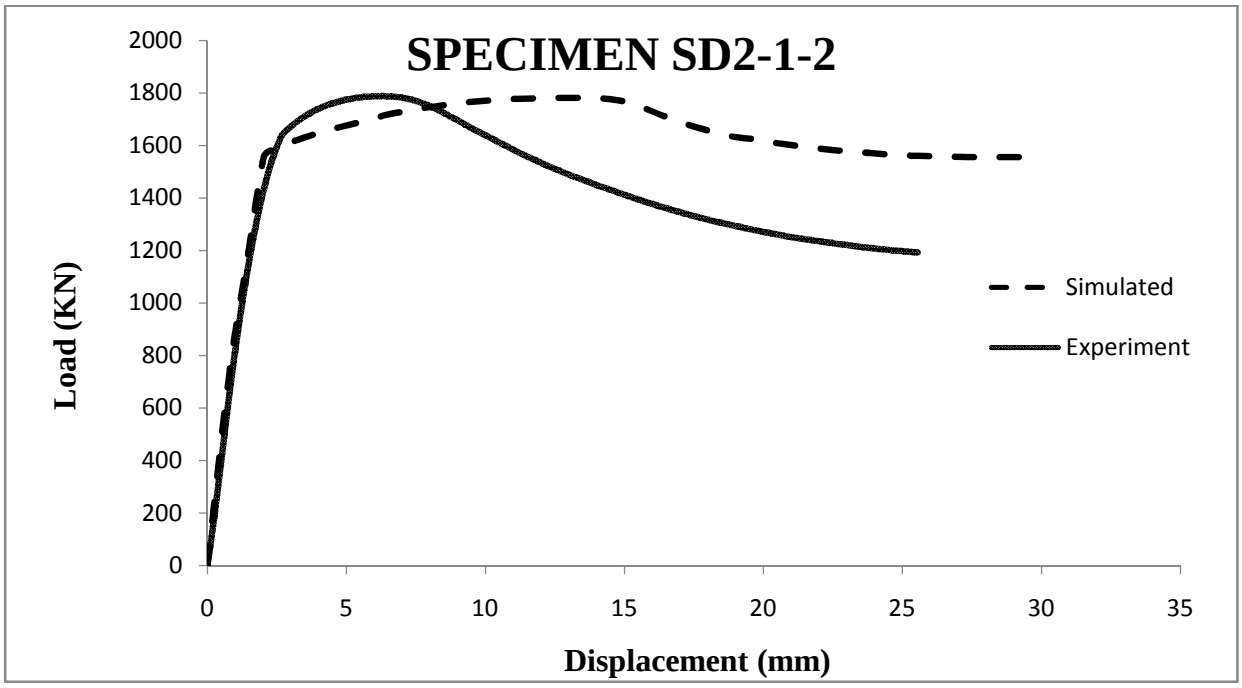

Figure 6.10(b) Comparison of experimental and numerical load-displacement curves for L7D square CFDST specimens, B=113.5 mm

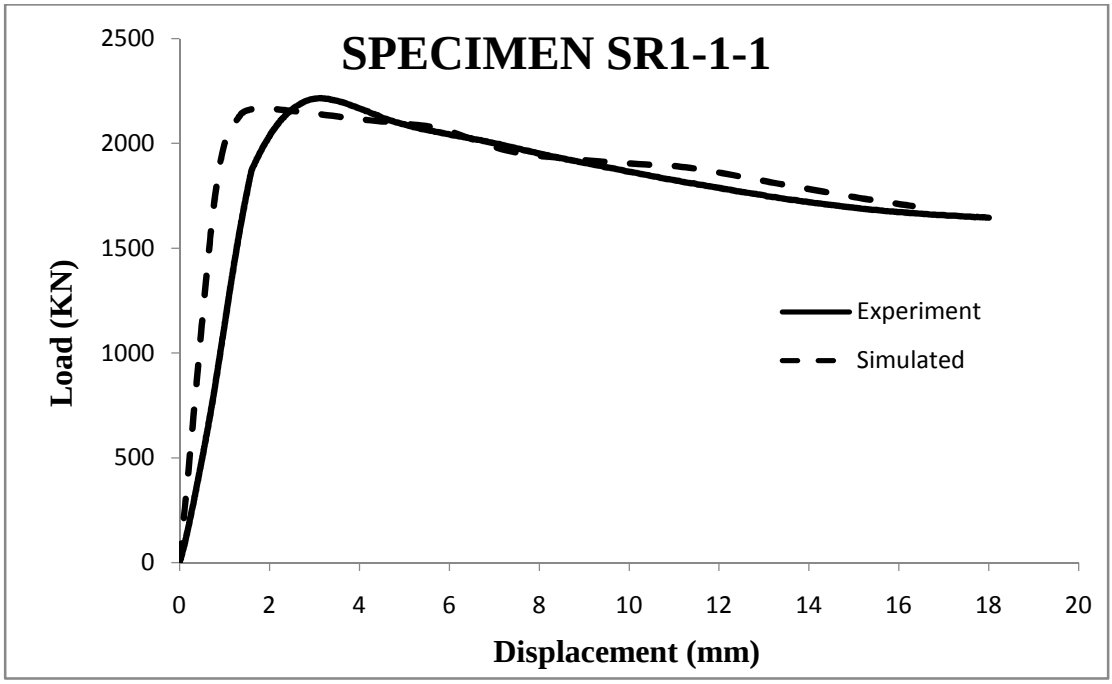

Figure 6.11(a) Comparison of experimental and numerical load-displacement curves for L3D square RCC-CFST specimens, B=150 mm

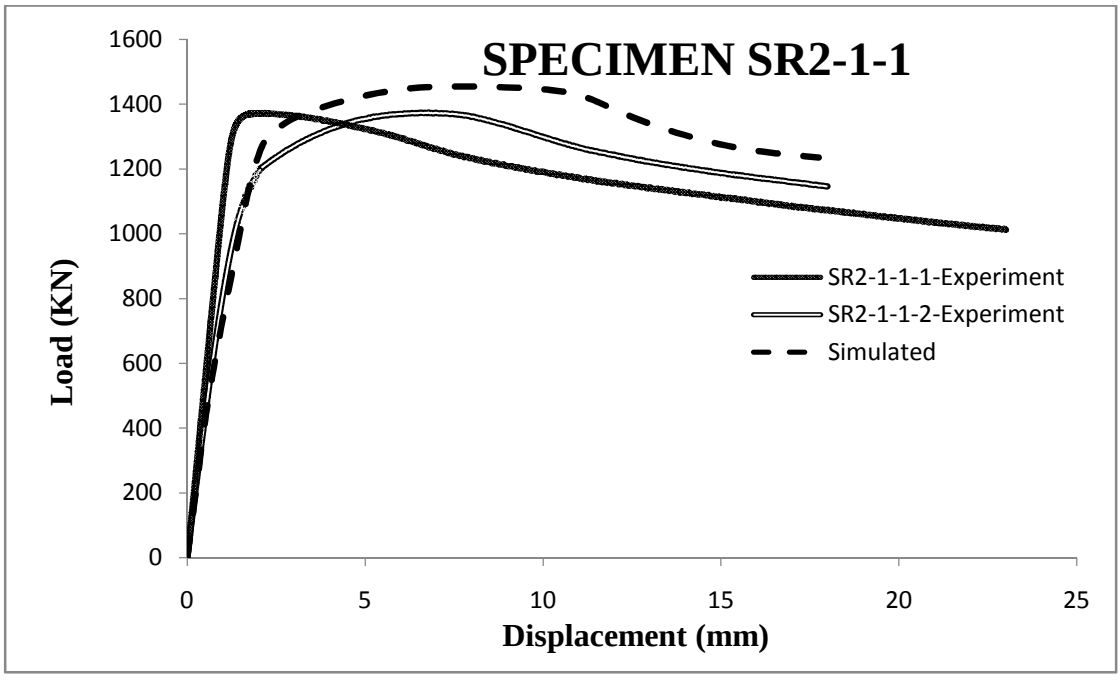

Figure 6.11(b) Comparison of experimental and numerical load-displacement curves for L7D square RCC-CFST specimens, B=113.5 mm

Tables 6.3, 6.4 and 6.5 give the simulated nominal and ultimate load, experimental yield load and ultimate load and yield displacements for CFST, RCC-CFST and for CFDST. The nominal capacity (P_n), experimental yield load (P_y), strength index (SI), and ductility index (DI) were calculated as explained in Sections 5.3.2 and 5.3.3.

Table 6.5 Experimental and numerical results for square CFST specimens

Length Category	Specimen ID	P_n (KN)	Δ_y (mm)	P_y (KN)	P_{5y} (KN)	P_u (KN)		SI	DI
						Experiment	Simulated		
L3D	SS1-1-1	1550.64	1.90	1770.45	1197.92	1772.42	1730.54	1.14	0.68
	SS1-1-2-1	1875.46	2.54	2033.40	1687.09	2140.09	2042.29	1.14	0.83
	SS1-1-2-2	1875.46	2.05	2176.22	1718.92	2196.00	2042.29	1.17	0.79
L7D	SS2-1-1	1218.98	5.00	1230.84	1010.11	1231.15	1232.83	1.01	0.82
	SS2-1-2-1	1363.42	4.81	1598.00	1234.32	1621.12	1657.11	1.19	0.77
	SS2-1-2-2	1363.42	4.89	1691.24	1382.65	1692.38	1657.11	1.24	0.82

Table 6.6 Experimental and numerical results of square CFDST specimens

Length Category	Specimen ID	P_n (KN)	Δ_y (mm)	P_y (KN)	P_{5y} (KN)	P_u (KN)		SI	DI
						Experimental	Simulated		
L3D	SD1-1-1-1	1748.66	2.25	1900.26	1425.13	1903.14	1730.27	1.09	0.73
	SD1-1-1-2	1748.66	2.16	1857.07	1337.04	1931.79	1730.27	1.10	0.76
	SD1-1-2	2045.21	3.10	2352.46	1921.80	2480.10	2276.32	1.21	0.82
L7D	SD2-1-1	1365.46	3.85	1372.85	986.23	1382.33	1395.09	1.01	0.72
	SD2-1-2	1565.81	3.97	1738.28	7.43	1787.33	1273.83	1.14	0.73

It can be concluded from Table 6.5 that strength index was highest in case of CFST core configuration for L3D and L7D specimens. Further, it can also be noticed that the strength index increases with the increase in thickness of steel for all tested specimens. However, the

trend of increase was higher in case of CFST and CFDST specimens as compared to RCC-CFST samples.

Table 6.7 Experimental and numerical results of square RCC-CFST specimens

Length Category	Specimen ID	P_n (KN)	Δ_y (mm)	P_y (KN)	P_{5y} (KN)	P_u (KN)		SI	DI
						Experimental	Simulated		
L3D	SR1-1-1-1	2181.43	2.57	2174.12	1758.63	2216.45	2167.88	1.02	0.81
L7D	SR2-1-1-1	1389.22	3.03	1363.34	1110.22	1372.27	1454.32	0.99	0.85
	SR2-1-1-2	1389.22	3.31	1289.62	1166.17	1375.02	1454.32	0.99	0.89

6.3.3 Ductility and Post Yield Behaviour

The Ductility Index DI of all specimens are shown in Tables 6.5 to 6.7. It can be concluded from the tables that all tested specimens showed strain softening behaviour. It is clear from the tables that both RCC-CFST and CFST single skin specimens generally displayed a DI higher than the CFDST square specimens for both L3D and L7D specimens. The maximum ductility was observed in RCC-CFST specimens for L7D category.

Also, the DI decreased with increase in D/t ratio for all core configurations. The trend in reduction was the highest in CFDST specimen, followed by the CFST and ultimately the RCC-CFST specimens

6.3.4 Equivalent Area of Steel

Specimens with L3D and L7D details were used to investigate the effect of use of equivalent cross-sectional area of steel in composite columns having two different core configurations (i.e. CFST and RCC-CFST). Area of steel including the cross-sectional area of rebars and cross-sectional area of steel tube remained same in RCC-CFST specimens as that of CFST specimens. There was a marginal difference due to limited availability of steel tubes and rebars commercially. In this Table, results of CFST specimens with greater thickness were compared with RCC-CFST specimens with smaller thickness. The axial load was normalized with respect to nominal cross-sectional capacity of each specimen calculated using Equation 5.1. The normalized load-displacement curves are shown in Figure 6.12. It can be concluded from Table 6.8 that enhancement in strength of L3D specimens was higher in CFST specimens (SI for both

samples is greater than 1.1) as compared to RCC-CFST specimens (SI=1.02). The same trend can also be observed in the case of L7D specimens.

Table 6.8 Comparison of square specimens with equivalent area of steel but different core configurations

	Specimen ID	L (mm)	D (mm)	t (mm)	f_y (MPa)	L/D	D/t	A_s (mm^2)	A_{sr} (mm^2)	A_s Total (mm^2)	SI	DI
L3D	**SS1-1-2-1**	**450**	**150x150**	**5.6**	**388**	**3.00**	**26.79**	**3235**	**0**	**22500**	**1.14**	**0.83**
	SS1-1-2-2	**450**	**150x150**	**5.6**	**388**	**3.00**	**26.79**	**3235**	**0**	**22500**	**1.17**	**0.79**
	SR1-1-1-1	450	150x150	3.75	413	3.00	40.00	2194	1118	21382	1.02	0.81
L7D	**SS2-1-2-1**	**900**	**113.5x113.5**	**5.16**	**456**	**7.93**	**22.00**	**2236**	**0**	**12882**	**1.19**	**0.77**
	SS2-1-2-2	**900**	**113.5x113.5**	**5.16**	**456**	**7.93**	**22.00**	**2236**	**0**	**12882**	**1.24**	**0.82**
	SR2-1-1-1	900	113.5x113.5	4.52	438	7.93	25.11	1970	314	12568	0.99	0.85
	SR2-1-1-2	900	113.5x113.5	4.52	438	7.93	25.11	1970	314	12568	0.99	0.89

This behaviour is expected since the steel tube provides better confinement than the longitudinal reinforcing bars.

Comparing the DI values for the two lengths categories, it can be seen from Table 6.8 that the DI was almost same for CFST specimen (averaged DI of SS1-2-1 and SS1-2-2 is 0.81) as compared to RCC-CFST specimen for L3D samples. However, in case of L7D samples, the DI was higher for RCC-CFST samples as compared to CFST samples. Therefore, it may be better advised to use RCC-CFST samples from the ductility point of view.

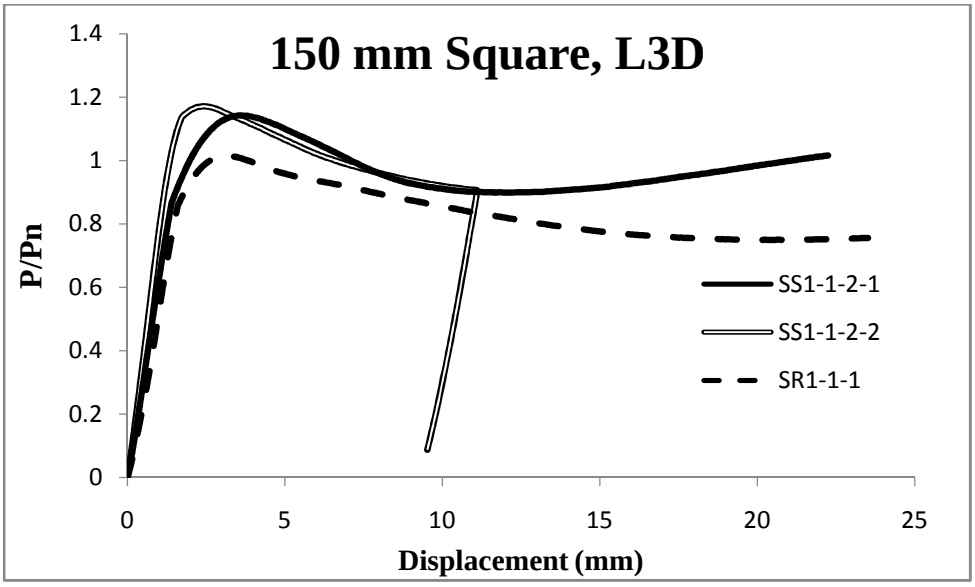

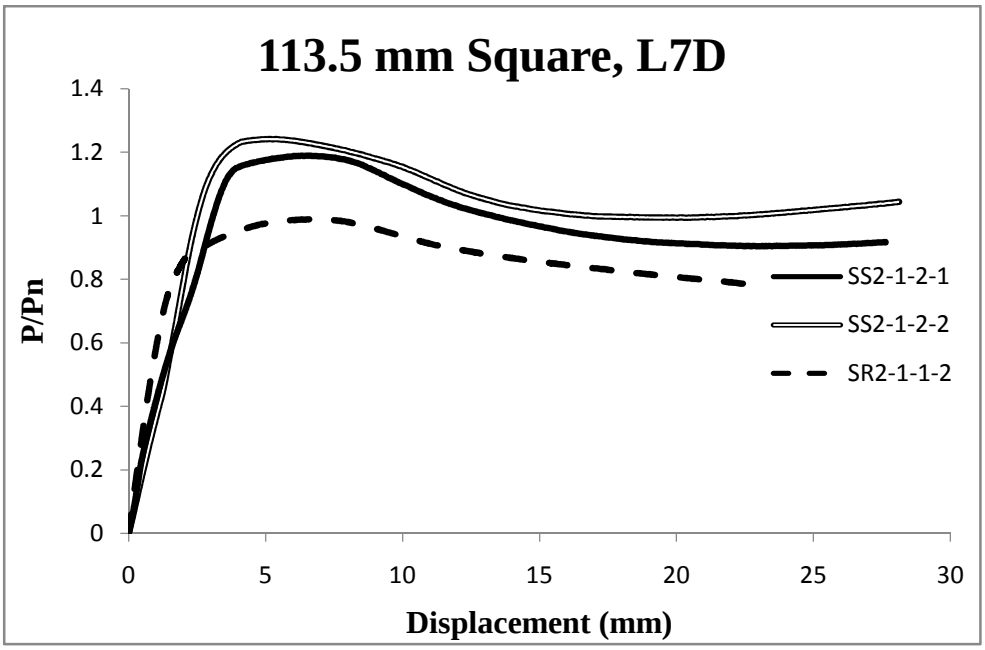

Figure 6.12 Comparison of load-displacement curves of square CFST and RCC-CFST specimens

6.4 CODAL RECOMMENDATIONS

Recommendations from seven International Codes are used to predict the axial load capacity of the tested specimens. The obtained capacities are compared with the measured strengths. The codes used are: ANSI/AISC 360 (2010), British Standard 5400 (BS 5400, 2005), Canadian Standard S016 (CSA) (S016, 2001), two Chinese Standards; CECS 28 (1990) (Zhang et al., 2007) and GJB and DL/T 4142 (2000) (Han, 2002), Euro Code 4 (EC4) (EN 1994, 2004) and Japanese Standard AIJ (2001) (Morino and Tsuda, 2003). The formulas and, detailed procedures of these codes are given in following sections.

6.4.1 American National Standards Institute/ American Institute of Steel Construction (ANSI/AISC360, 2010)

The plastic stress distribution method provided in ANSI/AISC360 (2010) is used for calculating the nominal strength of composite columns. In this procedure, the nominal strength of the composite section is computed based on plastic strength of steel and concrete without allowing for confinement. Crushing stress of concrete core is defined as 0.85 $f_c^{'}$ for square and rectangular cross-section. The cross-section area of steel should be at least 1% of the total area of composite cross-section for it to qualify as a CFST column.

Based on the cross-sectional slenderness (D/t), the code classified CFST columns subjected to compression into three categories: compact, non-compact or slender sections.

Compact sections:

For compact sections:

$$\frac{D}{t} \leq 2.26\sqrt{\frac{E_s}{f_y}} \qquad \text{For square and rectangular cross-sections} \qquad (6.1)$$

Non-compact sections:

The maximum D/t ratios for section to be classified as non-compact section are:

$$\frac{D}{t} \leq 3.00\sqrt{\frac{E_s}{f_y}} \qquad \text{For square and rectangular cross-sections} \qquad (6.2)$$

Slender sections

The maximum D/t ratios for section to be classified as slender are:

$\frac{D}{t} \leq 5.00\ \frac{E_s}{f_y}$ For square and rectangular cross-sections (6.3)

The nominal compressive strength for axially loaded composite columns should be determined for the limit state of flexural buckling based on column cross-sectional slenderness and global slenderness.

When $\frac{P_n}{P_{cr}} \leq 2.25$

$$P_u = P_n \left[0.658^{\left(\frac{P_n}{P_{cr}}\right)}\right] \quad (6.4\ a)$$

When $\frac{P_n}{P_{cr}} > 2.25$

$$P_u = 0.877\ P_{cr} \quad (6.4\ b)$$

where P_{cr} is elastic Euler buckling load calculated as:

$$P_{cr} = \frac{\pi^2}{(KL)^2}(EI)_{eff} \quad (6.5)$$

$$(EI)_{eff} = E_s I_s + E_r I_r + C_3 E_c I_c \quad (6.6)$$

$$C_3 = 0.6 + 2\left(\frac{A_s}{A_c + A_s}\right) \leq 0.9 \quad (6.7)$$

P_n is the nominal cross-sectional capacity based on material strength calculated as:

For compact sections

$$P_n = P_{n1} = A_s f_y + \emptyset f_c^{'}\left(A_c + A_r \frac{E_s}{E_c}\right) \quad (6.8)$$

where $\emptyset$ is strength reduction factor considered as 0.85 for square and rectangular sections.

For non-compact sections

$$P_n = P_{n2} = P_{n1} - \frac{P_{n1} - P_y}{(\lambda_r - \lambda_p)^2}(\lambda_m - \lambda_p)^2 \quad (6.9)$$

where λ_m is the maximum cross-sectional slenderness permitted and calculated as:

$\lambda_m = 5.00 \frac{E_s}{f_y}$ For square and rectangular cross-sections (6.10)

λ_r is the maximum cross-sectional slenderness permitted to be classified as non-compact section and that is :

$$\lambda_r = 3.00\sqrt{\frac{E_s}{f_y}} \quad \text{For square and rectangular cross-sections} \tag{6.11}$$

λ_p is the maximum cross-sectional slenderness permitted to be classified as a compact section and calculated as:

$$\lambda_p = 2.26\sqrt{\frac{E_s}{f_y}} \quad \text{For square and rectangular cross-sections} \tag{6.12}$$

$$P_y = A_s f_y + 0.7 f_c^{'}\left(A_c + A_r \frac{E_s}{E_c}\right) \tag{6.13}$$

For slender sections

$$P_n = P_{n3} = A_s f_{bl} + 0.7 f_c^{'}\left(A_c + A_r \frac{E_s}{E_c}\right) \tag{6.14}$$

where f_{bl} is the local buckling strength of steel tube calculated based on simplified Bryan's formula as (Galambos, 1998):

$$f_{bl} = \frac{9E_s}{\left(\frac{D}{t}\right)^2} \quad \text{For rectangular and square sections} \tag{6.15}$$

6.4.2 British Standard (BS 5400, 2005)

British standard (BS 5400, 2005) considers the composite action between steel and concrete for designing such composite columns in rectangular and square CFST. The method for designing the composite columns in this standard as follows:

Steel Tube

The steel tube thickness should follow the constraint

$$t \geq D\sqrt{\frac{f_y}{3E_s}} \quad \text{For rectangular and square sections} \tag{6.16}$$

Concrete core

The code limits the concrete contribution factor (P_c) to be within a specified range to permit the use of this approach for composite columns design. The columns having P_c lower than the minimum limit are designed as RCC columns and the columns having P_c higher than the maximum limit are designed as steel columns. Where:

$$P_c = \frac{0.45 A_c f'_{cu}}{P_n} \quad \text{For rectangular and square sections} \qquad (6.17)$$

Where, P_c is the concrete contribution factor (f'_{cu}) is the cube compressive strength of concrete, and f'_{cc} is the enhanced characteristics strength of concrete core calculated as:

$$f'_{cc} = f'_{cu} + C_1 \frac{t}{D} f_y \qquad (6.18)$$

P_n is the peak load carrying capacity of CFST column calculated as:

$$P_n = 0.95 A_s f'_y + 0.87 A_r f_{yr} + 0.45 A_c f'_{cu} \quad \text{For rectangular and square sections} \qquad (6.19)$$

$$f'_y = C_2 f_y \qquad (6.20)$$

The constants C_1 and C_2 are given in Table 3 of the code .

If the ratio L/D is lower than 12, the code classifies CFST column as short column and limits the ultimate limit state of load carrying capacity at failure to:

$$P_u = 0.85\, P_n \qquad (6.21)$$

The factor 0.85 is a reduction factor to allow the moments due to constructions. Columns having L/D ratio greater than 12 may be considered as long columns. In this case the capacity of the column should be calculated considering bending moment not less than 0.03 B.

6.4.3 Canadian Standard (S016, 2001)

Full composite resistance is specified in Canadian Standard S016 (2001) for hollow steel tubes completely filled with concrete. The limitations for using such columns in this code are:

$$\frac{D}{t} \geq \frac{1350}{\sqrt{f_y}} \qquad \text{For rectangular and square cross-sections} \qquad (6.22)$$

Grade of concrete should be between 20 MPa and 40 MPa for CFST columns. This code predicts the factored compressive strength of CFST columns by increasing the strength of concrete core due to confinement effect and reduces the strength of steel tube.

$$P_u = \left(\tau \emptyset_s A_s f_y + \tau' 0.85 \emptyset_c A_c f_c'\right)\left(1 + \bar{\lambda}^{2n}\right)^{-1/n} \quad (6.23)$$

where $\tau = \tau' = 1$ for rectangular and square columns having L/D ≥ 25. For CFST columns having L/D < 25:

$$\tau = \frac{1}{\sqrt{1+\rho+\rho^2}} \quad (6.24\text{ a})$$

$$\tau' = 1 + \left(\frac{25\rho^2\tau}{D/t}\right)\left(\frac{f_y}{0.85 f_c'}\right) \quad (6.24\text{ b})$$

where

$$\rho = 0.02(25 - L/D) \quad (6.25)$$

$$\overline{\lambda} = \sqrt{\frac{P_n}{P_e}} \quad (6.26)$$

P_n and P_e are nominal cross-sectional capacity and Euler buckling load, respectively calculated as

$$P_n = \tau A_s f_y + \tau' 0.85 A_c f_c' \quad (6.27)$$

$$P_e = \frac{\pi^2}{(KL)^2}(EI)_{eff} \quad (6.28)$$

$$(EI)_{eff} = E_s I_s + \frac{0.6 E_c I_c}{1+(C_{fs}/C_f)} \quad (6.29)$$

$$E_c = \left(3300\sqrt{f_c' + 6900}\right)\left(\frac{w_c}{2300}\right)^{1.5} \quad (6.30\text{ a})$$

For concrete having compressive strength between 20 MPa to 40 MPa, E_c can be calculated as:

$$E_c = 4500\sqrt{f_c'} \quad (6.30\text{ b})$$

Here $\bar{\lambda}$ is the relative slenderness parameter and w_c is the density of concrete. C_{fs} is defined as the sustained axial load on the column while C_f is the total axial load on the column. The ratio

of C_{fs}/C_f is taken as 1.0 for short-term loading condition. The constant n has been considered as 1.8 as recommended by the code. $\emptyset_s$ and $\emptyset_c$ are the nominal resistance factors for steel and concrete respectively and have been considered as 1.0.

6.4.4 Euro Code 4 (EN 1994, 2004)

There are two methods for designing composite columns in Euro Code 4 (EC4) (EN 1994, 2004). The columns in the present study have been designed using the Simplified Design Method, as explained in Section 5.4.5.

The steel contribution ratio, P_s, must be $0.2 \leq P_s \leq 0.9$. P_s is defined as:

$$P_s = \frac{A_s f_y}{P_{ud}} \tag{6.31}$$

If P_s is less than 0.2, the column may be designed as a reinforced concrete column. If P_s is larger than 0.9, the concrete contribution is ignored and the column is designed as a steel column. P_{ud} is design nominal plastic resistance of concrete filled steel tube (design nominal squash load) calculated as:

$$P_{ud} = A_s f_y + A_r f_{yr} + A_c f_c' \quad \text{For rectangular and square cross-section} \tag{6.32}$$

where A_r is the area of reinforcement bars, if any, f_{yr} is design yield stress of reinforcement bar, λ_s and λ_c are confinement parameters for steel tube and concrete core. λ_s and λ_c depend on relative slenderness ratio $\overline{\lambda}$, calculated as:

$$\overline{\lambda} = \sqrt{\frac{P_n}{P_{cr}}} \tag{6.33}$$

P_n is the plastic resistance of the composite cross-section to compression calculated using the nominal yield strength of steel tube and reinforcement bars and nominal compressive strength of concrete cylinder:

$$P_n = A_s f_y + A_r f_{yr} + A_c f_c' \tag{6.34}$$

P_{cr} is the critical buckling load:

$$P_{cr} = \frac{\pi^2 E I_{eff}}{L^2} \tag{6.35}$$

EI_{eff} is the effective elastic flexural stiffness of the composite column calculated as:

$$EI_{eff} = E_s I_s + E_r I_r + 0.6 E_{cm} I_c \quad (6.36)$$

E_r and I_r are modulus of elasticity and yield stress of reinforcement bars and E_{cm} is the mean secant modulus of elasticity for structural concrete calculated as:

$$E_{cm} = 22000 \left[\frac{f_{cm}}{10}\right]^{0.3} \quad (6.37)$$

where f_{cm} is mean compressive strength of concrete at 28 days age and calculated as:

$$f_{cm} = f_c^{'} + 8\ (MPa) \quad (6.38)$$

For columns having e/d <10:

$$\lambda_s = 0.25\left(3 + 2\overline{\lambda}\right) \leq 1.0 \quad (6.39)$$

$$\lambda_c = 4.9 - 18.5\overline{\lambda} + 17\overline{\lambda}^{\,2} \quad \geq 0 \quad (6.40)$$

The squash load of composite columns in axial compression is calculated as:

$$P_u = \chi\, P_{u1} \quad (6.41)$$

where P_u is the ultimate load carrying capacity of CFST columns and χ is reduction factor to account buckling effect.

$$\chi = \frac{1}{\Phi + \left(\Phi^2 - \overline{\lambda}^2\right)^{0.5}} \quad (6.42)$$

$$\Phi = 0.5 * (1 + \alpha\left(\overline{\lambda} - 0.2\right) + \overline{\lambda}^2) \quad (6.43)$$

where α is imperfection factor and has been taken as 0.34 as recommended by Hicks et al. (2002). For this code to be applicable:

$$D/t \leq 52 \times \sqrt{\frac{235}{f_y}} \text{ For rectangular and square CFST sections} \quad (6.44)$$

6.4.5 Architectural Institute of Japan (AIJ)

The details for calculating the allowable and ultimate compressive strength of CFST columns are given by Morino and Tsuda (2003). AIJ code classifies the CFST columns into three categories:

a) Short if KL/D ≤ 4: The axial load carrying capacity for short CFST columns is calculated by superimposing the strength of steel column and concrete column.

b) Long if KL/D > 12: The ultimate compressive strength of the long CFST columns is calculated as the summation of critical buckling loads of concrete column and steel column.

c) CFST columns having 4 < KL/D ≤ 12 are classified as Intermediate columns. The compressive strength of intermediate CFST columns is calculated using linear interpolation.

The details of calculating the load carrying capacity are:

For KL/D ≤ 4

$$P_{u1} = P_{uc} + P_{us} \tag{6.45}$$

where P_{u1} is the axial load carrying capacity of CFST column having KL/D ≤ 4, P_{uc} is the ultimate axial compressive load carried by concrete column, and $P_{us}$is the ultimate axial compressive load carried by steel column.

$$P_{uc} = 0.85 f_c^{'} A_c \tag{6.46}$$

$$P_{us} = f_y A_s \tag{6.47}$$

For 4 < KL/D ≤ 12

$$P_{u2} = P_{u1} - 0.125\left(P_{u1} - P_{u3,12}\right)\left(\frac{KL}{B} - 4\right) \tag{6.48}$$

Here P_{u2} is the load carrying capacity of column having 4 < KL/D ≤ 12 and$P_{u3,12}$ is the load carrying capacity of a virtual CFST column having same cross-section but with KL/D =12

For KL/D > 12

$$P_{u3} = A_c f_{crc} + A_s f_{crs} \tag{6.49}$$

where f_{crc} and f_{crs} are critical buckling stress of concrete column and steel column, respectively.

For $\overline{\lambda}_c \leq 1.0$

$$f_{crc} = \frac{2}{1+\sqrt{\overline{\lambda}_c^{\,4}+1}} 0.85 f_c^{'} \tag{6.50}$$

For $\overline{\lambda}_c > 1.0$

$$f_{crc} = 0.83 \times e^{\left(C_c(1-\overline{\lambda}_c)\right)} 0.85 f_c^{'} \tag{6.51}$$

where:

$$\overline{\lambda}_c = \frac{\lambda_c}{\pi}\sqrt{\varepsilon_{uc}} \tag{6.52}$$

$\overline{\lambda}_c$ is the relative slenderness parameter of concrete column and λ_c is the slenderness parameter of concrete column calculated as:

$$\lambda_c = \frac{KL}{r_c} \tag{6.53}$$

where r_c is the radius of gyration of concrete column and ε_{uc} is the ultimate axial strain of concrete column calculated as:

$$\varepsilon_{uc} = 0.93(0.85 f_c^{'})^{1/4} \times 10^{-3} \tag{6.54}$$

C_c is an empirical parameter calculated as:

$$C_c = 0.568 + 0.00612\, f_c^{'} \tag{6.55}$$

For $\overline{\lambda}_s < 0.3$

$$P_{crs} = f_y A_s \tag{6.56 a}$$

For $0.3 \leq \overline{\lambda}_s < 1.3$

$$P_{crs} = \left(1 - 0.545\left(\overline{\lambda}_s - 0.3\right)\right) f_y A_s \tag{6.56 b}$$

For $\overline{\lambda}_s \geq 1.3$

$$P_{crs} = \frac{P_{es}}{1.3} \quad (6.57$$

$$\overline{\lambda}_s = \frac{\lambda_s}{\pi}\sqrt{\frac{f_y}{E_s}} \quad (6.58)$$

$\overline{\lambda}_s$ is the relative slenderness parameter of steel column, $\lambda_s$is the slenderness parameter of steel column calculated as:

$$\lambda_s = \frac{KL}{r_s} \quad (6.59)$$

r_s is the radius of gyration of steel tube and P_{es} is the Euler buckling load of steel column calculated as:

$$P_{es} = \frac{\pi^2 E_s I_s}{(KL)^2} \quad (6.60)$$

6.4.6 Chinese Codes

There are four codes, i.e. DL/T 5085:1999, GJB 4142:2000, JCJ 01:89 and CECS 28:90 (as mentioned in Section 5.4.7) in China for designing CFST members. These codes are published in Chinese language and the code methodologies are also discussed in Han (2002), Zhang et al., (2007), Hatzigeorgiou (2008), and Lu and Zhao (2010).

The capacity of short CFST column in JCJ and CECS codes is calculated based on confinement theory. In this theory, the cross-sectional strength of steel tube and concrete core are calculated separately and then added to get the strength of composite cross-section. The details of these codes, as presented in Han (2002) and Zhang et al. (2007) are as follows:

CECS 28:90 code:

$$P_u = A_c f_{ck}\left(1 + \xi + \sqrt{\xi}\right) \quad (6.61)$$

Where:

$$\xi = \frac{A_s f_y}{A_c f_{ck}} \quad (6.62)$$

Here ξ is the confining factor. The value of ξ must lie between 0.03 and 3.0.

The DL/T and GJB codes work on the principle of unified theory i.e. A heterogeneous CFST cross-section consisting of concrete and steel is converted to an equivalent single composite cross-section. The procedure for calculating the load carrying capacity as per these codes is given as:

GJB 4142:2000 (Han, 2002) ***and DL/T 5085:1999*** (Lu and Zhao, 2010)

$$P_u = f_{scy} A_{sc} \tag{6.63}$$

f_{scy} and A_{sc} are the equivalent stress and area of new composite cross-section.

$$f_{scy} = (1.212 + B\xi + C\xi^2) f_{ck} \tag{6.64}$$

where B and C parameters are given (Han, 2002) for square and rectangular CFST columns as:

$$B = 0.1381 \frac{f_y}{235} + 0.7646 \tag{6.65}$$

$$C = -0.0727 \frac{f_{ck}}{20} + 0.0216 \tag{6.66}$$

$$A_{sc} = A_s + A_c \tag{6.67}$$

The value of f_{ck} (characteristics compressive strength of concrete core) is obtained using 67% of the compressive strength of concrete cubes as recommended by Han (2002).

It can be seen from the above equations that none of the codes give any formulas for prediction of load carrying capacity of Double skin concrete filled steel tubes (CFDST). Hence, while calculating the load capacity for the CFDST, the inner tube in CFDST specimen was considered in a similar way as the outer steel tube.

The load carrying capacities calculated from the different codes are shown in Table 6.5. The ratio of codal to experimental values is also shown in the table. It can be seen that all of the except the CECS Chinese code, all other codes give conservative results with most conservative results being obtained from the British code (BS code). The table also illustrates that the Chinese GJB code gives the best estimate for the load capacity of CFST columns, with the average ratio of predicted to experimental load capacity as 0.94. Further, Eurocode (EC4) and Canadian Standards (CSA) also predict the load capacities of CFST with a good degree of precision.

.

Table 6.9 Results of different International Codes used for predicting the axial capacities of square tested specimens

Core	Length Category	Specimens ID	$P_{u\text{-}EC4}$ (kN)	$\frac{EC4}{EXP}$	$P_{u\text{-}AISC}$ (kN)	$\frac{AISC}{EXP}$	$P_{u\text{-}BS}$ (kN)	$\frac{BS}{EXP}$	$P_{u\text{-}CSA}$ (kN)	$\frac{CSA}{EXP}$	$P_{u\text{-}AIJ}$ (kN)	$\frac{AIJ}{EXP}$	$P_{u\text{-}CECS}$ (kN)	$\frac{CECS}{EXP}$	$P_{u\text{-}GJB}$ (kN)	$\frac{GJB}{EXP}$
RCFST	**L3D**	SS1-1-1	1555.8	0.88	1453.4	0.82	1226.2	0.69	1458.1	0.82	1484.2	0.84	2139.5	1.21	1629.5	0.92
		SS1-1-2-1	1871.8	0.87	1773.3	0.83	1539.0	0.72	1778.3	0.83	1803.6	0.84	2563.1	1.20	1934.8	0.90
		SS1-1-2-2	1871.8	0.85	1773.3	0.81	1539.0	0.70	1778.3	0.81	1803.6	0.82	2563.1	1.18	1934.8	0.88
	L7D	SS2-1-1	1239.8	1.01	1131.6	0.92	1016.3	0.83	1154.3	0.94	1172.5	0.95	1359.5	1.11	1245.1	1.01
		SS2-1-2-1	1437.0	0.87	1276.0	0.79	1160.3	0.72	1302.8	0.80	1321.6	0.82	1513.1	0.93	1373.8	0.85
		SS2-1-2-2	1437.0	0.84	1276.0	0.80	1160.3	0.69	1302.8	0.77	1321.6	0.78	1513.1	0.90	1373.8	0.81
RCC-RCFST	**L3D**	SR1-1-1-1	2170.6	0.98	1787.7	0.81	1761.1	0.79	2072.8	0.94	2099.1	0.95	2905.7	1.31	2199.4	0.99
		SR1-1-1-2	2170.6	1.01	1787.7	0.91	1761.1	0.85	2072.8	0.97	2099.1	0.97	2905.7	1.31	2199.4	0.99
	L7D	SR2-1-1-1	1384.9	1.01	1248.6	0.91	1166.5	0.85	1325.5	0.96	1329.8	0.97	1527.7	1.11	1384.3	1.01
		SR2-1-1-2	1384.9	1.01	1248.6	0.90	1166.5	0.85	1325.5	0.96	1329.8	0.97	1527.7	1.11	1384.3	1.01
RCFDST	**L3D**	SD1-1-1-1	1708.3	0.90	1612.4	0.85	1391.0	0.72	1938.9	1.02	1642.4	0.86	2344.3	1.29	1779.1	0.93
		SD1-1-1-2	1708.3	0.88	1612.4	0.83	1391.0	0.73	1938.9	1.00	1642.4	0.85	2344.3	1.30	1779.1	0.92
		SD1-1-2-1	2024.0	0.82	1932.5	0.78	1703.8	0.69	2041.3	0.83	1961.7	0.80	2750.4	1.11	2062.0	0.83
		SD1-1-2-2	2024.0	0.81	1932.5	0.77	1703.8	0.69	2041.3	0.82	1961.7	0.79	2750.4	1.11	2062.0	0.83
	L7D	SD2-1-1	1392.3	0.78	1284.2	0.72	1181.0	0.66	1356.8	0.82	1331.0	0.74	1503.6	1.09	1337.4	0.97
		SD2-1-2	1519.9	0.84	1428.2	0.80	1325.3	0.74	1460.1	0.76	1480.2	0.82	1650.4	0.92	1430.2	0.80
Average				0.90		0.83		0.75		0.88		0.86		1.14		0.92
Standard Deviation				0.08		0.06		0.07		0.09		0.06		0.13		0.08
Coefficient of Variation (%)				8.91		7.15		8.74		9.99		8.87		11.86		8.19

6.5 CONCLUSIONS

The following conclusions can be drawn from the experimental and numerical results:

Mode of deformation

a. The L3D specimens were observed to fail by local buckling of steel tube followed by the crushing of concrete core (Figures 6.2, 6.4 and 6.6). Local Buckling in the top third of the sample beginning near the top edge was also the primary mode of failure in L7D specimens (Figures 6.3, 6.5 and 6.7).

b. Steel tube was separated from the concrete core at cross-sections where local buckling occurred. However, the separation was avoided near the corners for small thickness samples, while the thicker square tubes separated from concrete near the corners also (Figure 6.8).

Strength

a. Due to composite, enhanced strength (strength index SI >1) action was reported for all tested specimens (Tables 6.5 to 6.7).

b. The maximum strength index was observed in case of CFST core configuration for L3D and L7D specimens (Table 6.5).

c. Trend of increase in strength index due to increase in thickness of steel tubes was more in case of CFST and CFDST specimens as compared to RCC-CFST samples (Tables 6.5 to 6.7)..

Ductility

a. The ductility index was highest in RCC-CFST core configuration for L7D specimens. For L3D length category, both RCC-CFST and CFST configurations showed almost same ductility (Table 6.8).

b. Ductility index was lowest in CFDST specimens with L3D and L7D details (Tables 6.5 to 6.7).

Equivalent area of steeL

a. Strength Index was generally observed to decrease for both L3D and L7D specimens with the redistribution in area of steel from steel tube to longitudinal rebars (Table 6.8).

b. The ductility index was observed to be higher (or equal) for RCC-CFST specimens as compared to CFST single skin specimens for both length categories (Table 6.8).

Codal recommendations:

Among seven International Codes, the Chinese code (GJB) gives closest estimation for strength with 8% conservative estimations on average as compared to measured values (Table 6.9).

CHAPTER SEVEN

COLUMNS WITH RECTANGULAR CROSS-SECTIONS

7.1 GENERAL

The experimental and computational investigations on rectangular tubes filled with concrete are presented in this chapter. A total of fifteen specimens consisting of three different types; Concrete Filled Steel Tube Columns (CFST) (Figure 3.3); Concrete Filled Double Steel Tube Columns (CFDST) (Figure 3.4) and Reinforced Concrete Filled Steel Tube Columns (RCC-CFST) (Figure 3.5) were cast and tested under axial loading. Twenty nine specimens of varying outer cross-section (B x D; B refers to the smaller dimension of the rectangular section, D is the larger side), thicknesses (t) and lengths (L) were tested to study the effect of these parameters on structural response of the tubular columns. The effect of change in core configurations on the strength and ductility of the rectangular CFST columns was also studied. The CFST specimens were then modeled using the Finite Element model presented in Chapter 4. The results from numerical simulations were compared with the experimental results.

7.2 DETAILS OF SPECIMENS

Rectangular Composite columns of three different core configurations viz. Eighteen Concrete Filled Steel Tubular Columns (CFST), Seven Concrete Filled Double Skin Tubular Columns (CFDST) and Four Reinforced Concrete Filled Steel Tubular Columns (RCC-CFST) were tested in axial loading. Table 3.6 presents the Material properties of rectangular steel tubes used for preparing the specimens. Labeling of rectangular specimens used in this chapter is explained in Table 7.1 (a) and 7.1 (b).

Seven length categories were used for CFST specimens. Three categories were intermediate column specimens, while the other four length categories were designed as long columns.. Geometric Properties of rectangular CFST specimens are given in Table 7.2.

Table 7.1 Labelling of rectangular specimens

Typical ID: RPQ-L-M-N		
Character	Denotes	Value
R	Rectangular specimen	
p	Length Category	1: $6 \leq L/B \leq 7.5$
		2: L10B
		3: L13B
		4: L16B
		5: L19B
		6: L22B
Q	Core configuration	S: CFST
		D: CFDST
		R: RCC-CFST
L	Cross-section B x D of outer steel tube	1: 100 mmx200 mm
		2: 82 mm x145 mm
		3: 40 mm x 60 mm
M	Thickness of steel tube with cross-section B x D	1: first thickness
		2: second thickness
		3: third thickness
N	Specimen No. with same details	1: first specimen
		2: repeated (second)

Please note that the specimens of size 40 x 60 mm had initially given separate specimens IDs while testing; however, in this thesis, they are being presented (in Tables only; the experimental photographs follow the old IDs) following the conventions of Table 7.1 to avoid confusion. Table 7.2 (a) give the details of all Rectangular CFST samples. Table 7.2 (b) gives the details of old and new labels for the specimens of size 40 x 60 mm.

Two sizes of inner tubes have been used for Rectangular CFDST columns. However, the same size of inner tube was maintained for any one cross-section to avoid any effect due to change in inner tube. Steel tube with outer dimensions of 48 x 96 mm was used for L6B columns. The wall thickness of the tube was 3.83 MPa and the measured yield stress of the tube was 452 MPa. For L10B columns, the inner tube size was 40 x 60 mm, with a wall thickness of 2.63 mm and a yield stress of 458 MPa. Table 7.3 gives the details of rectangular CFDST specimens.

Table 7.2(a) Details of rectangular CFST specimens

Length Category		Specimen ID	L (mm)	B (mm)	D (mm)	t (mm)	D/t	L/B	fy (MPa)
Intermediate Specimens	L6B	RS1-1-1	600	100	200	3.80	52.63	6.00	401
		RS1-1-2-1	600	100	200	5.68	35.21	6.00	410
		RS1-1-2-2	600	100	200	5.68	35.21	6.00	410
	L7B	RS1-3-1-1	300	40	60	2.63	22.81	7.50	458
		RS1-3-1-2	300	40	60	2.63	22.81	7.50	458
	L10B	RS2-1-1	900	82	145	4.65	31.18	10.98	428
		RS2-1-2-1	900	82	145	5.15	28.16	10.98	424
		RS2-1-2-2	900	82	145	5.15	28.16	10.98	424
		RS2-3-1-1	420	40	60	2.63	22.81	10.50	458
		RS2-3-1-2	420	40	60	2.63	22.81	10.50	458
Long Specimens	L13B	RS3-3-1-1	540	40	60	2.63	22.81	13.50	458
		RS3-3-1-2	540	40	60	2.63	22.81	13.50	458
	L16B	RS4-3-1-1	660	40	60	2.63	22.81	16.50	458
		RS4-3-1-2	660	40	60	2.63	22.81	16.50	458
	L19B	RS5-3-1-1	780	40	60	2.63	22.81	19.50	458
		RS5-3-1-2	780	40	60	2.63	22.81	19.50	458
	L22B	RS6-3-1-1	900	40	60	2.63	22.81	22.50	458
		RS6-3-1-2	900	40	60	2.63	22.81	22.50	458

Table 7.2(b) Details of renamed rectangular CFST specimens

Old Specimen ID	New Specimen ID
R1-5-1	RS1-3-1-1
R1-5-2	RS1-3-1-2
R1-7-1	RS2-3-1-1
R1-7-2	RS2-3-1-2
R1-9-1	RS3-3-1-1
R1-9-2	RS3-3-1-2
R1-11-1	RS4-3-1-1
R1-11-2	RS4-3-1-2
R1-13-1	RS5-3-1-1
R1-13-2	RS5-3-1-2
R1-15-1	RS6-3-1-1
R1-15-2	RS6-3-1-2

The Rectangular RCC-CFST specimens were designed in the same way as square and circular RCC-CFST specimens. The outer thicker steel tube was redistributed as a steel tube of smaller thickness and some longitudinal rebars. Two length categories were used, i.e. L6B and L10B. The details of RCC-CFST rectangular specimens are given in Table 7.4.

Normal concrete of M30 grade was used to fill the hollow volume of the tubes. The cylinder strength of the mix was 32.05 MPa (see Table 5.5). The Finite element model proposed in Chapter 4 was used to numerically simulate the samples. The applicability of the model was extended by modeling tubular columns of different lengths and core configurations.

Table 7.3 Details of rectangular CFDST specimens

Length Category		Sample ID	L (mm)	Bo (mm)	Do (mm)	to (mm)	(D/t)o	(L/D)o	f_{yo} (MPa)
Intermediate Specimens	L6B	RD1-1-1-1	600	100	200	3.80	52.63	6.00	401
		RD1-1-1-2	600	100	200	3.80	52.63	6.00	401
		RD1-1-2-1	600	100	200	5.68	35.21	6.00	410
		RD1-1-2-2	600	100	200	5.68	35.21	6.00	410
	L10B	RD2-1-1	900	82	145	4.65	31.18	10.98	428
		RD2-1-2-1	900	82	145	5.15	28.16	10.98	424
		RD2-1-2-2	900	82	145	5.15	28.16	10.98	424

Table 7.4 Details of Rectangular RCC-CFST specimens

Length Category		Specimen ID	L (mm)	B (mm)	D (mm)	t (mm)	Reinf. (mm)	L/B	D/t	f_Y (MPa)
Intermediate Specimens	L6B	RR1-1-1-1	600	100	200	3.80	4Ø10+4Ø16	6.00	52.63	401
		RR1-1-1-2	600	100	200	3.80	4Ø10+4Ø16	6.00	52.63	401
	L10B	RR2-1-1-1	900	82	145	4.65	4Ø10	10.98	31.18	428
		RR2-1-1-2	900	82	145	4.65	4Ø10	10.98	31.18	428

7.3 RESULTS

7.3.1 Mode of Deformation

Figure 7.1(a) shows the tested rectangular single skin (CFST) specimens, while the tested rectangular double skin (CFDST) and Reinforced concrete tubular specimens (RCC-CFST) specimens are shown in Figure 7.1(b). Figures 7.2 to 7.8 show experimental and numerical deformed shapes for various rectangular CFST, CFDST and RCC-CFST specimens.

Figure 7.1(a) All tested Rectangular CFST specimens

Figure 7.1(b) All tested Rectangular CFDST and RCC-CFST specimens

Experiment **Simulated** **Experiment** **Simulated**

Figure 7.2 Comparison of Experimental and Simulated Deflected Shape of L6B 100 x 200 mm Rectangular CFST

It was observed that CFST specimens with 100 mm x 200 and 82 mm x 145 mm cross-sections failed by crushing of concrete followed by local buckling of steel tube for L6B and L10B. (Figures 7.2 and 7.4). Global buckling starting near the mid height was the general mode of failure of 40 mm x 60 mm cross-section CFST specimens (Figure 7.3). This behaviour indicated that the mode of failure varies with both specimen length and cross-section size. In specimens with smaller cross-sections, the ratio of area of steel to the gross area of cross-section is generally larger (The ratio of area of steel to the gross area of the composite was 0.11 to 0.19 for specimens with 100 mm x 200 and 82 mm x 145 mm cross-sections, while that of 40 mm x 60 mm cross-section was 0.21). This is because of the triaxial state of stress, due to which the longitudinal stress that the steel tube can carry is decreased (as per von Mises criterion), thereby reducing the global stability of the sample as the area of steel increases.

The L6B CFDST samples failed by outward local buckling of outer steel tube accompanied by the inner buckling of the inner tube. The L10B specimens however, failed in a mixed mode of global and local buckling.

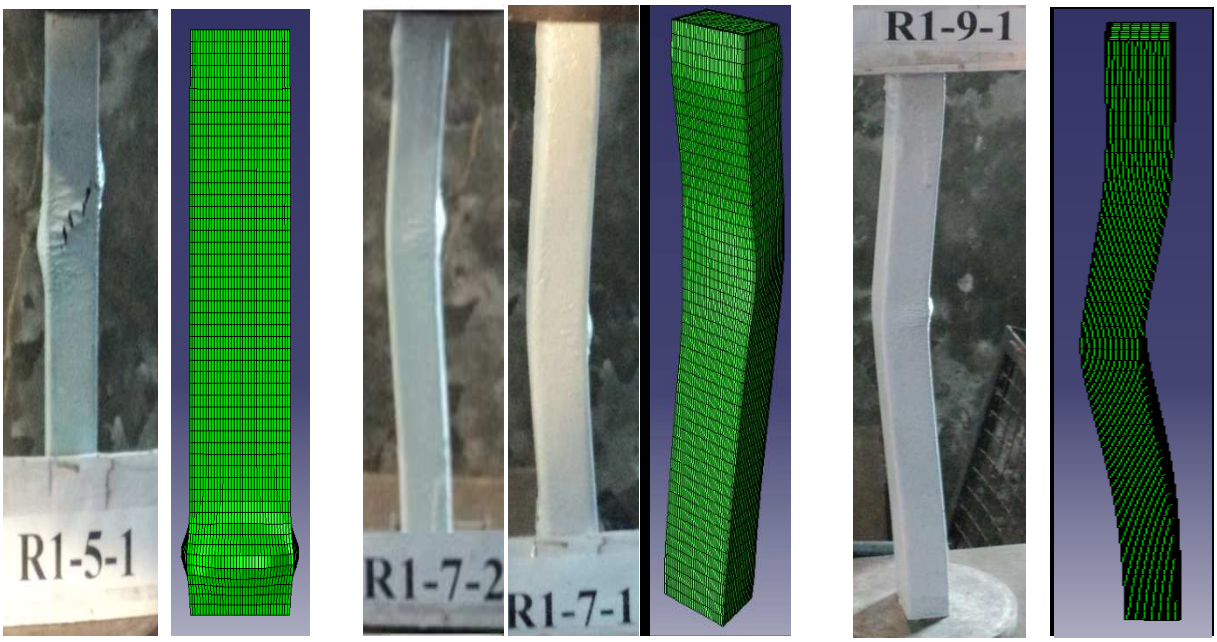

Experiment **Simulated** **Experiment** **Simulated** **Experiment** **Simulated**

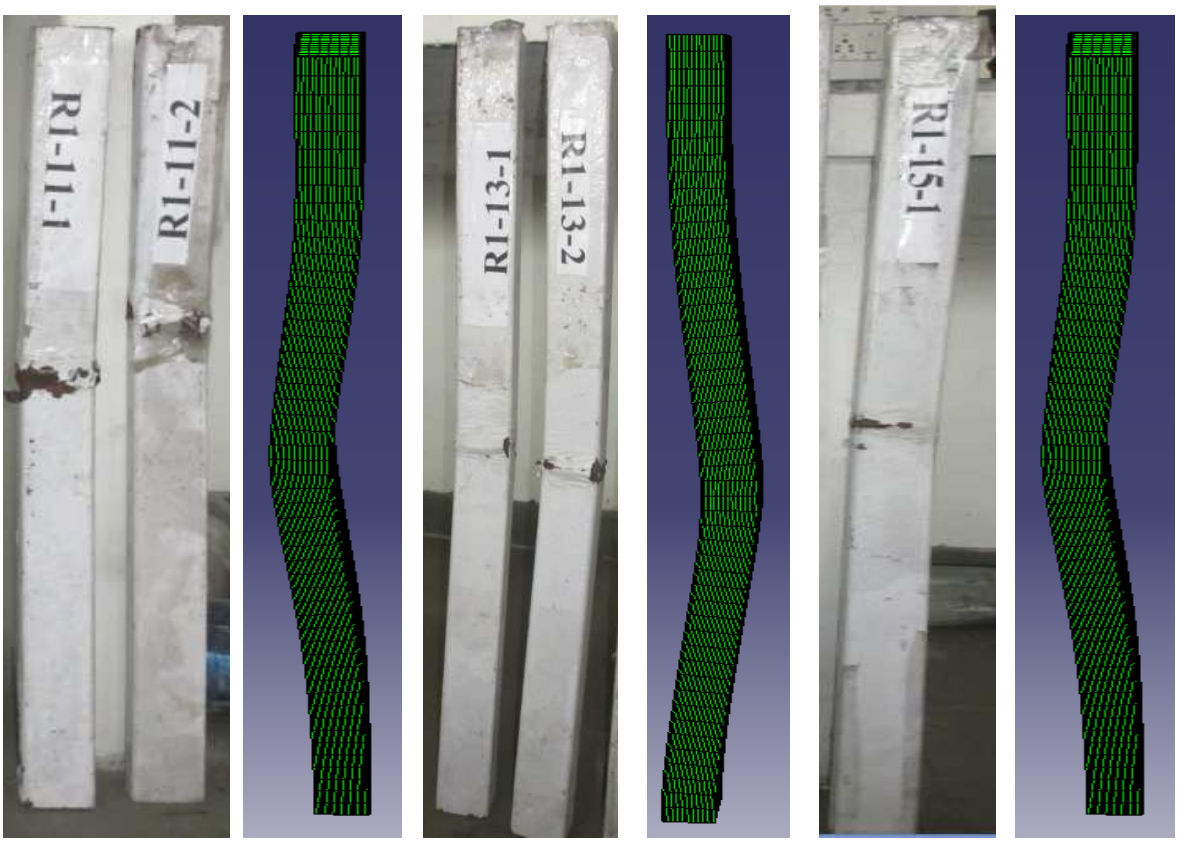

Experiment **Simulated** **Experiment** **Simulated** **Experiment** **Simulated**

Figure 7.3 Comparison of Experimental and Simulated Deflected Shape of 40 x 60 mm Rectangular CFST

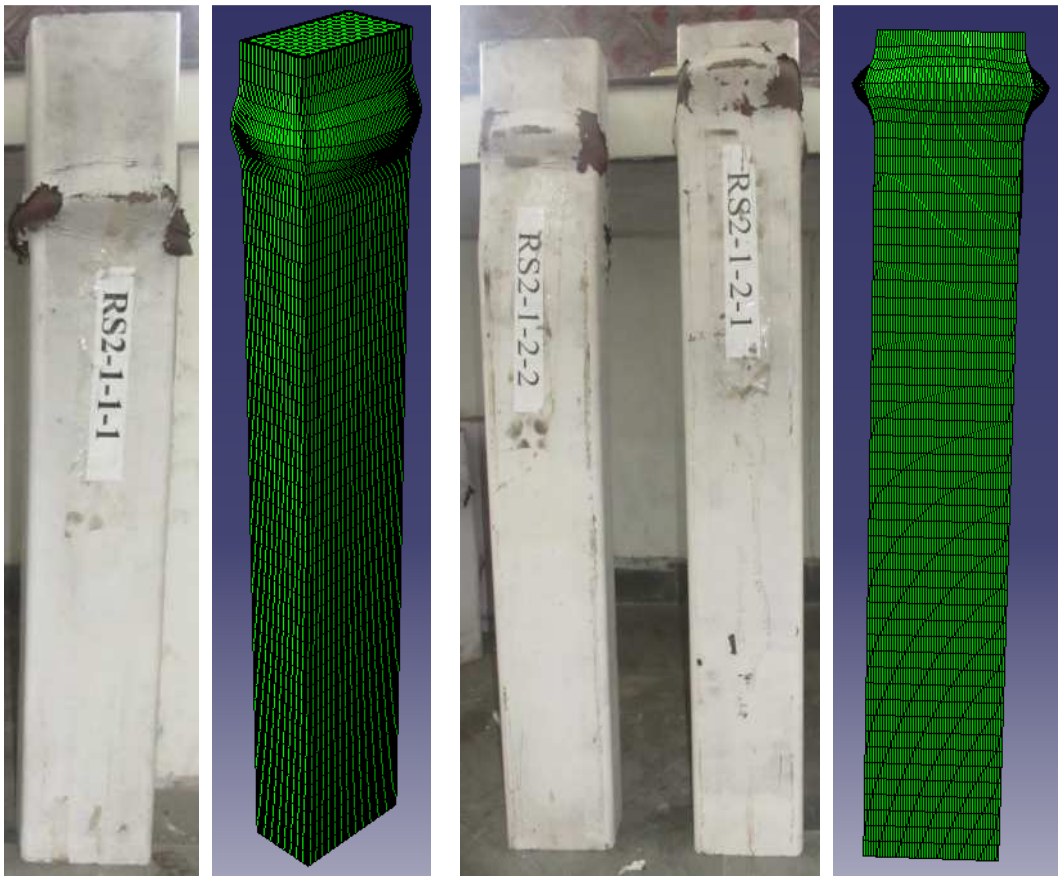

Experiment **Simulated** **Experiment** **Simulated**

Figure 7.4 Comparison of Experimental and Simulated Deflected Shape of L10B 82 x 145 mm Rectangular CFST

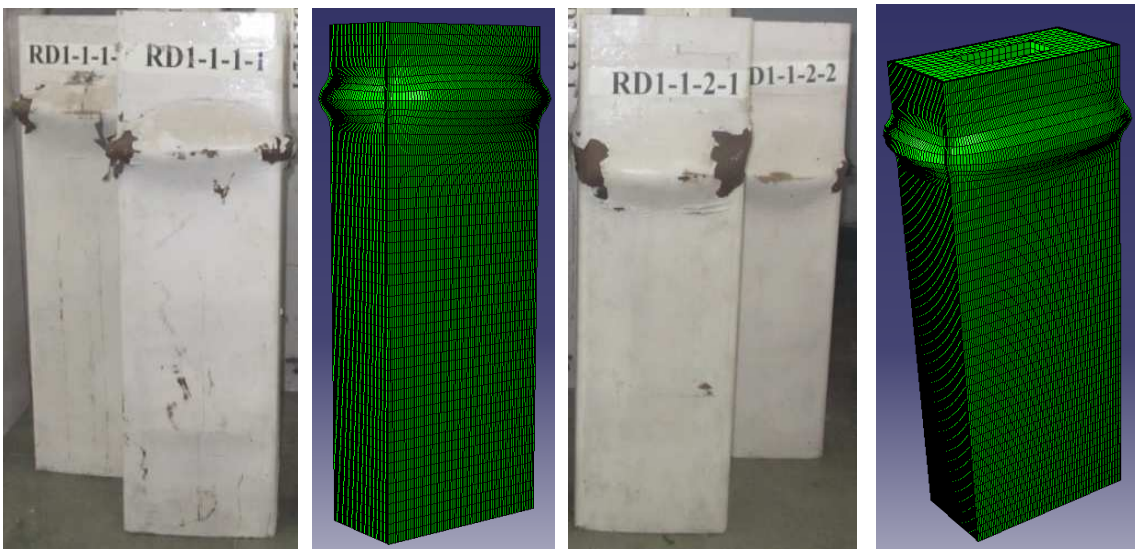

Experiment **Simulated** **Experiment** **Simulated**

Figure 7.5 Comparison of Experimental and Simulated Deflected Shape of L6B 100 x 200 mm Rectangular CFDST

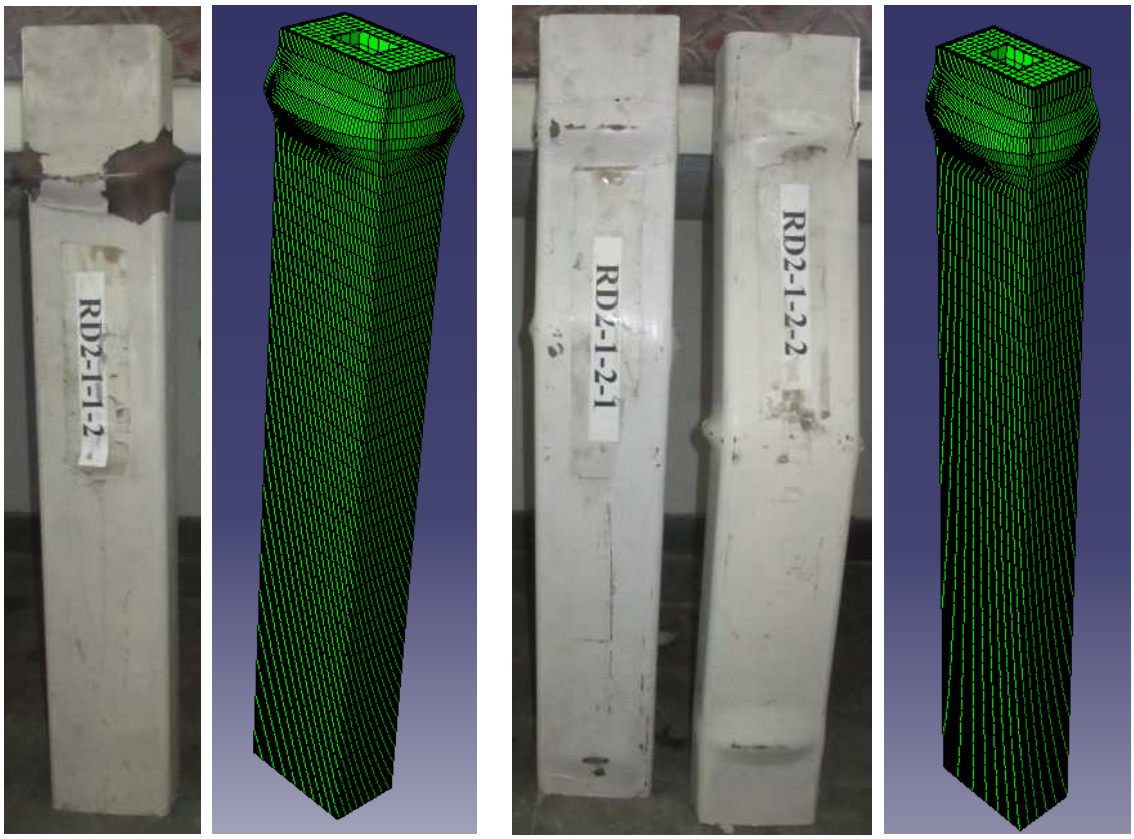

Experiment **Simulated** **Experiment** **Simulated**

Figure 7.6 Comparison of Experimental and Simulated Deflected Shape of L10B 82 x 145 mm Rectangular CFDST

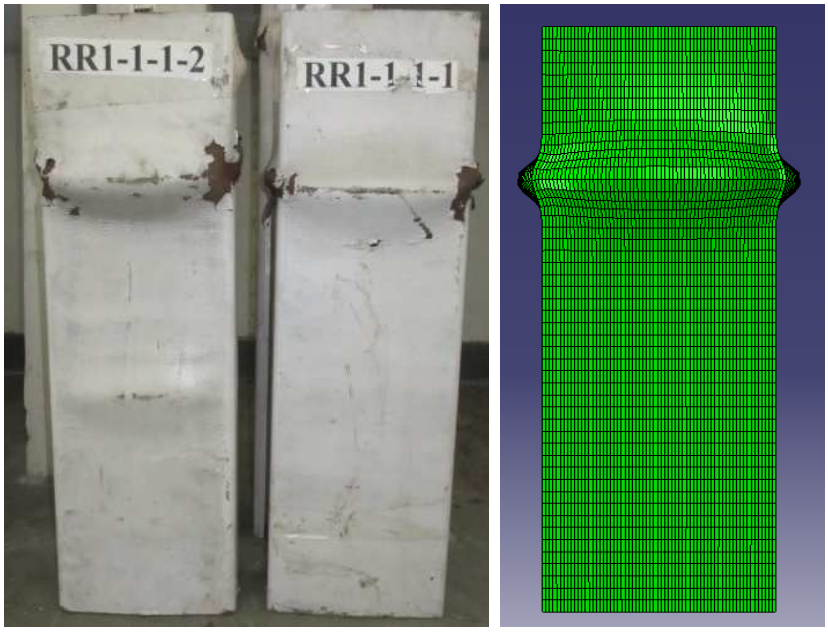

Experiment **Simulated**

Figure 7.7 Comparison of Experimental and Simulated Deflected Shape of L6B 100 x 200 mm Rectangular RCC-CFST

Experiment **Simulated**

Figure 7.8 Comparison of Experimental and Simulated Deflected Shape of L10B 82 x 145 mm Rectangular RCC-CFST

7.3.2 Strength

Figures 7.9, 7.10 and 7.11 show experimental and numerical load-displacement curves for Rectangular CFST, CFDST and RCC-CFST specimens, respectively. It can be concluded from Figures 7.9 to 7.11 that the axial capacity of specimens increases as the wall thickness of the specimens increases for all diameters, configurations and lengths. It can also be concluded that the proposed model gives acceptable results for load-displacement curves for all specimens and it is applicable to specimens with different lengths and different core configurations.

A glance at Figures 7.9 to 7.11 clearly shows that the proposed numerical model tends to become more conservative for samples of higher aspect ratio (D/B). The numerical load values are generally higher or quite close to experimental values for 40 x 60 mm rectangular samples (Aspect ratio=1.5; Figures 7.9(b) and (c)), while the model gives lower results than experimental for 100 x 200 mm samples (Aspect ratio=2.0)

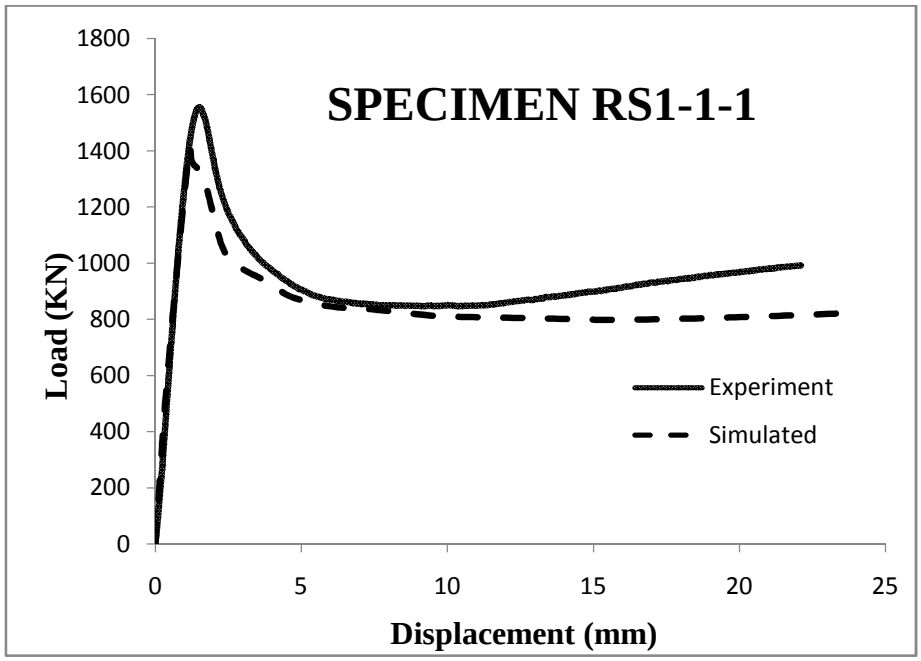

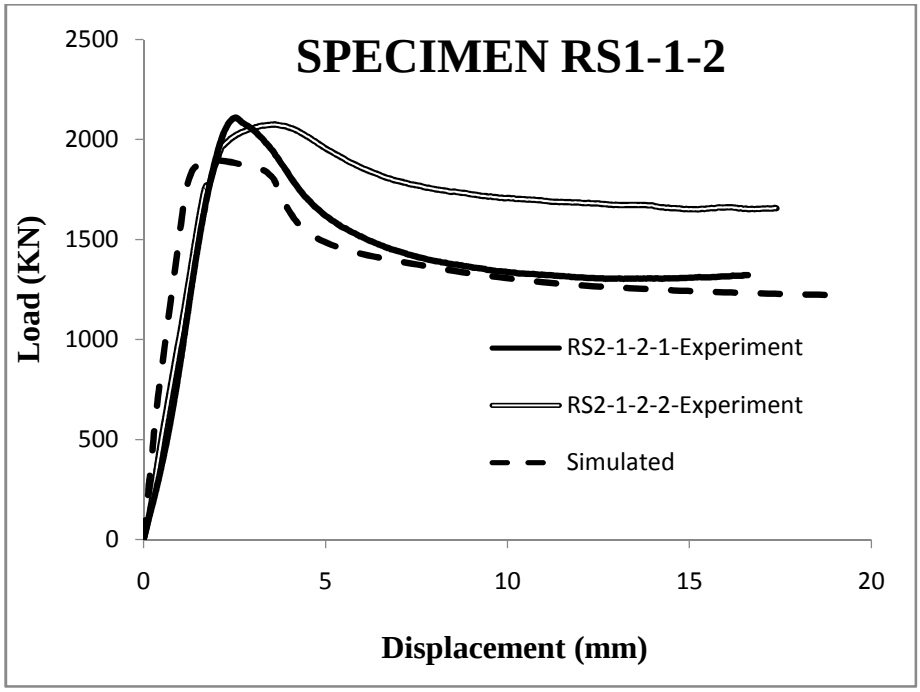

Figure 7.9(a) Comparison of experimental and numerical load-displacement curves for L6B 100 x 200 mm rectangular CFST specimens

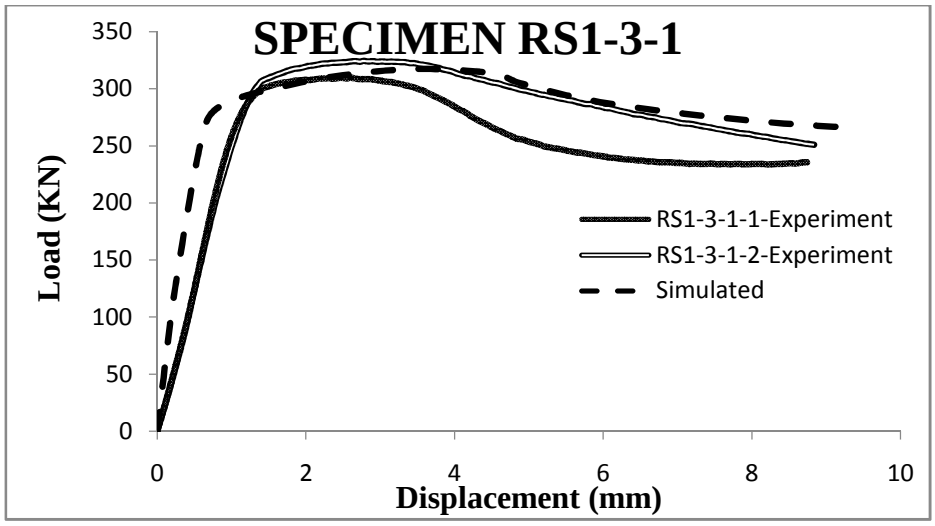

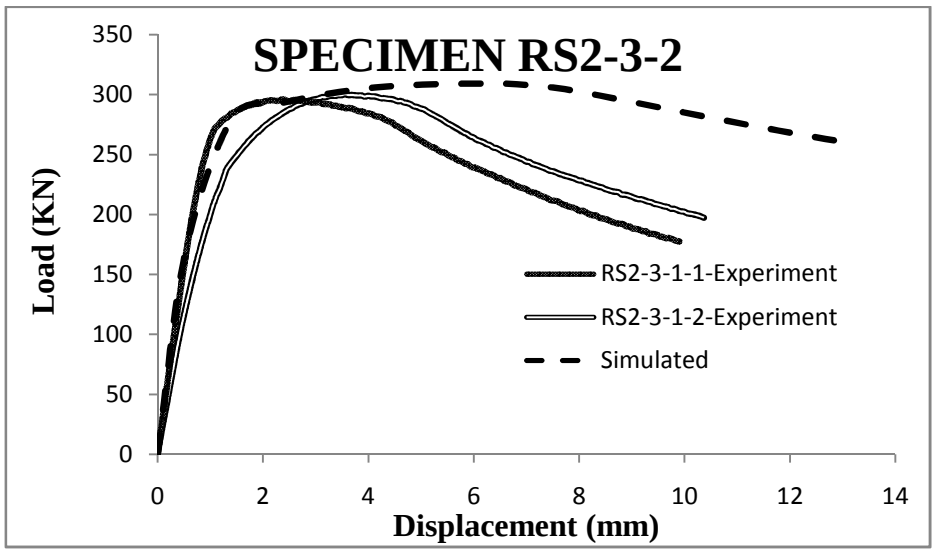

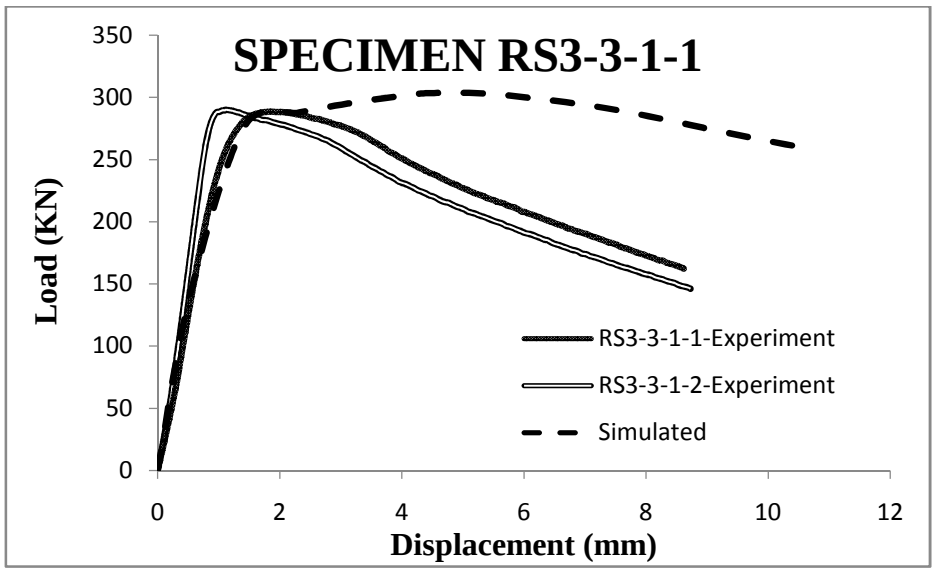

Figure 7.9(b) Comparison of experimental and numerical load-displacement curves for L7B, L10B and L13B 40 x 60 mm rectangular CFST specimens

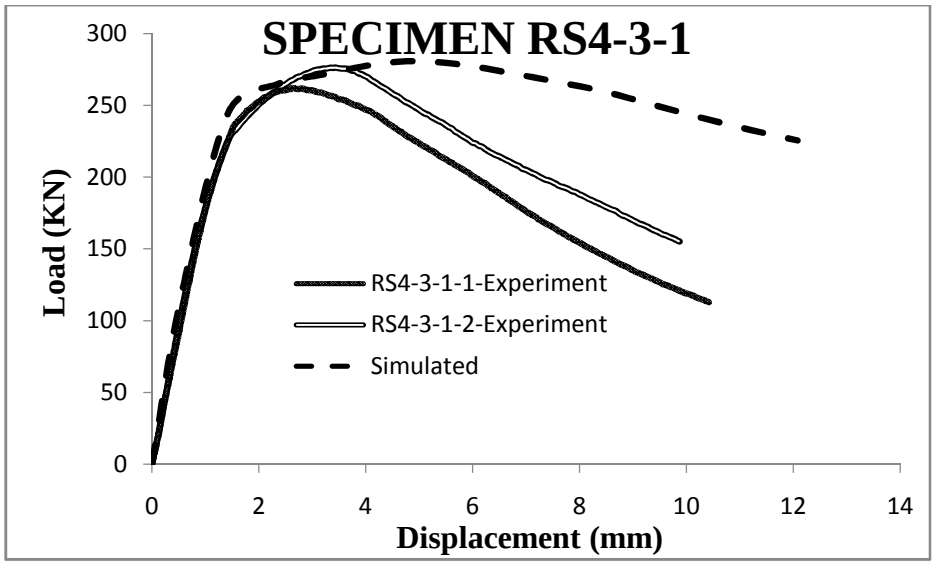

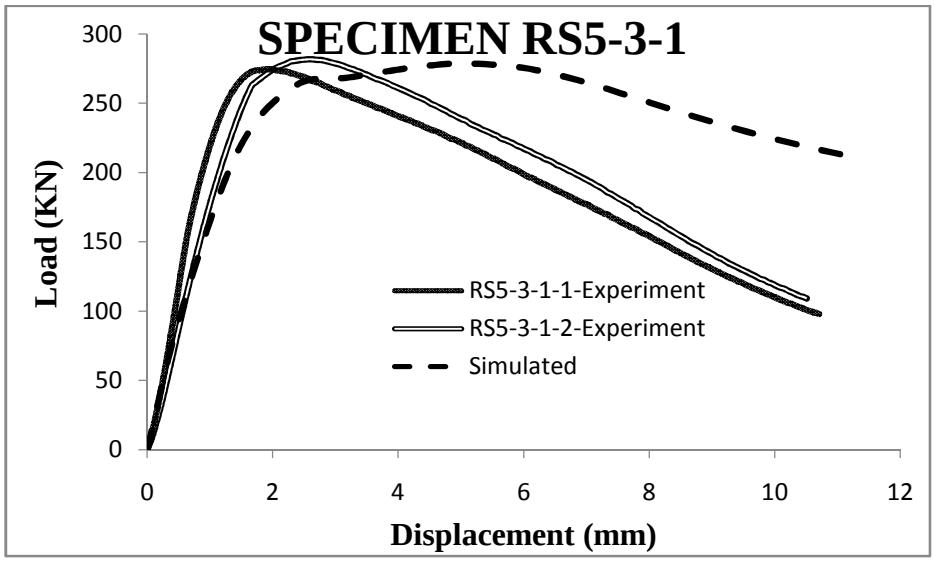

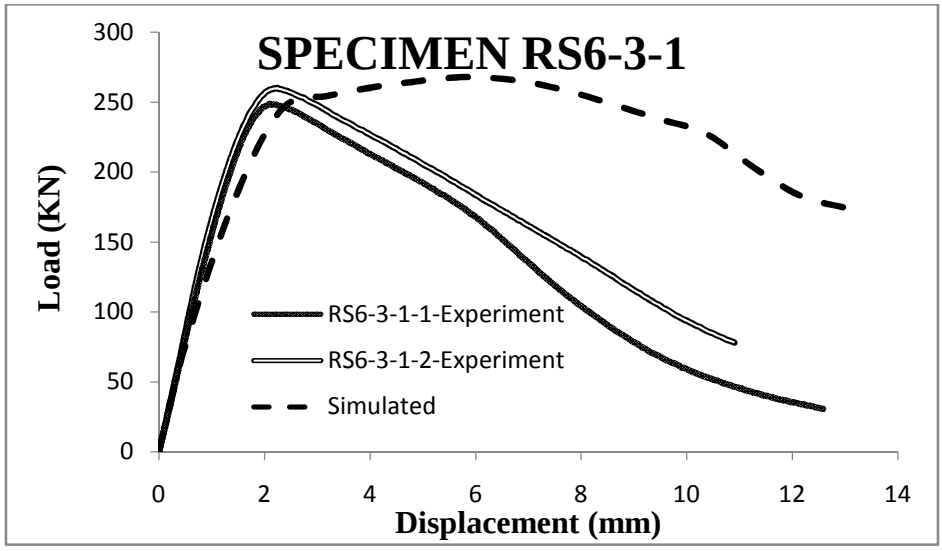

Figure 7.9(c) Comparison of experimental and numerical load-displacement curves for L16B, L19B and L22B 40 x 60 mm rectangular CFST specimens

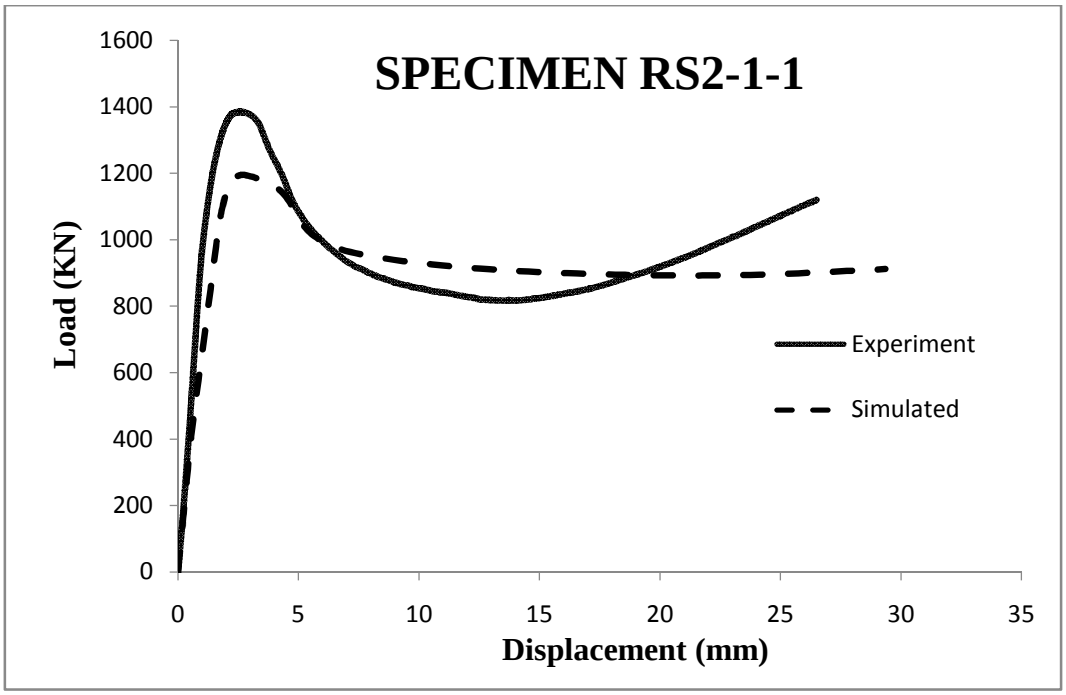

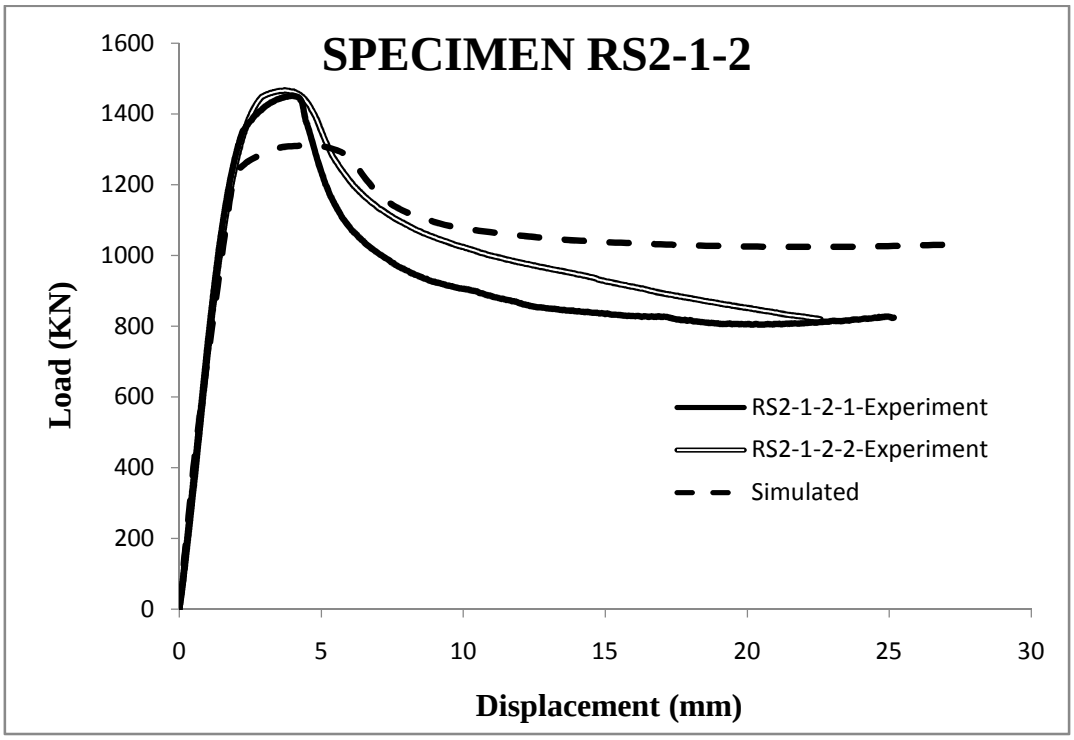

Figure 7.9(d) Comparison of experimental and numerical load-displacement curves for L10B 82 x 145 mm rectangular CFST specimens

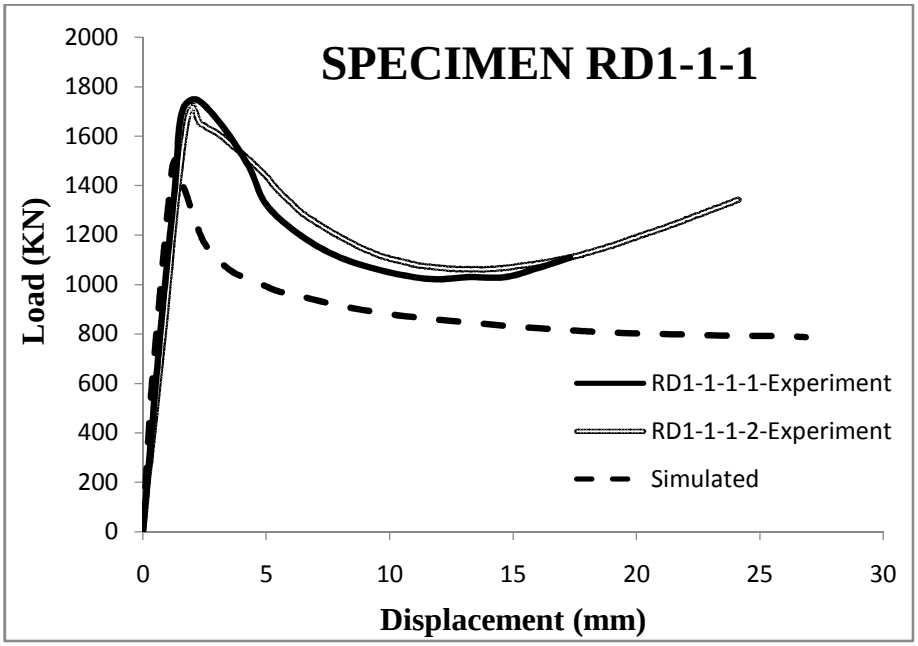

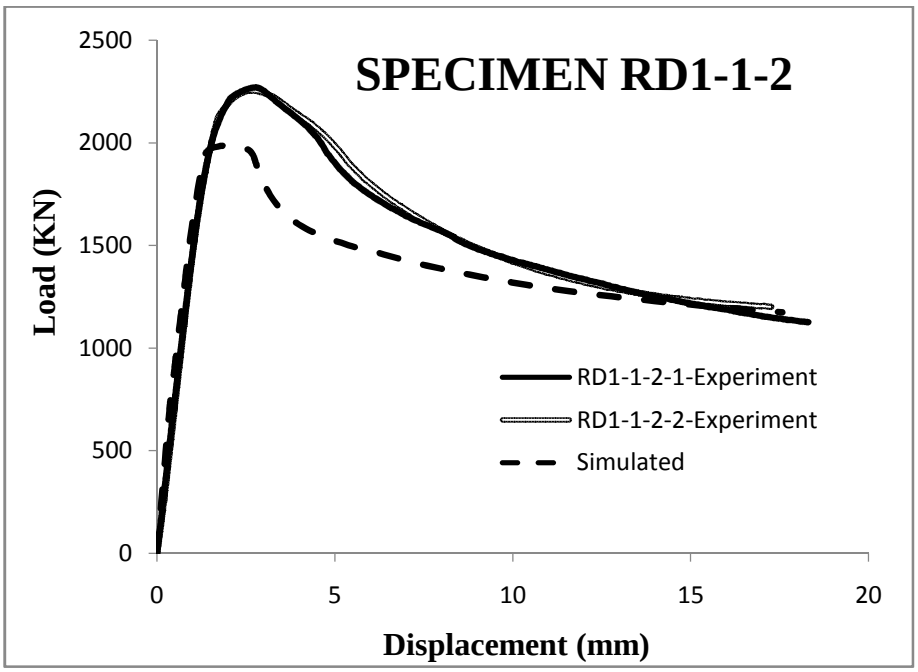

Figure 7.10(a) Comparison of experimental and numerical load-displacement curves for L6B 100 x 200 mm rectangular CFDST specimens

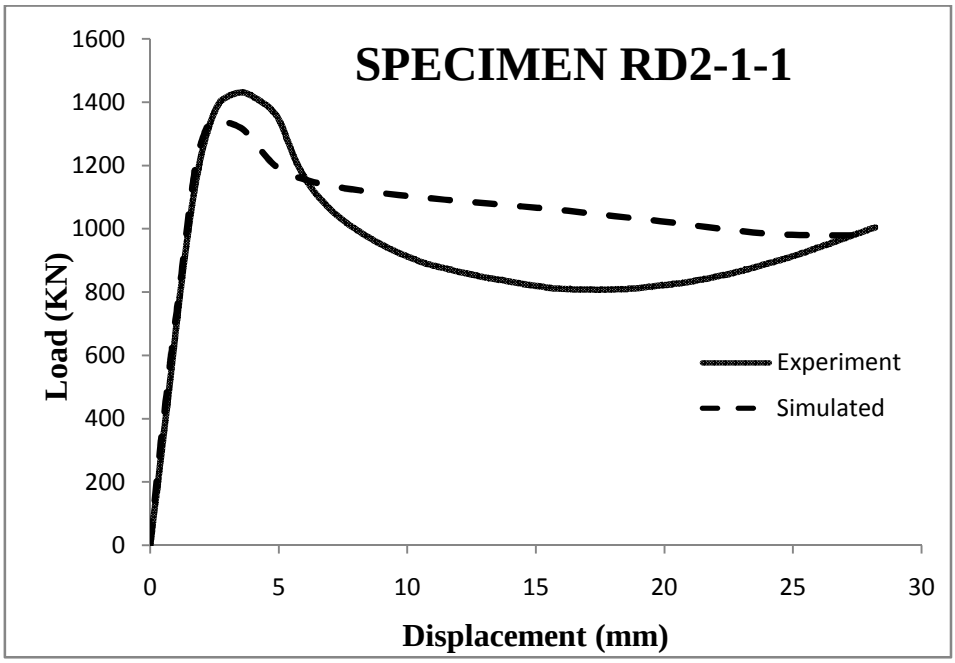

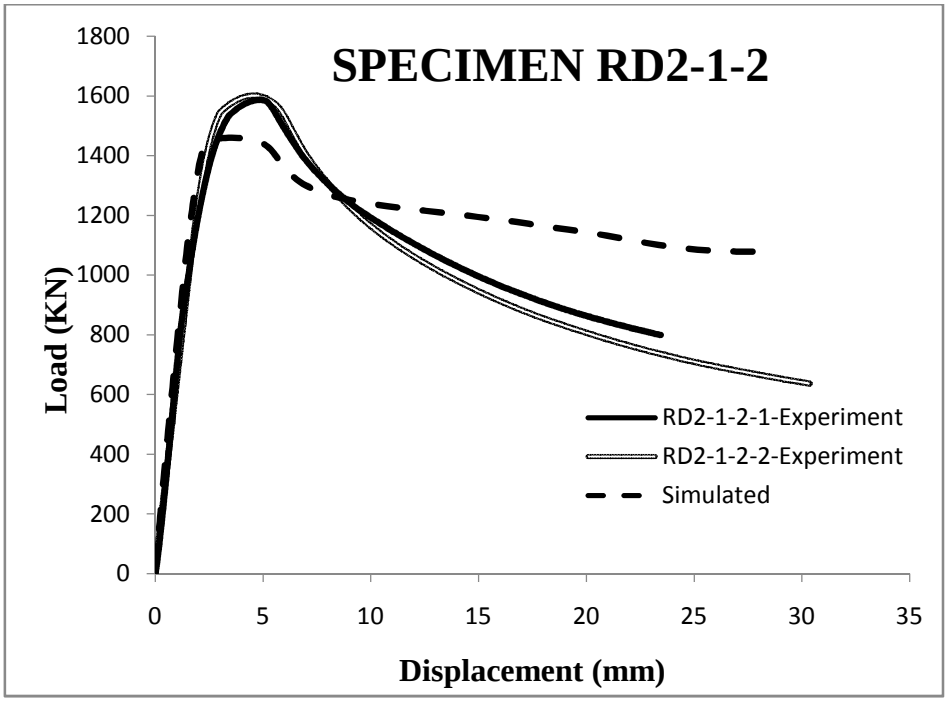

Figure 7.10(b) Comparison of experimental and numerical load-displacement curves for L10B 82 x 145 mm rectangular CFDST specimens

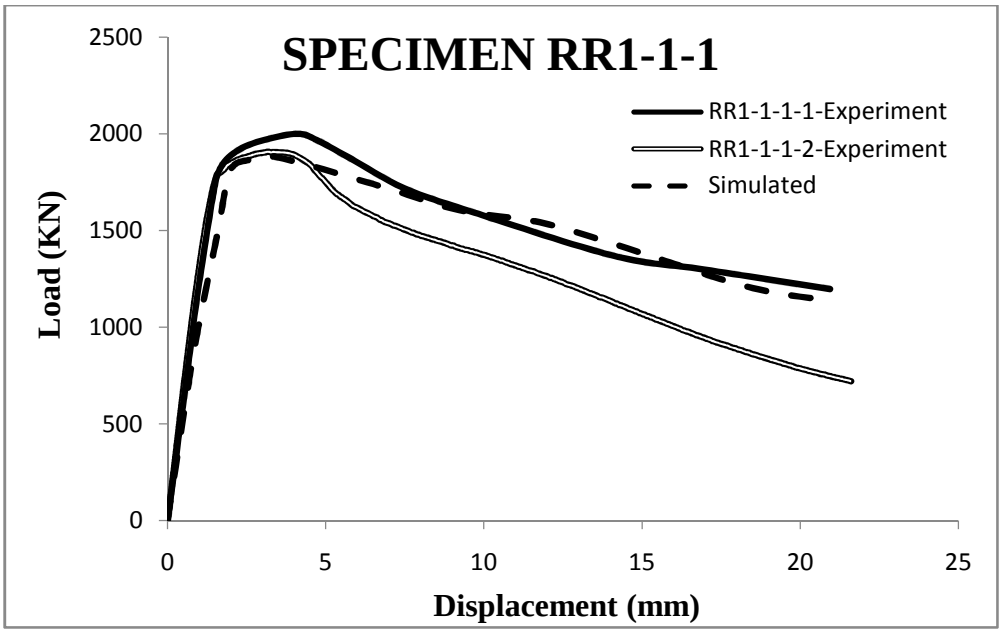

Figure 7.11(a) Comparison of experimental and numerical load-displacement curves for L6B 100 x 200 mm rectangular RCC-CFST specimens

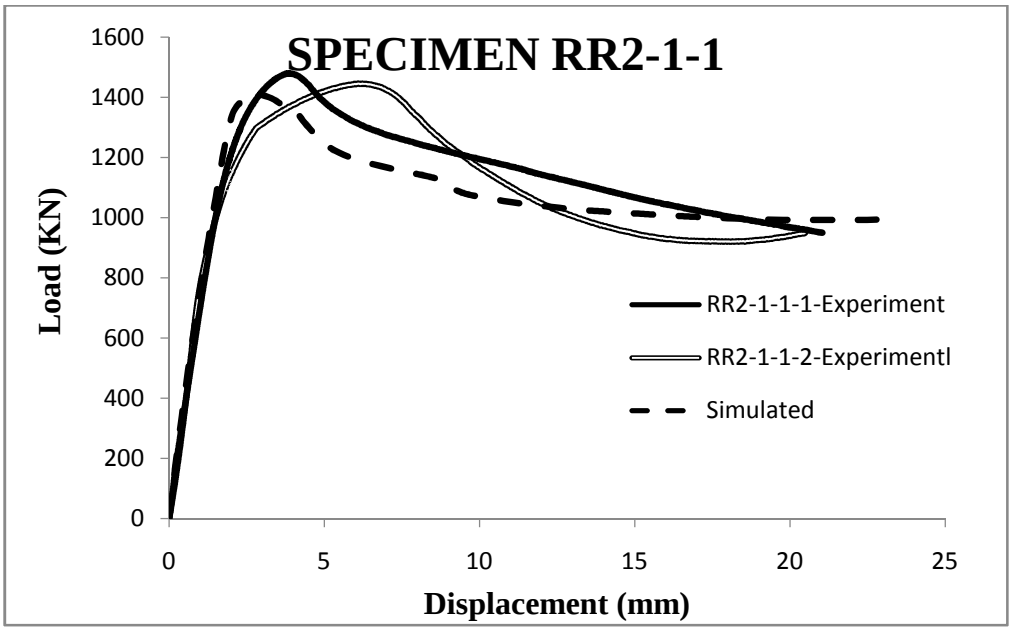

Figure 7.11(b) Comparison of experimental and numerical load-displacement curves for L10B 82 x 145 mm rectangular RCC-CFST specimens

Tables 7.5, 7.6 and 7.7 give the simulated nominal and ultimate load, experimental yield load and ultimate load and yield displacements for rectangular CFST, RCC-CFST and for CFDST. The nominal capacity (P_n), experimental yield load (P_y), strength index (SI), and ductility index (DI) were calculated as explained in Sections 5.3.2 and 5.3.3..

It can be concluded from Tables 7.5 to 7.7 that for specimens of same length category, strength index (SI) was highest for CFST specimens and lowest for CFDST specimens. Further, the SI decreased appreciably for all core configurations with increase in length. The trend of reduction of SI with length was lowest in case of CFDST specimens.

Table 7.5 Results of rectangular CFST specimens

Length Category	Specimen ID	P_n (KN)	Δ_y (mm)	P_y (KN)	P_{5y} (KN)	P_u (KN)		SI	DI
						Experiment	Simulated		
L6B	RS1-1-1	1438.96	1.99	1360.27	849.35	1555.16	1415.54	1.08	0.63
	RS1-1-2-1	1862.66	3.19	2016.75	1315.25	2109.35	1896.52	1.13	0.65
	RS1-1-2-2	1862.66	3.26	1753.23	1332.28	2080.92	1896.52	1.11	0.75
L7B	RS1-3-1-1	289.08	1.52	302.55	241.80	309.88	316.73	1.07	0.80
	RS1-3-1-2	289.08	1.52	311.62	261.56	325.36	316.73	1.13	0.84
L10B	RS2-1-1	1183.88	2.57	1246.70	3.92	1386.66	1194.03	1.17	0.69
	RS2-1-2-1	1255.43	3.43	1436.54	4.41	1451.64	1312.82	1.16	0.62
	RS2-1-2-2	1255.43	3.68	1401.91	4.06	1466.53	1312.82	1.17	0.63
	RS2-3-1-1	289.08	1.54	287.62	212.45	300.19	308.45	1.04	0.73
	RS2-3-1-2	289.08	1.85	266.55	213.87	298.04	308.45	1.03	0.81
L13B	RS3-3-1-1	289.08	1.78	288.32	165.76	288.32	302.34	1.00	0.58
	RS3-3-1-2	289.08	1.72	281.47	160.28	289.26	302.34	1.00	0.58
L16B	RS4-3-1-1	289.08	1.78	246.32	136.75	262.74	280.36	0.91	0.55
	RS4-3-1-2	289.08	1.83	244.66	146.10	276.05	280.36	0.95	0.57
L19B	RS5-3-1-1	289.08	1.91	265.31	129.85	281.87	271.86	0.98	0.49
	RS5-3-1-2	289.08	2.04	257.22	115.33	278.16	271.86	0.96	0.45
L22B	RS6-3-1-1	289.08	2.14	258.40	91.67	257.83	265.53	0.89	0.35
	RS6-3-1-2	289.08	1.80	239.32	81.40	254.32	265.53	0.88	0.34

Table 7.6 Results of rectangular CFDST specimens

Length Category	Specimen ID	P_n (KN)	Δ_y (mm)	P_y (KN)	P_{5y} (KN)	P_u (KN)		SI	DI
						Experiment	Simulated		
L6B	RD1-1-1-1	1788.06	2.81	1675.60	1005.48	1737.11	1505.54	0.89	0.60
	RD1-1-1-2	1788.06	2.9	1617.86	937.86	1718.47	1505.54	0.89	0.58
	RD1-1-2-1	2209.98	2.73	2269.12	1262.84	2270	1982.19	0.96	0.56
	RD1-1-2-2	2209.98	2.74	2253.87	1293.61	2254.49	1982.19	0.95	0.56
L10B	RD2-1-1	1336.56	3.89	1421.92	816.65	1430.26	1341.89	1.01	0.57
	RD2-1-2-1	1402.92	3.41	1533.29	858.48	1587.5	1459.88	1.07	0.56
	RD2-1-2-2	1410.21	3.26	1598.00	875.26	1598.53	1459.88	1.08	0.55

Table 7.7 Results of rectangular RCC-CFST specimens

Length Category	Specimen ID	P_n (KN)	Δ_y (mm)	P_y (KN)	P_{5y} (KN)	P_u (KN)		SI	DI
						Experiment	Simulated		
L6B	RR1-1-1-1	2042.44	2.70	1954.35	1397.65	2000.58	1886.54	0.98	0.71
	RR1-1-1-2	2042.44	2.62	1886.77	1194.00	1906.56	1886.54	0.93	0.64
L10B	RR2-1-1-1	1346.67	3.38	1458.67	1023.55	1479.18	1416.52	1.10	0.70
	RR2-1-1-2	1346.67	3.30	1332.17	924.83	1445.35	1416.52	1.07	0.70

7.3.3 Ductility and Post Yield Behaviour

Results of ductility index (DI) presented in Tables 7.5 to 7.7 show that all tested specimens exhibited strain softening behaviour. Further, the ductility index DI was maximum for CFST samples and lowest for CFDST samples, for a given length category. The DI decreased for all core configurations with increase in specimen length. Further, the CFDST specimens showed the lowest decrease in ductility with increase in length.

7.3.4 Length Effect

The results of specimens with 40 mm x 60 mm cross-section, tested for a wide range of length categories were studied to investigate the effect of length on load carrying capacity of CFST specimens. Effect of increase in length on SI is shown in Figure 7.12.

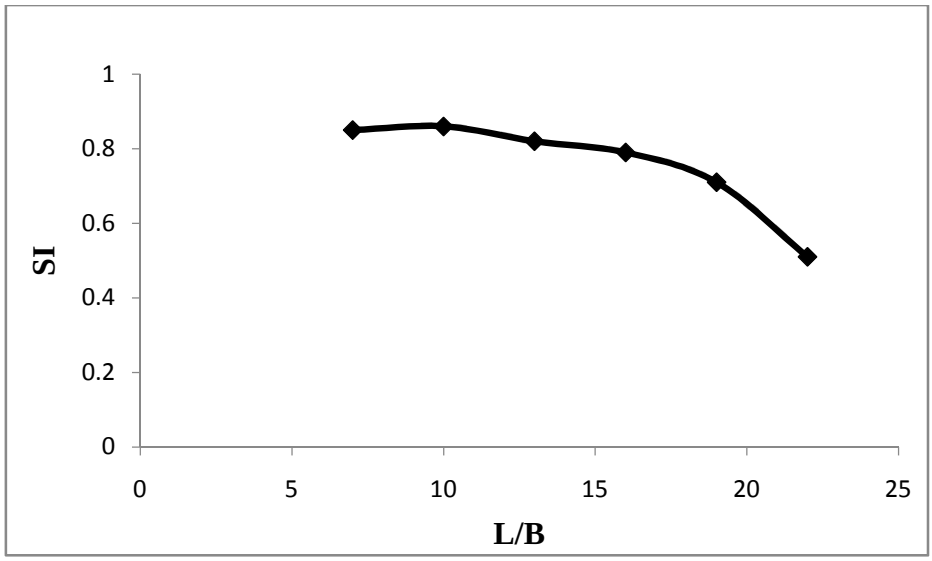

Figure 7.12 Effect of L/B ratio on Strength Index SI

It can be concluded from Figure 7.12 that the strength index of the CFST rectangular specimens decreases with increase in L/B.

The variation in ductility (DI) with L/B was plotted for 40 x 60 mm cross-sections, as shown in Figure 7.13. From the figure, it can be concluded that although the ductility reduces constantly with increase in length, the trend of reduction is accelerated beyond L/B=10.

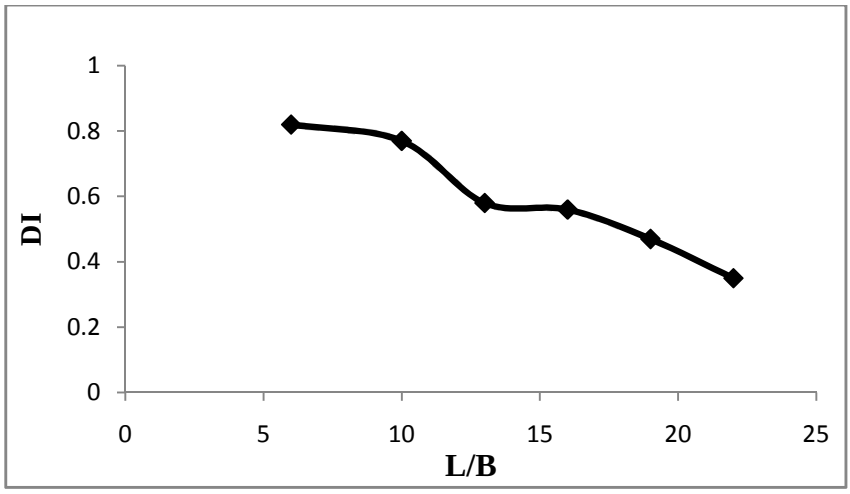

Figure 7.13 Effect of L/B ratio on Ductility Index DI

7.3.5 Equivalent Area of Steel

To study the effect of equivalent area of steel, specimens of L6B and L10B CFST and RCC-CFST were compared with each other (specimens of larger wall thickness of CFST were compared with smaller wall thickness and rebar samples of RCC-CFST). Details of specimens are listed in Table 7.8.The axial load was normalized with respect to nominal cross-sectional capacity of each specimen calculated using Equation 5.1. Figure 7.14 shows the normalized load-displacement curves for each specimen. It can be concluded from Table 7.8 that enhancement in strength of RCC-CFST was lower than that of CFST specimens. Such behaviour may be attributed to the fact that the rebars cannot provide same confining pressure provided by steel tube due to typically uniformly distributed area of steel in case of steel tube.

From Table 7.8, it can be seen that the ductility index for RCC-CFST specimens is slightly lower than that of corresponding CFST specimens for L6B columns. Further, the ductility was appreciably improved for RCC-CFST specimens as compared to CFST specimens for L10B specimens. Hence, it can be concluded that redistribution of area of steel in the form of rebars gives RCC-CFST with lower strength and comparable ductility.

Table 7.8 Comparison of rectangular specimens with equivalent area of steel but different core configurations

Specimen ID		L (mm)	B (mm)	D (mm)	t (mm)	f_y (MPa)	L/B	D/t	A_s (mm^2)	A_{sr} (mm^2)	SI	DI
L6B	**RS1-1-2-1**	**600**	**100**	**200**	**5.68**	**410**	**6.00**	**35.21**	**3279**	**0**	**1.16**	**0.65**
	RS1-1-2-2	**600**	**100**	**200**	**5.68**	**410**	**6.00**	**35.21**	**3279**	**0**	**1.17**	**0.75**
	RR1-1-1-1	600	100	200	3.80	401	6.00	52.63	2222	1118	0.98	0.71
	RR1-1-1-2	600	100	200	3.80	401	6.00	52.63	2222	1118	0.93	0.64
L10B	**RS2-1-2-1**	**900**	**82**	**145**	**5.15**	**424**	**10.98**	**28.16**	**2232**	**0**	**1.13**	**0.62**
	RS2-1-2-2	**900**	**82**	**145**	**5.15**	**424**	**10.98**	**28.16**	**2232**	**0**	**1.11**	**0.63**
	RR2-1-1-1	900	82	145	4.65	428	10.98	31.18	2025	314	1.10	0.70
	RR2-1-1-2	900	82	145	4.65	428	10.98	31.18	2025	314	1.07	0.70

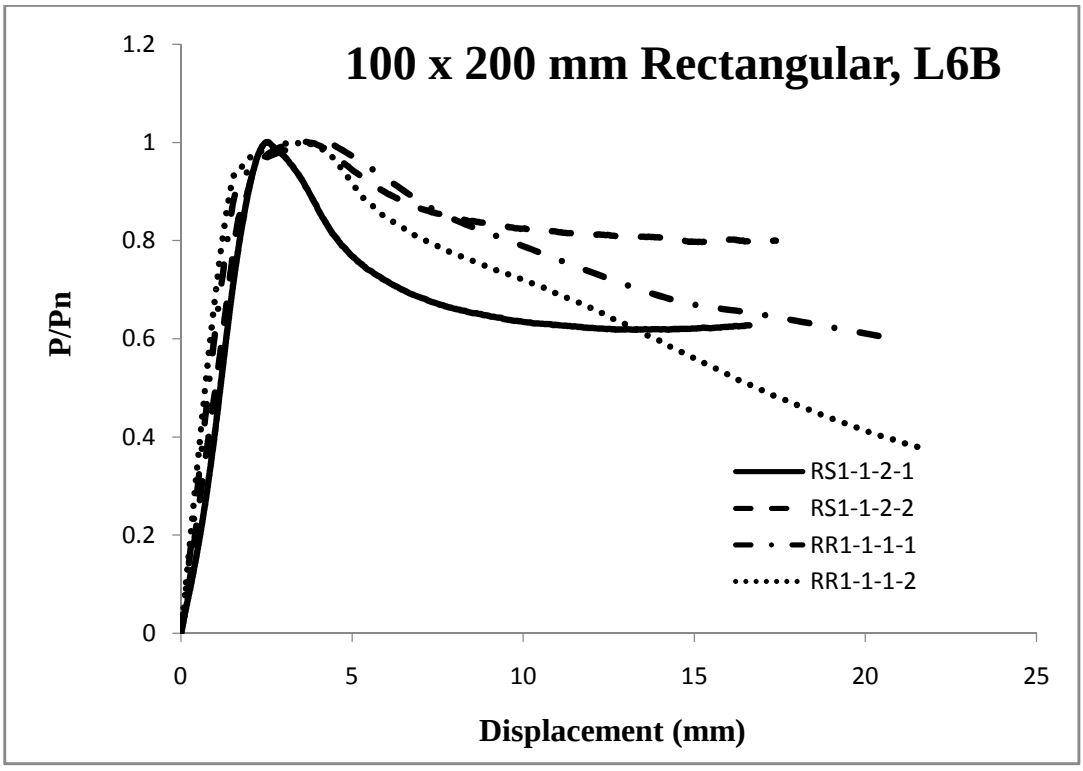

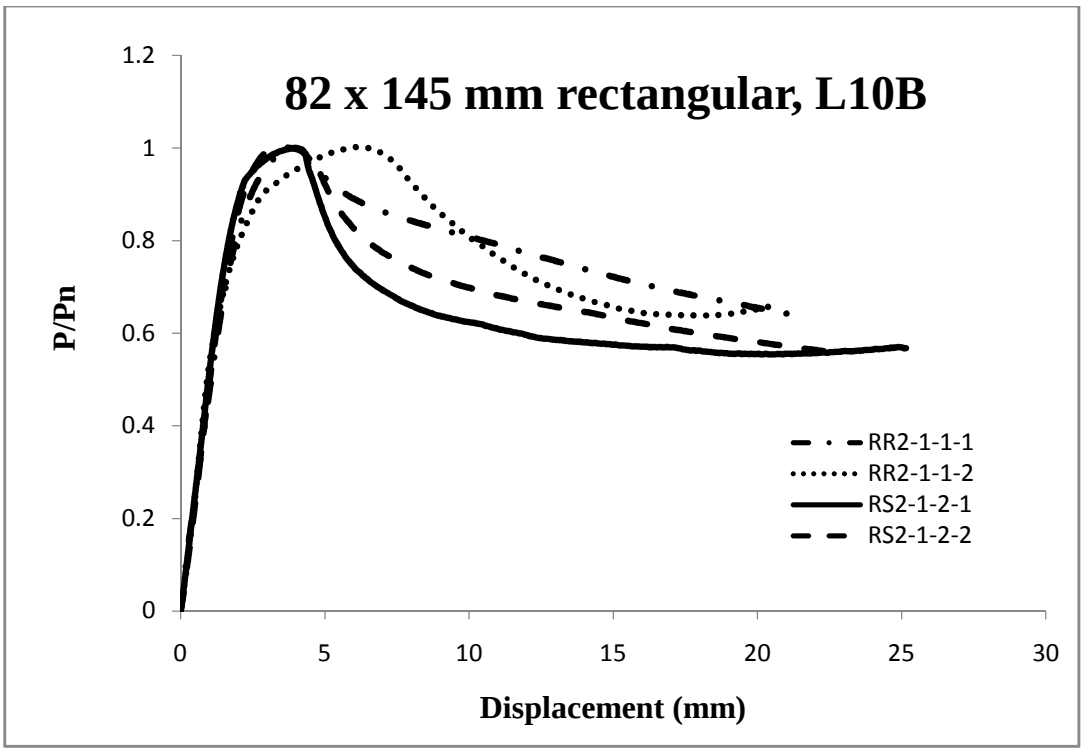

Figure 7.14 Comparison of load-displacement curves of rectangular CFST and RCC-CFST specimens

7.4 CODAL RECOMMENDATIONS

Equations from seven International Codes are used to predict the axial load capacity of the tested specimens. The obtained capacities are compared with the experimental strengths. The formulas and detailed procedures of these codes are given in various codes employed are given in Article 6.4.

The compared results of these codes are given in Table 7.5 .It can be observed that all codes, give conservative results with British Standard (BS) as the most conservative. It can also be concluded from Table 7.5 that the Chinese code CECS gives best estimations of the capacities with the ratio of (average of) all predicted to experimental capacities as 1.00. Some other codes like Eurocode (EC4) and GJB code also give a good idea of predicted load capacity.

Table 7.9 Results of seven International codes for predicting the capacities of experimental specimens

Length Category		Specimen ID	$P_{u\text{-}EC4}$ (kN)	$\frac{EC4}{EXP}$	$P_{u\text{-}AISC}$ (kN)	$\frac{AISC}{EXP}$	$P_{u\text{-}BS}$ (kN)	$\frac{BS}{EXP}$	$P_{u\text{-}CSA}$ (kN)	$\frac{CSA}{EXP}$	$P_{u\text{-}AIJ}$ (kN)	$\frac{AIJ}{EXP}$	$P_{u\text{-}CECS}$ (kN)	$\frac{CECS}{EXP}$	$P_{u\text{-}GJB}$ (kN)	$\frac{GJB}{EXP}$
RCFST	L6B	RS1-1-1	1460.0	0.94	1358.0	0.87	1166.0	0.75	1373.2	0.88	1396.6	0.90	1811.5	1.16	1525.8	0.98
		RS1-1-2-1	1879.4	0.89	1777.1	0.84	1577.7	0.75	1796.6	0.85	1819.9	0.86	2304.5	1.09	1923.6	0.91
		RS1-1-2-2	1879.4	0.90	1777.1	0.85	1577.7	0.76	1796.6	0.86	1819.9	0.87	2304.5	1.11	1923.6	0.92
	L7B	RS1-3-1-1	286.3	0.92	273.9	0.88	211.8	0.68	279.0	0.90	280.2	0.90	324.1	1.05	281.7	0.91
		RS1-3-1-2	286.3	0.88	273.9	0.84	211.8	0.65	279.0	0.86	280.2	0.86	324.1	1.00	281.7	0.87
	L10B	RS2-1-1	1182.2	0.85	1086.7	0.78	1000.8	0.72	1121.9	0.81	1121.4	0.81	1204.9	0.87	1202.6	0.87
		RS2-1-2-1	1255.4	0.86	1157.6	0.80	1072.9	0.74	1195.5	0.82	1194.4	0.82	1272.3	0.88	1260.2	0.87
		RS2-1-2-2	1255.4	0.86	1157.6	0.79	1072.9	0.73	1195.5	0.82	1194.4	0.81	1272.3	0.87	1260.2	0.86
		RS2-3-1-1	276.2	0.92	267.3	0.89	208.7	0.70	276.7	0.92	275.6	0.92	293.7	0.98	281.7	0.94
		RS2-3-1-2	276.2	0.93	267.3	0.90	208.7	0.70	276.7	0.93	275.6	0.92	293.7	0.99	281.7	0.95
	L13B	RS3-3-1-1	265.5	0.92	259.4	0.90	205.2	0.71	272.1	0.94	271.5	0.94	271.0	0.94	281.7	0.98
		RS3-3-1-2	265.5	0.92	259.4	0.90	205.2	0.71	272.1	0.94	271.5	0.94	271.0	0.94	281.7	0.97
	L16B	RS4-3-1-1	264.4	1.01	249.8	0.95	225.2	0.86	264.4	1.01	270.6	1.03	252.1	0.96	281.7	1.07
		RS4-3-1-2	264.4	0.96	249.8	0.90	225.2	0.82	264.4	0.96	270.6	0.98	252.1	0.91	281.7	1.02
	L19B	RS5-3-1-1	250.7	0.89	238.7	0.85	218.7	0.78	253.3	0.90	270.6	0.96	235.5	0.84	281.7	1.00
		RS5-3-1-2	250.7	0.90	238.7	0.86	218.7	0.79	253.3	0.91	270.6	0.97	235.5	0.85	281.7	1.01
	L22B	RS5-3-1-1	239.4	0.93	226.4	0.88	210.4	0.82	238.8	0.93	270.6	1.05	220.6	0.86	281.7	1.09
		RS5-3-1-2	239.4	0.94	226.4	0.89	210.4	0.83	238.8	0.94	270.6	1.06	220.6	0.87	281.7	1.11
RCC-RCFST	L6B	RR1-1-1-1	2074.4	1.04	1670.8	0.84	1701.5	0.85	1984.8	0.99	2003.6	1.00	2538.3	1.27	2074.2	1.04
		RR1-1-1-2	2074.4	1.09	1670.8	0.88	1701.5	0.89	1984.8	1.04	2003.6	1.05	2538.3	1.33	2074.2	1.09
	L10B	RR2-1-1-1	1371.4	0.93	1219.0	0.82	1151.0	0.78	1362.1	0.92	1294.6	0.88	1368.2	0.92	1332.3	0.90
		RR2-1-1-2	1371.4	0.95	1219.0	0.84	1151.0	0.80	1362.1	0.94	1294.6	0.90	1368.2	0.95	1332.3	0.92
RCFDST	L6B	RD1-1-1-1	1622.3	0.93	1697.0	0.98	1532.1	0.88	1719.2	0.99	1737.9	1.00	1973.6	1.14	1777.3	1.02
		RD1-1-1-2	1622.3	0.94	1697.0	0.99	1532.1	0.89	1719.2	1.00	1737.9	1.01	1973.6	1.15	1777.3	1.03
		RD1-1-2-1	2041.9	0.90	2115.8	0.93	1943.5	0.86	2144.1	0.94	2161.0	0.95	2428.4	1.07	2010.6	0.89
		RD1-1-2-2	2041.9	0.91	2115.8	0.94	1943.5	0.86	2144.1	0.95	2161.0	0.96	2428.4	1.08	2010.6	0.89
	L10B	RD2-1-1	1285.5	0.90	1236.6	0.86	1199.6	0.84	1283.5	0.90	1301.8	0.91	1273.6	0.89	1227.6	0.86
		RD2-1-2-1	1358.7	0.86	1307.7	0.82	1264.5	0.80	1357.6	0.86	1380.1	0.87	1337.1	0.84	1247.2	0.79
		RD2-1-2-2	1358.7	0.85	1307.7	0.82	1264.5	0.79	1357.6	0.85	1380.1	0.86	1337.1	0.84	1247.2	0.78
Average				0.92		0.87		0.78		0.92		0.93		0.99		0.95
Standard Deviation				0.05		0.05		0.07		0.06		0.06		0.13		0.09

7.5 CONCLUSIONS

Based on the experimental and numerical results, following conclusions can be drawn:

Mode of deformation

a. The failure mode in L6B specimens was observed to be crushing of concrete followed by local buckling of steel tube for all core configurations (Figures 7.2, 7.5 and 7.7).

b. CFST core configuration specimens of smaller cross-sections (40 x 60 mm) failed generally by global buckling (Figure 7.3)

c. RCC-CFST and CFST core configurations of L10B length category failed by local buckling near the top of the specimen. On the other hand, CFDST specimens failed showed a mixed failure mode of global and local buckling (Figures 7.4, 7.6 and 7.8).

Strength

a. Increase in strength was generally observed for L6B, L7B and L10B specimens with all core configurations. However, L6B CFDST and RCC-CFST specimens showed slightly reduced strength (Tables 7.6 and 7.7).

b. For categories beyond L10B, CFST specimens showed decrease in load carrying capacity with increase in length (Table 7.5).

c. Among all three core configurations, the highest enhancement in load carrying capacity was observed in CFST specimens in load carrying capacity. The lowest increase in load capacity was seen for CFDST specimens (Tables 7.5 to 7.7).

Ductility

a. All tested specimens showed strain softening behaviour (Tables 7.5 to 7.7).

b. For higher cross-sectional sizes, the ductility index (DI) was lowest for CFDST specimens and almost same for CFST and RCC-CFST specimens for specimens of lower lengths, and higher for RCC-CFST specimens of longer lengths (Tables 7.5 to 7.7).

Length effect

a. For CFST specimens, the strength index was found to decrease with increase in L/B ratio (Figure 7.12).

b. The ductility index was found to decrease with increase in length of the specimens. However, the specimens beyond L/B=10 showed marked decrease in ductility with increase in length (Figure 7.13).

Equivalent area of steel

a. The partial replacement of area of steel tube with longitudinal rebars was observed to give composite columns with slightly reduced strength and comparable ductility (Table 7.8).

b. Enhancement in strength of RCC-CFST was slightly lower than that of CFST specimens (Table 7.8).

c. For L6B specimens, ductility index (DI) was almost same in CFST columns and corresponding RCC-CFST specimens, whereas DI was significantly enhanced for L10B specimens with RCC-CFST core configuration as compared to CFST specimens.

Codal recommendations

a. Chinese code (CECS) gives best estimations of the capacities with average of capacities of all specimens as 0.99 multiplied by the average of all tested capacity (Table 7.9).

b. All the other codes gave conservative predictions, with British Standards (BS) being the most conservative (Table 7.9).

CHAPTER EIGHT

CONCLUSIONS

8.1 GENERAL

The results from the various experimental and numerical studies have already been detailed at the end of respective chapters. In this chapter, the conclusions for the various cross-sectional shapes and core configurations are compared with each other, and presented in a combined form for completeness.

8.2 CONCRETE FILLED STEEL TUBULAR (CFST) COLUMNS

8.2.1 Mode of Deformation

a. The primary mode of deformation of short circular, short square, and intermediate rectangular columns of large cross-sectional sizes (100 x 200 mm and 82 x 145 mm) was local buckling of steel tube accompanied by crushing of adjoining concrete for all core configurations (Figures 5.2, 5.4, 5.5, 5.7, 6.2, 6.4, 6.6 and Figures 7.2 to 7.8).

b. For all cross sectional shapes and core configurations, it was noted that debonding occurred between steel tube and concrete core at the location of local buckling of the tube, thereby indicating a loss of confining pressure at that location.

c. For short circular specimens, local buckling was initiated by the buckling of steel tube followed by the crushing of concrete core near the mid height and extending to the end s of the specimen.

d. For square and rectangular specimens, local buckling was initiated by crushing of concrete core followed by yielding of steel tube. The local buckling of rectangular specimens was always started first at the centre of wider side and extended to the corners of the tube.

e. CFDST specimens of all cross-sections failed outward buckling of outer steel tube accompanied by the inner local buckling of the inner steel tube.

f. For RCC-CFST specimens, the local buckling was initiated, close to the mid height near the location of ties. The longitudinal reinforcement bars generally buckled in the central region between the two ties (Figure 5.9(b)).

g. The mode of deformation was observed to vary with the length as well as the cross-sectional size of the specimen. Local buckling (or sometimes a combination of local and global buckling) was the mode of failure even in intermediate columns for square and rectangular columns (Figures 6.3, 6.5, 6.7, 7.4, 7.6 and 7.8). The intermediate circular composite columns and rectangular columns of small cross-sectional sizes (40 x 60 mm), however, failed predominantly be global buckling initiated at the mid height of the specimens for all core configurations (Figures 5.3, 5.6, 5.8, 7.3).

8.2.2 Strength

a. Increase in strength as compared to the nominal compressive squash load was reported for all the specimens due to composite action between steel and concrete. The specimens with smaller tube thickness generally showed smaller increase in capacity.

b. RCC-CFST specimens showed the highest improvement in strength in case of circular specimens (Figure 5.13). On the other hand, CFST single skin columns showed the maximum enhancement in case of square and rectangular specimens (Tables 6.5 and 7.5).

c. The increase in strength due to confinement was always lower for CFDST specimens as compared to CFST and RCC-CFST specimens for all cross-sectional shapes (Tables 5.5 to 5.7, 6.5 to 6.7 and 7.5 to 7.7).

d. Rectangular specimens showed enhanced strength for intermediate category specimens, whereas long specimens showed axial capacities lesser than the nominal capacities (Table 7.5)

e. The increase in strength was observed to decrease significantly with decrease in thickness of outer steel tube. However, the highest reduction in enhancement due to increase in thickness was observed in circular specimens.

8.2.3 Ductility

a. Nearly all the circular specimens showed strain hardening behaviour (DI>1, Table 5.5-5.7), whereas all tested square and rectangular specimens showed strain softening behaviour (DI<1, Tables 6.5-6.7 and 7.5-7.7).

b. Highest ductility in circular specimens was observed in CFST core configuration, whereas RCC-CFST core configuration showed the maximum ductility in case of square and rectangular specimens for specimens of higher lengths. For square and rectangular specimens of lower lengths, RCC-CFST and CFST specimens showed comparable ductility.

c. The ductility of CFDST specimens was observed to be lowest as compared to that of other core configurations (i.e. CFST and RCC-CFST) (Tables 5.5-5.7, 6.5-6.7 and 7.5-7.7).

8.2.4 Length effect

a. A drop in strength and ductility with increase in length for all tested specimens. The reduction was greater in specimens with greater wall thickness of the steel tube.

b. RCC-CFST specimens showed the lowest reduction in axial load due to increase in length among all the tested specimens.

8.2.5. Equivalent area of steel

a. A comparison of experimental results for CFST and RCC-CFST specimens for circular columns showed that the replacement of higher wall thickness of steel tube partially with rebars was justified from the viewpoints of strength and ductility. The enhancement in strength and strength generally decreased with the increase in area replaced. However, the columns still maintained their strain hardening behaviour (Table 5.9).

b. For square and rectangular specimens, decrease in strength index was observed after replacement of steel tube with reinforcing bars for all length categories. However, the ductility was generally of RCC-CFST specimens was generally higher than (or equal to) that of base CFST specimens (Tables 6.8 and 7.8)

8.2.6 Codal Recommendations

Codal recommendations available in ACI 318 (2008), ANSI/AISC 360 (2010), British Standard 5400 (BS 5400, 2005), Canadian Standard S016 (CSA) (S016, 2001), two Chinese Standards; CECS 28 (1990) (Zhang et al., 2007) and GJB and DL/T 4142 (2000) (Han, 2002). Euro Code 4 (EC4) (EN 1994, 2004) and Japanese Standard AIJ (2001) (Morino and Tsuda, 2003) of different countries are used to predict the load carrying capacities of different tested specimens. The main conclusions are summarized here:

a. Recommendations from all the codes generally gave conservative results for the load capacity of composite columns, with the British Standards (BS 5400,2005) being the most conservative of all (Tabels 5.10, 6.9 and 7.9).

b. Chinese code (CECS) and Canadian code CSA gave the best prediction of the load capacity of the circular specimens, with the average ratio (of all tested specimens) of codal to experimental values being 0.98 (Table 5.9).

c. Chinese code (GJB) gave the best estimate for load capacity of square columns, with 6 % conservative estimate (average of all specimens) as compared to experimental values. The next best estimate was given by EC4 (Table 6.8). For rectangular specimens, Chinese code (CECS) gave the closest prediction for the load capacities of the composite columns (Table 7.8).

8.2.7 Study of confinement pressure

The proposed numerical model was used to study the confining pressure provided by the steel tube to concrete core for 114.3 mm outer diameter circular columns of all core configurations. The variation of confinement pressure along the length and circumference of the specimen was studied and graphically presented. The following conclusions can be drawn from this study

a. The confining pressure values at the end regions of the CFT section are unusually high due to the end restraint applied by machine platens. In the region of the sample away from the machine platens, the confining pressure is almost constant for CFST i.e. Single Skin

Specimens. However, in CFDST columns, there is appreciable variation in confining pressure even in this middle region.

b. For RCC-CFST specimens, large jump in values of confining pressure was observed near the region of lateral ties (which is also the location of local buckling of steel tube). Further, the region between the ties was seen to give relatively much lower values of confining pressure (Figure 5.27).

c. The confinement pressure values obtained from the numerical model have been compared with the corresponding values from theoretical models from literature. It is observed that the theoretical models generally overestimate the value of confining pressure for specimens of higher length (Tables 5.11 and 5.12).

8.2.8 Digital Image Correlation

A new technique named Digital Image Correlation was used to get the in-situ strain distribution of a typical circular specimen during the actual experimental test. The specimen was CFST single skin intermediate column of 90 mm outer diameter. The images recorded from the apparatus at periodic intervals were calibrated to give material strains and the results compared with proposed numerical model. The results from numerical model were found in acceptable agreement with DIC results (Figure 5.37 and 5.39). More specimens of different lengths and cross-sections may be tested to better understand the deformation mechanics of composite tubular columns.

8.3 MAJOR CONTRIBUTIONS

8.3.1. Experimental study on Concrete Filled Steet Tubular (CFST) columns

A total of 81 specimens were tested in experimental study to study the behaviour of tubular columns of different cross-sectional shapes (circular, square and rectangular) and core configurations. Three core configurations namely, Concrete filled single steel tube (CFST), Concrete filled double steel tube (CFDST) and Reinforced concrete filled steel tube (RCC-CFST) was studied. The effect of different wall thickness of steel tube (t) and increase in length of specimen on the behaviour was studied and presented. The study generated a large database of varied experimental data for the research community.

8.3.2 Modeling and Numerical Simulations

A three-dimensional nonlinear Finite Element model for simulating the behaviour of circular, square and rectangular Concrete Filled Steel Tube (CFST) columns is presented in this chapter. An effort was made to provide a detailed procedure for Finite Element modelling and simulations of such columns using commercial software package ABAQUS 6.8. Composite action is modeled between concrete core and steel tube. Suitable constitutive models were used for simulating the behaviour of concrete in confinement. The proposed model was then verified by comparing its numerical results with selected experimental results available in literature.

The proposed model was then extended to widen its applicability to tubular columns of different lengths and core configurations. The aforementioned eighty one experimentally tested specimens (across different core configurations and lengths) were tested and results compared with experimental counterparts. In general, the numerical model was found to predict the deformed shapes and load deflection behavior of various core configurations with acceptable accuracy.

A pilot study of the confining pressure experienced by the concrete core was performed. The confining pressure was studied along the height and cross-sectional circumference of the specimen for various core configurations in circular samples. The results from the numerical model were compared with results of confining pressure from theoretical models proposed in literature. Using a new method of Digital Image Correlation, the experimental strain distribution of a typical circular intermediate length specimen was also obtained and compared with values from the ABAQUS model

8.4 FUTURE SCOPE

The following areas may be of interest to future researchers in this field:

1. The numerical study of confinement pressure in CFST is still at a very preliminary stage. Cross-sections of different shapes, sizes and core configurations may be analyzed by this method. The results from such models can be compared with the results from new apparatus like DIC. Suitable constitutive models may be proposed for confined concrete based on such studies.

2. The effect in reduction of thickness of steel tube in actual structures on account of corrosion on may be explored in future experimental studies. Attempts can also be made to integrate this behaviour in future analytical and numerical model.

3. The behaviour of beam-column and column-footing connections in field is still largely untouched.

4. Refinement of confined concrete model for modelling square and rectangular specimens filled with high strength concretes.

5. More investigations may be performed for new core configurations like CFDST and RCC-CFST members under various loading conditions such as

    - Composite members in eccentric loading (uniaxial and biaxial)
    - Composite loaded in pure bending
    - Composite loaded in cyclic loading

6. The behaviour of CFST members under extreme environments such as in Fire, seawater corrosion etc. may be explored.

LIST OF REFERENCES

[1] Abedi, K., Ferdousi, A., and Afshin, H. (2008). A novel steel section for concrete-filled tubular columns. Thin Walled Structures, 46(3), pp.310-319.

[2] Agrawal, S.K. (2003). Seismic Resistant Design and Construction. IGC-2003, Roorkee.

[3] Agrawal, Shailesh Kr., and Chourasia, Ajay. (2005). Experimental Investigation of Seismic Strengthening and Retrofitting Measures of RC Multistoried Buildings. Intl. Conf. on Advances in Concrete Composites and Structures, Structural Engineering Research Centre, Chennai.

[4] Alhozaimy, A., AL-Negheimish, A., Alawad, O. A., Jaafar, M. S., and Noorzaei, J. (2012-a). Binary and ternary effects of ground dune sand and blast furnace slag on the compressive strength of mortar. Cement and Concrete Composites, 34(6), pp.734–738.

[5] Alhozaimy, A., Jaafar, M. S., Al-Negheimish, A., Abdullah, A., Taufiq-Yap, Y. H., and Noorzaei, J. (2012-b). Properties of high strength concrete using white and dune sands under normal and autoclaved curing. Construction and Building Materials, 27(1), pp.218–222.

[6] ANSI/AISC:360-10. (2010). Specification for Structural Steel Buildings. American Institute of Steel Construction.

[7] ASTM E8/E8M-11. (2011). Standard Test Methods for Tension Testing of Metallic Materials. American Society for Testing and Materials.

[8] Baidya, N., Zhang, L., Mendis, P. A., and Fragomeni , S. (2012). Effect of construction sequence in the axial shortening behaviour of composite columns. From Materials to Structures: Advancement through Innovation (pp. 55 - 59). Sydney, Australia: Taylor and Francis Ltd., London Group.

[9] Balendra, T. (1983). A simplified model for lateral load analysis of asymmetrical buildings. Engineering Structures, 5(3), pp. 154-162.

[10] Bangash, M. Y. (2001). Manual of numerical methods in concrete: modelling and applications validated by experimental and site-monitoring data. London: Thomas Telford.

[11] Borsaikia, A., Talukdar, S., and Dutta, A. (2006). Study of modal parameters and vibration signatures of notched concrete prisms. Cement and Concrete Research, 36(3), pp 592 – 598.

[12] Bradford, M. A., Loh, H. Y., and Uy, B. (2002). Slenderness limits for filled circular steel tubes. Journal of constructional Steel Reserch, 58(2), pp 243-252.

[13] BS 5400. (2005). Steel, Concrete and Composite Bridges-Part 5: Code of Practice for the Design of Composite Bridges. British Standard Institute.

[14] Canadian Standard S016. (2001). Limit State Design of Steel Structures.

[15] Chakrabarti, A., Sheikh, A. H., Griffith, M., and Oehlers, D. J. (2013-a). Dynamic Response of composite beams with partial shear interactions using a higher order beam theory. Journal of Structural Engineering, ASCE, 139(1), pp 47-56.

[16] Chakrabarti, A., Sheikh, A. H., Griffith, M., and Oehlers, D. J. (2012-a). Analysis of composite beams with longitudinal and transverse partial interactions using higher order beam theory. International Journal of Mechanical Sciences, 59(1), pp 115-125.

[17] Chakrabarti, A., Sheikh, A. H., Griffith, M., and Oehlers, D. J. (2012-b). Analysis of composite beams with partial shear interaction using a higher order beam theory. Engineering Structures, 36(1), pp 283-291.

[18] Chakrabarti, A., Sheikh, A. H., Griffith, M., and Oehlers, D. J. (2013-b). Vibration and Buckling of composite beams with partial shear interactionsusing a higher order beam theory. International Journal of Structural and Civil Engineering Research, 1(2), pp 24-42.

[19] Chen, B.-C., and Wang, T.-L. (2009). Overview of concrete filled steel tube arch bridges in China. Practice Periodical on Structural Design and Construction-ASCE, 14(2), pp 70-80.

[20] Choubey, A., Sehgal, D.K., and Tandon, N. (2006). Finite element analysis of vessels to study changes in natural frequencies due to cracks. International Journal of Pressure Vessels and Piping, 83(3), pp.181-187.

[21] Chung, J., and Matsui, C. (2005). SRC Standards in Japan and Comparison of Various Standards for CFT Columns. Steel Structures 5, pp. 315-323.

[22] Dai, X., and Lam, D. (2010). Numerical modelling of the axial compressive behaviour of short concrete-filled elliptical steel columns. Jounal of Constructional Steel Research, 66, pp 931-942.

[23] Diapos ESDEP Anglais, Slides: Titles and Commentary, online paper http://www.systemx.fr/meca/cm/ESDEP/ Diapos ESDEP Anglais

[24] El chalakani, M., Zhao, X.-L., and Grzebieta, R. (2002). Tests on concrete filled double-skin (CHS outer and SHS inner) composite short columns under axial compression. Thin-Walled Structures, 40(5), pp 415-441.

[25] Ellobody, E., Young, B., and Lam, D. (2006). Behaviour of normal and high strength concrete-filled compact steel tube circular stub columns. Journal of Constructional Steel Research, 62(7), pp 706-715.

[26] Ellobody, E., and Young, B. (2006). Nonlinear analysis of concrete-filled steel SHS and RHS columns. Thin-Walled Structures, 44(8), pp. 919-930.

[27] EN 1994. (2004). Eurocode 4: Design of composite steel and concrete structures, Part 1-1: General Rules and Rules for Buildings. European Standard.

[28] Endo, T., Shioi, Y., Hasegawa, A., and Wang, H. J. (2000). Experimental study on reinforced concrete filled steel tubular structures. 25th Conference on Our World in Concrete and Structures, (pp. 279-286). Singapore.

[29] Furlong, R. W. (1967). Strength of steel-encased concrete beam columns. Journal of the Structural Division-Proceedings of American Society of Civil Engineers, 93(ST5), pp.113-124.

[30] Furlong, R. W. (1968). Design of steel-encased concrete beam-columns. Journal of the Structural Division-Proceeding of the American Society of Civil Engineers, 94(ST1), pp.267-281.

[31] Ganesan, N., Indira, P. V., and Santhosh Kumar, P. T. (2006-b). Ultimate Strength of Steel Fibre Reinforced Self Compacting Concrete Flexural Elements. The Indian Concrete Journal, 80(12), pp.8-15.

[32] Ganesan, N., Indira, P. V., and Santhosh Kumar, P. T. (2006-a). Durability aspects of Steel Fibre Reinforced SCC. The Indian Concrete Journal, 80(5), pp.31-37.

[33] Ganesh, N., Indira, P. V., and Prasad, S. R. (2010). Structural Behaviour of Steel Fibre Reinforced Concrete Wall Panels in Two-way In-plane Action. The Indian Concrete Journal, 84(10), pp.21-28.

[34] Gao, X. Y., Balendra, T., and Koh, C. G. (2013). Buckling strength of slender circular tubular steel braces strengthened by CFRP. Engineering Structures, 46(January), pp.547–556.

[35] Gardner, J., and Jacobson, R. (1967). Structural behavior of concrete filled steel tubes. ACI Journal, 64(7), pp.404-413.

[36] Ge, H., and Usami, T. (1992). Strength of concrete filled thin-walled steel box columns: Experiment. Journal of Structural Engineering, ASCE, 118(11), pp.3036-3054.

[37] Giakoumelis, G., and Lam, D. (2004). Axial capacity of circular concrete-filled tube columns. Journal of Constructional Steel Research, 60(7), pp.1049-1068.

[38] Gourley, B. C., Tort, C., Denavit, M. D., Schiller, P. H., and Hajjar, J. F. (2008). A Synopsis of Studies of the Monotonic and Cyclic Behavior of Concrete-Filled Steel Tube Members, Connections, and Frames. University of Illinois at Urbana, Department of Civil and Environmental Engineering. Champaign: NSEL.

[39] Gupta, P. K., Khaudhair, Ziyad. A., and Ahuja, A. K. (2014-a). Modeling, verifications, and investigation on behaviour of circular CFST columns. Structural Concrete, Paper in Press.

[40] Gupta, P. K., Sarda, S., and Kumar, M. (2007). Experimental and computational study of concrete filled steel tubular columns under axial loads. Journal of Constructional Steel Research, 63(2), pp.182–193.

[41] Han, L. H. (2002). Tests on stub columns of concrete-filled RHS sections. Journal of Constructional Steel Research, 58(3), pp.353-372.

[42] Hasegawa, A., and Xiamuxi, A. (2011). Experimental Study on RCFT Columns Using High Strength Concrete and Thin Steel Tube. The 2011 World Congress on Advances in Structural Engineering and Mechanics, (pp. 175-180). Seoul, Korea.

[43] Hatzigeorgiou, G. D. (2008). Numerical model for the behavior and capacity of circular CFT columns, Part I: Theory. Engineering Structures, 30(6), pp.1573-1578.

[44] Hicks, S. J., Newman, G. M., Edwards, M., and Ba, O. A. (2002). Design guide for SHS concrete filled columns, structural and conveyance business. Corus Tubes Company.

[45] Hu, H., Huang, C., Wu, M., and Wu, Y. M. (2003). Nonlinear Analysis of Axially loaded Concrete-Filled Tube Columns with Confinement Effect. Journal of Structural Engineering, 129(10), pp.1322-1329.

[46] Hu, H.-T., and Schnobrich, W. C. (1988). Nonlinear analysis of plain stress state reinforced concrete under short term monotonic loading. Structural Research Series, University of Illinois, Civil Engineering Studies.

[47] Hu, H.-T., and Schnobrich, W. C. (1989). Constitutive modeling of concrete by using nonassociated plasticity. Journal of Material in Civil Engineering-ASCE, 1(4), pp.199-216.

[48] Hu, H.-T., and Su, F.-C. (2011). Nolnlinear analysis of short concrete-filled double skin tube columns subjected to axial compressive forces. Marine Structures, 24(4), pp.319-337.

[49] Huang, C., Yeh, Y., Liu, G., Hu, H. T., Tsai, K., Weng, Y., et al. (2002). Axial Load Behavior of Stiffened Concrete-Filled Steel Columns. Journal of Structural Engineering,ASCE, 128(9), pp.1222-1230.

[50] Jaafar, M. S., Thanoon, W. A., Khan, S. R., and Trikha, D. (2002). Strength estimation of concrete in different environments using UPV. Pertanika Journal of Science and Technology, 10(2), pp.179 - 186.

[51] Johansson, M. (2002). The efficiency of passive confinement in CFT columns. Steel and Composite Structures, 2(5), pp.379-369.

[52] Kaustubh Dasgupta, Murty, C.V.R., and Agrawal, S.K. (2003). Seismic Shear Design of RC Structural Walls-Part-I, Review of Code Provisions. Indian Concrete Journal, 77(11), pp. 1423-1430.

[53] Knowles , R. B., and Park, R. (1969). Strength of concrete filled steel tubular columns. Journal of the structural division, Proceedings of the American Society of Civil Engineering, 95(ST12), pp.2565-2587.

[54] Knowles, R. B., and Park, R. (1970). Axial load design for concrete filled steel tubes. Journal of the structural division, Proceedings of American Society of Civil Engineers, 96(ST10), pp.2125-2153.

[55] Laskar, A. I., and Talukdar, S. (2008-a). Rheology of steel fiber reinforced concrete. Asian Journal of Civil Engineering, 9(2), pp.167-177.

[56] Laskar, A. I., and Talukdar, S. (2008-b). A new mix design method for high performance concrete. Asian Journal of Civil Engineering (Building and Housing), 9(1), pp.15-23.

[57] Laskar, A., and Talukdar, S. (2008-c). Rheological behavior of high performance concrete with mineral admixtures and their blending. Construction and Building Materials, 22(12), pp.2345–2354.

[58] Liang, Q. Q., and Fragomeni, S. (2009). Nonlinear analysis of circular concrete-filled steel tubular columns under axial loading. Journal of Constructional steel Research, 65(12), pp.2186-2196.

[59] Liu, D., Gho, W.-M., Yuan, J. (2003). Ultimate capacity of high-strength rectangular concrete-filled steel hollow section stub columns. Journal of Constructional Steel Research, 59(12), pp.1499-1515.

[60] Liu, D., Gho, W.-M. (2005). Axial load behaviour of high-strength rectangular concrete-filled steel tubular stub columns. Thin-Walled Structures, 43(8), pp.1131-1142.

[61] Lu, Z.-H., and Zhao, Y.-G. (2010). Suggested empirical models for the axial capacity of circular CFT stub columns. Journal of Constructional Steel Research, 66(6), pp.850–862.

[62] Mander, J. B., Priestley, M. J., and Park, R. (1988). Theoritical Stress-Strain model of confined concrete. Journal of Structural Engineering, 114(8), pp.1804-1826.

[63] Mehta, P. K., and Monterio, P. J. (2006). Concrete Microstructure, Properties, and Materials (Third Edition ed.). New Delhi: McGraw Hill Education (India) Private Limited.

[64] Menon, D., and Reddy, Y. N. (1998). Finite Element Modelling of Tall Slender Tubular Towers. Journal of Structural Engineering, SERC, 24, pp.243–246.

[65] Morino, S., and Tsuda, K. (2003). Design and construction of concrete-filled steel tube column system in Japan. Earthquake Engineering and Engineering Seismology, 4(1), pp.51-73.

[66] Nakanishi, K., Kitada, T., and Nakai, H. (1999). Experimental study on ultimate strength and ductility of concrete filled steel columns under strong earthquake. Journal of Constructional Steel Research, 51(3), pp.297-319.

[67] Natarajan, C. (2005). Characterization of permiability of fly ash concrete. The Journal of Corrosion Science and Engineering, 7(Preprint 34), pp.1-12.

[68] Natarajan, C., and Shifana Fatima, S. (2007). Influence of size effect on response of RC beam. Journal of Structural Engineering, 34(3), pp.166-177.

[69] Natarajan, C., and Srividya. (2005). Corrosion effects on high performance concrete. New Buildings Materials and Construction World, 10(12), pp. 49-54.

[70] Neogi, P. K., Sent, H. K., and Chapman, J. C. (1969). Concrete-filled tubular steel columns under eccentric loading. Journal of American Concrete Institute, 47(5), pp.187-195.

[71] Oliveira, W., Nardin, S., El Debs, A., and El Debs, M. (2009). Influence of concrete strength and length/diameter on the axial capacity of CFT columns. Journal of Constructional Steel Research, 65(12), pp.2103-2110.

[72] Partheepan, G., Sehgal, D.K., and Pandey, R.K. (2008). Finite Element Application to Estimate In-Service Material Properties using Miniature Specimen. World Academy of Science, Engineering and Technology, 2, pp. 477-483.

[73] Rai, S. K., and Prasad, J. (2005-a). Non-linear static analysis of shear wall in tall buildings. Proc. of International Structural Engineering Convention. Bangalore, India: Indian Institute of Science Bangalore.

[74] Rai, S. K., and Prasad, J. (2005-b). Non-linear static analysis of tall buildings. Proc. of 4th International Conference on Autoclaved Aerated Concrete- Innovation and Development, (pp. 89-100). London, UK.

[75] Rai, S. K., Prasad , J., and Ahuja, A. K. (2006). Reducing Drifts and damages in tall buildings by shear wall panels. Proc. of the National Conference on High Rise Buildings: Materials and Construction Practices. New Delhi, India.

[76] Raman, S. N., Ngo, T., Mendis, P., and Mahmud, H. B. (2011). High-strength rice husk ash concrete incorporating quarry dust as a partial substitute for sand. Construction and Building Materials, 25(7), pp.3123–3130.

[77] Ramesh, T., Prakash, R., and Shukla, K. K. (2010). Life cycle energy analysis of buildings: An overview. Energy and Buildings, 42(10), pp.1592–1600.

[78] Ramesh, T., Prakash, R., and Shukla, K. K. (2012). Life cycle energy analysis of a residential building with different envelopes and climates in Indian context. Applied Energy, 89(1), pp.193–202.

[79] Ramesh, T., Prakash, R., and Shukla, K. K. (2012). Life cycle approach in evaluating energy performance of residential buildings in Indian context. Energy and Buildings, 54(November), pp.259–265.

[80] Ravindrarajah, R. S., and Tam, C. T. (1985). Properties of concrete made with crushed concrete as coarse aggregate. Magazine of Concrete Research, 37(130), 29-38.

[81] Revathi, P., and Menon, D. (2005). Nonlinear finite element analysis of reinforced concrete beams. Journal of Structural Engineering, SERC.

[82] Richart, F. E., Brandtzaeg, A., and Brown, R. L. (1928). A study of the failure of concrete under combined compressive stresses. Bulletin No.185, University of Illinois-Engineering Experimental Station.

[83] Roeder, W. Charles, Lehman E. Dawn, and Bishop E. (2010). Strength and Stiffness of Circular Concrete Filled Tubes. Journal of Structural Engineering, ASCE

[84] Saenz, L. P. (1964). Discussion of Equation for the stress-strain curve of concrete by P. Desaui and S. Krishnan. ACI Journal, 61, pp.1229-1235.

[85] Sakino, K., Nakahara, H., Morino, S., and Nishiyama, I. (2004). Behavior of Centrally Loaded Concrete-Filled Steel-Tube Short Columns. Jouranl of Structural Engineering, ASCE, 130(2), pp.180-188.

[86] Salmanpour, A., and Mojsilovic, L. (2013). Application of Digital Image correlation for strain measurements of large masonary walls. Proceedings, 5th Asia Pacific Congress on Computational Mechanics, Singapore, December 11-14, 2013, Paper No. 1128.

[87] Schneider, S. (1998). Axially loaded concrete-filled steel tubes. Journal of Structural Engineeing, ASCE, 124(10), pp.1125-1138.

[88] Shakir-Khalil, H., and Zeghiche, J. (1989). Experimental behaviour of concrete-filled rectangular hollow-section columns. The Structural Engineer, 67(19), pp.346-353.

[89] Shams, M. H. (1997, January). Non-linear evaluation of concrete-filled steel tubular columns, PhD Dissertation. New Jersey Institute of Technology, Department of Civil and Environmental Engineering, New Jersey, USA.

[90] Shams, M., and Saadeghvaziri, M. (1997). State of the Art of Concrete-Filled Steel Tubular Columns. ACI Structural Journal, 94(5), pp.558-569.

[91] Shams, M., and Saadeghvaziri, M. A. (1999). Nonlinear response of concrete-filled steel tubular columns under axial loading. ACI Structural Journal, 96(6), pp.1009-1018.

[92] Shanmugam, N. E., and Lakshmi, B. (2001). State of art report on steel-concrete composite columns. Journal of constructional steel research, 57, pp.1041-1080.

[93] Sofi, M., van Deventer, J. S., Mendis, P. A., and Lukey, G. C. (2007). Engineering properties of inorganic polymer concretes (IPCs). Cement and Concrete Research, 37(2), pp.251–257.

[94] Sridevi, B., and Agrawal, S.K. (1991). 2D Finite Element Model for Planar Failure along a Joint. Indian Geotechnical Conference.

[95] Srinivasan , S., and Menon, D. (2003). RC rectangular column sections under biaxial eccentric compression-an improved design recommendation. Journal of Structural Engineering, SERC, 29(4), pp.205-211.

[96] Susantha, K. A., GE, H., and Usami, T. (2001). A capacity prediction procedures for concrete-filled steel columns. Journal of Earthquake Engineering, 5(4), pp.483-520.

[97] Tan, K. T., Bhowmik, T., and Balendra, T. (2013). Confinement model for FRP-bonded capsule-shaped concrete columns. Engineering Structures, 51(June), pp.51-59.

[98] Tao, Z., and Han, L.-H. (2006). Behaviour of concrete-filled double skin rectangular steel tubular beam-column. Journal of Constructional Steel Research, 62(7), pp.631-646.

[99] Tao, Z., Han, L.-H., and Zhao, X.-L. (2004). Behaviour of concrete-filled double skin (CHS inner and CHS outer) steel tubular stub columns and beam-columns. Journal of Constructional Steel Research, 60(8), pp.1129-1158.

[100] Thanoon, W. A., Hamed, A. M., Noorzaei, J., Jaafar, M. S., and Al-Silayvani, B. J. (2004-a). Inelastic analysis of composite sections. Computers and Structures, 82(20-21), pp.1649–1656.

[101] Thanoon, W. A., Paul, D., Jaafar, M. S., and Trikha, D. N. (2004-b). Influence of torsion on the inelastic response of three-dimensional r.c. frames. Finite Element in Analysis and Design, 40(5-6), pp.611–628.

[102] Tomii, M., Yoshimura, K. and Morishita, Y. (1977). Experimental studies on concrete-filled steel tubular stub columns under concentric loading. Proc. of the International Colloquium on Stability of Structures under Static and Dynamic Loads, Washington: SSRC/ASCE. pp. 718-741

[103] Umar, A., Abbas, H., and Sehgal, D.K. (1994). An extrapolation technique for prediction using coarse mesh. Proc. of 10th Symposium on Earthquake Engineering, Roorkee, India, pp. 547-558.

[104] Umar, A., Abbas, H., Qadeer, A., and Sehgal, D.K. (1996). Prediction of error in finite element results. Computers and Structures- COMPUT STRUCT, 60(3), pp. 471-480.

[105] Uy, B. (1998-a). Ductility, strength and stability of concrete-filled fabricated steel box columns for tall buildings. Structural Design of Tall Buildings, 7(2), pp.113–133.

[106] Uy, B. (1998-b). Local and post-local buckling of concrete filled steel welded box columns. Journal of Constructional Steel Research, 47, pp.47-72.

[107] Uy, B. (2000). Strength of concrete filled steel box columns incorporating local buckling. Journal of Structural Engineering, 126(3), pp.341-352.

[108] Wheeler, A., and Pircher, M. (2002) The Influence of Material Properties on the Local Buckling of Concrete Filled Steel Tubes. Advances in Building Technology, I, pp. 215-222.

[109] Wu, D., Sofi, M., and Mendis, P. (2010). High strength concrete for sustainable construction. International Conference on Sustainable Built Environment (ICSBE-2010), (pp. 434-442). Kandy.

[110] Xiamuxi, A., and Akira , H. (2012). A study on axial compressive behaviors of reinforced concrete filled tubular steel columns. Journal of Constructional Steel Research, 76(September), pp.144-154.

[111] Xiamuxi, A., Hasegawa, A., and Shioi, Y. (2011, Novemeber). Nonlinear Analysis of RCFT columns under axial forces with confinement effect and failure history. Proceeding of Constructional Steel, 9, pp.49-56.

[112] Yang, Y., Han, L., and Wu, X. (2008). Concrete Shrinkage and Creep in Recycled Aggregate Concrete-Filled Steel Tubes. Advances in Structural Engineering, 11(4). pp.383-396

[113] Yang, Y.-F., and Han, L.-H. (2006). Experimental behaviour of recycled aggregate concrete filled steel tubular columns. Journal of Constructional Steel Research, 62(12), pp.1310-1324.

[114] Yu, Q., Tao, Z., Liu, W., and Chen Z.-B. (2010). Analysis and calculations of steel tube confined concrete (STCC) stub columns. Journal of Constructional Steel Research, 66, pp.53-64.

[115] Zhang, S., Ma, X., and Goode, C. D. (2007). Comparison between Chinese and three worldwide codes for circular concrete-filled steel tube members. Chinese scientific papers online,http://www.paper.edu.cn.

[116] Zhao, X.-L., and Grzebieta, R. (2002). Strength and ductility of concrete filled double skin (SHS inner and SHS outer) tubes. Thin-Walled Structures, 40(2), pp.199-213.

LIST OF PUBLICATIONS

JOURNALS

1. Heaven Singh**,** P.K. Gupta (2013). Numerical Modeling of Rectangular Concrete Filled Steel Tubular Short Columns. International Journal of Scientific and Engineering Research. Vol. 4, Issue 5, pp. 170-173.
2. P.K. Gupta, V.K. Verma, Heaven Singh, Ziyad Kubba and Nabam Ajay (2013). Ductility and energy absorbing capacity of concrete filled UPVC tubes. International Journal of Construction Materials and Structures. Vol. 1, No. 1, April 2013, pp. 1-10
3. P.K. Gupta, Heaven Singh (2014). Numerical study of confinement in short concrete filled steel tube columns. Latin American Journal of Solids and Structures. Vol. 11, No. 8, pp. 1445-1462.
4. P.K. Gupta, V.K. Verma, Ziyad A. Khaudhair and Heaven Singh (2014). Effect of tube area on the behavior of concrete filled tubular columns. Computers and Concrete, Techno-Press (In Press).

CONFERENCES

1. P.K. Gupta, Heaven Singh (2012). Numerical study of tubed concrete filled short columns. 5th Asian Concrete Federation (ACF) Conference, October 26-28, Pattaya, Thailand.
2. P.K. Gupta, Heaven Singh (2012). Numerical study of concrete filled tubular columns under axial compression. 8th Structural Engineering Convention (SEC), December 19-21, SVNIT Surat, Gujrat, India.
3. P.K. Gupta, Heaven Singh (2012). Analytical Study of Concrete-Filled Tubes in Axial Compression. 28th NCCE & National Seminar on Role of Infrastructure for Sustainable Development, 12-14 October, IEI Roorkee, India. Awarded the Best Paper Award in the conference in the category “Advances in Construction Materials and Technologies”